Development of a Quality System to Control DNA, Endotoxin and Particulates as part of an Extracorporeal Bioartificial Liver Medical Device

Amir Gander

2011

UCL Centre for Hepatology
UCL Medical School, Hampstead Campus
Department of Medicine
University College London

Declaration

I, Amir Gander confirm that the work presented in this thesis is my own. Where information has been derived from other sources, I confirm that this has been indicated in the thesis.

Abstract

The Bioartificial Liver Devices (BAL) could provide treatment for acute liver failure by supporting patients awaiting transplantation or aid the process of liver regeneration. For use within a clinical setting, a number of regulatory criteria must be met, including controlling DNA, endotoxins and particulates. The aim of this thesis was to begin the development of a system to control plasma quality returning to the patient.

Methods for DNA, endotoxin and particulates detection were established with human plasma to measure sensitivity for use with the BAL system. DNA detection by QPCR using Alu repeats were validated for use as an analytical method to demonstration DNA removal, achieving a Limit of Quantification (LoQ) of 0.1ng/ml DNA. Endotoxin analysis utilised a fluorescent derivative of the widely used LAL assay to increase sensitivity, enabling 2EU/ml to be detectable. Particulates down to 1μm were measured using laser light obscuration.

Initially the removal of particulates from alginate as a starting material (alginate prior to encapsulation) was shown, using filtration by depth charge filter, sand bed filtration and gas solid cyclonic filtration. Encapsulated bead integrity, cell function and growth were compromised with all techniques of filtering alginate in solution, including depth charged and sand bed filtration. Conversely, gas solid cyclonic filtration maintained bead integrity, cell growth and function.

Testing potential DNA levels in the large scale BAL system required the development of a scaled down model of the BAL treatment phase, replicating the large scale BAL system with cell number to plasma volume ratio. This provided an indication of the DNA challenge a removal system at a large scale would need to contend with, predicted to be 68ng/ml for a full scale BAL. A scaled down filtration model was then established to model the DNA removal capability of different 3M® Cuno® DNA depth charged filters. This established a requirement for a predicted surface area of 1300cm^2 to achieve complete DNA removal. The volumetric capacity of the filters were calculated using established filter blockage models, in order to scale the capacity to the full BAL system size.

Finally, the chosen depth charge filter was tested at a large scale with the extracorporeal BAL system, spiking human plasma with DNA and endotoxin, whilst measuring endotoxin and DNA removal over 8 hours of treatment.

Acknowledgements

I would like to thank Dr Clare Selden, Professor Barry Fuller and Professor Humphrey Hodgson for their supervision and guidance throughout this project. I would also like to thank the Liver Group Charity for funding my studentship and this research.

The scaled down filtration system would not have been possible without the help of Liz Joyce at the medical electronics department for the many hours and late nights put into the work. For the development of the filtration model I would like to thank both Nigel Silver and Peter Koklitis at 3M® Cuno® for their patience and friendly advice. I would like to acknowledge the huge effort that Timea Grego and Ian Stuttervant at the UCL Department of Civil Engineering for contributing to this thesis from the work Timea preformed for her MSc.

To those entire Liver group and other colleagues in the Department of Hepatology and elsewhere, past and present, who have provided scientific advice, moral support, thank you.

Last but not least thank you to my family and especially Shafaq, who I could not have asked for more from and will be eternally grateful!

Table of Contents

List of Figures

List of Tables

List of Abbreviations

AFP	α-fetoprotein
a-MEM	Alpha Minimal Essential Medium
3D	3-dimensional
ALF	Acute Liver Failure
AMC-BAL	Amsterdam Medical Centre Bioartificial Liver Device
BAL	Bioartificial Liver Device
BCA	Bicinchoninic Acid
BSA	Bovine Serum Albumin
cfcDNA	Cell free circulating DNA
CSTPE (plasma)	Cobe® Spectra® therapeutic plasma exchange (plasma)
CV	Coefficient of Variance
DE	Diatomaceous Earth
DMSO	Dimethyl Sulfoxide
ELAD	Extracorporeal Liver Assist Device
EPDM	ethylene propylene diene monomer
cGMP	current Good Manufacturing Practice
FBB	Fluidised Bed Bioreactor
FCS	Foetal Calf Serum
FDA	Fluorescein diacetate
FFP	(Human) Fresh Frozen Plasma
HBSS	Hanks Balanced Salt Solution
ISO	International Organisation for Standardisation
LAL	Limulus Amebocyte Lysate
LoD	Limit of Detection
LoQ	Limit of Quantification
NBS	National Blood Service
PERV	Pig Endogenous Retro-Virus
PI	Propidium Iodide
PTFE	Poly tetra Flouro-Ethelyne
RPM	Revolutions per Minute
RPS	Revolutions per Second
SOP`	Standard Operating Procedure
TRH	Thyroid Releasing Hormone
UV	Ultra Violet

Chapter 1
General Introduction

This Chapter will present the background of the liver, liver disease, and substantiate the need for clinical development of the bioartificial liver device.

1. General Introduction

The fields of human organ replacement and regeneration using bioengineered solutions have blossomed into potential treatment for many diseases, from bioartificial tracheal, lung and heart transplants[1-3] to extracorporeal bioartificial kidney and pancreas[4]. The central tenet of these approaches is that organ replacement is drastically improved by using living cells that are able to replace functions that are often insufficient in artificial organ replacement or intensive care treatments alone.

Worldwide, the annual mortality rate of patients suffering from hepatic liver failure is over 2 million[5], which clearly illustrates a need for better liver replacement therapies.

1.1. The Liver

In order to understand the pathology of the liver, this section will briefly discuss the relevant macroanatomy, microanatomy, and function of the liver.

1.1.1. Structure and Function of the Liver

The human liver is one of the largest organs, situated at the top of the upper abdomen, beneath the diaphragm, it is protected by the ribcage (Figure 1-1A)[6] and comprises of two main lobes, the right and left, separated by the falciform ligament (anterior view on Figure 1-1B), and two smaller lobes, the caudate and quadrate lobes (posterior view Figure 1-1B). The liver mass is on average 1500g and taking around 25% of cardiac output, second only to the brain, arriving via the hepatic artery at ~400ml/min. It is connected to the small intestines by the portal vein transporting blood at 1000-1200ml/min from gastrointestinal tract and spleen to the liver[7]. A second blood supply maintains the liver with oxygen saturated blood from the heart via the aorta[8].

Figure 1-1: Morphological anatomy of the Liver. A; Showing the location of the Liver in the upper abdomen protected by the rib cage. B; Magnification of the liver, illustrating the morphological anatomy of the liver, comprising of the left and right lobe separated by the falciform ligament, shown in the anterior view, with the posterior view showing the hepatic vein, proper hepatic artery, the portal vein, and the common bile duct. (Modified from the Encyclopaedia Britannica and www.fattyliver.com)

Branches of the hepatic artery and portal vein feed the dual blood supply through the liver lobules, constituting segments that are defined at histological scale[9] (Figure 1-2C). The area between the hepatic venule and the hepatic artery is comprised of both hepatocytes and non-parenchymal cells (e.g. Kupffer cells and stellate cells). Blood passes from branches of the hepatic portal vein and the hepatic artery, during which over 500 different synthetic and detoxifaecatory functions occur, before entering the systemic blood supply via the central vein[10].

The presence of an oxygen, hormone and substrate concentration gradient, from the portal vein to the hepatic artery, causes zonal Hepatic heterogeneity shown in Figure 1-2B[11-13] (Figure 1-2C). For example, the oxygen concentration changes from ~85μmol/L at the

hepatic artery to ~40μmol/L at the hepatic venule[14], leading to hepatocytes in the specific zones performing distinct functions related to the environment, which form the basis for the model of the acinus functional unit illustrated in Figure 1-2C.

Figure 1-2 : Microanatomy of the liver. A; arterial and venous branches supply ~ 1 x 10^6 liver lobules (in the whole liver), a morphological unit of the liver. B; a detailed section of a lobule illustrating the blood entering through the portal vein and hepatic artery to flow through the sinusoids which are lined by hepatocytes, exiting through the hepatic vein. Hepatocytes distributed across the sinusoid are split into three functional zones: 1, 2, and 3. C; the acinus as defined by the orientation around the afferent vascular system of the portal vein and hepatic artery, describing the smallest functional subunit (Modified from American College of Surgeons [15], and American National Institute of alcohol Abuse [16])

An important hepatic function is bile production, regulated by hormonal and molecular signals carried in venous and arterial blood[17]. Bile drains into the biliary system (Figure 1-2B), which is formed by a network of channels connected to the common hepatic duct, (Figure 1-1B posterior view and Figure 1-2B) before being released into the small intestines [18]. It contains many organic salts as well as exogenous and endogenous amphipathic compounds, such as bilirubin, fatty acids, drugs, and toxins, both aiding excretion of toxins and emulsification of lipids for adsorption. [19,20].

1.1.2. Cell Numbers, Types, and Function.

The liver is commonly segmented into 8 functional subunits each of which contains approximately 1 million lobules (Figure 1-2A). A single lobule contains, on average, between 100,000 and 200,000 hepatocytes, giving a total of $1 \times 10^{11} – 2 \times 10^{11}$ hepatocytes in the liver. However, with only 35% of the original cell volume of 7×10^{10} hepatocytes, the liver can sustain a healthy individual[21,22]. Other cell types, which form part of the liver and play a vital role in a functional system are summarised in Table 1-1.

Cell Type	Function	Description
Hepatocytes	Oxidative metabolism	O2 gradient dictates level depending on proximity to portal vein[14,23]
	Carbohydrate metabolism	Aerobic respiration is favoured hepatocytes in periportal region[24,25]
	Lipid metabolism	Hypoglycaemia induces formation of ketone bodies, and inhibition of lipid metabolism[26]
	Amino acid metabolism and Detoxification	Excess is catabolised into ammonia. Gluconeogenesis occurs when glycogen and fatty acids are exhausted[26,27]
	Bile formation	Bile production is stored in the gall bladder before being excreted into the digestive system to aid lipid emulsification, and digestion and excretion [26]
	Biotransformation and detoxification	Cytochrome P450 proteins are responsible for detoxification, biotransformation include T4 to T3 de-iodinisation stimulated by thyroid stimulating hormone (TSH) [28]
Kupffer Cells	Macrophages residing in the liver sinusoid	Antigen presentation, cytokine release and mediation of pathogen response[29]
Liver Sinusoidal Endothelial Cells	Barrier forming the sinusoid and the space of Disse	Line the inner wall of the sinusoid containing fenestrations of 100 - 200nm to allow diffusion[20]
Stellate Cells	Produce extracellular matrix for hepatocytes growth	Located in the space of Disse producing matrix proteins such as collagen[30]

Table 1-1 Summary of cell type and function making up the human liver.

1.2. Liver Failure

Liver failure is a condition where the liver can no longer perform normal metabolic and synthetic functions. The development of liver failure is categorised into either chronic or acute liver failure, depending on the nature of the insult and the progression of the disease. Chronic liver failure develops due to progressive liver injury followed by regeneration over a long period, resulting in development of cirrhosis and fibrosis replacing functional hepatocytes[31]. Acute liver failure occurs through the death of large numbers of hepatocytes, in a short period of time leading to compromised liver function as defined by hepatic encephalopathy and a lack of protein synthesis. The leading global cause of acute liver failure is viral Hepatitis, with the exception of the UK and USA where acetaminophen (Paracetamol) is the primary cause[32].

1.2.1. Chronic Liver Failure

Despite chronic liver injury causing widespread cirrhotic tissue damage the liver has functional capacity for prolonged periods before acute-on-chronic liver failure ensues, exhibiting the aetiology of acute liver failure described in section 1.2.2.

1.2.1.1. Toxic Substances Leading to Chronic Liver Disease

Long term abuse of toxic substances such as alcohol can lead to different hepatic conditions including alcoholic liver disease where hepatocytes swell and change their metabolism, and fatty liver disease with excess fat builds up in the liver. As a result of persistent hepatitis caused by these conditions, liver cirrhosis develops, eventually leading to organ failure[33].

1.2.1.2. Viral Hepatitis

Currently five main categories of viral hepatitis have been defined: A, B, C, D and E, of which B, C and D are parenterally transmitted and have shown progress to chronic hepatitis. Infected patients can be treated with anti-viral drugs but persistent infection can lead to progression of chronic hepatitis whereby the liver sustains inflammation and damage [34].

1.2.1.3. Metabolic Disorders of the Liver Disorders

Metabolic disorders often do not directly cause liver damage, but lead to either a build-up of toxin, an increased susceptibility to pathogens or manifestation of carcinoma, ultimately causing development of cirrhosis and fibrinogenesis and potentially acute-on-chronic liver failure. An example of fibrotic metabolic disorders is hemochromatosis, which arises from excess iron accumulation in the liver and pancreas, leading to cirrhosis and potentially acute-on-chronic liver failure[35].

1.2.1.4. Treatment of Chronic Liver Disease

Most chronic liver diseases mentioned are treatable with relevant drugs only causing major problems if they are not diagnosed or are neglected, allowing cirrhosis and fibrosis to develop. Eventually, the liver becomes decompensated leading to acute-on-chronic liver failure[36], which

the Liver Group BAL system could treat, although it is primarily targeted at acute liver failure patients.

1.2.2. Acute Liver Failure

1.2.2.1. Toxic Liver Injury

The liver is vulnerable to toxic injury due to its pivotal role in biotransformation and metabolite processing for excretion into the bile, potentially leading to hepatic necrosis and acute liver failure [37]. Two aspects dictate hepatotoxic effect, dosage and the properties of the metabolite for biotransformation. For example, a relatively high concentration (200mg/kg person) of acetaminophen (Paracetamol) can cause acute liver failure [38], whereas a comparatively low concentration of carbon tetrachloride (200µg/ml)[39]) leads to the same outcome. Both are metabolised by the CYP-P450 group of enzymes to form toxic compounds carbon trichloride and dichlorocarbene (from CCl_4), and N-acetyl-*p*-benzoquinoneimine (from acetaminophen) causing hepatotoxicity[40].

1.2.2.2. Viral Induced Injury

Of the five main types, Hepatitis B (HBV) is the main cause of viral acute liver failure[41], attributable to the immune response through a substantial induction of pro-inflammatory interleukin-12 release from Kupffer cells[42].

1.2.2.3. Treatment of Acute Liver Failure

Treatment of acute liver failure is predominantly focused on intensive care practices, based on four principles: prevention and treatment of complications; substitution of substances no longer synthesised; promotion of liver regeneration; bridging the gap before transplantation or regeneration. Liver transplantation was first reported in 1967[43] and is now the treatment of choice, if liver regeneration fails, but is limited by inadequate donor numbers. A report to the UK house of Lords in 2008 stated that despite increases in donor availability, 15% of people on waiting lists die before receiving a transplant[44]. This is reflected in the USA where in 2007, 6494 liver transplants were performed, with 17,000 remaining on the waiting list, of which 2000 died. Furthermore, the longer a patient is on the transplant list the less favourable the transplant outcome is, due to the deterioration of their condition[45].

1.3. Extracorporeal Liver Replacement Technology

In order to bridge the gap prior to transplantation or to support patient physiology to promote liver regeneration, liver replacement technologies seek to replace vital liver functions, with one or a combination of mechanical, chemical or biological means.

1.3.1. Artificial Liver Systems

Artificial liver systems aim to cleanse the blood or plasma through physical or chemical means, in order to mimic the detoxifacatory function of the liver. They are usually based on membrane separation associated with columns or suspensions of sorbents such as charcoal or ion exchange resins or albumin exchange.

1.3.1.1. Liver Dialysis

Liver dialysis works on the principle of a concentration gradient between a semi-permeable membrane removing toxins from the blood. For example, HemoCleanse® uses a semi-permeable membrane with a 4-5kDa cut-off, which separates patient blood from a solution containing sorbent activated charcoal and cation exchange resin. Toxins in plasma from fulminant hepatic failure (FHF) patients, in particular non-ionic compounds, adsorb onto the charcoal, with the cation exchange resin binding to ionic compounds. Unfortunately, the technique shows no survival benefit in patients suffering from FHF, although an improvement in transplant recovery of 71% vs. 35.7% was shown, with treated vs. untreated FHF patients. Despite the modest improvement, it shows that the principle of removing toxins by substituting for liver function may work[46].

Developments in dialysis technology used more sophisticated approaches, essentially based on dialysis with the incorporation of sorbent technologies. One such device named MARS® (Molecular Absorbance in a Recycled System) shown on Figure 1-3, uses a 50kDa membrane for dialysis of lipophilic, albumin bound toxins from patient albumin, to extracorporeal albumin present on the counter side of the membrane. However, no significant survival benefit was seen, in of 90 patients treated with MARS before transplantation, a significant improvement in life quality was observed for post liver transplanted patients, which showed to be more cost effective than conventional hospital treatment[47]. This illustrates that the concept of replacing liver function has great potential; the question now is how to make it more effective.

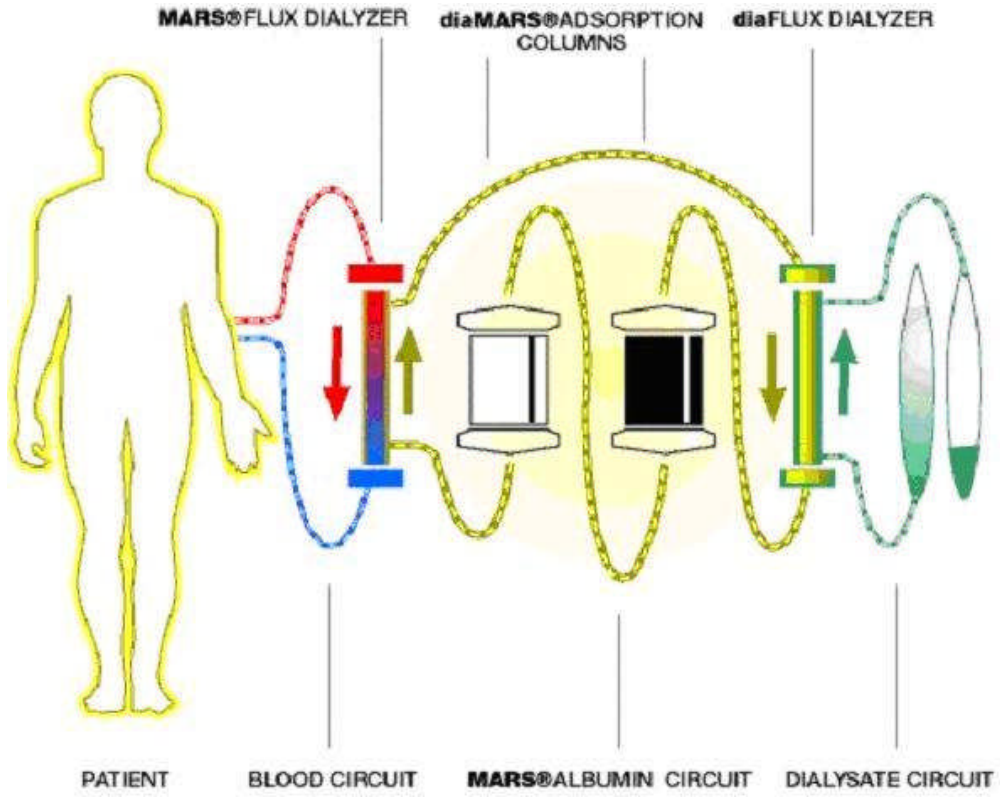

Figure 1-3: Molecular Adsorbent Recycling System (MARS®). Patient plasma passes by a 50kDa dialysis membrane with clean albumin, facilitating the absorption of hydrophobic toxins from the patient's albumin, whilst preventing protein transfer. The albumin is then partially rejuvenated by passing through an anionic exchange and activated charcoal column.[47]

1.3.2. Bioartificial Liver Machines

Artificial liver systems cannot perform the full gamut of functions necessary to substitute liver function for therapeutic benefit, as defined by a definite improvement in survival outcome. With over 500 functions provided for by the liver[26] the only practical approach is utilising a biological element. As a consequence, the focus of system design shifts from dissection of individual liver functions for artificial replacement to designing a system which can sustain

Sufficient living cells adequate for treatment. These aspects are inextricably linked with cell type, the growth media and the ability to achieve and maintain a cell mass comparable to a third of a native liver, normally sufficient for maintaining liver function in humans[48]. Furthermore, the system needs to be a bedside treatment, with fully regulatory approved components available at extremely short notice, requiring a means of long term cell storage through cryopreservation[49]

1.3.2.1. Cell Source

The biological element to the bioartificial liver is crucial for treatment efficacy, requiring a balance between proliferative potential in cell culture, functional capability, possible patient immunogenicity, and cell source availability. Table 1-2 summarises different considerations that are important for cell choice.

Cell Source	Advantages	Disadvantages
Autologous cells harvested from patients (primary Hepatocytes from patient)	• No immune reaction • Low risk of infection • Near native level of hepatic function	• Prohibitively limited availability • Potentially poor quality of cells • Limit proliferative capacity
Allogeneic cells collected from donors (primary hepatocytes from donors)	• Better availability compare to patient source • Ability to pool cells • Near native level of hepatic function	• Risk of immune response • Risk of disease transmission • Limit growth capacity
Allogeneic cell lines (Carcinoma cell line)	• High availability • Almost infinite cell growth capacity • High cell density achievable	• Loss of cell function • Potential tumourigenicity • Potentially undesirable protein expression Regulatory issues with use
Xenobiotic cells source harvested from different species, e.g. pigs	• High availability • Near native functionality	• Risk of pathogen transmission (e.g. PERV) • Non-human protein production • Regulatory issues with use

Table 1-2: Potential cell sources for Bioartificial liver systems. Outlining advantages and disadvantages.

The use of primary human hepatocytes, either from the patient or from donors would immediately appear to be the best choice, due to their near native level of hepatic function, low risk of infection and lack of immune induction. However, limited availability of primary human hepatocytes, especially from the patient, coupled with a limited ability to culture them to the required cell density and maintain differentiation for prolonged periods, present major obstacles for their use in a BAL system[50-52]. Animal primary hepatocytes solve the issue of availability, but bring with it many other issues, not least the potential risk of transferring endogenous retroviral elements, as well as increasing the probability of bacterial and viral infections crossing the species barrier[52-54].

Other cell sources include a burgeoning area of stem cells, where groups have induced differentiation of mouse induced pluripotent and embryonic stem cells into cells of hepatic lineage. The cells are then cultured for application to a hollow fibre cell matrix, constructed from polyethersulfone, to produce functioning cells with comparable function to primary mouse hepatocytes[52,55].

A popular cell source for BAL systems is the HepG2 cell line and various derivatives including; C3A cells, HepG2/tk, and HepG2 cells[56-59]. The advantage of these is an inexhaustible source of cells, although function may be compromised in comparison to primary hepatocytes[56,60]. However, many of the lacking functions can be up regulated using genetic modification[58,59], oxygenation and chemical induction, e.g. refampsin [61,62].

1.3.2.2. Hollow Fibre Bioartificial Liver Systems

Hollow fibre bioreactors were the first generation of bioartificial livers entered into clinical trials. They are based on the design for kidney dialysis, where the specific cells types are suspended in cold collagen, then injected into the hollow fibre cartridge, which is then perfused with warm media causing gelation of the collagen and contraction cell-collagen suspension. This provides a space for the plasma/blood to pass adjacent to the cells/collagen matrix[63].

A multitude of cell types have been used with this technology, such as the HepaAssist BAL, using cryopreserved primary porcine hepatocytes[64], the ELAD BAL (extracorporeal liver assist device) using C3A cells, a HepG2 cell line derivative [65], the MELS-BAL (modular extracorporeal liver support) and utilising primary human hepatocytes from donors[66], amongst many others. A recent study with 1 x 10^8 primary human hepatocytes in a hollow fibre system showed maintenance of viability over two weeks, although physiological and function

parameters, such as urea production, glucose consumption, and non-essential amino acid synthesis rapidly declined during this time[51].

1.3.2.3. Microfluidics

An area of increased interest is the use of micro-fluidics with micro-electro-mechanical (MEM) technology, working on a micrometre to millimetre scale to mimic the liver vasculature, by etching silicon wafers with channels and attaching electrodes and other chemical functional groups such as cell adhesion proteins[52,67]. One such microfluidics device, is designed to form an artificial micro-liver, provides capillary like space where hepatocytes (HepG2 cells) are seeded, forming tissue similar to that of a native liver, showing a maintenance of cell viability and up regulation of function[68]. A polyethersulfone membrane barrier, containing 0.22μm pores, also provides a structure analogous to the fenestrations of the endothelial layer.

Recent developments have the ability to mimic sinusoids by introducing a co-culture system into a precisely etched chamber by positioning cells through di-electrophoresis, showing the same flow characteristics as a sinusoid[52,69]. Despite some exciting developments, a microfluidics device would currently be impractical to manufacture a device at a large enough scale for human clinical application, due to the low cell numbers relative to the size of the devices. However, it does illustrate the importance of improving intercellular contacts to better model the native liver architecture.

1.3.2.4. Examples of BAL Systems in Clinical or Pre-Clinical Trials

A number of bioartificial livers have gone through pre-clinical and clinical trials, but none have reached full clinical use. Some of the hollow fibre devices previously mentioned is outlined in Table 1-3. A development away from hollow fibre technology has been to apply hyper-fluidisation methodology on encapsulated spheroid cells to increase mass transfer and allow direct perfusate contact with cells. A recent study using HepG2 cells encapsulated in alginate beads, showed improved survival times in pigs suffering from fulminant hepatic failure. The alginate beads were coated in chitosan, increasing the stability of the beads in plasma, and housed in a chamber which induced bead fluidisation when passing plasma through[70]. Other Bioartificial Liver systems recently involved in clinical trials are summarised in Table 1-3.

Name of technology	Bioreactor Type	Method of Perfusion	Cell type	Clinical Trials
HepAssist[64]	Hollow fibre with two compartments, cells attach to dextran micro carriers on outside of hollow fibre, includes charcoal perfusion chamber and oxygenation by perfusate	Plasma passes through fibre lumen	Human Hepatocyte C3A cell line	Phase I Randomised trial, ALF survival: 73% vs. 59% control
ELAD[65,71]	Hollow fibre with 2 compartments, dialysis style cartridge, oxygenation by perfusate	Plasma passes through fibre lumen	Primary porcine hepatocytes	Randomised phase I trials: improvement in survival between controls
MELS[66,72]	Hollow fibre capillary system with 4 interwoven compartments, with independent function; media inflow, media outflow O_2/ CO_2/ heat exchange.	Plasma through fibre lumen	Primary human or porcine hepatocytes	Phase I trials: 7 of 8 patients carried to liver transplant with 100% transplant success rate after 3 years
Radial Flow Bioreactor[73]	Two hollow fibre compartment, oxygenation by direct cell contact with perfusate,	Radial plasma flow through mesh across cells	Primary porcine hepatocytes	Phase 1 trials: improvement to encephalopathy ammonium levels

Table 1-3, Summary of Bioartificial Liver systems which have undergone clinical trials. All are based on hollow fibre technology.

1.4. The Liver Group BAL

The Liver Group BAL currently utilises HepG2 cells (Heptoma blastoma cell line sub group), but is able to accommodate other proliferative cells lines, encapsulated inside 500µm alginate hydrogel beads to form cell spheroids, cultured to optimal function, which can then be fluidised by perfusion with plasma at ~400 ml/min in the same extracorporeal chamber.

1.4.1. Bulk Cell Growth

The growth phase commences by seeding the alginate hydrogel with a low number of cells per bead. After which, cells proliferate to between 30-100 million cells/ml of alginate beads in a fluidised bed configuration, being sufficient to achieve at least 35% of the native liver cell mass for a 75 kg individual (7 x 10^{10}), with ~1.2L of alginate beads. Growth is maintained over 9-12 days of culturing in modified culture medium, applying microgravity fluidisation to form multi-cellular spheroids with cell-to-cell communication via gap junctions, desmosomes, and microvilli, illustrated in Figure 1-4. As with other 3-D technologies, this too shows an increase in cell proliferative and functional performance compared with monolayer[74].

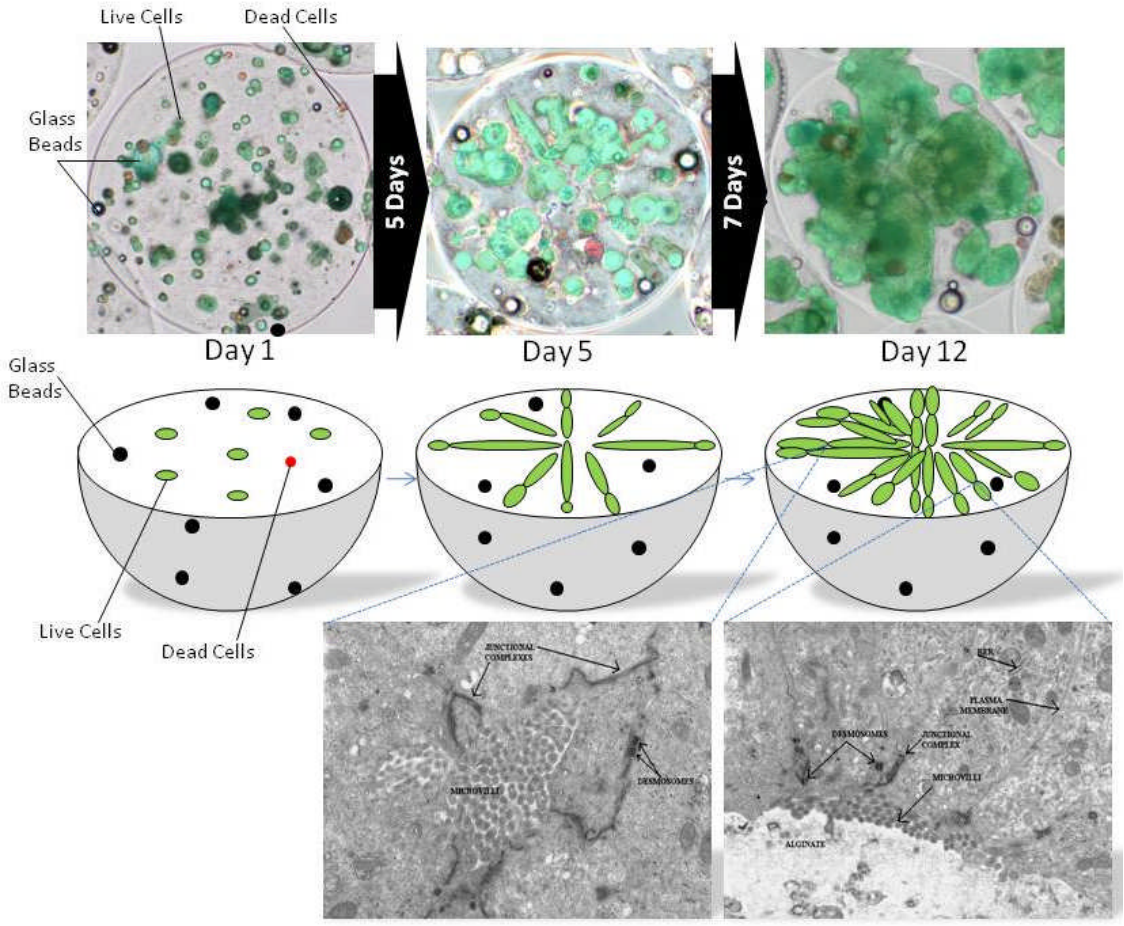

Figure 1-4: HepG2 cell encapsulated in alginate grown in modified media over 12 days to form multi-cellular spheroids. Cell viability was measured by green FDA staining, overlaid with red PI staining for non-viable cells. Cells grow out from single cells to form multi cellular spheroids with cell-to-cell contact, as illustrated in the transmission electron microscope images.

1.4.2. Microgravity

A microgravity environment is provided by movement of each bead in a stable continuous loop, with drag created by the upward fluid velocity forcing beads from the bottom of the fluidised bed to the top, where gravitational force due to the density of beads eventually becomes greater than the force of the plasma drag (Figure 1-5). The chamber provides a consistent environment between growth and treatment phase, allowing cell growth, washing and bead perfusion with human plasma, thereby removing risk of contamination from exchanging chambers.

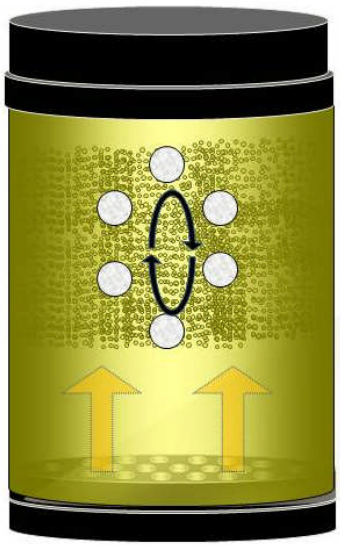

Figure 1-5: Microgravity in the BAL chamber. The small beads represent the bead bed, one bead is enlarged for clarification. Drag as a result of flow velocity causes the beads to move to the top of the fluidised bed. The density of the bead becomes sufficient to overcome the drag, through gravitational forces to fall to the bottom of the bead bed.

1.4.3. Treatment Phase

The biomass grown in modified culture medium is washed in human plasma before installation into a dual circuit system, as illustrated in Figure 1-6. In the primary circuit, blood from the patient is separated into plasma using the Cobe® Spectra® plasmapheresis system. Plasma is then passed into the secondary circuit, which contains the fluidised biomass providing nourishment and detoxification for the plasma.

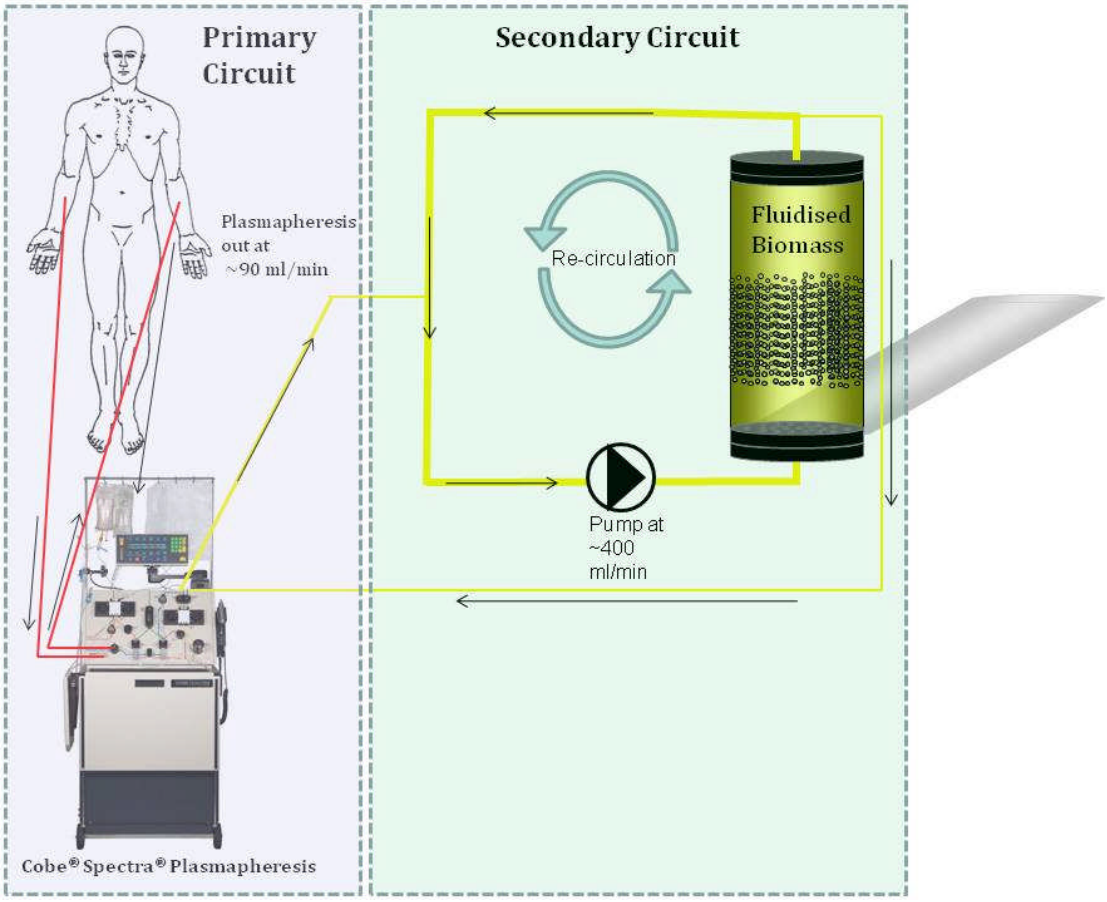

Figure 1-6: Liver Group BAL treatment phase, comprising two circuits. The primary circuit separates plasma from the patient using the Cobe® Spectra® aphaeresis system. The secondary circuit contains the cell biomass, which nourishes and detoxifies the plasma supplied by the primary circuit a number of times before returning to the Cobe® Spectra® Aphaeresis system and the patient.

Treatment can occurs for up to 8 hours where preliminary studies in rabbit models of hepatic failure showed high levels of liver specific function as well as improved systemic parameters indicative of liver failure (diastolic blood pressure and transjugular venous oxygen saturation)[57,74]. In addition to this, beads exposed to an *in vitro* model of human acute liver failure plasma showed maintenance of viability, bilirubin conjugation, CYP450-1A activity and urea synthesis [75]. In addition to this beads were tested in a large pig trial with full results pending, but did show improvement in clotting function, protein synthesis, and bilirubin conjugation amongst others.

1.5. Further Liver Group BAL Developments

To provide adequate nourishment and detoxification to patient's plasma, whilst maintaining patient safety, a balance needs to be struck between cell function, viability and number, as well as integrity of beads and clinical safety. One particularly crucial balance is that of cell function and proliferation. In comparison to primary human hepatocytes some HepG2 cell functions are down-regulated, whereas the contrary is true for HepG2 cell proliferation compared with primary hepatocytes[76]. For the BAL system, sufficiently sized and stable cell bulk is necessary to provide treatment. As previously mentioned, HepG2 function can be up regulated, whereas stability of cell function or proliferation cannot be easily maintained for a BAL application using primary hepatocytes.

A key aspect to market approval of the BAL medical device is the characterisation, evaluation and control of contaminants [77]. There are two vital features to control contaminants in the BAL system: patient safety, and regulatory compliance. These points are not mutually exclusive; regulatory bodies provide a framework for research and manufacture standardisation through stipulating requirements for compliance, by entrenching safety through traceability, stringent testing, and validation of efficacy. These criteria are delivered by implementing particular management tools through quality manuals, validated research, and validated analytical tools implemented through well-defined Standard Operating Procedures (SOPs) and personnel training documentation. SOP's are standard manuals and protocols to institute standardisation, not only as part of experimentation but through to laboratory practices and management structures.

It is important to incorporate safety and efficacy by establishing quality systems, beginning with the development of validated analytical methods to support them. Three contaminants, which are of significant regulatory importance and are cell associated will be the focus of this thesis; cell debris, DNA and endotoxin. Another important contaminant is particulates within the alginate starting material and will also be discussed. Some of the health aspects of these contaminants will be mentioned as an explanation for the regulations relating to these contaminants in a medical device.

The aspects of BAL bead integrity and clinical safety mainly relating to contamination transfer from components of the device to the patient. This includes alginate/cell fragments from the biomass, DNA from HepG2 cells, various components from the alginate matrix and endotoxin within the system. This will be the focus of this thesis with each chapter detailing the specific concerns related to the aforementioned contaminants. An overview of aspects not dealt with in later chapters will be outlined now.

1.5.1. Alginate

Alginate is a family of linear anionic polysaccharides, which form linear chains by covalent linking through the 1-4 carbon of -D-mannuronate (M) and its C-5 epimer α-L-guluronate (G), both in pyranose ring form. It is relatively abundant in nature, mainly produced by *Pseudomonas* bacteria and *Macrocystis pyrifera*, *Ascophyllum nodosum*, and various types of *Laminaria* seaweed[78]. For commercial use, however, extraction from seaweed is most common. Alginate solubilisation in water, when in linear chains, is achieved by forming the monovalent salt during extraction and processing. Once solubilised the electrostatic anionic repulsion between chains produces an intramolecular extended random coil structure, forming a gum with relatively high dynamic viscosity[79]. Dynamic viscosity increases exponentially with increased molecular mass, whilst the flexibility of the linear chains increase in the order of GG < MM <MG. As a result, the ratio of G and M directly influences the dynamic viscosity of the solution at a given concentration[80].

1.5.1.1. Ionotropic Gelation of Alginate

Ionotropic gelation of alginate (referred to as encapsulation), to form insoluble beads, can use Calcium as the divalent cation, to form cross linkers between anionic polymeric chains. Other alkaline earth metals can also be used, with the affinity decreasing thus; $Ba^{2+} > Sr^{2+} > Ca^{2+} >> Mg^{2+}$ [81], but increasing in biocompatibility. The gel forms by alginate chains linking between carboxylic acid groups on adjacent chains with the calcium in between[78].

1.5.1.2. Important Alginate Parameters for the BAL

Alginate beads are most commonly produced using a variety of techniques to form droplets or beads that undergo cross-linking in a polymerisation buffer containing calcium ions. This is termed external gelation, as the greatest Ca^{2+} concentration is on the outside of the bead, causing an increase in alginate chain formation on the edge of the bead[82]. As a result, this type of encapsulation provides an external protective layer for cells whilst providing sufficient internal space for cell growth[74,75].

The non-toxic nature of alginate itself and the process of making beads lend itself to use in a biomedical device. Bead formation occurs at neutral pH with no need for organic solvents, which maintains cell viability. Despite this, the use of relatively high Ca^{2+} concentrations required to facilitate cross-linking can be damaging to cells if exposed for a prolonged periods of time[83]. Furthermore, conditions that may cause excessive levels of shear stress to the cells during encapsulation may lead to a reduction in viability, although some shear stress can be tolerated[84].

For application to the BAL system, the formation of beads relies on the correct viscosity of the unpolymerised alginate, to form suitable bead morphology to facilitate cell growth and function, whilst maintaining a robust matrix over 8 – 12 days of growth, and up to 12 hours of plasma treatment, as well as cryopreservation and storage over long periods[49]. The ability to form a non-homogenous alginate cross-linking environment with adequate pore size to allow sufficient mass transfer between the cells and media/plasma is also crucial.

Anions with the ability to chelate Ca^{2+} such as citrate, EDTA, and phosphate need to be controlled in the BAL environment to maintain bead integrity[81], which is the reason for supplying additional calcium to FFP (fresh frozen plasma) that uses citrate as an anticoagulant.

1.5.1.3. Alginate Purification

During the development of the Liver Group BAL system, a set of alginate parameters have been carefully established, which are crucial for the successful encapsulation and growth of HepG2 cells, as well as bead integrity during the treatment phase in plasma[75]. Currently, analytical grade alginate is used, which has been perfectly adequate for research purposes, but requires purification to become clinical grade (detailed further in Chapter 3), as amongst other issues visible particulates can be seen under a phase contrast microscope at between 1-20μm in size, which cause alginate discolouration.

Many groups have undertaken purification protocols to produce medical grade alginate, for the purposes of reducing, or eliminating biocompatibility issues, mainly related to long term cell transplantation into a patient[78,85-87]. These applications include alginate encapsulation providing protection against immune rejection for islet cells for the treatment of diabetes[88,89]. This requires the pore size to be regulated to prevent cellular and IgG penetration to prevent immune response[90]. The methods used to attain the required grade of alginate focus on lengthy phenol, acetone and ethanol extraction steps, followed by filter sterilisation, which cause changes to alginate properties, particularly viscosity and M: G: MG ratio[87].

One focus of this thesis will be the removal of particulates from alginate which cause discolouration, without affecting alginate properties, cell growth, function and viability for incorporation into the BAL system.

1.5.2. DNA release from the Biomass

1.5.2.1. Justification for DNA Control

There exists some debate about the true risk of circulating DNA in the blood supply, named cell free circulating DNA (cfcDNA)[91].The presence of cfcDNA has been shown in healthy human blood at relatively low levels, first defined by Mandel and Metais[92], and confirmed many time since [93-99], suggesting cfcDNA in an autologous setting poses little risk to health. One report showed 59±15ng/ml of DNA, using Picogreen fluorescence [94].

Despite the apparent lack of risk, other sources of cfcDNA have been reported to have originated from active cellular DNA release by lymphocytes, releasing double stranded DNA as part of a immunogenic homeostatic mechanism[100]. In addition to this, some cfcDNA from necrotic cell death has contributed to the total cfcDNA in healthy patients as well as patients with various forms of carcinoma [98,99,101,102]. Since DNA may have a role in immune response and is associated with release from carcinoma cells, the World Health Organisation (WHO) has proclaimed DNA from cell lines as a contaminant, forming the basis for the guidelines adopted by the major regulatory bodies[103]. Consequently, HepG2 cell DNA released from the extracorporeal biomass into the patients' plasma during BAL treatment must be controlled.

1.5.2.2. Origin of cfcDNA

The origin of cfcDNA in healthy patients is predominantly from apoptotic cell death as opposed to necrotic cell death [98,99,101,104]. However, the mechanism of cfcDNA release from cells having undergone apoptosis remains relatively unclear. Apoptosis is a tightly controlled process of cell death, producing apoptotic bodies, which house the DNA fragments of between 180-200bps [105]. By DNAse I activity, apoptotic bodies are endocytosed by macrophages, where membrane fusion with lysosomes results in complete degradation of the apoptotic bodies, with DNAse I breaking DNA down into nucleotides[106]. The logical conclusion is that DNA would not be detectable, which is clearly not the case.

Detectable levels of cfcDNA spawned an entire field concerned with quantifying DNA in plasma, from forensics [107,108] to disease diagnostics[107,109]. For diagnosis of disease, either an increase in total cfcDNA levels is measured inferring increase in cell death, or DNA markers for specific disease states are detected within background cfcDNA. These include detecting higher cfcDNA levels with autoimmune disease [110] and trauma [111] or detecting a specific DNA cancer marker[99,104,112-114]. In liver disease, there may be potential in using plasma DNA levels as an indicator of disease, where apoptotic and necrotic cfcDNA were shown to have been released from mice that have had liver injury, 3 hours after induction [115].

1.5.3. Endotoxins in the BAL

1.5.3.1. Bacterial Endotoxins

Endotoxins describe lipopolysaccharides (LPS) or lipooligosaccharide (LOS) that originate predominantly from the outer cell membrane of various gram negative bacteria, such as *Escherichia coli, Salmonella, Shigella, Pseudomonas, Neisseria, Haemophilus influenzae, Bordetella pertussis* and *Vibrio cholera.* Endotoxins mainly remain associated to the cell membrane until the organism undergoes disintegration due to complement and phagocytic immune responses. LPS are complex amphiphilic molecules approximately 10kDa in size, varying widely depending on bacterial species, although all sharing the common architecture of a lipid A region, as well as O and R polysaccharide regions. The Lipid A region contains the hydrophobic intra-membrane spanning domain allowing anchorage onto the bacterial outer cell membrane. The polysaccharide regions vary depending on the bacterial species, particularly with the O polysaccharide region and are associated with bacterial virulence, phagocyte resistance, and protection against complement and anti-body reaction[116].

1.5.3.2. Endotoxin Contamination in the BAL

With the clinical use of the Liver Group BAL system, the majority of endotoxin contamination is likely to originate from the patients rather than from the BAL system itself. To be compliant with ISO (International organisation for Standardisation) and GMP (good manufacturing Practice) standards, that define how devices are manufactured for market approval, construction of the BAL will be performed in an aseptically controlled environment [77,117,118], reducing the endotoxin to negligible levels. The endotoxin levels in patients can contribute to the aetiology of ALF. Patients suffering from ALF who underwent liver transplantation, showed an elevated level of endotoxin before and during anhepatic phase (46.5 ± 6.7 pg/mL endotoxin), only significantly reducing after 24 hours (to 19.3 ± 1.5 pg/ml endotoxin), and not returning to normal levels until 7 days later (13.2 ± 1.0pg/ml endotoxin vs. 10.6 ± 0.8pg/ml for healthy patient). In addition to this, patients with the highest endotoxin levels exhibited greater numbers of complications during treatment[119].

The normal physiological response to endotoxins and pathogens is mediated by Kupffer cells, residing in the liver sinusoid, coming into contact with materials absorbed by the gastrointestinal tract, being the principal liver cell for phagocytosis, cytokine release and antigen presentation. They are crucial to the liver function by mediating pathogen response as well as tolerance, and are associated with release of inflammatory mediators growth factors and reactive oxygen species [29,120]. Kupffer cells, and LSEC, are involved with uptake and clearance of endotoxins. In response to endotoxin or bacterial presence, Kupffer cells produce cytokines, chemokines and reactive oxygen species, which mediate a pro-inflammatory

responses and can contribute to further liver injury[120]. However, under non-inflamed physiological conditions, Kupffer cells develop endotoxin tolerance[121] by expressing anti-inflammatory mediators such as IL-10, and endogenous prostanoids and TGFβ.

The levels of endotoxin reported in ALF patients compared with those permitted by regulatory authorities for parenterals, are lower, i.e. 25EU/ml (2,500pg/ml) endotoxin in 1ml of parenteral solution compared with 10.6 ± 8pg/ml in 75kg patient. The rationale behind this may be the systemic dilution of parenterals when administered to a patient with 3L of blood.

The regulatory requirements for removal of contaminants from the BAL system predominantly focus on measurement and control of levels. Therefore, methods of measurement and control will be discussed.

1.6. Contamination Removal

1.6.1. Current Approaches to Contaminant Removal

As mentioned previously, artificial livers have been used to remove toxins in the plasma of patients suffering from ALF. Other groups working bioartificial liver systems have recognised the problem of potential cellular contaminants, particularly when using xenogeneic cell sources. In these cases, Pig Endogenous RetroViruses (PERV) were shown to be expressed in the supernatant of microencapsulated porcine hepatocytes cell cultures in a BAL system, and then proceeded to infect primary human hepatocytes and cell lines when exposed to the same supernatant[54,122]. In these studies, the suggestion is made that altering the pore size of the alginate beads could prevent PERV escape, a tactic that may negatively influence nourishment of plasma from the ALF patient.

The AMC-BAL, which utilises primary porcine hepatocytes, performed a small trial on 14 patients, collecting plasma after treatment to assess PERV infection by QPCR. In no cases was infection detected[123]. A comment made at the end of the Yang group summarised the results well: "We therefore suggest that more extensive preclinical studies focused on bio-safety to be conducted."[54]

Although indications are that DNA, or specifically PERVs in this context, does not pose a risk, *in vitro* studies do show a potential risk. Furthermore, the fact that no BAL has attained FDA approval is not exclusively due to contamination risk, but taking a proactive approach to contaminant removal is surely preferable to performing extensive bio-safety studies to establish the lack of risk.

Other contaminants such as endotoxin have been removed from sepsis patients using charcoal adsorption, immobilised protein column, and ion-exchange filtration. A particular study immobilised the anti-biotic polymyxin B, which has been shown to be toxic to the central nervous system and the kidneys, but was immobilized on polystyrene fibres, to render it safe. Perfusing patient plasma through the column with the immobilised polymyxin B alleviated symptoms associated with sepsis, by hydrophobic and ionic binding to endotoxins[124,125].

Overall, the use of activated charcoal has been used to remove toxins in plasma from ALF patients, such as endotoxins. However, they have been shown to be non-specific, also removing beneficial products such as fibrinogen and amino acids[124]. Another approach must therefore be found that is more selective toward particular toxins, whilst allowing transit of important synthetic compounds.

1.6.2.Filtration

The uses of filtration for removal of toxins from blood and plasma have been previously established, providing a potential means of contaminant removal for the Liver Group BAL[124,126,127].

Removal of contaminant from blood by filtration can take two approaches, either crossflow of dead end filtration. Dead-end-filtration describes the method passing the entire feed solution through a membrane or bed, with particulates being retained on the filter, as illustrated in Figure 1-7a. This has been extensively used for removing large and small particulates (~100's of μm to ~0.05μm) from solutions using a variety of media from sand, weaved cellulose, paper, and cotton amongst many others[128].

Cross flow, filtration uses a membrane situated at the lower point of the laminar flow, adsorbing particles that come in to contact with the filter as, illustrated Figure 1-7b. The technology originates from reverse osmosis for desalting sea water and has progressed through ultra-filtration of macromolecules, to microfiltration of particles between 0.02 -10μm[129].

Figure 1-7: comparison between dead end filtration and crossflow filtration. Dead-end filtration passes entire liquid volume through the filter. Crossflow filter remove particles from the section of laminar flow in contact with the filter, allowing some liquid to pass through the filter. Obtained from Brainerd et. al[130].

1.6.2.1. Dead End Filter Application

Membrane Filtration

The most common material used for this type of filter is cellulose and polyethersulfone (PES) with filtration relying on physically retaining particulates in the liquids by size exclusion. Micro-filters are defined as porous membranes by exhibiting a specific cut-off, usually

removing particulates is above 0.1µm, such as bacteria whilst allowing protein transit, thereby producing a sterile solution. Ultra-filtration usually concerns particles of less than 0.1µm. The main problem with membrane filters is the low volumetric capacity due to a reliance on physical retention and rapid spoiling in complex liquids[131]

Depth filter

Depth filters are composed of porous interwoven media, able to retain particles throughout the matrix of the filter. They are commonly used in pharmaceutical applications to remove larger insoluble particulates whilst maintaining a high volumetric capacity. Unlike membrane filters, which would quickly foul with high particle feed streams, the depth filters have a level of graded density across the filter media. The grading often decreases in density from the top layer of the filter, although sometimes the greatest density is found in the centre of the filter[132,133].

Due to variable gradation, the porosity of the depth filter is referred to as nominal porosity. Porosity is defined by the ratio of open space relative to the volume of the filter media, measuring the porosity as either absolute porosity or nominal porosity. Absolute porosity is measured by electron microscopy, where the actual sizes of the pores are measured. For depth filters this cannot be accurately performed, so nominal porosity is used. For this, a challenge using a defined range of particle size is applied to the filter, the range being determined by statistical significance for removal, providing a nominal porosity range[133,134].

Two types of depth filter are commonly available: fibre woven and sintered. Sintered filters, such as ceramic, metal, or porous plastic filters, are formed by fusing particles together under heat and pressure, with the spaces between the particles forming the flow path. Fibre filters are formed by spinning or weaving cellulose or polypropylene into a mesh or cloth-like structure, using an adhesive to retain the fibres in the capsule[132-135].

Depth filters rely on a torturous liquid path across the depth of the filter to retain particles, as there is little uniformity of structure across the membrane, as illustrated in Figure 1-8. One problem with depth charged filters is the relatively unpredictable nature in comparison to membrane filters. When testing charged depth filters, a series of destructive challenges are applied to representative samples to assess volumetric capacity, particle retention, and general rating of the filter for a particular environment{Baker, 2004 531 /id;Cuno, 2007 242 /id;Stacey, 2007 530 /id}.

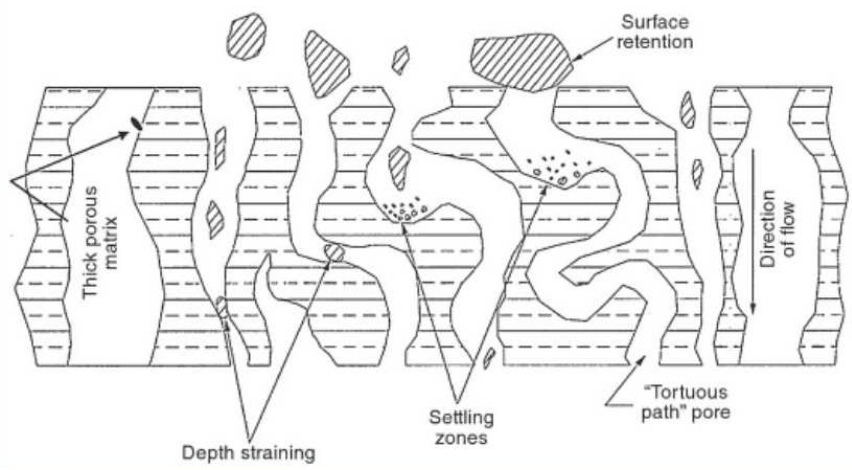

Figure 1-8: Representation of the fluid flow through a depth filter. Different non-uniform paths cause retention of specific porosities.

Improving retention capacity of these filters often utilises charged molecules, referred to as filter aids, bound on the surface of the fibres or sinters, to adsorb opposing charged compounds in the fluid. The filter aids comprise a combination of activated carbon, diatomaceous earth (SiO_2H_2O), or perlite. These increase the efficiency of filtration compared with size exclusion alone, having the ability to adsorb compounds smaller than the pore size of the filter[135]. Therefore, a positively charged onto the filter aid can remove endotoxin and DNA from water and cell broth[137-139]. Virus particles added to pure protein solutions were also removed by depth charged filters[140].

1.6.2.2. Cross-Flow Filtration Application

Cross-flow filters have been widely utilised in blood purification, particularly for haemodialysis in place of centrifugation. The membranes have a pore size of between 0.2-0.8µm to retain platelets and blood cells whilst allowing the transit of plasma and proteins such as immunoglobulins. This provides an un-traumatic separation method for blood cells, and is often used for this purpose, although the cost of replacing the filter due to fouling is considerably more expensive than centrifugation, so is used on rare occasions[131].

In other fields, however, the running cost of centrifuging large quantities of cell broth for biopharmaceutical processing can contributed to a third of running costs. In these cases, a distinct advantage of cross-flow filtration in comparison to other filtration types was the ability to separate solutions with large suspended particles from the liquid containing the compound of interest[141].

During the cross flow filtration processes used for the purification of process fluids, a recirculating system is often used, where the fluid that did not penetrate the filter re-circulates and re-enters the filter, as illustrated in Figure 1-9.

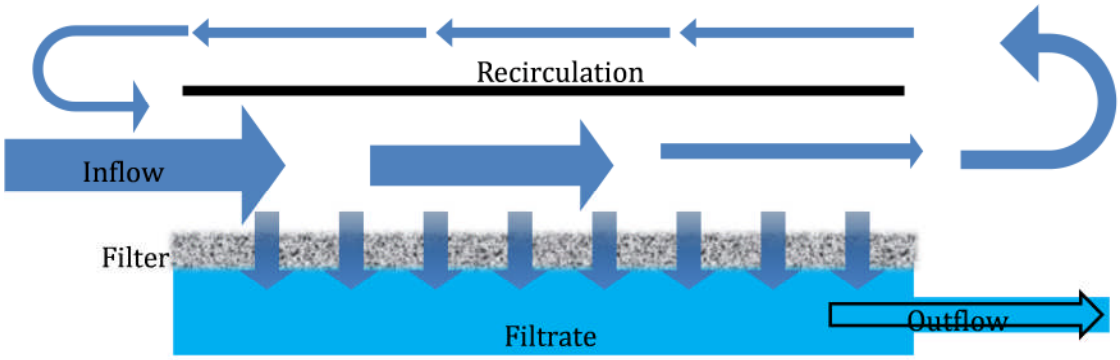

Figure 1-9: Recirculating crossflow filtration. The inflow of liquid passes into the crossflow filter, where some penetrates the filter and is taken to the next stage of the process. The unfiltered liquid is re-circulated for re-entry into the crossflow filter.

Although this type of filtration greatly increases capacity, due to less membrane fouling compared to dead-end filtration, the concentration of contaminant and process fluid can be problematic over long periods of time. For the BAL application, using a filter capsule with a recirculating system may not be practical due to a potential build-up of contaminants and protein from the BAL system. Furthermore, the flow rate of the outflow may not be as controllable as dead-end filtration, even during blockage of dead-end filters, a pump system can compensate for changes in flow. If excessive pressure is placed upon the crossflow filter, to balance flow rate the efficiency of filtration may be severely compromised[142].

Consequently, although crossflow filtration is a potential solution for contaminant removal in the BAL, (due to use with blood products), for the ability to remove molecules such as DNA and endotoxin, whilst allowing transit of proteins, (as with bioprocessing fluids), depth charged filters appear to be more suitable.

1.6.2.3. 3M® Cuno® Depth Charged Filters

A series of depth charged filters have been developed by 3M® Cuno® to filter cell broth and bioprocessing fluids, as illustrated in Table 1-4 .

Zeta Plus® Formulation	Filter Media	Filter Aids	Pharmaceutical Grades	Primary Application
A Grade	**Glass microfibers & Cellulose**	**None**	**01AP**	**Coarse pre-filtration Front end of blood plasma fractionation**
C grade	**Cellulose**	**DE, perlite**	**10CP, 30CP, 50CP, 60CP, 70CP**	**Blood plasma fractionation Haze removal Endotoxin reduction**
S Grade	**Cellulose**	**DE, perlite**	**05SP, 10SP, 30SP, 50SP, 60SP, 90SP**	**Final sterile membrane protection Buffer/solvent pre-filtration Chromatography column protection Reduction of contaminating DNA Endotoxin reduction**
LA/CA/SA/ Aluminium series	**Cellulose**	**DE, Pre-extracted acid washed**	**30LA, 60LA, 90LA, 10CA, 30CA, 50CA, 60CA, 70CA, 30SA, 50SA, 60SA, 90SA**	**Blood plasma fractionation Endotoxin reduction DNA reduction Extra low levels of extractables Membrane protection Post fermenter clarification**
LP series	**Cellulose (optimised for no β-glucan release)**	**DE, perlite**	**30LP, 60LP, 90LP**	**Blood fractionation Membrane protection Endotoxin reduction**
ZA series	**Cellulose**	**DE, Pre-extracted acid washed**	**30ZA05A, 60ZA05A, 90ZA05A**	**Endotoxin reduction in water DNA removal**
Zeta Carbon™	**Cellulose**	**Activate Carbon**	**R11SP, R12SP, R31SP, R32SP, R51SP, R52SP**	**Decolourisation Blood fractionation Endotoxin reduction**
Delipid	**Cellulose**	**Precipitated silica, perlite**	**DEL 1**	**Lipid reduction from blood plasma fractions Pre-chromatography column lipid reduction**

Table 1-4: filter grades and description of properties[136,142]. DE refers to diatomaceous earth.

Each type of filter has a specific application to biopharmaceutical and medical applications based upon specific properties, balancing filter nominal porosity and charge. The nominal porosity will dictate the manner of filter blockage and the resulting volumetric capacity. As described previously, a disadvantage of dead-end filtration compared with crossflow filtration is the potential for fouling due to particles depositing deep within the filter. The correct filter nominal porosity is crucial in providing volumetric and contaminant capacity.

Some of the filters are available as double layered filter capsules, which provide a convenient, clean, and low dead volume solution for protecting smaller nominal porosity filters with a larger porosity filter directly upstream. By testing the ZA, S and LP series filters, in Table 1-4, which are designed for DNA removal in complex solutions, for volumetric, DNA and endotoxin capacity in plasma a viable filtration system for the BAL could be established.

1.7. General Aims and Hypothesis

Hypothesis:

Contamination removal from the BAL system is possible using different filtration methods.

1.7.1. Thesis Aims

The development of a research stage medical device to be fully licensed for humans use requires a series of developments to ensure safety and efficacy of the device according to regulatory stipulations. One approach in ensuring that licensing occurs in a timely fashion is to incorporate regulatory stipulations, where appropriate, into the research process.

Measurement and control of extraneous contaminants, from the medical device, which may enter the patient, are important factors in gaining regulatory approval and to demonstrate device safety. For the BAL system cell debris, including DNA from the BAL system is an important contaminant to measure and control, as is particulates present within the alginate starting material.

The aims of the thesis are:

1. Establish models of the BAL system to gain statistical significance.
2. Establish a contaminant quantity in the BAL system.
    a. Detect DNA and endotoxins in BAL Plasma.
    b. Validate protocols, where possible.
3. Using the scale BAL model, determine the level of contaminants present
4. Remove contaminants.
    a. Use detection protocols to show contaminant removal by filtration.
5. Test removal system in the large scale BAL.
6. Remove particulate contamination from alginate as a starting material.

The Next chapter details the general methods used in the thesis.

General Methods

This Chapter describes the methods used in all subsequent chapters. Greater detail will be provided at the beginning of each chapter for methods specific only to that chapter

2. Methods

All items are from Sigma-Aldrich® unless stated.

2.1 Cell Culture Methods

2.1.1 Monolayer Cell Culture

2.1.1.1 Monolayer HepG2 Cell Culture

HepG2 cells were primarily utilised for the majority of the cell based work as the current cell line of choice for the BAL.

Materials

- **Supplemented Culture Medium**
  - α-MEM with Ribonucleosides and Deoxyribonucleosides (Invitrogen™)
  - HepG2 cells (ECACC, Wiltshire, UK)
  - 10% Foetal Calf Serum
  - 1.25µg/ml Fungizone
  - 0.04µg/ml Hydrocortisone
  - 9.5µg/ml Insulin
  - 2mM L-Glutamine
  - 50µg/ml Linoleic Acid BSA
  - 100Uml/Penicillin/0.1mg/ml Streptomycin (Lonza®)
  - 0.002µg/ml Sodium Selenite
  - 0.04µg/ml Thyroid Releasing Hormone

- **Other Materials**
  - 2% Trypan Blue in PBS
  - PBS
    - 137mM NaCl
    - 2.7mM KCl VWR International (BDH 101983K)
    - 8mM $Na_2HPO_4.2H_2O$
    - 1.76mM KH_2PO_4
  - Haemocytometer
  - Nunc™ 175cm^2 Flasks
  - HBSS
  - 2% Trypsin in PBS
    - PBS as Above
    - 17mM Citrate
    - 0.53mM EDTA
    - 111mM Glucose
  - All α-MEM supplements were pooled per 500ml media bottle and filter sterilised, through a 0.2µm membrane filter.

HepG2 Cell Seeding

HepG2 cell culture was initiated using a seeding density of 2 x 10^6 cells/ml suspended in 30ml supplemented culture media, contained in a T175 flask. Laying the flasks flat in a humidified incubator at 37°C, 95% air and 5% CO_2, cells naturally attached, leaving them for 4-5 days until

60-80% confluent. Every 2 days the culture media was replaced using supplemented α-MEM media pre-warmed to 37°C.

HepG2 Cell Passaging

Passaging cells began with 3 washes with 10ml HBSS to remove residual protein; followed by adding 10ml filter sterilised and pre-warmed (37 °C) Trypsin and incubating the flask for 1-2 minutes at 37°C, periodically knocking the side of the flask to assist cell detachment. To deactivate the Trypsin, 30ml α-MEM with 10 % FCS at 37 °C was added, followed by decanting into 50 ml Nunc™ centrifuge tubes, for centrifugation at 300 g for 4 minutes at room temperature. Discarding the supernatant, the pellet was re-suspended in 5ml supplemented α-MEM culture medium, passing the cell suspension through a 27G syringe 5 times, to disperse cell aggregates.

The required cell density was added to a culture flask, of relevant size, to provide the required final cell numbers after a designated time of culture. This number was calculated based on an empirically derived assumption that HepG2 cells on average double in number every 2 days. For example, if 8.0 $x10^7$ cells are required for encapsulation, then a Nunc™ triple would be seeded with 5 x 10^6 cells and cultured for 8 days.

2.1.1.2 Cell Number and Viability using Trypan Blue Exclusion on a Haemocytometer

Cell number and viability were measured using the Trypan blue exclusion method, by adding 20µl cell suspension to 160µl HBSS, then 20µl of 2% Trypan blue in PBS, incubating at room temperature for 2 minutes. Taking 9µl of the cell suspension and adding to a haemocytometer slide, at 10 x magnification, fully stained blue cells were counted as non-viable and unstained cells as viable, calculating percentage viability using the ratio of these counts. This was repeated 5 times from the same suspension to obtain a mean and standard deviation.

2.1.2 Monolayer Primary Liver Cell Culture

Primary liver cells were obtained from patients with liver metastasis, and isolated and frozen in liquid nitrogen.

Materials

- Williams E media (PAA®)
  - 10% FCS

Cells were revived as described in Section 2.1.2.2, and cultured on collagen coated plates as described in section 2.1.2.1, in Williams E media as in section 2.1.1.1, with medium changes every day. The purpose of this was to isolate DNA so cells were cultured for up to 4 days then harvested as in section 2.1.1.1.

2.1.2.1 Collagen Coating Plates for Primary Liver Cell Attachment

Materials

- Tendons from rat tails
- 10 mM Acetic acid (Sigma-Aldrich®)
- 6 well plate (Nunc™)
- HBSS (Lonza®)
- 0.9% NaCl (Sigma-Aldrich®)

Collagen Extraction

Rat tail tendons removed from cadaveric rats were weighed and dissolved in 300ml 10mM acetic acid for every 1g of tendon and stirred over 2-3 days at 4°C. Collagen solution was centrifuged at 800g for 2 hours to remove any remaining undigested rat tail and stored at 4°C for 1 up to 1 month.

Plate Preparation

To each well of a 6 well plate 2ml of the collagen was added to each well and incubated at room temperature for 5 minutes. Each plate was washed 3 times with 4ml of HBSS, using the final wash to check for any changes in the phenol red colour, confirming the absence of acetic acid. Traces of HBSS were removed by washing with 2ml of 0.9% NaCl, checking for any remaining red colouration. These plates were sterilised using 30 minutes of UV-C exposure, and sealed with parafilm® for storage.

2.1.2.2 Cryopreservation and Revival of Cells

Materials

- DMSO (Invitrogen®)
- FCS (Thermo-Scientific® Hyclone®)
- Cryovials (Nunc™)

To minimise variation in cell function and growth characteristics, cell lines were maintained in culture for a maximum of 10 continuous passages. Accordingly, a small cell bank was established to standardise the cell source, which was used for cell encapsulation.

Cryopreservation

Immediately after trypsinisation, cells were re-suspended in culture medium at a density of $1x10^7$ cells/ml, and divided into 1 ml aliquots. To the aliquots, an equal volume of freezing mix (90% FCS + 10% DMSO) was added and transferred to Cryovials®, placing at -80°C overnight, in a polystyrene container lined with cotton wool, causing the freezing rate to reach approximately 1°C/minute. The cells were then transferred to liquid nitrogen (-196°C) for long term storage.

Cell revival

Cells in Cryovials® were thawed quickly by placing in a 37°C water bath, immediately transferring to a 50 ml centrifuge tube, as soon as the last visible ice crystal melted. To this, 10mls of medium was added drop wise over 5 minutes, followed by centrifugation at 300g for 4 minutes at room temperature. Discarding the supernatant, cells were re-suspended in 15mls of medium and then transferred to a Nunc™ T80 flask. Following attachment, medium was replenished and cells maintained in monolayer culture as described in 2.1.1.1.

2.1.3 3D HepG2 Cell Culture

3D cell culture was either achieved through encapsulation using the Inotech® micro-encapsulator for smaller scale experiments from 10 – 50ml of beads (section 2.1.3.5) or GeniaLab® Jetcutter™ (section 2.1.3.6) encapsulation system, from 100ml to 2L beads.

2.1.3.1 Cell Culture for Encapsulation

For small scale experiments, using the Inotech® micro-encapsulator, 100ml of alginate/media mix was prepared, as outlined in section 2.1.3.2. In order to grow sufficient cell numbers, a triple layered Nunc™ culture flask was seeded as in section 2.1.1.1, which at 60-80% confluency provided between 6.0 x 10^7 and 1.0 x 10^8 HepG2 cells, sufficient for 120 – 200ml of alginate/media mix at 0.5x10^6cell/ml seeding density.

Provision of larger scale culture for the GeniaLab® Jetcutter™ encapsulation was performed by other member of the group and is described in Section 2.1.3.6.

2.1.3.2 1% alginate solution

Materials

- 2% Alginate solution (1% final concentration when in 1:1 ratio with medium)
  - Alginic acid powder (cat no. 180947)
  - 150 mM NaCl
  - 15 mM HEPES
  - NaOH for pH adjustment

Preparation and sterilisation of 1% alginate

A 2% solution was made by gradually adding 2g Alginic acid-sodium salt, to 100ml, sterile, 150mM NaCl and 15mM HEPES solution, under constant agitation (pH 7.4 with NaOH), and left stirring overnight in the dark. It was then sterilised at 121°C for 10 minutes, the size of the vessel during autoclaving was scaled (e.g. 250ml glass reagent bottle for 100ml alginate, and 2.5L bottle for 1L alginate), thereby maintaining identical heating treatments between encapsulations. If the Jetcutter® system was used, 2% 10-50µm glass beads (dry sterilised by heating to 180 °C for 3 hours) were added to the 1:1, alginate: cell/medium mix.

2.1.3.3 Cell number using Nucleocounter® Spectrophotometer for 3D culture

Materials

- PBS pH 7.4
- 16mM EDTA/0.15M NaCl, pH 7.4
- Nucleocounter® nucleocassettes (Chemometec®)
- Reagent A100: Lysis buffer (Chemometec®)
- Reagent B: Stabilising buffer (Chemometec®)
- Nucleocounter® YC-100™ cell counter

Isolation of Cells from Beads and Cell Number Determination using Nucleocounter

A 0.25 ml aliquot of beads was transferred to a 2ml Eppendorf® micro-centrifuge tube, then washed with HBSS, carefully removing as much liquid as possible before making up the total volume to 2ml with 16mM EDTA/0.15M NaCl and incubating for 10 minutes at 37°C, causing the dissolution of the alginate and release of cells. The cells were then pelleted by centrifuging at 13000g for 5 minutes. Discarding the supernatant, the pellet was re-suspended by vigorous vortexing in the volume of PBS outlined in Table 2-1, reliant on numbers of day of growth.

Days of growth in Culture	Re-suspension volume (µl)
0-1	200
2-3	300
4-5	600
> 6	1000

Table 2-1: Re-suspension volume of cell isolated from Beads grown for different days in static culture

An equal volume of lysis Buffer Reagent A100 was added, vortexing for 1 minute to ensure uniform cell lysis. The same volume of stabilisation buffer Reagent B was added, mixing by briefly vortexing and loaded onto the Nucleocassette® then inserting into the Nuceocounter®.

The Nucleocounter provides a cell/ml value below 2 x 10^6 cells/ml LoD, requiring back calculation to derive the original cell number/ml of alginate beads.

Equation 2-1: N x *Z* = Cell Number

Where N (cell/ml) is reading from Nucleocounter and Z is the multiplication factor to account for dilutions.

Equation 2-2: $Z = \frac{3}{V_B} \times V_{PBS}$

Where V_B is the volume of alginate beads (mL) and V_{PBS} is the volume of PBS used to re-suspend the cell pellet (mL).

2.1.3.4 Determination of Viability in Beads using FDA, PI staining for 3D culture

Materials

- FDA (fluorescein diacetate)
- PI (propidium iodide)
- PBS $^{Ca+ Mg+}$ (Lonza)

Cell Viability Protocol

A 200µl sample of beads was taken and added to a 1.6ml micro-centrifuge tube, washing with 1.4ml PBS^{Ca+Mg} to remove residual culture medium; if the sample was in 100% plasma, the wash was repeated. The beads were re-suspended in a final volume of 500µl PBS^{Ca+Mg} to which 20µl of PI and 10µl of FDA were added in quick succession, gently agitating for 90 seconds on the bench. To remove excess stain, the beads were washed with 1.4ml PBS^{Ca+Mg}, finally re-suspending in 500µl PBS^{Ca+Mg}. A portion of this was transferred to a microscope slide, removing excess liquid, to be visualised using the Nikon® Eclipse microscope with the DX1200 camera and Lucia G imaging software. An excitation filter of 510-560ηm and an emission filter of 590nm was applied for PI fluorescent measurement, and an excitation filter of 465-495nm and an emission filter of 515-555nm for FDA. The viability was calculated using the Lucia software measuring integral pixel density of the images, deriving viability using equation 1:

Equation 2-3:
$$\% \text{ viability} = \left(\frac{\text{FDA integral density}}{\text{FDA integral density} + \text{PI integral density}} \right) \times 100$$

Where FDA integral density counts pixel density of living cells stained with FDA and PI integral density is the pixel density of dead cells stained with PI.

2.1.3.5 Inotech™ Cell Encapsulation

Materials

- Alginic acid solution
  - Alginic acid Sodium salt
  - 150 mM NaCl (Invitrogen™)
  - 15 mM HEPES (Lonza®)
- Polymerisation Buffer
  - 204 mM $CaCl_2$
  - 150 mM NaCl
  - 15 mM HEPES
  - 0.05% Pluronic acid
- High Glucose (HG) Media
  - α-MEM as described in section 2.1.1
  - 25 mM of D-Glucose,
- Volumetric flasks
- Schott bottle
- Magnetic flea
- Syringe filter
- Baked Pyrex beakers (3 hours at 180°C)
- Stainless steel forceps

- Inotech syringe pump system (Inotech, Dottiken, Switzerland)
- Bottomless beaker and Elastic band
- Nylon mesh
- DMEM supplemented with 10% FCS,
- 100Uml/Penicillin/0.1mg/ml Streptomycin (Lonza®)
- 1.25 µg/ml Fungizone
- Inotech IER-20 Cell Encapsulator (Inotech, Dottiken, Switzerland),

Inotech™ Principle

To provide sufficient volumes of beads for small scale experiments, the Inotech IER-20 Cell Encapsulator system was used, which operates by passing the alginate/media mix through a small nozzle to create a laminar liquid flow that is broken into equally sized droplets by superimposing vibrations. An additional electrostatic dispersion unit generated a uniform charge on the surface of each droplet, by passing through an electrostatic field, causing droplets to repel, thus preventing agglomeration, and forming a coned shaped descent into the polymerisation buffer. Upon contact with polymerisation buffer containing Ca^{2+}, cross linking between β-D-mannuronate (M) and α-L-guluronate (G) polymers occurs, fully forming the alginate beads.

1) Syringe
2) Syringe pump
3) Nozzle input
4) Electromagnetic pulsation unit
5) 200µm nozzle
6) Electrode
7) Reaction vessel (open vessel used)
8) Waste and bypass unit
9) Polymerisation buffer input (not used)
10) Pressurisation value (not used)
11) Vibration frequency generator
12) Electromagnetic charge generator
13) Stroboscope
14) Stirrer
15) Collection vessel (not used)

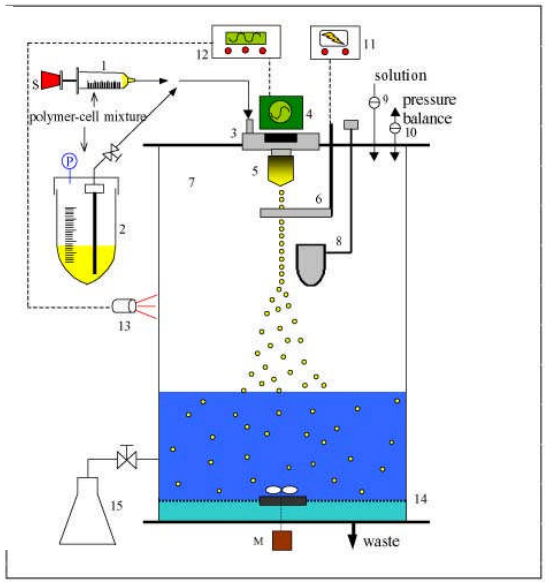

Figure 2-1: Schematic diagram of the Inotech® microencapsulator. 50:50 alginate/media mix is passed through a 200µm nozzle (5) creating a laminar flow, which is broken to equally sized droplets by superimposed vibration (11), it then passes through an electromagnetic field to impose charge on the droplets (4), giving a cone shaped descent into the polymerisation buffer.

2.1.3.5.1 Inotech™ Encapsulation Protocol

Cells were cultured as in section 2.1.1, harvested and diluted in media and were added to the alginate in a 50:50 ratio, with a final seed density of 0.5 x 10^6 cells/ml of mix. A 50ml syringe with the mix was placed onto the Inotech system at position (1) in Figure 2-1; the parameters listed below were applied to the system to produce beads of ~500 μm in diameter:

- 1295Hz on the vibration frequency generator, (11) Figure 2-1.
- 0.5 volts on the electromagnetic charge generator, (12) Figure 2-1.
- 12.7ml/min on the syringe pump, (2) Figure 2-1.

The beads then fall into the polymerisation buffer containing Ca^{2+} promoting polymerisation of the homopolymer sugar residues, incubating for 10 minutes, prior to being poured through a 200μm mesh sieve (prepared using a bottomless beaker and mesh attached using an elastic band, retaining the beads on the mesh). They were then twice washed in D-MEM containing 10% FCS, to remove polymerisation buffer to prevent over polymerisation. A volume of 100ml HepG2 cell and Alginate mix, typically provided 20ml of HepG2 encapsulated Alginate beads. Subsequent solutions that come into contact with the beads were controlled for Ca^{2+}.

2.1.3.6 Jetcutter encapsulation

This protocol was performed by other members of the Liver Group, and is detailed in Appendix I.

Jetcutter® principle

The Jet Cutter encapsulation enables the production of large volumes of beads, and is currently the method of choice for encapsulating cells for use with the full scale Bioartificial Liver system.

The Jetcutter® system consists of a pressurised chamber, which forces the alginate/cell/media mix through a nozzle at a controlled rate. The stream then passes through a cutting tool with asymmetrically arranged wires, which are inclined relative to the vertical solid stream of liquid, resulting in a horizontal cut as the tool passes through the liquid stream. The cylindrical segment then forms a bead due to surface tension whilst descending to the polymerisation buffer.

2.2 DNA Detection Methods

The aim of detecting DNA within the BAL system is to ensure that contamination from the HepG2 cells in this form is not transmitted to the patient. A number of approaches were tested to establish a detection method for routine use with the BAL system. These focussed on attaining a Limit of Detection (LoD) so that defined DNA concentrations and the cell numbers relating to those DNA concentrations could be detected to sufficient sensitivity to detect small changed in HepG2 viability (<1%).

2.2.1 DNA Extraction Methods

In order to measure DNA removal, and to test DNA detection methods, DNA was extracted from different cells.

2.2.1.1 Qiagen® QIAamp® DNA Extraction Kit

This kit is based on DNA binding to the column with a number of wash steps and proteinase K steps to remove contaminants.

Materials

- 1ug/ml Proteinase K
- Qiagen® QIAamp® Columns
- PBS
- Qiagen® QIAamp® AL Lysis buffer
- Qiagen® QIAamp® AW1 wash buffer
- Qiagen® QIAamp® AW2 wash buffer
- 100 % ethanol
- Qiagen® QIAamp® AE buffer
  - 10 mM TrisHCl
  - 0.5 mM EDTA
- Thermo-scientific® Nanodrop® ND1000™ spectrophotometer.

Qiagen® QIAamp® DNA Isolation Protocol

Each column is designed to extract DNA from 0.5 x 10^6 cells, therefore from a Nunc™ T25 flask which can yield 5 x 10^6 cells, 10 columns were utilised simultaneously. To each 1.5 ml Eppendorf® micro centrifuge tube, 20µl of Proteinase K was added followed by adding 200µl of cell suspension at 2.5 x 10^6 million cells/ml. To this, 200 µl of AL lysis buffer was added, incubating at 56 °C for 10 minutes. After briefly centrifuging at 1000g for 30 seconds to collect the solution in the bottom, 200µl of ethanol was added and vortexed for 15 seconds. The entire mixture was carefully pipetted into the column, and centrifuged at 6000g for 1 minute, discarding the flow through. The DNA attached to the column was washed sequentially, by initially adding 500µl of AW1 wash buffer, centrifuging at 6000g for 1 minute, followed by a second wash with AW2 wash buffer, centrifuging as before. Again, the flow through was discarded and a final centrifugation was performed at 20,000g for 3 minutes to remove any residual liquid. Each column was then placed into a clean centrifuge tube, adding 50µl of AE elution buffer and centrifuged at 6000g for 1 minute. The flow through was then analysed on the

Nanodrop® spectrophotometer at 260ηm and 280ηm giving a measure of DNA concentration and purity.

2.2.2 Simplified Mammalian DNA isolation Procedure

This protocol was obtained from Laird et al.[143] and was used to obtain high molecular weight genomic DNA from cell culture.

Materials

- Lysis Buffer
  - 100 mM TrisHCl
  - 5 mM EDTA
  - 0.2 % SDS
  - 200 mM NaCl
  - 100 µg Proteinase K (freshly added)
- 100 % Isopropanol

DNA Isolation Protocol

Cells were cultured as in section 2.1.1, in a Nunc™ T80 flask to 80% confluency. The culture medium removed and the cells washed 3 times with HBSS, to which 5 ml lysis buffer was added and incubated for 4 hours at 37°C. To this, 5ml of isopropanol was added mixing gently for 5 minutes, to allow the DNA to precipitate and aggregate, then transferring the entire solution into a 50 ml Nunc™ tube. Using a clean pipette tip, the DNA aggregate was gently moved to above the liquid to allow the isopropanol to dry for 10 minutes. The DNA aggregate was then transferred to an Eppendorf® tube for re-suspension in DNAse-and-RNAse-free water.

2.2.3 Hoechst Dye Staining

Materials

- PBS
- 0.1 M NaOH
- 1 M TrisHCl pH 7
- 1 mg/ml Hoechst Dye 33342 in water
- Applied Biosystems Cytofluor® Fluorescence plate reader
- TNE buffer
  - 10 mM TrisHCl
  - 200 mM NaCl,
  - 1 mM EDTA,

Hoechst Dye Purpose

The *bis*-benzimide fluorophore Hoechst dye was used to quantify calculated DNA concentrations in water compared to media and plasma to assess efficacy of the assay in different environments, and to determine DNA concentration from lysing a pre-determined cell number in 48 well plates.

Determining Limit of Detection (LoD) with DNA Standards

A seven point DNA standard curve was prepared by serial dilution, with final concentrations between 0.078µg/ml and 5µg/ml in 500µl TNE buffer, or plasma, respectively. To this 500µl of 1µg/ml Hoechst dye was added and immediately read on the Cytofluor® plate reader using 360ηm excitation filter (bandwidth of 50) and 480ηm emission filter (bandwidth of 20). An arbitrary fluorescence unit was converted to the known standard concentration, whilst ensuring the gain was set so that the blank showed a signal in the order of 10^4 times greater than the lowest sample signal, typically set at 90.

2.2.4 PCR and QPCR with Alu Repeats

Due to the proven sensitivity of QPCR, shown in other applications for detecting DNA in plasma[144-147], this was the natural progression from a chemical approach to DNA quantification within a complex solution such as plasma. Initial optimisation and testing of primers was performed by PCR amplification then analysis on a 2% agarose gel. Two sets of primers, specific for the Alu repeat consensus sequence, were taken from Umetani et al.[148], and utilised in separate reactions to produce 115bp and 247bp Alu repeat amplicons.

2.2.4.1 Conventional PCR

Materials

- TBE Buffer
  - 0.9 M Tris base
  - 0.9 M Boric Acid
  - 20 mM EDTA
- 2 % Agarose Gel
  - 2 g Agarose
  - 100 ml TBE buffer

PCR Stock solutions

- 2x Hot Star Taq® Polymerase (Qiagen®)
  - 200 µM dNTP's and
  - 1.25 units Taq Polymerase in
  - 2x PCR Buffer.
  - 1.5 mM $MgCl_2$
- Certified DNase, RNase free PCR H_2O (Bioline®)
- 28mM $MgCl_2$ (Sigma-Aldrich®)
- 100µM 247bp primer (Sigma®)
  - Forward: 5′-**GTGGCTCACGCCTGTAATC**-3
  - Reverse: 5′-**CAGGCTGGAGTGCAGTGG**-3'
- 100µM 115bp primer
  - Forward: 5′-**CCTGAGGTCAGGAGTTCGAG**-3′
  - Reverse: 5′-**CCCGAGTAGCTGGGATTACA**-3′

1x PCR mix

- 10µl Hot Star Taq® Polymerase (concentration: 1x)
- 1µl 10µM Forward Primer (concentration: 400 nM)
- 1µl 10µM Forward Primer (concentration: 400 nM)
- 3µl 23mM $MgCl_2$ (concentration: 5 mM in total, 1.5 mM + 3.5 mM)

- Total 15µl + 5µl sample
- iCycler 96 well PCR machine (BioRad®)
- 0.5ml PCR tubes

PCR protocol

As a complement to QPCR described in section 2.2.4.3, optimisation and confirmation of the amplicon size relative to the melt curve was undertaken using conventional PCRs, using the iCycler® PCR machine.

Cycle:

95 °C 5 minutes
95 °C 15 seconds
64 °C 30 seconds
72 °C 30 seconds
} 30 Cycles
72 °C 10 minutes

2.2.4.2 PCR Template Treatment for Sample Purification

Materials

- 200 ng/µl stock Human Genomic DNA (Bioline®)
- TTE buffer for plasma sample purification
  - 16 µg proteinase K (lyophilised into 0.2ml PCR tubes from 1mg/ml stock) (Sigma-Aldrich®)
  - 50 mM Tris Base
  - 1 mM EDTA
- 2.5% Tween-20
- Certified RNA, DNA, pyrogen, RNase and DNase free filtered Pipette tips (Starlabs®)
- Certified RNA, DNA, pyrogen, RNase and DNase free 2 ml, 0.5 ml and 0.2 ml tubes
- Certified RNA, DNA, pyrogen, RNase and DNase free 0.1 ml Rotorgene PCR tubes (Corbette®, Qiagen®)
- Rotorgene 3000 (Corbette®, Qiagen®)
- Edwards® Lyophiliser

As a result of using plasma directly in the PCR reaction, interference from proteins and other constituents of plasma was reduced using proteinase K treatment and dilution with TTE buffer. Initially, 20µL of plasma was added to a 0.5ml PCR tube containing 16µL pre-lyophilised proteinase K and 20µL of TTE buffer, and then incubated at 50°C for 45 minutes. To this an extra 160µl of TTE buffer was added followed by deactivating proteinase K at 95°C for 10 minutes, producing a white precipitate removed by centrifugation at 13,000g for 10 minutes. A volume of 5µL of this supernatant was added to the PCR mix being equivalent to 0.5µL of original sample.

2.2.4.3 Quantitative Real Time Genomic PCR

Material

PCR Stock solutions

- Same as 2.2.4.1, with the addition of
- 10,000 x SybrGreen I (Biogene®)

1x PCR mix

- 10 µl Hot Star Taq® Polymerase (concentration: 1x)
- 0.5 µl 1/1000 SYBR Green I (concentration: 0.25 x)
- 1 µl 10 µM Forward Primer (concentration: 400 nM)
- 1 µl 10 µM Forward Primer (concentration: 400 nM)
- 2.5 µl 28 mM $MgCl_2$ (concentration: 5 mM)
- Total 15 µl + 5µl sample

Alu Repeat QPCR protocol

The absolute DNA concentration was determined using a five point standard curve, in triplicate, from 0.01pg to 100pg DNA, giving a sample limit of detection (LoD) of 0.1pg/µl DNA. Samples were run on the Rotor Gene™ 3000 PCR machine.

Cycle:

95 °C 5 minutes

95 °C 15 seconds
64 °C 30 seconds
72 °C 30 seconds
} 40 Cycles

72 °C 10 minutes

Melt curve from 45 °C to 95 °C at 1 °C per minute.

2.3 Small Scale BAL Experimental Setup

Principle of the Scale BAL

In order to provide a means to analyse specific parameters of the large scale BAL system with sufficient replicates for statistical significance, a scale model of the BAL system was developed, prior to implementation on a large scale system, which focussed on:

- DNA release in media, healthy human plasma, and acute liver failure plasma
- Bead integrity and debris release from fragmented beads,

Due to the flexibility of the model both the bioreactor growth phase and the treatment phase can be modelled. For the bioreactor growth phase, media with FBS or media with FFP were used in the columns, if modelling the BAL system FFP, acute liver failure plasma, renal failure plasma, or pig plasma were used, depending on the large scale BAL system parameter being tested.

Materials

- Fresh Frozen Plasma from healthy patients (FFP)(Citrated)
  - 1 M $CaCl_2$
  - 4 Units/ml plasma Sodium Heparin
  - 100Uml/Penicillin/0.1mg/ml Streptomycin (Lonza®)
  - 1.25µg/ml Fungizone (Invitrogen™)
  - 25mM Glucose

- Acute Liver Failure Plasma
  - Obtained from acute liver failure patient plasma exchange using the Cobe Spectra® Apheresis System
  - Same additions as FFP, except no addition of $CaCl_2$.

- Renal Failure Plasma
  - Obtained from plasma exchange of renal failure patients using the Cobe Spectra® Apheresis System
  - Same additions as FFP
- Pig Plasma
  - Obtained from BAL treatment of pig with a portal vein shunt to model acute liver failure separated using the Cobe Spectra® Apheresis System.
  - Heparinised during treatment at 20 Units/ml plasma Sodium Heparin
  - Same additions as FFP

- Watson-Marlow 520Du peristaltic pump with a 10 channel pump head
- α-MEM with Ribonucleotides and Deoxyribonucleosides (Invitrogen™)
  - Supplemented as of section 2.1.1.1
- Sterilised Column setup:

- Glass column and fittings representing the chamber holding the beads (shown in Figure 2-2.

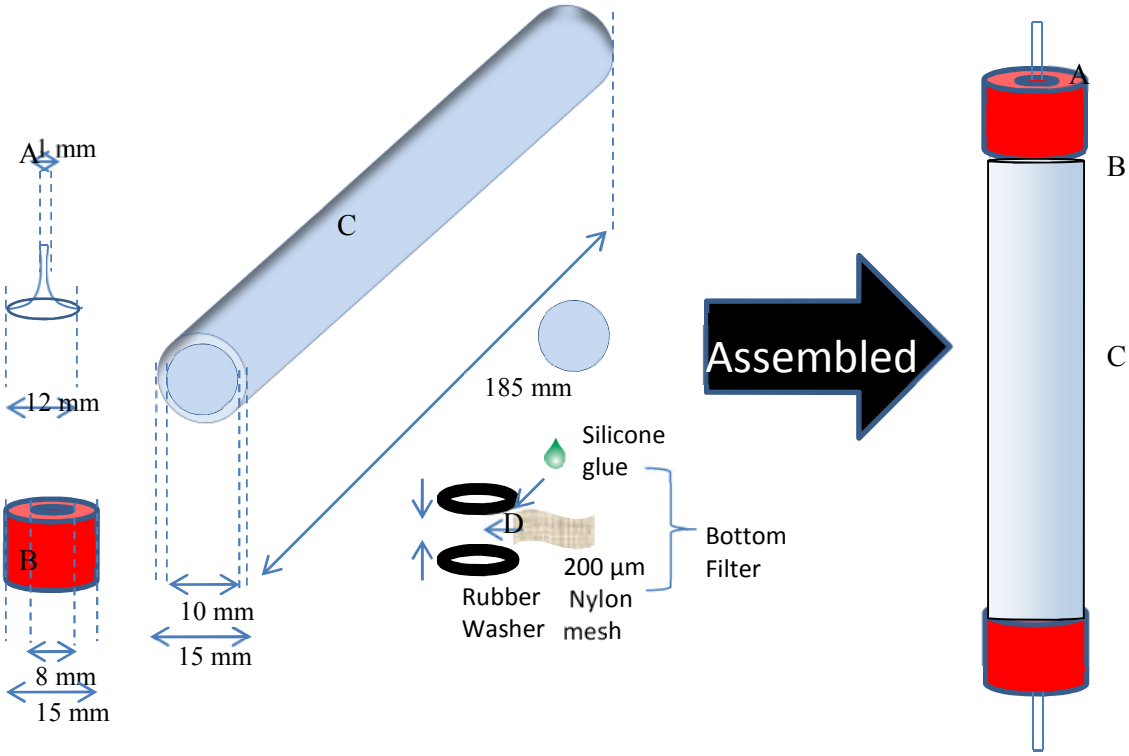

Figure 2-2; the column set-up was used to provide a scale BAL chamber. A; tapered glass fitting, was placed on the top of the glass column, with a 1.2mm rubber washer in between to provide a seal between the column and the silicone tubing. B; polypropylene screw cap (with an 8 mm hole), which holds the glass fitting, washer and column in place. The glass column has on either end a thread, which enables the attachment of the cap. C; glass column. D Bead filter to prevent bead escaping through the bottom when flow is off, comprising two rubber O-rings and a 200µm nylon mesh secured with silicon glue.

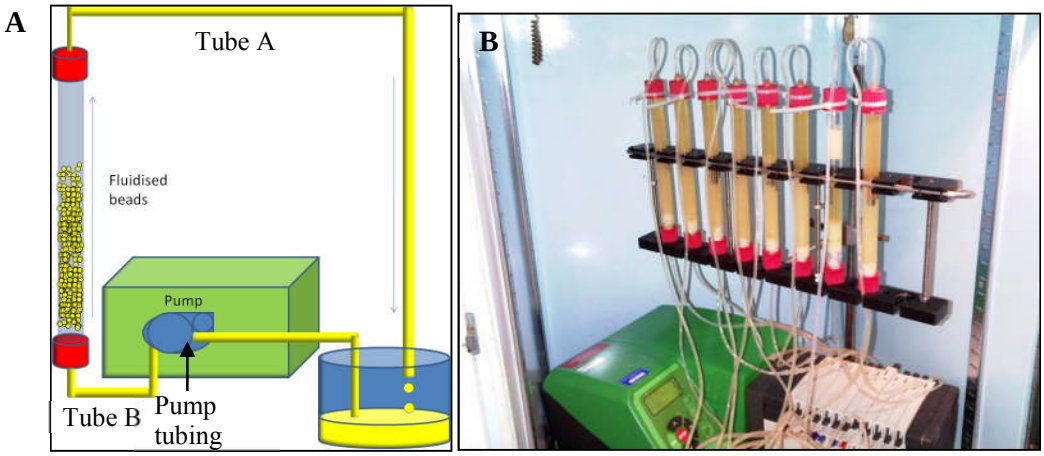

Figure 2-3: Column setup for scale BAL system. A; the layout of a single column, in series with the pump and the reservoir, tubing letters denote the differing length of tubing used (A, 75 cm; B, 50 cm; Pump tubing 45 cm). B; 8 columns in an incubator maintained at 37°C and 5% CO2, using the Watson Marlow® Multichannel pump to perfuse beads with plasma/ and or media, over 8 hours.

- Tubing between the pump and the reservoir. Figure 2-3 A shows the position of each length of silicone tubing, also summarised below:

  - Tube A: top of column to the reservoir; 75cm
  - Tube B: from pump to the bottom of column; 50cm
  - Pump tubing: attached to the reservoir then passes through the pump; 45cm (2.7mm bore size, 0.5mm wall thickness)

- 75ml polypropylene bottle
- 9 column holder (shown in Figure 2-3 B)
- Watson Marlow multichannel pump
- Filter at bottom of column to retain beads when pump is off
  - Two 1.2 mm x 0.5 mm rubber washer
  - 200 µm nylon mesh

- Complete media with 24 mM D-Glucose
- 2% Trypan blue in PBS
- FDA and PI staining
- Dry sterilised beaker (180 °C 3hours)
- PBS^{+ca} (Lonza®)
- HBSS (Lonza®)
- 100% ethanol
- 70% IMS
- Sampling septum
- Serological pipette
- Sterile Steel spoon
- Sterile 10 ml syringe

2.3.1 Assembly of the Scale BAL Model

As illustrated in Figure 2-2, the column comprises a 15 ml glass tube with screw threads at each end. A rubber washer was placed between this and a tapered glass fitting, held in place by securing the polypropylene cap, also engineered with screw thread, so that the tapered glass fitting can pass through the 8mm hole in the top of the cap, which is in turn attached to 2.7mm internal diameter silicone tubing. At the bottom end of the column the washer is modified to incorporate a 200µm nylon mesh, by cutting 6mm radius circular sections of nylon mesh, and attaching two washers on either side of the mesh by silicone glue illustrated in Figure 2-2, to form a liquid permeable, but bead impermeable membrane. The filter/washer are constructed 2 days prior to the experiment, allowing the silicone glue to set overnight, then sterilising for 1 hour by immersing in 70% IMS then washing with 100% ethanol, placing in a Class II microbiological safety tissue cabinet, to dry for 30 minutes.

Columns were constructed on the bench as illustrated in Figure 2-3A with specific tube lengths outlined below Figure 2-3, then placed in a sterilising bag for autoclaving at 121°C for 30 minutes (the cap on one end of each column was left loose to allow steam penetration). After sterilisation, the bags containing the columns were placed in a Class II microbiological safety tissue cabinet, where a sample port was added to a T-piece with luer fittings, fitted prior to sterilisation. Whilst still in the tissue cabinet, the columns and tubing from the reservoir to the

column were placed on a multi-column rack able to hold 9 at one time (Figure 2-3B) and primed with liquid (plasma or media depending on experiment) to just above the bottom filter using a sterile syringe, to prevent bubbles passing through the beads. The columns were then ready to add beads outlined in Section 2.3.2.

A day prior to commencing the experiment an incubator was set at 37°C and 5% CO_2, to house columns for the duration of the experiment commonly spanning between 5 and 12 hours. Usually hourly samples of 300µl were taken through the septum attached to the reservoir for later analysis. For some experiments, however, the frequency of sampling was reduced so that no more than 10% of the original volume would be removed.

2.3.2 Preparation of Beads for Addition to the Scale Model

Cells were initially cultured as in section 2.1.1, then encapsulated either using the Inotech® microencapsulator as outlined in section 2.1.3.5, and grown in static culture or encapsulated using the Jetcutter microencapsulator outlined in section 2.1.3.6, and grown in the fluidised bed bioreactor over 7 to 12 days allowing experimentation in plasma. Beads were extracted using a serological pipette from either the bioreactor or static culture, and passed through a 200µm mesh covering the underside of a bottomless beaker held over a sterile container, causing the beads to be retained on the mesh.

The beads were then lowered into a second sterile beaker containing 500ml PBS^{+Ca}, and agitated briefly by swirling the beaker, leaving them for 5 minutes to allow the diffusion of PBS^{+Ca} into the beads. With a sterile steel spoon, the beads were gradually transferred into sterile 15ml Nunc™ centrifuge tubes already containing 7ml of HBSS, plasma or media (depending on the experiment), allowing the beads to settle. Thus enabling the measurement of bead volume with the graduations on the exterior of the tube, each addition of beads required 3 minutes to settle. With the desired bead volume, sufficient diluent was added to achieve a 15 ml total volume, inverting the tube gently 5-10 times to completely re-suspend the beads, followed by un-screwing the top of the column and pouring the content in the glass column.

2.3.3 Determination of Plasma / Media ratio

The ratio between media or plasma and beads related to whether the bioreactor growth phase or the BAL system was being modelled. For example, modelling the full scale BAL with 500 ml beads in 8L of plasma (4L in chamber, 1L reservoir, 1L in the circuit tubing, 0.5L in the Cobe Spectra® Aphaeresis unit and 1.5L in the pig) was equivalent to a ratio of 16ml of plasma to 1ml of beads in the scale column experiment. To provide adequate bead volume for fluidisation 5ml beads with 80ml plasma would have been used (15ml in column, 3ml in tubing and 62ml in the reservoir).

2.3.4 Modelling Flow Rates between the Scale Model and BAL System

An essential condition the BAL scale model was to replicate the flow rate used to fluidise the beads regardless of the experiment. An insufficient flow rate would cause inadequate fluidisation, thereby inhibiting mass transfer between the cells and the surrounding environment. Excessive flow rates may result in beads incurring shear stress damaged or providing excessive upward force causing them to escape from the chamber. These parameters have been established with the use of mathematical models and empirical observation. To replicate a volumetric flow rate from the large BAL system to the scale BAL system, the corresponding linear flow rate for the large system was calculated then replicated in the small scale BAL system, back calculating the relevant volumetric flow rate for the scale BAL. As a consequence, the linear flow rate in the large scale BAL would be identical to that of the scale BAL model, resulting in the same fluid characteristics being encountered by the beads in the large and small scale BAL model.

2.3.4.1 Calculating the Bioreactor and Large Scale BAL Volumetric and Linear Flow Rates

The linear flow rate describes the movement of liquid over a distance, and was calculated from the volumetric flow rate, as follows:

The linear flow rate was determined for a given large scale BAL or bioreactor system that was to be modelled using equation 2-4:

Equation 2-4: $F_L = F_v / D$

Where F_v is the volumetric flow rate (m^3sec^{-1}), and D (m^2) is the cross sectional area of the bioreactor chamber and F_L is the linear flow rate (ms^{-1}).

F_v was converted from $mlmin^{-1}$ to m^3sec^{-1}, as follows:

- F_{V1} is in $mlmin^{-1}$ and is set on the peristaltic pump
- F_{V1} $1x10^{-6}$ (cm^3min^{-1} to m^3min^{-1}) = F_{V2}
- $F_{V2} / 60$ ($m^3min^{-1}$to m^3sec^{-1}) = F_v

The cross sectional area, D, was calculated using equation 2-4:

Equation 2-4: $D = \pi r^2$

Where r is the radius of the chamber or the column in m.

Using this equation to establish the linear flow rate in the large scale model, the same linear flow rate was implemented in the scale BAL model, by calculating the required volumetric flow rate to achieve the given linear flow rate. The Watson-Marlow® peristaltic pump used for the scale BAL system provided a single speed to drive a multichannel pump head.

For example, where the bioreactor utilised a 342 $mlmin^{-1}$ volumetric flow rate to provide a 1.5 bead bed expansion in media (described in section 2.1.3) the linear flow rate was calculated as 3.23×10^{-4} ms^{-1}; equation 2-5 provided the volumetric flow rate required to match the linear flow rate, which was a re-arrangement of Equation 2-4, including the unit conversions.

Equation 2-5: $F_{Vs} = 6^5 F_L D_1$

Where F_{Vs} ($mlmin^{-1}$), is the volumetric flow rate for the small scale BAL model, F_L is the linear flow rate (ms^{-1}) from equation 1, and D_1 (m^2) is the cross sectional area of the column.

Having established the volumetric flow rate required, the 2.74mm bore pump tubing was calibrated for volumetric flow rate relative to RPM of the pump. To verify the correct flow rate was being used, the bed expansion observed in the column should be identical to that of the bioreactor using the same density of liquid, i.e. Media with 10% FFP, or media with 10% FBS.

2.3.5 "Worst Case Scenario" BAL Model

Materials

- Complete media as described in Section 2.1.1.1
- Plasma as in Section 2.3
- 50 Nunc® tubes
- 0.15 M HEPES (Lonza®)

End-Over-End Mixing Protocol

To trigger complete cell death, causing cell DNA and debris release, the relevant bead to media/plasma ratio was calculated in the same manner as section 2.3.3. Beads encapsulated using the Jetcutter® and cultured in the Bioreactor for 12 days were placed in a 50ml Nunc® with 20ml of complete supplemented media or plasma with 0.15 M HEPES buffer, incubating at 37°C for 2 days, whilst mixing end-over-end on a cell mixer. The conditioned supernatant was then removed and used as a "worst case scenario" of DNA and cell debris release.

2.4 ELISA Protocols

All the ELISA protocols have been optimised to work with the same protocol, only differing in the antibodies used.

2.4.1 AFP ELISA 10% FBS media

Alpha-fetoprotein (AFP) is thought to be a foetal counterpart to albumin and is generally used as a biomarker for hepatic carcinoma[149]. We have harnessed this expression by HepG2 cells to evaluate cellular synthetic performance in the presence of plasma, where excessive albumin background would inhibit sensitivity and accuracy of the assay.

2.4.2 Albumin ELISA

Albumin quantification served as an indicator of cell function when cells were not in the presence of human plasma, as the background albumin in plasma was too high to measure the production from HepG2 cells. However, during filtration experiments albumin was measured in plasma to establish whether the filter was removing albumin as a highly abundant protein, merely requiring a change in concentration to be detected.

2.4.3 Fibrinogen ELISA

Fibrinogen whilst also being an indicator of cell function, at a size of 340kDa[150] provided a means of ensuring that proteins were not being excluded from alginate secretion nor filtered out based on size.

2.4.4 Alpha-1-antitrypsin (AAT) ELISA

AAT provided another liver specific protein for assessment of HepG2 function.

Materials

- Nunc™ ELISA 96 well plate
- Primary antibody Table 2-2
- Secondary antibody Table 2-2
- ELISA 96 well immunosorbent plates (Nunc®)
- Coating Buffer
  - 0.6 mM Na_2CO_3
  - 1.4 mM $NaHCO_3$
  - pH 9.6 with 1 M NaOH
- PBS Tween-20
  - PBS
  - 0.05 % v/v Tween-20
- Blocking Buffer
  - PBS
  - 5% w/v powdered milk
- OPD (o-phenylenediamine dihydrochloride), H_2O_2 solution
  - 6 µl/L H_2O_2
  - 4 mg/L OPD
- 1 M H_2SO_4

2.4.5 ELISA Protocol

Primary Antibody Adsorption

In order to adsorb the primary antibody onto the immunosorbent 96 well plate, the stock antibody was diluted as shown in Table 2-2 in coating buffer, adding 100µl to each well, and then sealing the plate for overnight incubation at 4°C. The next day the plate was washed 3 times with PBS-Tween-20 and liquid flicked off; 100µl of blocking buffer was added to each well and incubated for 1 hour at room temperature, to block any remaining antibody binding sites on the plate.

Sample and Standard Preparation

Sufficient sample and standards were prepared to perform triplicate analysis, with a 5 point standard curve starting from 200ng/ml prepared by serial dilution in supplemented culture media or plasma. Samples were also diluted in media or plasma, using pre-determined dilution factors in anticipation of obtaining optical densities equidistant from the top and bottom standard (this was determined by using the same ELISA protocol with a matrix of sample dilutions analysed relative to a standard curve). Finally, a pre-prepared QC control was used to validate the ELISA, and was obtained by pooling media from 10 separate HepG2 cell cultures. Following the addition of 100µl of standard and sample, the plate was incubated at 37ºC for at 2 hours.

Secondary Antibody Addition

To remove any unbound antigen, the plate was washed 3 times with PBS-Tween-20 and briefly dried. Secondary antibody was diluted 1/2000 in blocking buffer, to block any remaining primary antibody binding sites and therefore reducing false positives. To each well 100µl was added, incubating for 1 hour on the bench, then washed 5 times.

Colorimetric Development

The secondary antibody used is conjugated with horseradish peroxidise (HRP), which catalyses the oxidation of OPD with H_2O_2 to form 2, 3-diaminophenazine, producing an orange/brown colour read spectrophotometrically at 492ηm. This change is directly proportional to antigen concentration, and varies with time up to a saturation point. Therefore, care was taken to ensure each sample had identical development time. To each sample 100µl of OPD / H_2O_2 solution was added at timed intervals, incubating in the dark for 5 minutes to allow colour development. The reaction was stopped with the addition of 50µl 1M H_2SO_4 added at timed intervals.

ELISA Antigen	Primary Antibody Source and Catalogue Number	Primary Antibody Dilution	Secondary Antibody Source and Catalogue Number	Secondary Antibody Dilution
Albumin	DAKO (cat # A0001)	1/1000	Abcam (cat # ab24458-200)	1/1000
AFP	cat # ab10071	1/1000	ab10072	1/3500
Fibrinogen				
Alpha-1-antitrypsin	Dako (cat # A0012)	1/1000	Abcam (cat # ab7635-s)	1/2000
Prothrombin	Abcam (cat # ab9020-1 and).	1/10	Ab53597-200	1/3000

Table 2-2 Antibody and source dilution factors for ELISA protocol

2.5 A Model for Filtration of Plasma in the BAL System

The filtration model assembly allowed the capacity and throughput of the filters to be tested and scale up to remove DNA and endotoxin in the full scale BAL system.

Materials

- 1.6 mm wall thickness thick, 4.6 mm bore size Watson-Marlow Silicone tubing from water bath to the pump.
- 1.6 mm wall thickness, 4.6 mm bore size Watson-Marlow PVC link tubing between the pump and filter, as protection from possible increased pressure due to back pressure.
- 1.6 mm wall thickness, 4.6 mm bore size Watson-Marlow Marprene™ peristaltic pump tubing between the pump and filter, as protection from higher pressure.
- 3M® Cuno® Zeta Plus™ Maximiser™ Filters
  - 60ZA50A dual layer filter
  - 90ZA05A dual layer filter

- 3M® Cuno® Plus EXP™ Filters
  - 05SP (BC0030A - 05SP)
  - 10SP (BC0030A - 10SP)
  - 30SP (BC0030A - 30SP)
  - 50SP (BC0030A - 50SP)
  - 60SP (BC0030A - 60SP)
  - 90SP (BC0030A - 90SP)

- Plasma
  - FFP plasma
  - Plasma from Cobe® Spectra® therapeutic plasma exchange
  - Pig acute liver failure plasma from plasma exchange

- Pressure transducers assembly
  - Smith Medical® Medex™ Optimax Medical Pressure transducers
  - ADintruments® PowerLab® data acquisition system
  - LabChart® 4 data acquisition software
  - Modified data cables described in section 2.5.1

- Volume measurement Assembly
  - A&D® GX 2000® Top plate balance
  - Serial RS232 to USB converter
  - RsWeight® version 100 Data acquisition software

- Other materials
  - Water bath at 37°C
  - 4.6mm Watson Marlow® pump tubing
  - Watson Marlow® 520 Du pump
  - Sterile dry baked at 180 °C for 3 hours
  - Certified sterile, DNA and pyrogen free 15ml Nunc® centrifuge tubes
  - Certified sterile, DNA and pyrogen free 2 ml Eppendorf® tubes
  - Sterile DNA and Endotoxin Free Filtered Pipette tips
  - Timer
  - 25 g/L Virkon® disinfectant (containing potassium peroxymonosulphate, sodium dodecylbenzenesulfonate, sulphamic acid; and inorganic buffers)

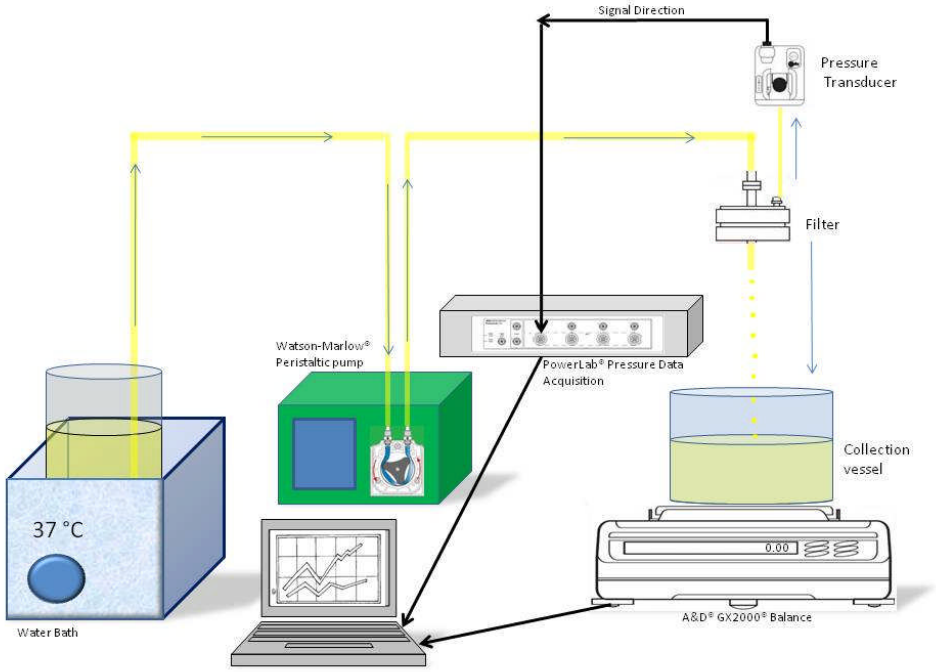

Figure 2-4: Filtration model assembly. The Watson-Marlow® peristaltic pump forces plasma/media from the water bath, at 37°C, to the filter where a pressure transducer measures back pressure. The filtrate then passes to a collection vessel on a top loading balance. The analogue signal from the pressure transducer is converted to a digital signal using the PowerLab® data acquisition system, recording reading on LabChart 4 program. The analogue signal from the A&D balance passes through an analogue to digital converter into the A&D WinCT data logging program. This provides real-time data acquisition to measure filtration function (capacity, flux and volumetric throughput).

2.5.1 Construction of PowerLab and Pressure Gauge

In order to sufficiently model the filter system for the BAL, a series of data acquisition and fluid systems were integrated to provide data for real time filter performance required to upscale for the full scale BAL system.

PowerLab Data acquisition System

The PowerLab® Data Acquisition system is able to read most analogue signals with the relevant conditioners and amplifiers to provide a real time digital signal, which is read by LabChart® 4 software.

Principle of the Transducer

The Medex® pressure transducers consisted of a strain gauge mounted on a thin diaphragm wired to a Wheatstone bridge circuit, creating a load cell. To power the load cell, a regulated DC voltage was provided by the PowerLab®. As a result of using specific medical grade pressure transducers they required modification for integration with the PowerLab® system. Figure 2-5 shows a circuit diagram of the connection between the pressure transducer and the

PowerLab® data acquisition system, comprising the strain gauge, to the Wheatstone bridge, then to the signal conditioner and finally the PowerLab®.

The strain gauge consisted of a stretched strip of metal, which under strain became thinner, changing resistance between 30Ω to 300kΩ, end-to-end, proportionally to the strain applied. The degree of imbalance in resistance was measured between different arms of the Wheatstone bridge circuit, providing a measure of the strain applied. This worked by the resistor R3 (Figure 2-5) and the strain gauge being set to an equal resistance with no force was applied; arms R1 and R2 were set at identical resistance to each other, so a symmetrical balance occurred and output voltage was zero. When a strain was applied the resistance of the gauge changed causing an imbalance in voltage, transmitting a micro voltage to the PowerLab® for signal conditioning, amplifying the signal to 200mV.

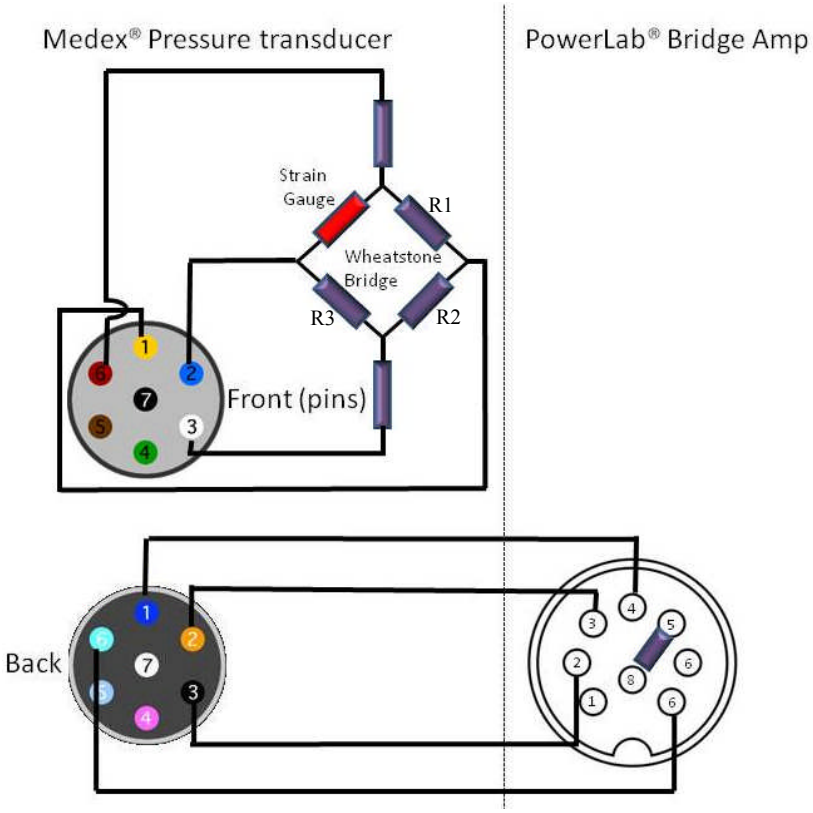

Figure 2-5: A Wheatstone bridge circuit. This is the basis of Medex® pressure transducer, consisting of four resistors that change resistance according to the strain applied by the diaphragm of the transducer.

2.5.2 Preparation of the Filtration Assembly

All the tubing was pre-assembled, with the tubing length adjusted for the requirements of specific experiments. Sterility was maintained in order to model the large scale BAL system and to reduce any contamination, the tubing assembly and the filter were autoclaved for 20 minutes at 121 °C. Prior to autoclaving the filter, 500 ml of MilliQ water passed through then purged with air.

Plasma was held in a baked sterile beaker, and covered with aluminium foil while pre-warming to 37°C in the water bath; in the same water bath a sterile beaker of MilliQ water was also pre-warmed for washing and calibration (Section 2.5.3). Meanwhile the tubing assembly was put in place as shown in Figure 2-4, again passing 500ml of MilliQ water through the filter, then purging with air.

2.5.3 Initial Filter Model Protocol

The pump was calibrated with the pre-warmed MilliQ water, to relate RPM to the volumetric flow rate, then purging the whole system with air, before priming with Plasma. To prime the filter with plasma, the air vent on the upside of the filter was opened to fill the top layer of the filter capsule. Once full, both the pressure transducer and the tube between the filter and the pressure transducer were primed with plasma, taking care to remove any air bubbles.

With the whole system primed, with exception of the filter membrane itself and the bottom end of the filter capsule, the data acquisition systems were started and the pump turned on to the required RPM for the given flow rate. It took a few moments to prime bottom end of the filter and the tubing below it, however, this provided sufficient time for the pump to reach speed.

2.5.4 Sampling and Data Acquisition during Filter Model Protocol

At regular intervals 1ml samples were taken from the collection vessel and immediately aliquoted into 2ml Eppendorf® tubes and frozen to -20°C. As a result of this, temporary reduction in the mass of the vessel was observed which was later accounted for when analysing data. During the course of the filtration experiment the progressive pressure increase determined the end of the experiment, and the frequency of sample taking. According to 3M® Cuno® the filters are designed to withstand a differential pressure up to 40psig (equivalent to 2.7 bar or 2026 mmHg). Considering atmospheric pressure at 1 atmosphere equivalent to 1.01295 Bar or 760 mmHg, the maximal differential pressure for the filter model was set at 1200mmHg (2026 mmHg – 760 mmHg = 1266 mmHg). If the pressure increased quickly then the samples were taken with greater frequency to ensure that any point of contaminant breakthrough in the form of DNA or endotoxin could be recorded.

2.5.5 Termination of Filter Model Experiment and Data Analysis

At the end of the experiment, the entire system, including the filter, was purged with 2L MilliQ water, whilst measuring the pressure to determine the extent of the pressure attributable to the plasma, and the amount of pressure remaining due to blockage of the filter. Finally, the entire system excluding the filter was washed with 2L of 25g/L Virkon® then washed again with 5 L of MilliQ water.

2.6 Testing Endotoxin in Plasma by Fluorometric *Limulus* Amoebocyte Lysate Assay

Materials

- All materials were from Lonza® unless otherwise stated
- Fluorescence buffer
  - 1 part Fluorescence Enzyme Solution,
  - 4 parts Assay Buffer, B50-658, 5.0 ml/vial
  - 5 parts Fluorogenic Substrate,
- 20 EU/ml *E. coli* Endotoxin, O55:B5, E50-643,
- LAL Reagent Water, 30 ml/vial.
- 1 ml endotoxin free glass tubes, baked for 3 hours at 250 °C
- Endotoxin free, sterile filtered pipette tips (Starlab®)
- Endotoxin free, sterile 96 well plate (Nunc®)
- LAL certified endotoxin free water

Principle of Fluorometric Endotoxin Assay

Endotoxin testing is based upon a Gram-negative bacterial infection of *Limulus polyphemus*, the horseshoe crab, resulting in a potentially fatal intravascular[151,152] . At the molecular level, a serine protease catalytic coagulation cascade results in the gelation of *Limulus* blood. This cascade is used in the *Limulus* Amebocyte Lysate Assay (LAL)[153].

Chromogenic assays developed from utilising the enzymatic cascade, shown in Figure 2-6A, where the protease cascade activates a chromogenic change. However, due to the possibility that glucans in the solution may activate this cascade, producing false positives, another option was used. The recombinant Factor C (Figure 2-6B) directly interacts with the endotoxin, causing a fluorometeric change proportional to the level of endotoxin, which is more sensitive and robust compared with the chromogenic assay.

Figure 2-6: LAL assay enzyme cascade A; The enzyme cascade found in the *Limulus polyphemus* when in the presence of gram-negative bacteria, modified in the form of an assay utilising a chromogenic substrate or turbidity testing to relate amount of endotoxin proportionately to colour of turbidity change. B; The recombinant Factor C which only binds endotoxin to cause a fluorescent change, by passing the possibility of false negatives from the presence of Glucan. Obtained from Lonza®[154],

Preparation of the Endotoxin facilities

Environmental endotoxin contamination was averted by following a number of procedural and technical protocols. A dedicated room was used for analysis, using a dedicated category 3 biological safety tissue cabinet to provide a sterile environment. The room was maintained as a clean room, using separate robes, wearing hair nets and face mask to reduce the probability of bacterial and endotoxin contamination into the room. All glassware was baked at 250°C for 3 hours and only certified endotoxin free sterile plastic ware in the form of pipette tips were used. To decontaminate the room and the tissue hood after sterilisation using UV light, Virkon® and 70% IMS, the surfaces were exposed to 0.1M NaOH in 60% Ethanol for at least 6 hours, which promoted endotoxin hydrolysis followed by dissolution, finally wiping surfaces with endotoxin free water.

Endotoxin Assay Protocol

To a 96-well plate, 100µl of sample was added in triplicate, either a standard curve, water blanks, a quality control sample, or unknown test samples, incubating at 37°C for 10 minutes. Meanwhile the stock fluorescence buffer was mixed, in the following ratio:

- 1 x fluorescence buffer:
  - 1 x fluorescence enzyme
  - 4 x assay buffer
  - 5 x fluorogenic substrate

Sufficient stock was made to accommodate 100µl for all samples, standards, and blanks. At timed intervals, 100µl of fluorescence buffer was added to each well and the fluorescence read at 380ηm excitation and 440ηm emission wavelengths; this constituted the blank fluorescence. The plate was then incubated for 1 hour at 37°C and read again at the same wavelengths, subtracting the blank reading from the 1 hour reading.

Preparation of Standards and samples

Endotoxin standards were prepared from the lyophilized *E. coli* O55:B5 endotoxin reconstituted with LAL Reagent water to yield a 20EU/ml stock solution, agitating vigorously for at least 15 minutes at high speed on a vortex mixer (This was of particular importance, for standards and samples stored in glass containers, which endotoxin readily binds to). Immediately prior to administering standards or samples, each was agitated again for 20 seconds by vortexing. A four point logarithmic standard curve was prepared from 0.1EU/ml to 10EU/ml by serial dilution and analysis in quadruplicate.

Inhibition from components of the plasma samples were reduced by diluting to 0.5% with in endotoxin free water, then heating samples at 70°C for 20 minutes. A positive control was included in each sample preparation, where a 1EU/ml plasma sample was prepared, and treated in an identical manner, to ensure that reduction in inhibition was confirmed.

2.6.1 Preparing and Extraction of Lipopolysaccharides to Spike Plasma for Filtration

The aim was to produce at least 500 mg of dry cell mass, for extraction of lipopolysaccharides

2.6.1.1 Materials

- *E.Coli* with DR7 vector containing XL -1 blue and Kanamycin resistance
- 35g/L L Broth, autoclaved
- Kanamycin 1/1000 dilution of 50 mg/ml stock solution
- 200 µg/ml Proteinase K (1 mg/ml stock)
- TM buffer, with added DNase and RNAse Buffer
  - 10mM TrisHCl
  - 2mM $MgCl_2$
  - 200 µg/ml DNAse (10mg/ml stock)
  - 50 µg/ml RNAse (10mg/ml stock)
- TSE Buffer at pH 7
  - 0.1M EDTA (Ethylenediaminetetraacetic acid)
  - 10mM TrisHCl
  - 2 %SDS (sodium dodecyl sulphate)
- 95% Ethanol in 0.375 M MgC_2 at 0 °C
- 2 %SDS in 0.1 M EDTA
- 25mM $MgCl_2$
- Sterile (by autoclaving at 121 °C) glass 500ml, 1 L and 5 L conical flask
- Sterile 50ml Nunc® centrifuge tube
- Beckman- Coulter® J6-MI floor centrifuge
  - JS-4.2A Aries™ series rotor
- Beckman- Coulter® 80K LE floor centrifuge
  - 70 Ti rotor
- Edwards Lyophiliser
- Pestle and mortar at -20 °C

Preparation of *E.Coli* Cells for LPS Extraction

A 2ml solution of L broth was added to a 50 ml Nunc™ centrifuge tube, with 1/1000 dilution of 50ug/ml Kanamycin then inoculated with 50µl of *E. coli* Glycerol Stock and incubated overnight at 37°C, with constant circular agitation. The following day the 2ml inoculum was added to 200 ml L Broth (with Kanamycin) in a 500ml sterile conical flask, incubating for 8 hours at 37°C, with constant circular agitation. This inoculum was added to 2 x 1L L broth (with Kanamycin) contained in 2 x 5L Conical flasks incubated overnight at 37°C, with constant circular agitation.

To isolate the E.Coli, the 2 x 1L broths were centrifuged at 8000g for 10 minutes at 4°C in sterile 1L Beckman- Coulter® centrifuge tubes in the J6-MI floor centrifuge using the JS-4.2A Aries™ series rotor. Discarding the supernatant, each of the 2 pellets were re-suspended in the 50ml TM buffer, with no DNAse or RNAse added, and separated into 4 sterile 50ml Nunc®

tubes, freezing at -80°C overnight. In order to gather dry homogenised cell mass, the frozen samples were lyophilised for 32 hours then ground into a fine powder in a pestle and mortar, (previously incubated at -20°C).

Extracting Lipopolysaccharides from the Dry Cell Mass

The remainder of the protocol is designed for 500mg of dry weight, greater or less than this quantity would have necessitated a proportional alteration in the amount of each solution used. In addition to this, any centrifugation step above 4000g was performed in sterile 100ml Beckman-Coulter® centrifuge tubes in the Beckmann-Coulter ® 80K LE floor centrifuge using the 70Ti rotor; otherwise a conventional bench top centrifuge was used .

500mg of dry *E.Coli* cell powder was re-suspended in 15ml TM buffer contained in a 50ml Nunc® tube and vortexed thoroughly; adding 150µl of 10mg/ml DNAse and 37.5µl of 10mg/ml RNAse, giving 200µg/ml and 50µg/ml final concentrations, respectively, incubating at 37°C for 4 hours. The first step of protein removal was initiated with the addition of 10ml of TSE buffer, vortexing for 5 minutes to mix and then centrifuging at 50,000g for 30 minutes at 20°C. Decanting the supernatant into 50ml Nunc® tubes, 200µg/ml of proteinase K was added and incubated overnight at 37°C with constant rotary agitation. A white precipitate appeared at this stage, which was removed by centrifugation at 1000g for 10 minutes. The supernatant was decanted and allowed to cool for 30 minutes, followed by adding two volumes of 0.375 M $MgCl_2$ in 95% ethanol at 0°C, finally centrifuging at 12,000 g for 15 minutes at 2–4 °C.

A second protein removal step was performed by re-suspending the pellet in 25ml TSE buffer, and sonicated for 15 minutes to dislodge the pellet and all residual lipopolysaccharides from the centrifuge tube. This time a lower concentration of 25ug/ml proteinase K was added (due to lower contaminant levels), again incubating overnight at 37°C with rotary agitation, and centrifuging at 1000g to remove any precipitate. Two volumes of 0.375M $MgCl_2$ in 95 % ethanol at 0 °C were again added, centrifuging at 12,000 g for 30 minutes at 2 -4°C.

A final wash step consisted of re-suspending the pellet in 15mM TrisHCl and sonicating for 15 minutes. The solution was finally centrifuged at 200,000 g for 2 hours at 12 °C, re-suspended in sterile MilliQ water.

2.8 PMAS SBSS Liquid Particulate Counter

Materials

- PMASS GmbH SBSS Particulate counter with the HCB-LD-50/50 sensor provided by PMT Ltd.
- diH_2O treated with the MilliQ System

Principle of Particulate Counting using the PMAS System

The PMAS particulate counter detects light scattering due to the presence of particulates in a sample. A laser light was passed through the sample, where any loss in light was detected by sensor attributing loss in signal proportionately to size and frequency of particulates. As a result, a fully quantitative measure of particulates was provided, giving both a size distribution and total particulate count per ml of sample.

Particulate Counting Protocol

The Particulate counter was first calibrated by passing through a solution, which contained defined size and concentration of latex beads at 10ml/min, assigning an mV change in signal to a particulate size illustrated in Table 2-3. Prior to sample analysis, the instrument was flushed with 500ml of MilliQ treated diH_2O. The parameters for analysis were set at 10ml/min, measuring 0 to 20 particulate sizes with 50ml sample volumes. In order to reduce the effect of superimposing particulates introducing inaccuracy into the measurement, samples were diluted in MilliQ treated RO water. The effect of superimposition was evaluated by incrementally testing diluted samples until the particulate measurement showed a linear distribution in line with the dilution, i.e. a samples serially diluted ½ must show a ½ in particulate number between dilutions.

Particulate size (µm)	Change in signal (mV)	Particulate size (µm)	Change in signal (mV)
1	101	**11**	1771.3
2	321	**12**	1835.9
3	513	**13**	1892
4	714	**14**	1944.3
5	1030.9	**15**	1992.1
6	1259.5	**16**	2037.7
7	1399.7	**17**	2081.9
8	1512.2	**18**	2167.2
9	1611	**19**	2209
10	1697	**20**	2250.5

Table 2-3: Calibration values for the particulate counter. Values obtained by passing defined sizes of 1,000 beads/ml solutions of latex beads through the PAMAS GmbH SBSS particulate counter to determine the mV change, which is then entered into the software to determine sample particulate size and frequency.

Chapter 3
Alginate Purification

This Chapter details experiments to remove particulates from alginate using different filtration methods, measuring efficacy by rheometry, bead sphericity and encapsulated HepG2 cell growth and function. The sand filtration was performed in partnership with Timea Grego as part of her MSc project, as the UCL Department of Civil Engineering

3. Alginate Purification

3.1 Introduction

For encapsulation of HepG2 cells, analytical grade sodium alginate powder is currently used and is perfectly adequate for research purposes, but falls short of meeting some of the standards attributed to medical grade alginate (Table 3). Medical grade alginate has been used in small quantities, mainly as a scaffold for cell implantation[155, 156], but has two drawbacks for use within the BAL system; firstly it is prohibitively expensive at the necessary BAL scale, and the properties of alginate are not necessarily appropriate for encapsulation in a fluidised bed system, over 8-10days.

One aspect of attaining medical grade alginate is purity as a starting material[157-160], which will be tackled in this chapter. The main focus will be the level of particulates between 1 and 20μm in diameter that remains in the alginate supplied by Sigma-Aldrich™ that is visible under a phase contrast microscope. Other groups have purified alginate for biotechnology application, often using lengthy extraction and filtration processes[161-163] that often adds to the cost of supplying alginate and affects the final properties. Therefore, an in-house method is required, starting with the removal of particulates, whilst maintaining alginate properties.

Control of alginate as a starting material can be distinguished from controlling particulates entering the patient during alginate bead fluidisation, as particulates trapped within alginate beads may not escape to enter the patient, although this cannot be relied upon. Furthermore, the basis of many regulations regarding particulates is derived from possible immunogenic reactions[166]. One such example is the development of phlebitis from particulate exposure with intravenous therapies[167]. As a consequence, compliant intravenous therapies must control and eliminate particulates within regulatory limits for the specific markets, as illustrated Table 3-1. These particulate levels relate to fluid directly infused into patients, so may not directly relate to the BAL system; however, it could be argued that plasma from the patient will be in direct contact with the alginate beads in the BAL circuit and therefore is analogous to direct infusion. As a result, the particulate levels in Table 3-1 were used as a guide.

Pharmacopeia source	*Particle size (μm)*	*Particle limit in 1cm³*
USA,	2	1000
UK,	5	100
Australia	10	50
	20	5
	25	5

Table 3-1: Particulate size and frequency admissible in water for parenteral medicines within specified regulatory jurisdiction.

Other regulatory considerations relating to alginate during the treatment phase have been tested *in vitro* and *in vivo* to meet fundamental requirements such as: immunogenicity, integrity as a cell support and reactivity with human, pig and rabbit[74,75,168,169]. Although controlling particulates in the starting material will be the focus, a quality management strategy, where particulates will be removed directly from the plasma upon re-entry into the patient is another possible approach.

Any alginate purification technique must maintain alginate properties outlined in the Thesis Introduction. These include: the ability to encapsulate cells, promote cell growth, cell function, and maintenance of viability for 8 – 12 days in fluidised bed 3D culture, as well as preserve bead integrity throughout the growth and treatment phase.

3.2 Summary of Chapter

Several different principles of purification will be tested to remove particulates whilst maintaining the required alginate properties for use within the entire BAL system. In brief the three approaches are:

- Filtration through depth charged filter
- Sand Filtration
- Gas Solid Cyclonic Filtration

3.3 Methods

3.3.1 Characterising Particulate Contamination in Analytical Grade Alginate

3.3.1.1 Particulates Measurement in 2% Alginate using Phase Contrast Microscopy

Materials

- Phase contrast microscope.
- Lucia G Software.
- Glass slide.
- Glass Cover slip.
- Calibration graticule.

Particulate Measurement

Alginate was prepared as detailed in Methods Section 2.1.3.2, carefully adding 250µl to a glass slide, then protecting the sample with a glass cover slip, analysing at 160x magnification on a phase contrast microscope, calibrated using a calibration graticule. Particulate size and frequency were evaluated using a function in the Lucia G® software, enabling lines to be drawn across the diameter of the particulates in a given field. Different fields across the slide were randomly chosen counting a total of 100 particulates across each slide. This provided a distribution of sizes reflecting the population distribution of particulates.

This method was semi-quantitative as total particulate numbers could not be determined, although it did provide a measurement of particulates in alginate for preliminary sample analysis.

3.3.1.2 PMAS SBSS Liquid Particulate Counter

Materials

- PMASS GmbH SBSS Particulate counter with the HCB-LD-50/50 sensor provided by PMT Ltd.
- MilliQ treated RO H_2O.
- Clean glass 250ml beaker.

Principle of Particulate Counting using the PMAS System

The PMAS particulate counter detects the extent of light scattered by particulates in a solution. Laser light was passed through the sample, where any loss in light transmission was detected by a sensor calibrated to attribute loss in signal proportionately to size and frequency of particulates. As a result, this provided an objective and quantitative measure of particulates, giving both a size distribution and total particulate count per ml of sample. However, to maintain accurate particulate measurement the samples required dilution to between 0.01% and 0.001% to prevent particulate agglomeration or overlapping interference, which may distort detection.

Particulate Counting Protocol

Calibration of the particulate counter used a solution containing defined size and concentration of latex beads at 10ml/min, assigning an mV change in signal to particulate sizes, as illustrated in Figure 3-1. Prior to sample analysis, the instrument was washed with 500ml of MilliQ treated RO H_2O. The parameters for analysis were set at 10ml/min, measuring 0µm to 20µm particulate size with 10ml sample volume.

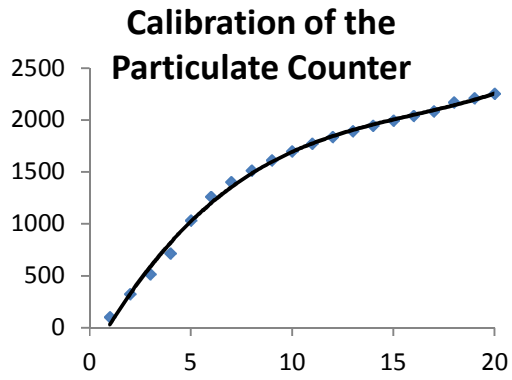

Figure 3-1: Calibration curve for the particulate counting. The curve was obtained by passing defined sizes of 1,000 beads/ml solutions of latex beads through the PAMAS GmbH SBSS particulate counter to determine the mV change, which was then entered into the software to determine sample particulate size and frequency.

3.3.2 Alginate Lyophilisation and Reconstitution

Materials

- Sodium Alginate (Sigma-Aldrich®)
- Dry ice
- Acetone (Sigma-Aldrich®)
- Round bottomed Winchester flask
- Edwards lyophiliser

For encapsulation, as described in Methods Section 2.3, 2% alginate was diluted to 1% by adding cell and media mix to a 1:1 ratio. For filtration, however, the relatively high the viscosity of 1% alginate (0.25Pas, equivalent to 250cPois) required dilution to 0.2%. Consequently, after filtration, the alginate solution was lyophilised and reconstitution in preparation for encapsulation, as illustrated in Figure 3-2.

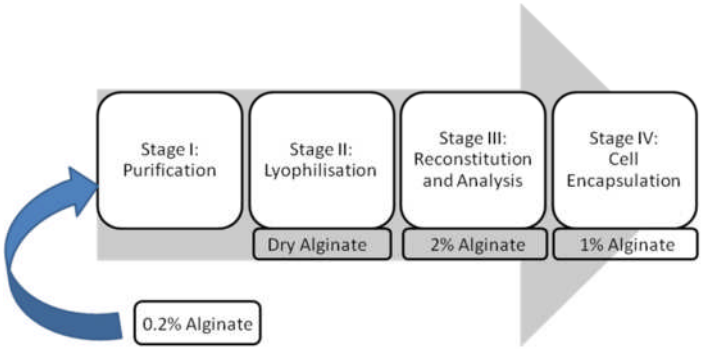

Figure 3-2: Alginate filtration process. This included alginate dilution, filtration and reconstitution: 0.2% alginate solution was diluted in HEPES buffered 0.15M NaCl, pH 7.4; stage I consisted of a filtration step; stage II involved shell freezing the alginate filtrate in round bottomed flasks using dry ice acetone bath, followed by lyophilisation over 3-5 days; stage III entailed reconstituting the alginate with sterile MilliQ treated RO diH_2O, to the desired alginate concentration; stage IV used the alginate initially to encapsulate empty beads to verify bead integrity then proceeding with HepG2 cells.

Processing of Alginate from Filtration to Encapsulation

A volume of 2% alginate was diluted to 0.2% with MilliQ treated RO H_2O for filtration in stage I. Stage II commenced by adding 200ml of filtrate to a round bottomed Winchester flask for shell freezing, by adding dry ice to an acetone bath, whilst rotating the bottom of a 1L Winchester flask in the bath (this was performed in a fume cupboard). The alginate gradually froze in increasing layers on the inside of the Winchester flask. Once complete, the flasks were stored at -80°C for lyophilisation over 2-3 days to leave a shell of dry alginate. The dry alginate was reconstituted in MilliQ treated RO H_2O to get 2% alginate solution, for particulate analysis or encapsulation.

3.3.3 Rheometry of Alginate

Materials

- Bohlin® CVO automated dynamic shear rheometer
- Graduated cone upper spinning plate
- Na alginate

Rheometry Principle

Changes to alginate molecular composition, attributable to filtration, were determined by rheometry. This provided a numeric comparison of shear stress (which is related to viscosity and in turn related to the size and distribution of polymer components) between filtered and unfiltered alginate solutions, based on the way the solution behaves when increased shear stresses were applied. The alginate solution was placed between two adjacent surfaces, where the upper surface rotated and the lower surface remained stationary. As the shear rate of the upper surface was incrementally increased, the resistance in the fluid was evaluated by a sensor attached to the axle of the upper surface, which was expressed as shear stress. Viscosity was then directly calculated from shear stress using Equation 3-1:

Equation 3-1: $\text{Viscosity (Pas)} = \frac{\text{Shear Stress (Pa)}}{\text{Shear rate } (s^{-1})}$

Where viscosity (Pas) is equal to the detected shear stress (Pa) divided by the shear rate applied (s^{-1}).

The way a solution responds to shear rate can be placed into two broad catagories; Newtonian and non-Newtonian fluids. Newtonian fluids do not change viscosity with increased shear stress as shown in Figure 3-3; these include fluids such as water and human plasma. Non-Newtonian fluids do change viscosity when shear is applied and are further subdivided depending on the response to the applied shear.

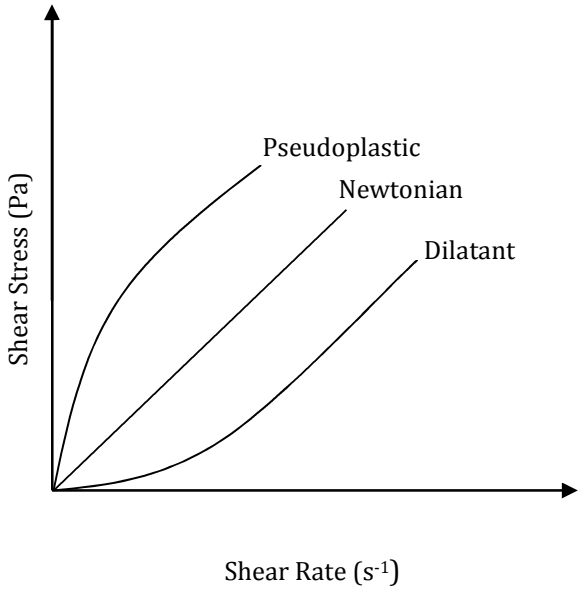

Figure 3-3: Flow curves representing Newtonian and non-Newtonian fluids. Non-Newtonian fluids change shear stress with changes to shear rate; as shear rate increases pseudoplastics show a concave downward curve for shear stress, whereas dilatants fluids show an upwards concave curve for shear stress. Newtonian fluids do not change shear stress as shear rate increases. This provides an indication of intermolecular interactions within the solution.

Rheometry Protocol

Prior to sample analysis the plates were cleaned with MilliQ treated RO H_2O followed by adding 1ml of 2% alginate sample to the center of the bottom plate. The top plate was then lowered to leave a 500µm gap between the center of the plates. An initial high shear of 250RPS was imposed for 5 seconds to remove air bubbles and ensure uniform distribution of alginate across the plate. After this, the shear measurement began at 0 shear rate, increasing in velocity by 10 RPS every 30 seconds. A sensor measuring resistance from the alginate solution provided a real time shear stress output on the Malvern® software.

Alginate viscosity was determined by measuring the mean viscosity over the range of shear rates, with the variance expressing the non-Newtonian change in viscosity over shear rate. To

measure mean viscosity for both Newtonian and non-Newtonian fluids a representative shear rate can be chosen for the given set of samples, so that the variance illustrates the spread of results at a particular shear rate. For the purposes of alginate purification, measuring alginate viscosity across shear rates and deriving a variance provided an indication of Newtonian vs. non-Newtonian fluid characteristics.

3.3.4. Filtration of Alginate using Cuno® Filters.

Materials

- 3M Cuno® filters
- Watson-Marlow® D510U pump

Principle of Depth Charged Filtration for Alginate

As described in Section 1.6.2 in the Introduction, depth charged filters work on two principles: the physical porosity of the filters, and the charge of the filter media. Due to the nature of the particulates, the charge cannot be easily determined, instead relying on the porosity of the filter to remove particulates.

Filtration Protocol

Filters were autoclaved to gain sterility, which would be essential if used for large scale alginate production. The filters were prepared for this by being flushed with 500ml of MilliQ treated RO H_2O, at 25ml/min, discarding the flow through then purging with air to leave the filter media moist. Following autoclaving at 121°C for 20 minutes, another 500ml water flush and air purge was performed. Samples of 0.2% alginate were passed through the filter at 10 ml/min, taking 1ml samples every 30 seconds for particulate analysis (Methods Section 3.3.1).

3.3.5. Sand Filtration

Sand filtration was performed by the UCL Civil Engineering Department, for full protocol, please refer to Appendix II.

Sand Filtration Principle

Fine sand filtration more conventionally serves as a means of removing particulates in industrial water purification and many bioengineering processes[170]. As Figure 3-4 illustrates, granular media filtration (e.g. sand) can retain particulates from 1μm to 1000μm, depending on sand sizes used.

Figure 3-4: Different filtration approaches for purification of solutions. Granular media filtration (sand) can remove particulates of between 1µm to 1mm[171].

3.3.6 Measurement of Bead Size and Sphericity after Filtration Processes

Materials

- Phase contrast microscope
- Lucia G software
- Calibration graticule

Bead Size and Sphericity Protocol

Measurement of bead size and sphericity provided a means of assessing the effects of different purification protocols on the integrity of beads, for cell growth and to prevent inhibition to bead fluidisation through deformation.

Initially, a calibration graticule was used to measure a defined length for each magnification. Images of alginate beads taken, using the Lucia G microscope, were analysed for bead size and sphericity, by drawing two perpendicular lines across the diameter, incorporating the longest diameter of a given bead. This was repeated 100 times to provide a statistically representative analysis of the beads. One of the diameters was used to evaluate bead size and the combination of the two perpendicular diameters were used to evaluate sphericity as expressed by Equation 3-2. Accordingly, a figure closer to 0 depicts greater sphericity, whereas a higher figure indicates greater deformation.

Equation 3-2: $S = 1 - (d_2 / d_1)$

Where the sphericity, S (dimensionless) is equal to the longest diameter, d_1 (µm) divided by the perpendicular diameter, d_2 (µm).

Visualisation of Particulates in an Alginate Bead

In order to visualise the particulates in the alginate, beads were encapsulated and analysed under a phase contrast microscope, Figure 3-5.

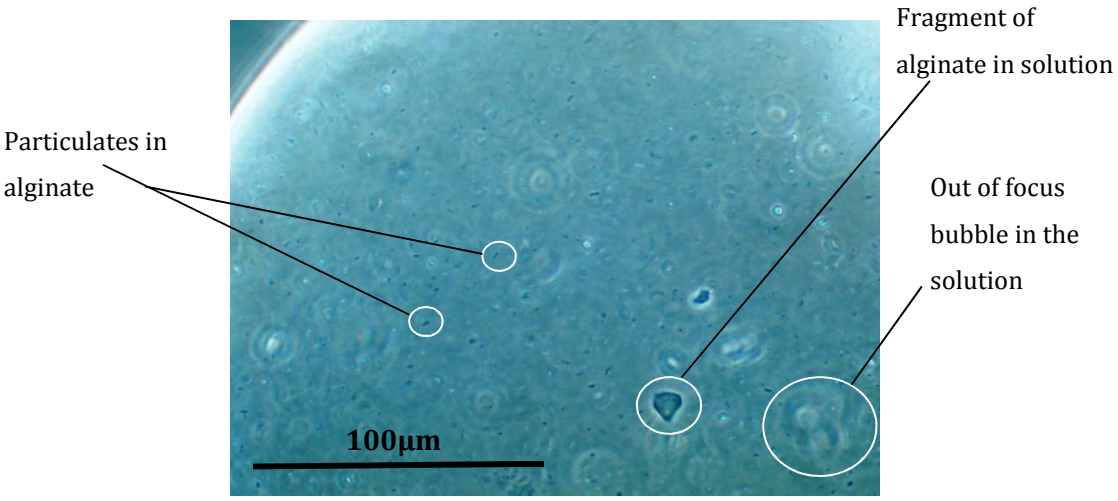

Figure 3-5: Particulates visible in an encapsulated alginate bead. This used 160 x magnification.

3.4 Results

For the purposes of clarity, this chapter will present each set of relevant results with a short introduction and discussion, as many of the experiments performed were relatively disparate.

3.4.1 Changes in Alginate Property due to Sterilisation

3.4.1.1 Introduction to Alginate Sterilisation

Sterility is of vital importance to any intravenous medical device. Alginate is highly heat labile[78], alginate sterilisation (121°C for 10 minutes), causes a reduction in alginate viscosity crucial for cell growth and function whilst maintaining bead integrity (data not shown). Conventional autoclaving protocols often use 121°C for 20 minutes to provide sterility, which causes alginate viscosity to reduce to an extent which compromises bead integrity. To distinguish between autoclaving for different times, in the remainder of the chapter, **sterilised** alginate will refer to **10 minutes at 121°C**, whereas **autoclaving** will refer to **20 minutes at 121°C**. The change in viscosity between sterilised and autoclaved alginate were evaluated by rheometry, arring at the ideal viscosity for successful encapsulation. The sterility of the alginate sterilised for 10 minutes at 121°C was emperically assessed due to the lack of infection over 8-10 days of culture.

3.4.1.2 Results from Rheometric Analysis of Alginate

Autoclaving alginate (20 minutes at 121°C) caused a 6-fold decrease in mean viscosity compared with unautoclaved alginate, as illustrated in Figure 3-6A and Figure 3-6C. A 2.25 fold reduction in viscosity, was observed between unautoclaved and **sterilised** alginate (Figure 3-6B). This clearly illustrates the highly heat labile nature of alginate polymeric chains. For all subsequent experiments, alginate was sterilised in an autoclave for 10 minutes at 121°C, as is currently the practice for the large scale BAL growth phase in our group.

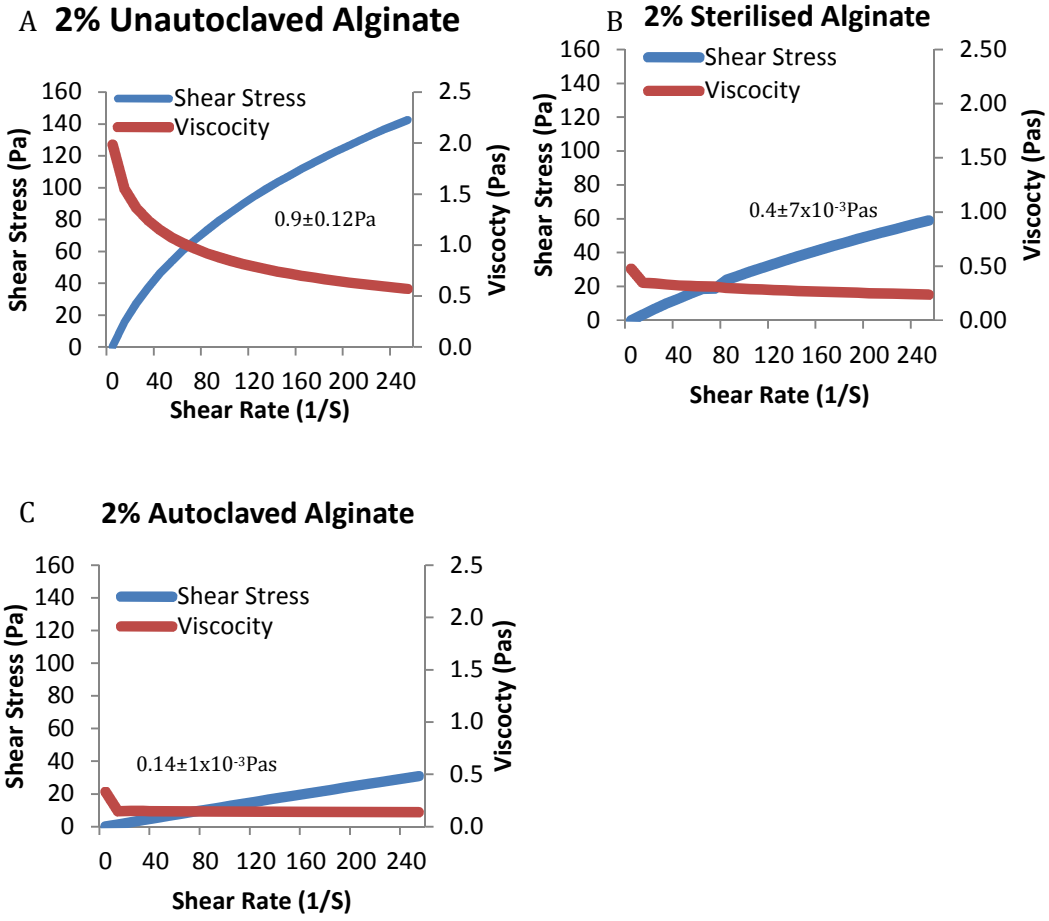

Figure 3-6: Rheometric analysis of sterilising alginate. The viscosity of 2% alginate changes significantly between 10 and 20 minutes at 121°C. A; 2% unautoclaved, unsterilized alginate solution, mean viscosity of 0.9±0.12Pas. B; 2% alginate sterilised at 121°C for 10 minutes, mean viscosity of 0.4±7x10^{-3}Pas. C; 2% alginate autoclaved for 20 minutes at 121°C, mean viscosity of 0.14±1x10^{-3}Pas.

3.4.1.3 Discussion of Alginate Sterilisation

Clearly, the exposure of a 2% alginate solution to heat treatment decreases viscosity of the solution, which has been shown by others[172]. As mentioned in the General Methods Section 2.1.3, sterilisation of alginate is controlled by using specific vessels for certain alginate volumes (100ml in a 250ml glass bottle) to ensure uniform bulk density between experiments, as well as replicating the time the alginate is at 121°C (10 minutes). As a result, a 2% solution of alginate should maintain a viscosity of 0.4±7x10^{-3} Pas to maintain the required encapsulation properties for the BAL system.

3.4.2 Effect of Lyophilisation on Alginate Properties

To confirm that filtration was the primary cause of any alteration in alginate properties, any changes as a result of dissolution, freezing, lyophilisation, and reconstitution were assessed (described in Section 3.3.2). As part of the development of the BAL system, the dissolution of alginic acid salt powder has become standardised to prevent any changes in alginate properties. The effects of freezing alginate have also been previously established as having no effect on alginate properties. Therefore, the viscosities of unfiltered, un-lyophilised, and lyophilised alginate (both un-sterilised) were determined to ensure the lyophilisation had no effect on alginate properties. The mean viscosity of un-lyophilised alginate sample was 0.9±0.12Pas, as compared with 0.9±0.11Pas for lyophilised alginate sample. This was further illustrated in Figure 3-7 where change in shear stress and viscosity with increased shear rate show almost identical curves.

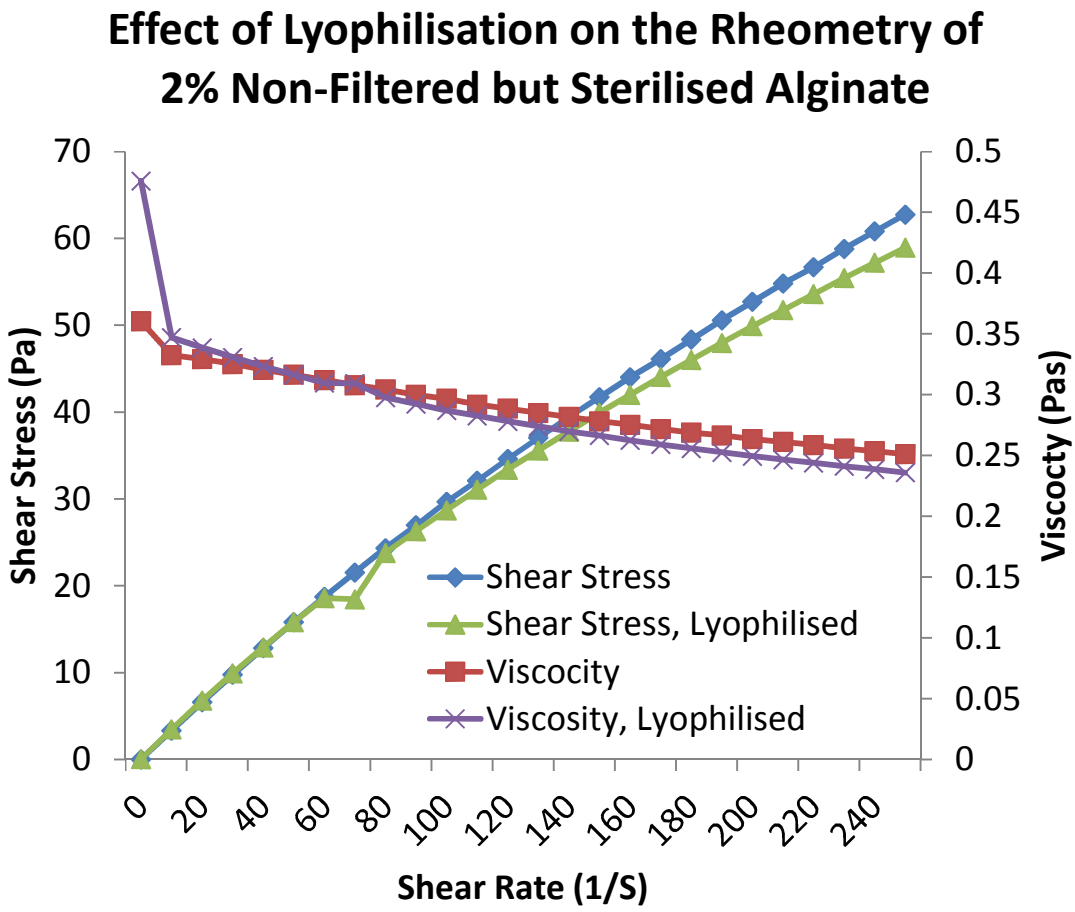

Figure 3-7: The process of shell freezing, lyophilisation, and reconstitution did not change alginate properties. Un-lyophilised, unfiltered and unautoclaved alginate showed a mean viscosity of 0.9±1.2Pas (Figure 3-6A), compared with a mean of 0.9±0.11PAS for Lyophilised, unautoclaved and unfiltered alginate.

3.4.3 Depth Charge Filtration

3.4.3.1 Introduction

As described in Section 1.6.2.3 of the Introduction, Cuno® SP filters are designed for downstream bioprocessing clarification. To make a preliminary assessment of particulate retention capability of depth charged filters, the filtered alginate solution was analysed under phase contrast microscope, as mentioned in Methods Section 3.3.1. With the filtered alginate, cells were encapsulated as described in General Methods Section 2.1.3.2.

3.4.3.2 Results of Alginate Filtration using Cuno® Depth Charged Filters

Alginate filtered through both 10SP filter media (1 – 4.5µm nominal porosity) and 05SP filter media (1.5 – 10µm nominal porosity), showed a modest decrease in particulate size distribution, using a phase contrast microscope (data not shown). Despite this, the properties of alginate were compromised; inhibiting encapsulation as illustrated in Figure 3-8 and Table 3-2 with reduced sphericity. After 2 days of cell culture, beads made with filtered alginate lost integrity and began to dissolve.

Alginate type	Bead Size (µm)	Sphericity
Unfiltered Alginate	**494±27**	**0.25±0.026**
05SP Filtered Alginate	**475±41**	**0.80±0. 14**
10SP Filtered Alginate	**432±87**	**0.92±0.25**

Table 3-2: Sphericity and bead size of encapsulated alginate beads filtered with Cuno® Filters. Bead size and sphericity were altered as a result of filtration.

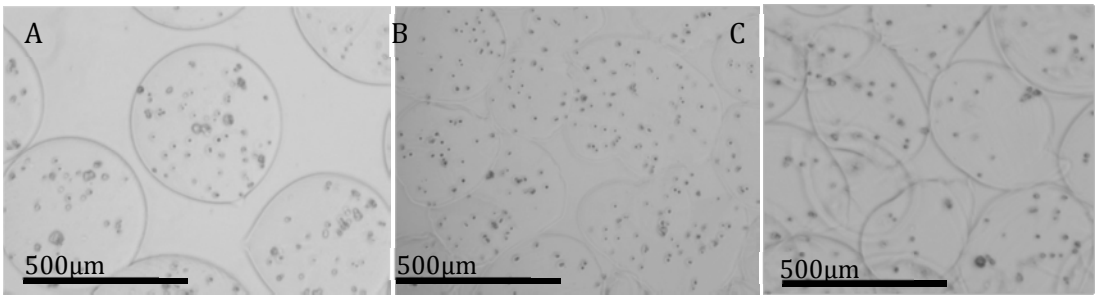

Figure 3-8: HepG2 cells encapsulated with alginate filtered through depth charged filters. A; un-filtered alginate. B; alginate filtered through a 05SP filter. C; alginate filtered through a 10SP filter.

3.4.3.3. Discussion of Cuno® Depth Charged Filtration

As a result of the beads dissolving after only 2 days, possibly due to a drastic alteration in alginate composition, no further experiments were performed with depth charged filters.

3.4.4. Preliminary Sand Filtration

3.4.4.1. Introduction to Preliminary Sand Filtration

In order to assess the ability for sand filtration to remove particulates from alginate, a set of preliminary experiments were performed, by measuring change in sand particulate distribution by phase contrast microscopy, as detailed in Methods Section 3.3.1. Prior to this, size of sand grains used in the filter measured, again using phase contrast microscopy, to ascertain the correct flow rate and sand bed height for filtration, (detailed in Appendix II). Measurements of sand size distribution were made using a standard phase contrast microscope.

Following this, bead integrity was determined by encapsulating alginate without cells and measuring bead size and sphericity. Finally, HepG2 cells were encapsulated in alginate to measure cell function and growth over 12 days.

3.4.4.2. Results of Preliminary Sand Filtration

Measurement of Sand Size

Sand size was measured to determine correct flow rate for filtration. Sand at 129±31µm was categorised as fine sand, whereas sand at 523±114µm was categorised as coarse sand.

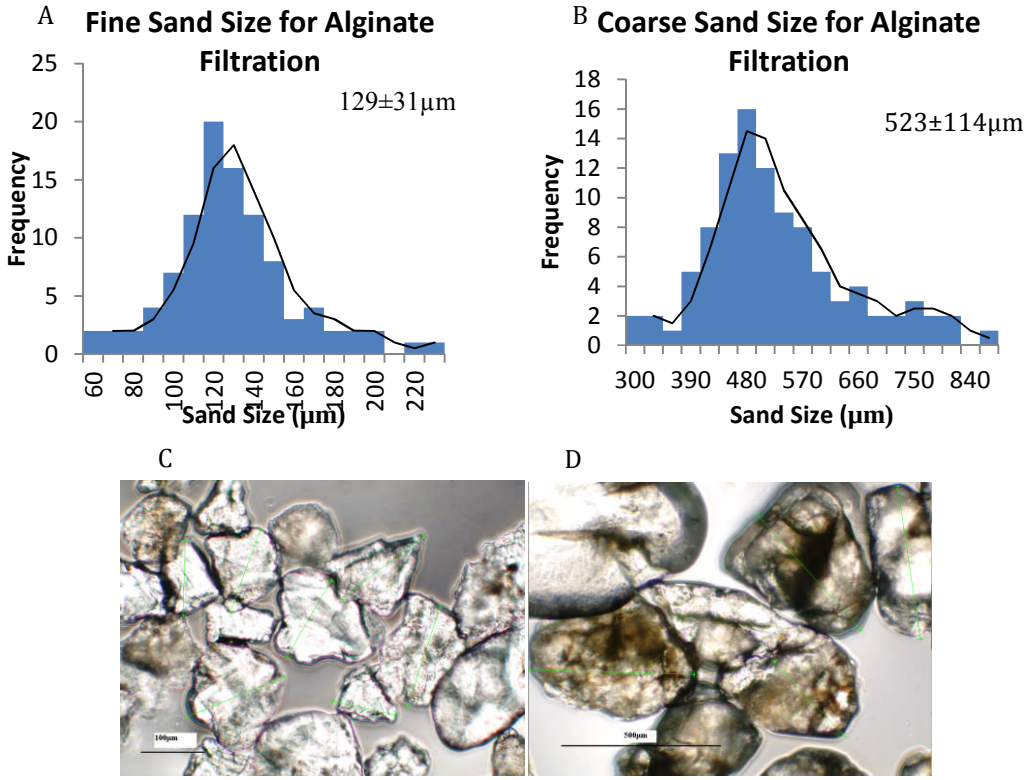

Figure 3-9: Fine and coarse sand sizes, for alginate filtration, were measured using phase contrast microscopy. A; Fine sand size distribution with a mean size of 129±31µm. B; Coarse sand size distribution with a mean size of 523±114µm. C; phase contrast image of 129±31µm sand grains at 40 x magnification. D; phase contrast image of 523±114µm at 20x magnification.

Preliminary Particulate Analysis

Unfiltered alginate showed a mean particulate size of 5±2µm, whereas alginate filtered through coarse sand bed (523±114µm) showed a reduction in particular size distribution to 4±1.5µm. Filtration through a fine sand bed (129±31µm) further decreased particulate size distribution to 3±1µm. This confirmed that particulates were being retained by the sand bed, thereby reducing the larger sized particulates, as illustrated in Figure 3-10.

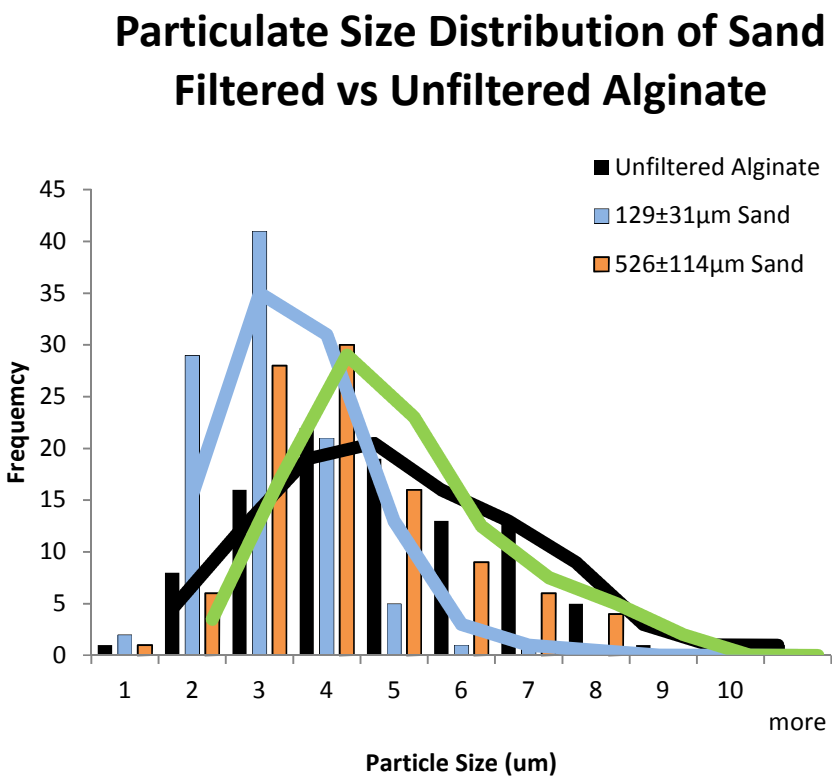

Figure 3-10: Larger particulates were removed from sand filtration, increasing in efficiency with smaller sand size. Unfiltered alginate (Black) was compared with alginate filtered through a fine sand bed (129±31µm) (Red), and alginate filtered through a coarse sand bed (526±114µm) (Green) and unfiltered alginate. Each distribution represents 100 particulates on a single slide. The particulate size distributions were; 5±2µm (unfiltered alginate), 4±1.5µm (526±114µm sand), and 3±1µm (129±31µm Sand). No stats available due to semi quantitative nature of analysis.

Alginate encapsulation without cells

Bead size showed no significant change between unfiltered and filtered alginate (n=100, p=0.1927), as shown in Figure 3-11. However, bead shape was significantly compromised as measured by bead sphericity (p=0.0059, n=100, Figure 3-11).

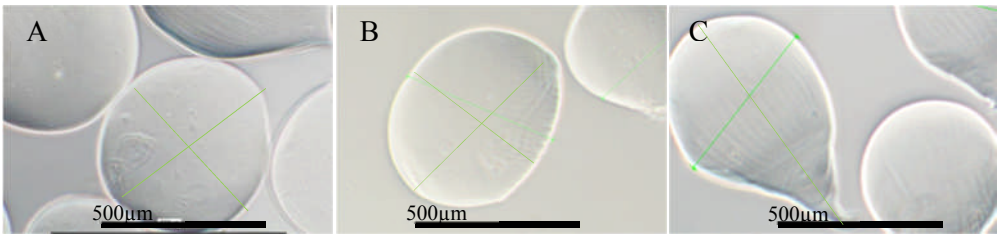

Figure 3-11: Preliminary experiments by encapsulating sand filtered alginate. Encapsulation was successful with all samples, although some changes in bead shape were observed. A; 1% unfiltered alginate. B; 1% alginate filtered through coarse sand bead (526±31µm). C; 1 % alginate filtered through sand bed (129±31µm). Green lines show measurement of diameter to determine bead size and sphericity.

Alginate type	Bead Size (µm)	Sphericity
Unfiltered	**492±17**	**0.12±0.0012**
Coarse sand filtered (526±31µm)	**489±28**	**0.84±0.04**
Fine sand filtered (129±31µm)	**478±25**	**0.90±0.12**

Table 3-3: Bead size shows no significant change due to filtration(n=100, p=0.1927), whereas sphericity as measured by perpendicular diameter measurement shows significant change (n=100 for each sample, *ANOVA* showed: bead size P=0.0059, bead sphericity p=0.1).

The sphericity of beads showed a significant change with filtered alginate, but no change in bead size, as can be seen with the formation of tails illustrated in Figure 3-11 B and C. Despite this, the bead shape was deemed sufficient to assess any changes in cell proliferation and function, as measured by viable cell growth and albumin production, respectively.

Alginate Encapsulation with Cells

HepG2 cells encapsulated in sand filtered alginate and cultured in a static environment over 12 days (Methods 2.1.3), showed no significant difference in viable cell numbers and albumin production (Figure 3-12A and B, ANOVA on viable cell growth n=5, P=0.54; ANOVA on albumin production n=5, P=0.058).

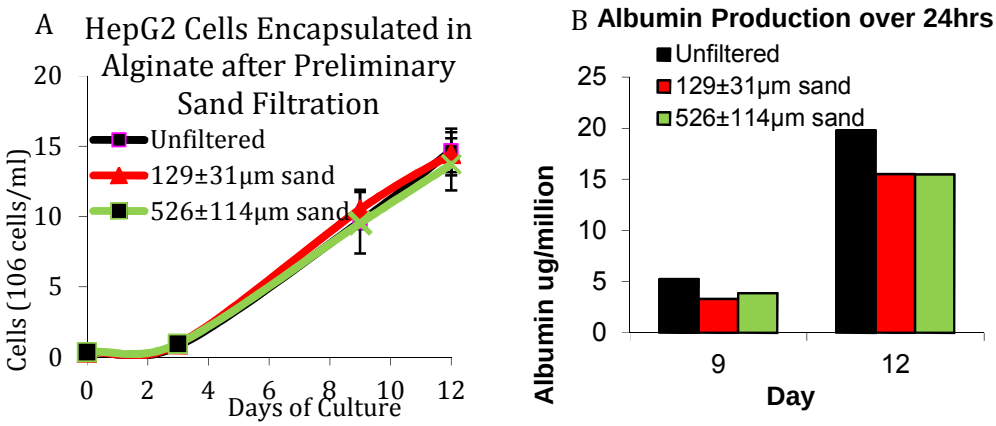

Figure 3-12: Viable cell growth and albumin production were not significantly affected by filtration (ANOVA on viable cell growth n=5, P0.54) (ANOVA on albumin production n=5, P=0.058). Cells were grown over 12 days in static cell culture using Alpha-MEM supplemented media (Methods Section 2.1.3). A; Viable cell number per ml of beads over 12 days B; Albumin production over 24 hours on day 9 and 12.

3.4.4.3 Discussion of Prelimenary Sand Filtration

Preliminary sand filtration experiments showed encouraging results with a reduction in alginate particulate size distribution, with only a modest change in bead integrity and no effect in cell growth or cell function. To increase the efficiency of filtration, the sand size was reduced then the particulate numbers and size were more accurately measured, as detailed in Methods Section 3.3.1.2.

3.4.5 Alginate Filtration with Reduced Sand Size

3.4.5.1 Introduction for Alginate Filtration with Reduced Sand Size

Despite some changes in bead morphology, viable cell number and function showed no significant differences. Therefore, to increase particulate removal efficiency whilst maintaining acceptable bead morphology, smaller sizes of sand were obtained from Sebelco® who provided sand size distribution, as illustrated in Figure 3-13. This data originated from experiments using a series of sieves to trap sand of a particular size range, denoted by "particulate size", also showing the defined blend prepared by Sebelco®.

Three types of sand filtration media were prepared from the sand size analysis in Figure 3-13: RH70, RH110 and a 50:50 mix of RH70 and RH110. The mixed sand was referred to as dual layered filter media and was backwashed a number of times to produce a gradient of sand sizes from larger particulates at the bottom, to smaller at the top of the filtration column. This was performed by the collaborators at the UCL department of Civil Engineering.

Particulates within alginate were then measured by laser light obscuration as detailed in Methods Section 3.3.1.2. Compared to a light microscope, laser light obscuration provided two important improvements: a value of total alginate particulates per ml of sample; as well as a true evaluation of the number smaller alginate particulates, being greater in number than larger particulates (Figure 3-14).

To assess integrity prior to a full cellular encapsulation the filtered alginate was used for encapsulation without cells. However, filtered alginate exhibited extensive bead deformation as shown in Figure 3-15. One possible way to correct for poor bead morphology using filtered alginate could be to increase the concentration of filtered alginate during polymerisation and encapsulation. Ordinarily a 2% concentration was mixed with media/cells to give a 1% final concentration, as described in General Methods Section 2.1.3.2. Alginate concentration was increased prior to encapsulation with RH110 and RH70 sand filtered alginate (Figure 3-16).

Optimal alginate concentration was determined by observing restored alginate bead integrity in terms of sphericity and bead diameter, alginate was filtered through the dual layered filter consisting of both RH110 and RH70 sand, (described in Methods Section 3.3.5). By combining Sibelco® RH70 and RH110, filter media the particulate retention may be further optimised as described in Section 3.3.5. Both the RH110 and RH70 were mixed at a ratio of 50:50 to form a single new sand blend, for alginate filtration as before.

Alginate filtered with RH110 and dual layered reduced particulate levels with the greatest efficiency (Figure 3-19 and 3-20). Therefore, this alginate was used to encapsulate HepG2 cells to measure growth and function.

Finally, rheometric analysis of the three sand filtered alginate types was used to determine the changes in bead integrity in terms of viscosity as a measure of the extent of alginate compositional change (Figure 3-21).

Results Alginate Filtration with Reduced Sand Size

The RH110 sand showed a mean sand size distribution of 102 ±30µm, whereas RH70 Sand showed a mean size distribution of 149±56µm, when analysed by Sibelco®

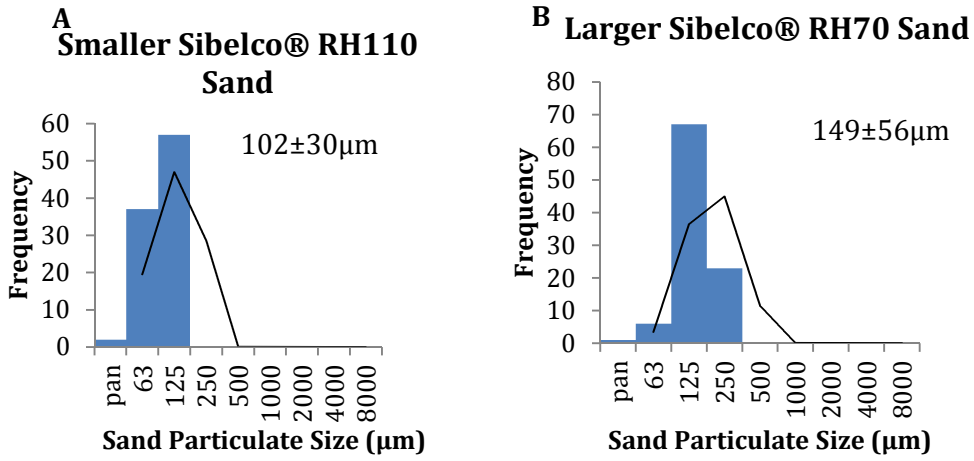

Figure 3-13: Sibelco® provided defined sand blends by using a series of sieves to trap the sand as denoted by particulate size. A; RH110 sand with a mean size distribution of 149±56µm. B; RH70 Sand with a mean size distribution of 102±30µm.

Particulate Analysis by Light Obscuration

Particulate analysis of alginate filtered with Sibelco® sand showed a reduction in particulate number with both RH70 and RH110 sand, with the finer RH110 showing the greatest particulate removal efficiency, as illustrated in Figure 3-14.

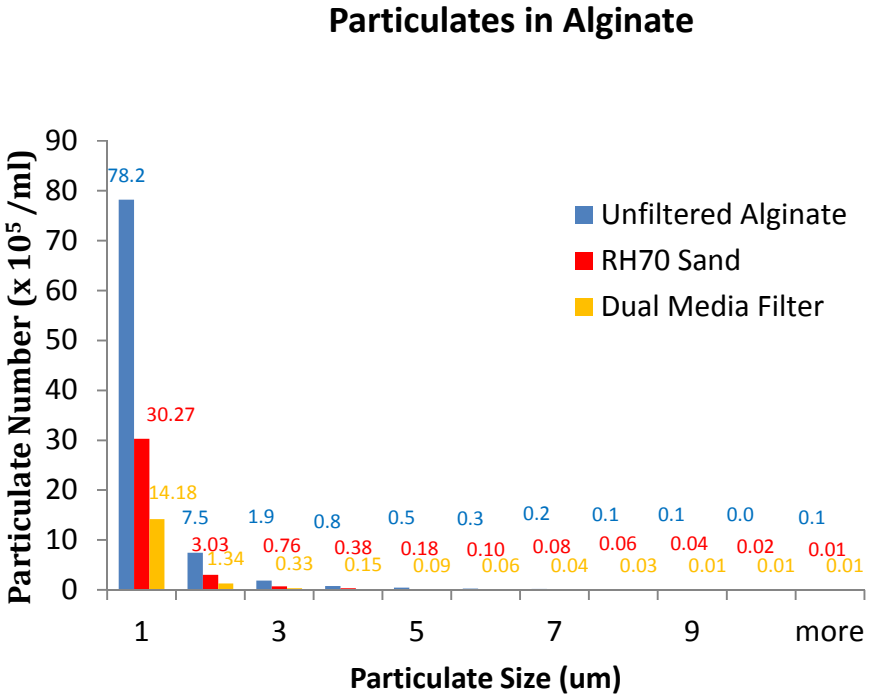

Figure 3-14: Particulate size and frequency in RH70 and RH110 sand filtered alginate. Particulate numbers reduced in sand filtered alginate compared with unfiltered alginate, as measured by the GmbH PMAS SBSS particulate counter by laser light obscuration. RH110 sand composed by larger grains showed a lower level of reduction compared with the finer RH70 sand. Numbers on the figure represent the numbers of particulates x10^5 for clarity.

Filtered Alginate Encapsulation without Cells

As a result of deformation to alginate beads illustrated in Figure 3-15, sphericity and bead size were not measured. Unfortunately, the beads in Figure 3-15 B and C were deemed unsuitable for cellular encapsulation.

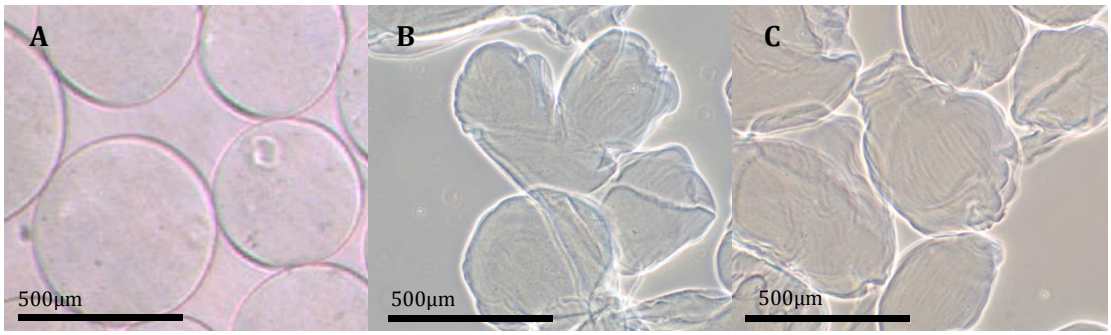

Figure 3-15: Bead integrity with RH70 and RH110 sand filtered alginate. Bead integrity was significantly reduced with RH70 and RH110 sand filtration. Beads were encapsulated without cells to assess integrity prior to full cellular encapsulation. Unfortunately, beads were deemed unsuitable for cellular encapsulation. A; Unfiltered alginate. B; RH70 sand. C; RH110 sand.

Increasing Alginate Concentration to Restore Bead Morphology

Increasing alginate concentration increases the viscosity of the solution as illustrated in Figure 3-16, using unfiltered alginate.

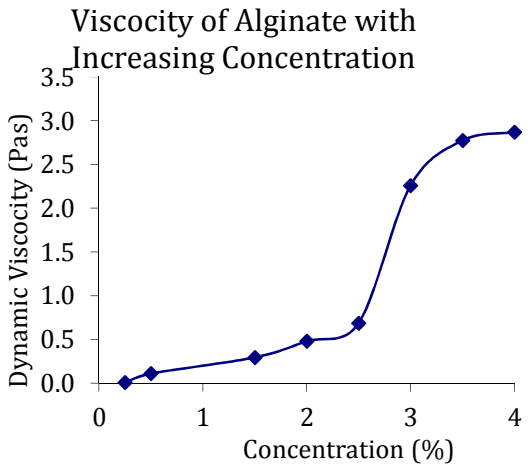

Figure 3-16: Change in alginate viscosity with increased concentration. As alginate concentration was increased, viscosity increases in a non-linear manner, as measured by rheometry (detailed in Methods Section 3.3.3), with increasing unfiltered alginate concentration. This used unfiltered alginate.

A series of increased alginate concentrations were used to encapsulate alginate without cells; analysing bead size and sphericity (Table 3-4), until at 1.875% final concentration (3.75% prior to encapsulation), bead morphology was restored (Figure 3-17). Bead size and sphericity showed no significant difference, analysing by ANOVA, n=100 p=0.25 with bead size, and sphericity of n=100 p=0.084.

After encapsulation, the viscosity of 3.75% filtered alginate was 0.98±0.147Pa (RH110) and 1.12±0.26Pa (RH70) filtered alginate.

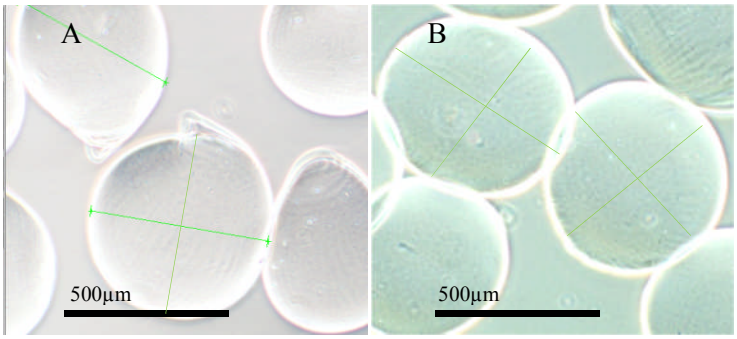

Figure 3-17: Bead morphology after increasing alginate concentration. Alginate encapsulated at 1.875% final concentrations (normally 1%), reconstituting dry alginate to 3.75% alginate for encapsulation.

Alginate type	Bead Size (µm)	Sphericity
Unfiltered	498±26	$0.12\pm1.2x10^{-3}$
Smaller RH110 Sand	481±13	0.22±0.011
Larger RH70 Sand	485±10	0.36±0.04

Table 3-4: Bead morphology was restored by increasing alginate concentration to 1.875% alginate, as measured by bead size and sphericity (n=100 for each sample, ANOVA showed: bead size P=0.25, bead sphericity p=0.084).

Dual Layered Sand Filtration

Particulates and Bead Integrity

Filtration with the dual media reduced particulate levels, compared with unfiltered alginate, and further improved removal efficiency relative to RH110 sand, as illustrated in Figure 3-19. However, bead integrity was compromised as a result of filtration through the dual layered sand (Figure 3-18A). Despite this, increasing the alginate concentration to 1.875% (final concentration, from 3.75% reconstitution) restored bead morphology, similarly to RH70 and RH110 alginate filtrates. Mean bead size was restored to 479±17µm and sphericity to $0.22\pm4.2x10^{-3}$, showing no significant difference with unfiltered beads (*t*-test, bead size n=100, p=0. 32).

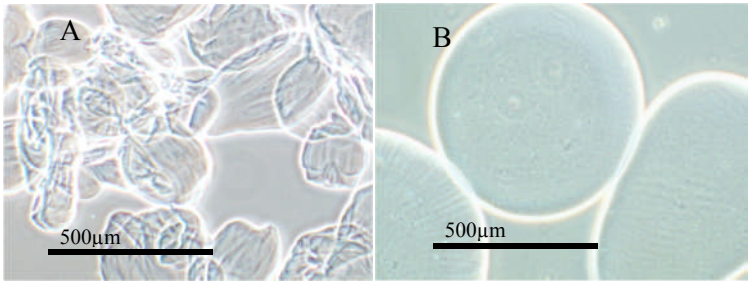

Figure 3-18: Bead integrity was again compromised by encapsulating without cells at 1% final alginate concentration (reconstituted to 2%), but restored after increasing alginate concentration to 1.875% (reconstituted at 3.75%). A; Alginate filtered through the dual media filter. B; Dual media filtered alginate shows no significant difference in bead size or sphericity compared to unfiltered alginate (n=100, p=0.32 bead size; n=100, p=0.12 for P sphericity).

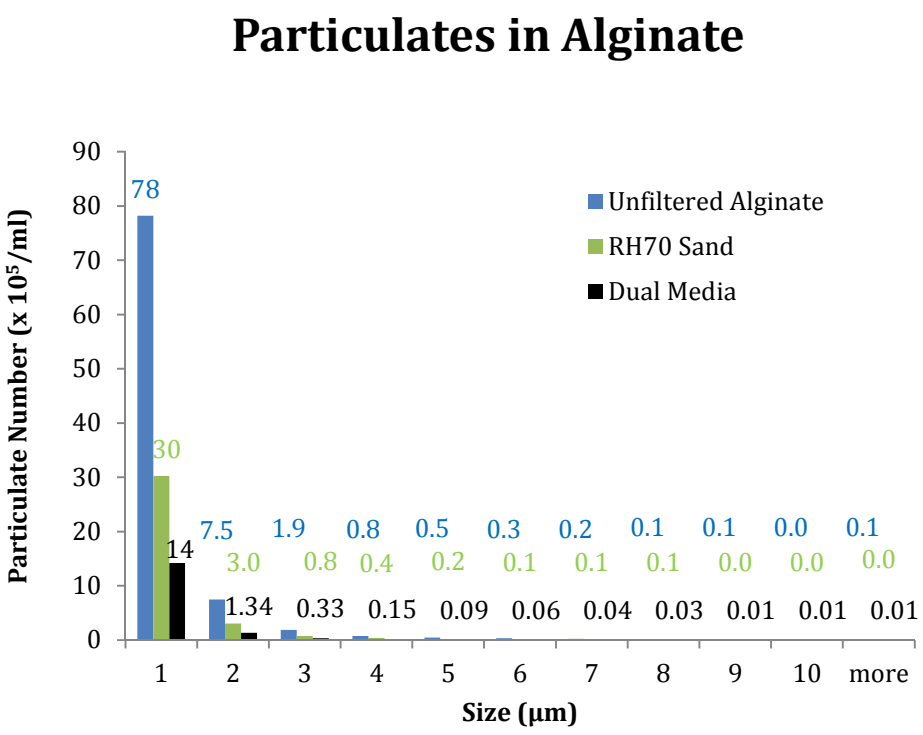

Figure 3-19: Alginate particulate content was reduced by dual sand media filtration, compared with unfiltered and RH70 filtered sand. Numbers above the x-axis were included for clarity, reflecting particulate numbers x10^5 for different alginate filtration states. Numbers above bars were added for clarity, signifying the particulate number x10^5/ml.

Cell Number and Function

Encapsulation of HepG2 cells in alginate filtered with RH70 and dual media showed a significant difference in viable cell growth, shown in Figure 3-20A (ANOVA n=5, p=0.0012), despite no significant difference in albumin production, as illustrated in Figure 3-20 B (ANOVA n=5, p=0.38). Having restored bead morphology by increasing alginate concentration, cell growth was inhibited.

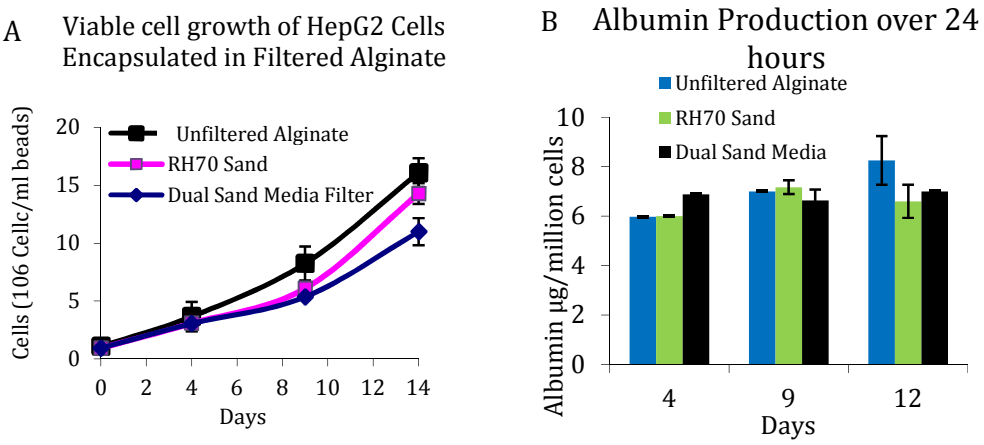

Figure 3-20: HepG2 growth and Cell function in sand filtered alginate encapsulated at 1.875%. Cell growth was significantly affected by alginate filtration (ANOVA n=5, p=0.0012), whereas albumin production was unaffected by alginate filtration (ANOVA n=5, p=0.38). A; Viable cell growth over 14 days of static culture in Alpha MEM media. B; Albumin production n days 4, 9, and 12.

Rheometric Analysis of Sand Filtered Alginate.

Rheometry of Alginate Filtered with RH110 and RH70

Comparing viscosity of unfiltered alginate with filtered alginates showed differing viscosities, possibly resulting from compositional changes. Filtered alginate exhibited more Newtonian fluid characteristics, where shear rate had little effect on viscosity, as illustrated in Figure 3-21. Alginate filtered through the smaller RH110 sand showed a mean viscosity of $3.6x10^{-2} \pm 9.1x10^{-6}$Pas, similar to alginate filtered through the larger RH70 sand with mean viscosity of $0.0492 \pm 7.3x10^{-4}$Pas. Unfiltered alginate showed a viscosity of 0.4±0.007Pas, exhibiting non-Newtonian fluid characteristics as shown in Figure 3-6B.

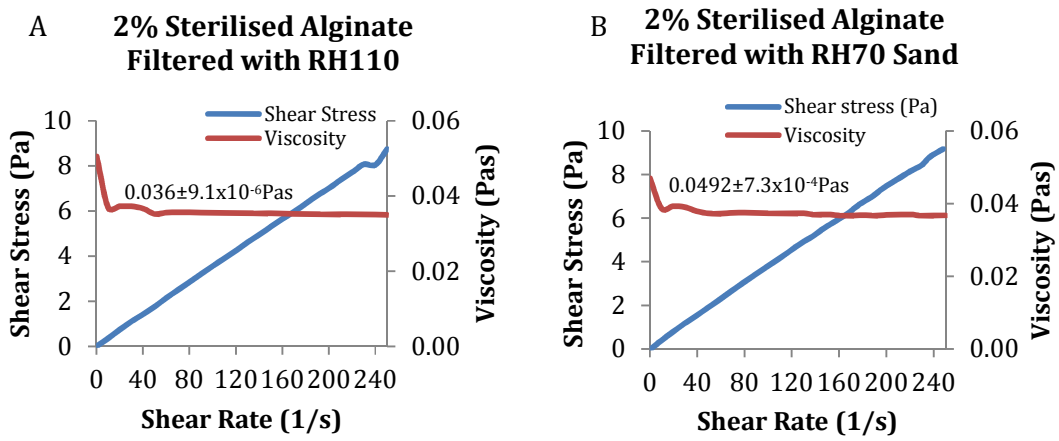

Figure 3-21: Filtered alginate had reduced viscosity exhibiting Newtonian fluid characteristics compared with unfiltered alginate (Figure 3-6B). A; 2% alginate filtered with RH110 sand, mean viscosity $3.6x10^{-2}$ ± $9.6x10^{-6}$Pas. B; 2% alginate filtered with RH70 sand mean viscosity of $3.78±4.7x10^{-5}$Pas.

Rheometry of Dual layered samples

The viscosity of 2% alginate filtered through the dual layered filter media was reduced from 0.4±0.007Pas for unfiltered sterilised alginate to $0.05±1.3x10^{-4}$Pas for dual layered filtered alginate, shown in Figure 3-22. This demonstrated both lower mean viscosity as well as a reduced variance, indicating reduction in non-Newtonian fluid characteristics due to lower viscosity. By increasing the alginate concentration, the viscosity of dual sand layered alginate was increased from $0.05±1.3x10^{-4}$Pas to 0.5±0.009Pas.

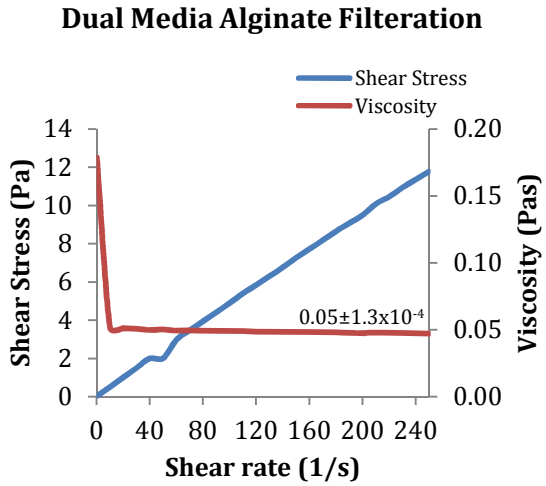

Figure 3-22: Filtration through the dual layered media caused a reduction in viscosity to exhibit Newtonian fluid characteristics. Mean viscosity of $0.05±1.3x10^{-4}$Pas excluding the first 10 RPS increase in shear rate.

3.4.5.3 Discussion of Alginate Filtration by Reduced Sand Size

Increasing the filtration efficiency by reducing sand size or using the dual layered sand filter resulted in bead integrity being severely compromised (Figure 3-15 and Figure 3-

18). A reduction in alginate viscosity confirmed this, with an 8-fold and an 11-fold reduction, from 0.4±0.007Pas (ideal alginate viscosity) to $0.05\pm1.3\times10^{-4}$ and $0.036\pm9.1\times10^{-6}$Pas, for dual layered and RH110 sand filtration, respectively. This reduction in viscosity probably did not affect the bead formation during transit between the encapsulator nozzle and the polymerisation buffer, but distorting upon impact with the surface tension of the polymerisation buffer, despite pluronic acid being added to reduce this effect.

Mitigating the loss in viscosity by increasing alginate concentration to1.875% (3.75% alginate concentration for reconstitution) during encapsulation restored bead integrity, as measured by bead morphology (sphericity and size). Although, the limitations of viscosity and beads morphology analyses were revealed when the perceived bead integrity was improved, but the alginate viscosity increased from 0.4±0.007Pa to 0.5±0.009Pa, 0.98±0.147Pa, and 1.12±0.26Pa for dual sand, RH110 sand and RH70 sand filtered alginate, respectively. As a result, cell growth was compromised as illustrated in Figure 3-17 and Figure 3-20; if the alginate encapsulation concentration was reduced to below 1.875% significant bead deformation would occur. Consequently, a balance could not be reached between sufficient bead integrity, to withstand fluidisation in a BAL growth and treatment phase, and achieving the required viscosity of 0.4±0.007Pa. Potential causes of the reduction in cell growth as a result of higher alginate concentration could have been an increase in internal alginate cross-linking physically inhibiting cell growth. Alternatively, alginate bead porosity has been shown to decrease with increased alginate concentration, therefore inhibiting mass transfer and indirectly reducing cell growth[173], although with protein levels unaffected by increasing alginate concentration, this seems unlikely.

3.4.6 Gas Solid Cyclonic Filtration of Dry Alginate

3.4.6.1 Introduction

Filtering alginate whilst in solution caused changes in viscosity coupled with reduction in cell growth. Therefore, another approach was taken in the form of filtering alginate in dry state by gas solid cyclonic filtration. This approach can be visualised as akin to the ancient process of "winnowing" to purify wheat grains by removing soil particles and other debris. Powder in dry state is passed into the top of a cylinder contained within it an upward cyclonic air flow. Depending on the speed of the flow and height of the cylinder, smaller particles would escape at the top quicker than larger particles (otherwise drop out of the bottom) as illustrated in Figure 3-23. It has been extensively used in many industrial applications from plastic fragment separation to dust removal from gaslines and could provide a means of fractionating alginate particles from pure alginate powder; as a result, they are often industrial sized machines with a high throughput capability[174]. The Air filtration was performed by The Department of Civil Engineering at the University of Miskolc, Hungary.

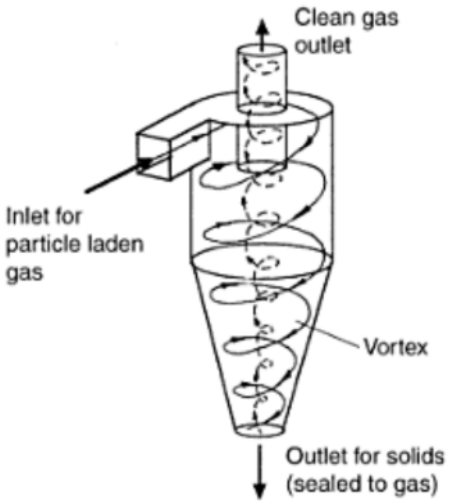

Figure 3-23: Gas solid cyclonic filtration unit. An upward cyclone separates dry particle travelling in a downward direction by size according to the upward thrust of the air and the weight of the particulates.

With the alginate obtained from this type of filtration, the same rheometric, and cell encapsulation studies were performed to determine effect of bead integrity, composition of alginate and effect of growth and function of the beads.

3.4.6.2 Results of Particulates Removal by Gas solid Cyclonic Filtration of Alginate

Gas solid cyclonic filtration reduced particulates within alginate to approximately the same levels as dual layered media filtration as illustrated in Figure 3-24.

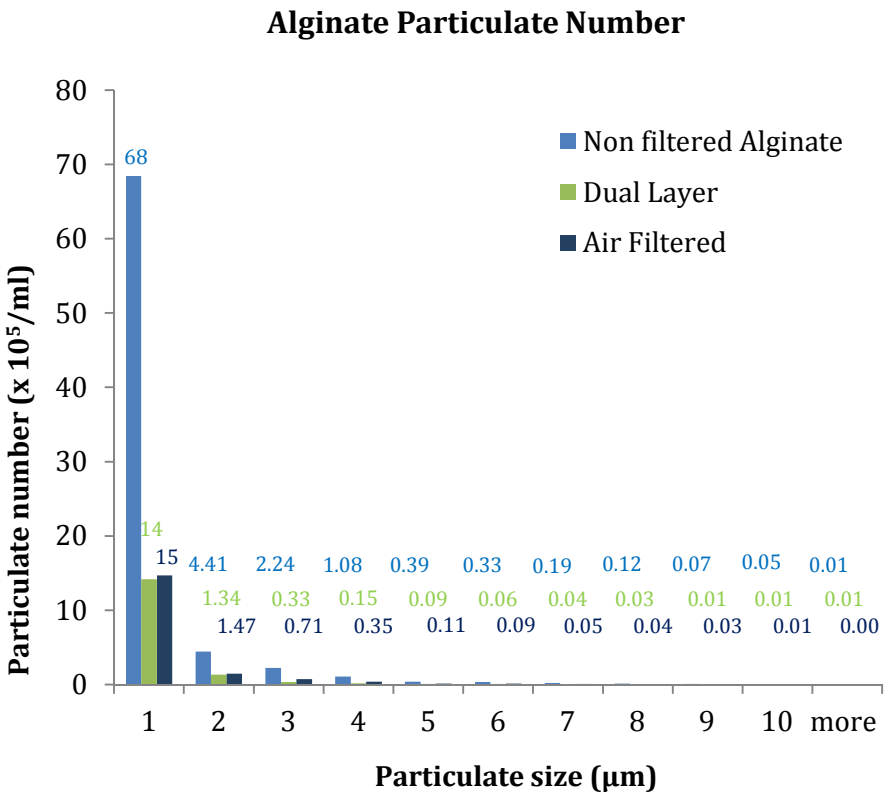

Figure 3-24: Gas solid cyclonic filtration of alginate reduced particulates to similar levels as dual media sand filtration, compared with unfiltered alginate. Values were included on the graph to represent particulate numbers x10^5, for clarity.

Rheometry of Air filtered samples

Unlike alginate filtered after reconstitution, gas solid cyclonic filtration did not change the viscosity of reconstituted alginate compared with unfiltered alginate, shown in Figure 3-25 (mean unfiltered at 0.291±8.6x10^{-4}Pas, vs. air filtered at 0.288±2.6x10^{-3}Pas).

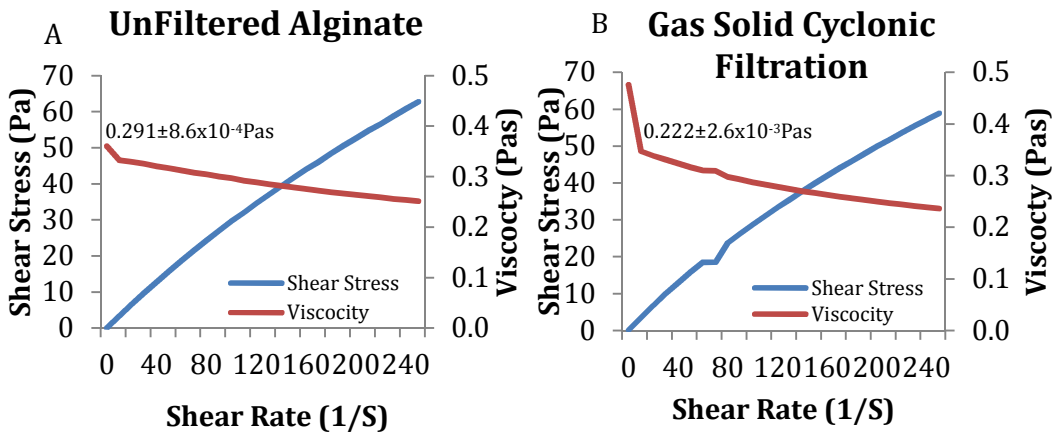

Figure 3-25: Gas solid cyclonic filtered and unfiltered alginate, reconstituted to 2% Viscosity maintained the same viscosity. A: mean unfiltered alginate viscosity at 0.291±8.6x10-4Pas. B; air filtered viscosity at 0.222±2.6x10-3Pas.

Encapsulation with HepG2 Cells of Air Filtered Alginate

Viable Cell Growth

Viable cell numbers were unaffected by gas solid cyclonic filtration of alginate, (two tailed t-test n=5, p=0.57).

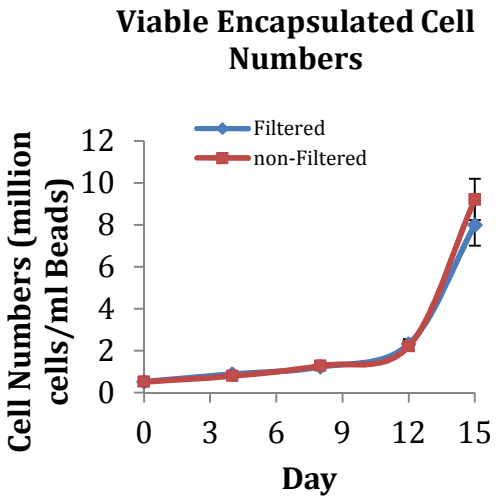

Figure 3-26: No significant difference in viable HepG2 cells numbers between unfiltered and gas solid cyclonic filtered alginate. (2 tailed t-test n=5, P=0.57)

Function of Cells Encapsulated

Cell function was also unaffected by alginate filtration as shown in Figure 3-27; four HepG2 specific proteins, albumin, AFP (α-Fetoprotein) and α-1-antitrypsin, and fibrinogen assayed by ELISA, showed no significant changes to protein production between samples on each day.

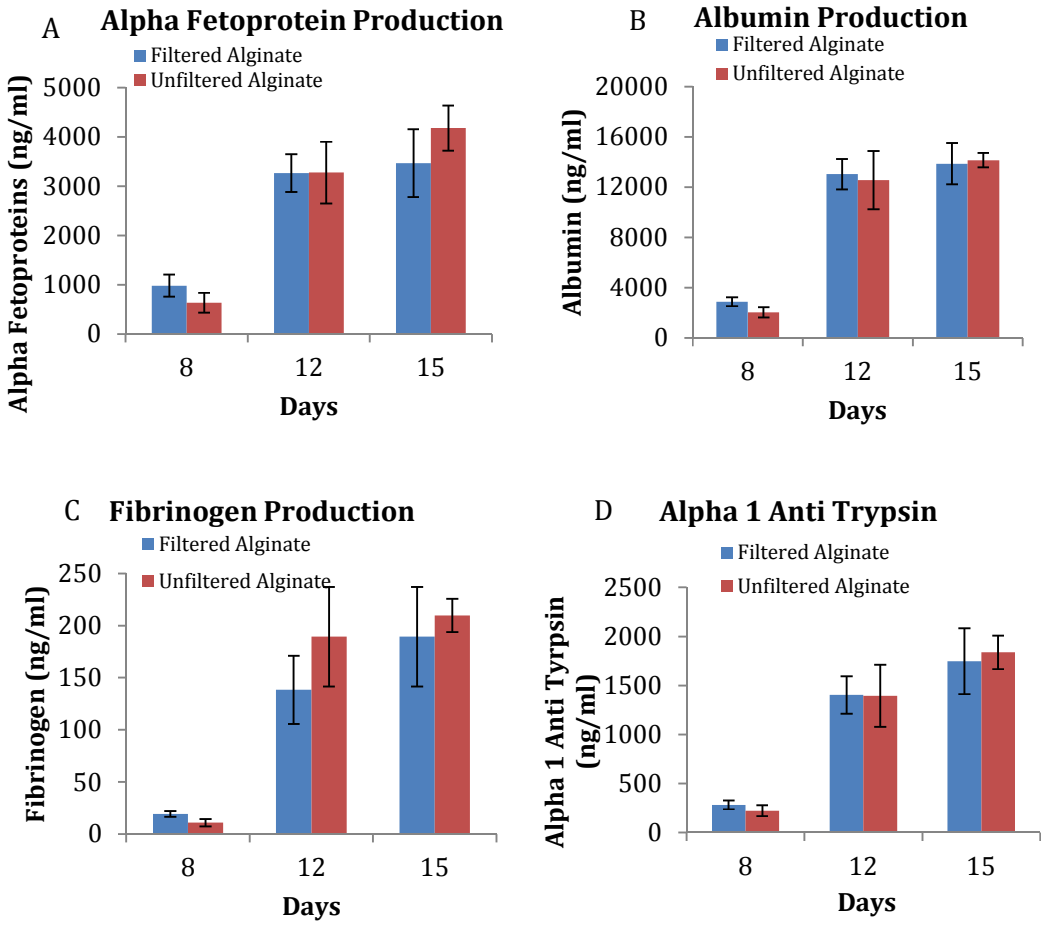

Figure 3-27: Gas solid cyclonic filtration did not significantly affect production of four proteins expressed in encapsulated HepG2 cells, over 24 hours, in static culture on days 8, 12 and 15 (Methods Section 2.1.2) as measured by ELISA (Methods Section 2.5). A; Alpha fetoprotein production (n=5, P=0.47). B; Albumin Production (n= 5, p=0.14). C; Fibrinogen Production (n=5, p=0.42). D; Alpha 1 Anti Trypsin (n=5, p=0.095).

3.3.4 Comparison of Alginate Particulates in Injectables and Air Filtered Alginate

As illustrated in Table 3-5, the reduction of particulate levels had been achieved by gas solid cyclonic filtration in comparison to unfiltered alginate. However, particulate levels still remain higher than the acceptable range for parenterals.

Pharmacopeia source	Particle size (μm)	Particle limit in (10^5/ml)	Particulates in Air filtered alginate (10^5/ml)	Particulates in Unfiltered alginate (10^5/ml)
USA	2	0.1	16.47	72.41
UK	5	0.01	1.06	3.71
Australia	10	0.005	0.32	0.76
	20	0.0005	0	0.01
	25	0.0005	0	0.01

Table 3-5: Alginate particulates are compliant for injectables for particulates of 10, 20 and 25μm, but approximately 10 times the acceptable levels for 2 and 5 μm particulate sizes.

3.5 Conclusions of Alginate Filtration Findings

The development of a standardised HepG2 cell encapsulation protocol, with analytical grade alginate, has produced robust alginate beads capable of withstanding 12 days of cell culture (BAL growth Phase), and 8 hours of perfusion with plasma from an ALF patient (BAL treatment phase). A central feature of the protocol is the sterilisation step (sterilised by autoclaving for 10 minutes) causing a 2.25-fold reduction in alginate viscosity, producing alginate with 0.4±0.007Pas mean viscosity (with the variance illustrating the change in viscosity with increased shear stress). For particulate reduction and other future purification methods, the central tenet will be the maintenance of these alginate bead properties.

Throughout the numerous steps of alginate reconstitution and lyophilisation only direct filtration introduced a change in viscosity, suggesting either a decrease in overall alginate polymer concentration or the selective retention of G uronic acid chains over M and MG by the sand, that have been shown to be important in alginate viscosity[162]. If a reduction in alginate concentration was the cause, increasing alginate concentration at encapsulation should have reversed the reduction in bead integrity. Alternatively, modification of alginate polymer chain length has been attributed to changes in alginate viscosity during purification[87].These purification protocols, often lengthy; involve a series of acetic acid and ethanol extraction and dialysis steps, which bring about in changes to alginate chain lengths[86,175-178]. The stability of alginate solutions (not cross-linked) over much longer periods than the 2-4 days taken for sand filtration has been established in diH_2O at pH 7-9 for more than 1 month[179]. Furthermore, the inert nature of sand is important for the more common application in water purification[128], so it is unlikely to have catalysed the shortening of alginate polymer chains. Chain shortening has only been reported when storing in diH_2O at pH 4.5 as a consequence of acid hydrolysis, the pH during alginate filtration was always maintained at pH 7.4 with HEPES buffer. Others have attributed changes to alginate viscosity when purifying pharmaceutical grade alginate to the removal of constituent contaminants, specifically protein (COOH group of particular importance), showing an inverse relationship between viscosity and protein content[87,175,180,181]. The nominal porosity of the sand filter media would be too large to prevent protein transit, as illustrated in Figure 3-4, therefore supporting the original idea that preferential removal of M and MG over G uronic acid chains caused the changes to viscosity.

Regardless of gas solid cyclonic filtration being at the preliminary stages of development, a clear potential for removing particulates was shown. For the study to be widened, analytical methods to measure and standardise alginate contamination levels and M/G composition need to be incorporated for the current analytical grade alginate. In addition to this extraction and chemical analysis of particulates may aid the air filtration optimisation. The most likely origin

of the alginate particulates is residual fibrous cellulose from extraction[182], which can be confirmed using the Updegraff acetic acid colorimetric assay[181].

In addition to characterising alginate particulates, other contaminants could be analysed using X-ray photoelectronic spectroscopy providing all alginate molecular components including elemental composition and electronic state of the surface 1-10nm of an alginate sample[87]. This would include evaluation of heavy metal content. In addition to this, others have accurately measured total residual protein contamination derived from the source, using fluorescent compounds, which bind amine groups in the primary structure of the protein, such as the amine group at the end[175]. An optimised version of the Pierce BCA (bicinchoninic acid) protein assay, named the Micro BCA, has been used to measure protein contaminants, but is less sensitive[183]. The bulk properties of the alginate, against which all purification protocols should be measured, could use two central techniques: measurement of viscosity to provide a valuable quality control tool for final bead shape[87]; C^{13}-NMR to accurately quantify specific M, G and MG composition in filtered alginate[177]. The cumulative information of these techniques will evaluate the composition of analytical grade alginate in terms of both particulate and molecular scale contaminants, as well as vital compositional information.

Most groups who have in-house alginate purification methods require improvement in biocompatibility for encapsulated cell transplantation, often reporting changes to alginate properties as a consequence of lengthy complicated purification techniques[86,175-178]. The Liver Group BAL has two distinct advantages over alginate transplantation: the BAL is not directly in contact with cellular components of the immune system, so some of the biocompatibility issues may be alleviated; the treatment time is for 8 hours, as opposed to up to 12 months for some alginate encapsulated cell transplantations[176]. As a result, if the composition and contaminants of alginate can be controlled and shown to be biocompatible, regulatory compliance may be attainable despite the presence of higher contaminants compared with other biomedical applications.

The Next Chapter will focus on detection methods for DNA and endotoxin in the context of the BAL system, with specific attention to validating the protocols where appropriate for future use for as analytical methods.

Chapter 4 Quantification of BAL Biological Contaminants

This Chapter details different methods for DNA and Endotoxin detection in human plasma, for use with the Liver Group BAL system.

4. Quantification of BAL Biological Contaminants

4.1 Introduction

Biological contaminants within the BAL system, will originate primarily from the biomass in the form of cell debris DNA and endotoxin from the system. Although much more of the endotoxin is likely to originate from the patient[119,184]. In order to develop methods of removing such contaminants methods were developed to quantify them in the BAL context.

4.1.1 Detection of Cell Debris

The importance of preventing foreign cell fragments from passing into a patient has been clearly defined, cellular debris in the form of cell membranes as well as fractions of cell organelles, have been shown to cause an immune response[185]. Therefore, avoiding HepG2 cell debris from entering the patient during BAL treatment has become an important stipulation, in terms of asserting the safety and efficacy of the system and in gaining regulatory market approval[77,186]. Currently the large scale BAL system utilises a 200µm meshes prevents transit of alginate bead and large alginate and cellular fragments from the fluidised bed to the patient. With the use of charged depth filters described in later chapters, cell fragments down to 0.3µm should be retained by the filter[187,188].

4.1.2 DNA Contamination

4.1.2.1. Detecting DNA in BAL Plasma

For the purposes of detecting DNA in the BAL system, QPCR can be used to determine total DNA levels. Two potential approaches for quantitative polymerase chain reaction of genomic DNA (qPCR) analysis in human plasma could be used: detecting DNA based on primers specific for a gene locus, as used to detect *Tuberculosis* by primers specific for the MBP62[107,189]; or targeting primers for repeating genetic elements such as Alu repeats[148]. If the principle of QPCR using a primer specific to a particular gene *locus* is applied to measuring total DNA, sensitivity may be compromised as only DNA with the specific gene will be amplified. Alternatively, detecting repeating genetic elements are found in large numbers across the genome increasing the probability of a DNA fragment containing the element, such as Alu repeats.

Another approach could utilise the ability for fluorescent molecules such as Hoechst dye or Picogreen, to indiscriminately bind DNA <200bp and <500bp, respectively. It may provide greater accuracy, as DNA amplification by QPCR requires the presence of a consensus sequence[94,148,190].

4.1.2.2. Alu Repeat QPCR to Determine DNA Integrity

A way of quantifying DNA in plasma for diagnostic purposes was developed by Umetani et al. who measured cfcDNA (cell free circulating DNA) for diagnosis of Colorectal or Periampullary Cancers, both associated with necrotic cell death[148]. The concentration of cfcDNA from apoptotic and necrotic cell death were determined in separate reactions, to provide a measure of necrosis from the carcinoma. The ratio between background apoptotic cfcDNA and carcinoma necrotic cfcDNA was referred to as DNA integrity reflecting the ratio between the two and was calculated using Equation 4-1:

Equation 4-1: $\text{DNA integrity} = Q_{247} / Q_{115}$

Where DNA integrity (dimensionless) is equal to DNA concentration of DNA from necrotic cell death, Q_{247} (ng/ml) divided by total DNA, Q_{115} (ng/ml).

Total DNA was determined using a primer set specific for a 115bp stretch of the Alu repeat consensus sequence, amplifying DNA from apoptotic cell death containing the 115bp sequence (apoptosis truncating DNA to 180-200bp in length). DNA from necrotic cell death (truncated to >300bp in length) was amplified using a primer set specific for a 247bp stretch of the Alu consensus sequence, only binding to DNA containing the entire sequence. Equation 4-1 reflects the ratio between these concentrations.

The Alu repeat Gene

The primers were based on Alu tandem repeated genetic elements, making up around 10.8% of the human genome numbering over 1,179,211 copies in total. Alu repeats are found ubiquitously across the primate genomes as illustrated in Figure 4-1A[191]. Alu genetic elements comprise three evolutionarily based subunits all with a 282bp conserved consensus sequence, although 6 other abundant subfamilies also exist[191-197].

Figure 4-1: Alu repeat repetitive elements are found ubiquitously across the primate genome originating from three main evolutionary subfamilies. A; Analysis of the human genome project sequence by bioinformatics PERL programme showed Alu repeat sequences ubiquitously across the genome. B; Analysis using the same program revealed the three main subfamilies and further subdivisions of Alu repeat family. Obtained from Grover et.al[191].

4.1.2.3 QPCR method Validation

Choosing the appropriate validation methods for an analytical method depends upon the specific requirements of the situation. Further discussion regarding the wider implications of specific validation criteria and requirements for regulatory compliance will be made in the Discussion Chapters. For the purposes of creating a QPCR method, which is fit for purpose, reliable and robust in detecting DNA in human plasma for pre-clinical and clinical trials, the focus was on precision, DNA recovery, robustness, linearity, and sensitivity.

Precision is defined as being the closeness of agreement between independent measurements, obtained under stipulated conditions[198]. It is important that the samples go through the entire testing procedure (from collection, purification, and analysis) performed on identical samples, providing measure of sample spread and the highest and lowest points. Crucially the precision of data does not reflect trueness, which is the closeness of data in relation to a reference standard. Measurement of precision relies on the coefficient of variance (CV), defined by the standard deviation divided by the mean of the results expressed as a percentage. The greater the CV figure is, the lower the constitutive precision of the results are[199].

A measure of precision utilises repeatability analysis, which uses the same analyst, instrument laboratory, over a short period to show the constitutive error within the method, expressing as precision. As a result a measure of random variability in the more specific manner is obtained.

A measure of precision (used in this chapter) was reproducibility that reflects variation using the identical method and samples under different conditions. This measure of precision was evaluated for two reasons: to confirm the effects of changing the QPCR conditions; to provide information for further validation if the method is transferred to a certified analytical laboratory.

Recovery was one of the most important parameters measured due to the relatively low levels of DNA in large volumes of plasma. If DNA loss was incurred from purification or extraction of the sample, then the method may not provide the sensitivity necessary for regulatory compliance[103]. Recovery analysis usually involves the addition of an analyte to a representative sample put through the purification and analytical process, for evaluation against the original amount added, expressed as a percentage.

Sensitivity is usually defined as the lowest level of analyte that can be measured, but can vary depending on the field in which the term is applied[199]. In the context of the QPCR, the sensitivity is defined as the lowest quantifiable DNA concentration or the limit of quantification (LoQ). Therefore the lowest DNA concentration that could yield a meaningful repeatable result was used.

4.1.3 Endotoxin Contamination

Quantification of endotoxin in plasma provides many challenges; many of the components of plasma will inhibit the reaction, including heparin, divalent cationic proteins, Penicillin. Dilution of plasma has been shown to reduce the interference of the substances mentioned, followed by heating which also causes release of protein bound endotoxin increasing the sensitivity of the endotoxin assay[200].

4.1.3.1 Determination of Endotoxin

In order to determine the level of Endotoxin removal by any quality system, an appropriate endotoxin assay was developed as described in Methods Section 2.6 and tested in Section 0. The sensitivity of the endotoxin assay was determined by using a zero calibrator, where a negative sample was repeated, calculating the mean and standard deviation of the fluorescence unit. The LoQ was established as the mean value + 10 x the standard deviation, using the lowest quantifiable endotoxin level that is above this figure[199].

4.1.4. Small BAL Scale Model

The scale BAL model detailed in Methods Section 2.3 served as a means of establishing contaminant levels in sufficient numbers to gain statistical power. During the large scale BAL treatment phase, the chamber (which holds the biomass) and tubing are primed with plasma, from healthy patients. Accordingly, during the first part of treatment, plasma from healthy patients will be continually diluted with plasma from the ALF patient. Therefore, testing alginate encapsulated HepG2 cells over 8 hours in undiluted plasma from an ALF patient, presents a worst case scenario for the large scale BAL system.

The plasma used in the scale model was tested by the Royal Free Clinical Biochemistry laboratory to confirm the characteristic ALF and healthy plasma markers, shown in Figure 4-3.

4.1.5 Defining Characteristic Plasma Markers and Parameters

4.1.5.1 Plasma from Patients with Liver Failure

One treatment for ALF patients is therapeutic plasma exchange[126]., where the patient's plasma is replaced with healthy plasma. We have exploited this opportunity to acquire large volumes of human ALF plasma by storing the "waste" plasma at -20°C until required. To confirm the extent of ALF diagnostic markers, described below, for liver failure, were measured by the clinical biochemistry department at the Royal Free Hospital.

Alkaline Phosphatase

Alkaline phosphatases are a group of enzymes found in a wide variety of tissue, particularly concentrated in Liver, bile duct, kidney and bone. They hydrolyse a number of organic phosphate esters into inorganic phosphates and organic radicals. A low level of alkaline phosphatase is an indicator of fulminant Wilkinson's disease or severe liver disease where liver function is severely comprised[32,203].

Alanine transaminase

Amino transaminases are a group of enzymes involved with amino acid synthesis by transferring amine groups. Alanine transaminase is a cytosolic enzyme predominantly found in the liver. Hepatotoxicity leads to release into the blood and elevated levels, and due to the relative localisation in the liver, it is a good indicator of liver damage[32,203].

Albumin

Albumin is an important protein synthesised by the liver, a decreased level indicates failure in liver synthetic function often associated with chronic liver disease. Due to the 20 day half-life of albumin, validity of this test is reliant on the speed of liver failure onset[32].

C - reactive protein

Acute phase proteins are a class of proteins mainly synthesised in the liver in response to inflammation including: coagulation proteins (fibrinogen, prothrombin), transport proteins (heptoglobin), complement proteins and C-reactive protein[204]. The extent of inflammation can be determined by testing for C-reactive protein providing a measure of systemic inflammation[32].

4.1.5.2 Fresh Frozen Plasma (FFP)

Fresh frozen plasma (FFP) is collected from blood donations under strict guidelines as to the processing of the samples. Whole blood is routinely processed either by centrifuged at between 1000-2000rcf for 15 minutes or filtration to provide specified plasma parameters[205]:

- Leukocyte depletion more than 99% with fewer than 5 x 10^6 with a 95% confidence interval
- 0.8% haemolysis as measured at the end of shelf life of plasma as part of process validation
- Total protein >50g/L
- Platelet content < 30 x 10^9/L
- Red Cells < 6 x 10^9/L

4.2 Methods

4.2.1 Small Scale BAL Models

Detail of the scale BAL model assembly was described in Methods Section 2.3.

Materials

- All materials, other than those stated below, are detailed in Methods Section 2.3, 2.3.1, 2.3.2, 2.3.3 and 2.3.4.

4.2.1.1 Small Scale BAL Model with Plasma from Healthy and ALF Patients

Materials

- Healthy plasma in the form of pooled FFP (Fresh Frozen Plasma)
  - Same addition as in Methods Section 2.3
  - Four units of Rhesus negative blood group B plasma were pooled totalling 1072ml
- ALF Plasma from TPE (therapeutic plasma exchange)
  - Same addition as detailed in Methods Section 2.3
  - Rhesus positive, blood group A

The viability and function of alginate encapsulated HepG2 cells were tested in both plasma from healthy and ALF patients. Prior to addition to the scale BAL system, characteristic markers for ALF, as outlined in Section 4.1.5, were tested in both types of plasma by the Clinical Biochemistry laboratory at the Royal Free Hospital (Appendix V). After which, 50ml plasma aliquots were made of both plasma types for immediate freezing at -80°C, in order to use the same plasma conditions across experiments.

HepG2 cells were encapsulated using the large scale JetCutter® encapsulation system, and cultured in the large scale bioreactor as described in Methods Section 2.1.3. To each column 5ml of beads was added to a total plasma volume of 80ml held in the column and reservoir, for 8 hours of perfusion. Each plasma condition was in duplicate (four columns in total) for each large scale encapsulation, repeating with five sets of beads. Total viable cell numbers were determined using FDA and PI staining (Methods Section 2.1.3.4) and total cell number using a Nucleocounter (Methods Section 2.1.3.3) at the beginning and end of each 8 hours experiment.

4.2.1.2. Small Scale BAL with Different Flow Velocities

Materials

- Volumetric Flask
- 10 Channel Watson-Marlow® pump
- Plasma
- Silicone tubing
- Greater details in Methods Section 2.3

HepG2 cells were encapsulated using the Inotech® microencapsulator and placed in static cultured over 14 days, as described in Methods Section 2.1.2.5. With each encapsulation, six columns were assembled with duplicates for each of the three flow velocities created, using three different bore sizes of pump tubing, 2.79mm, 1.52mm and 1.14mm.

Initially, the ten-channel pump was calibrated with plasma from healthy patients using the 2.79mm bore size tube to convert pump RPM to volumetric flow rate ($mlmin^{-1}$). The volumetric output was measured by disassembling the lower end of the column, in a sterile tissue cabinet, and measuring the flow over time, using a volumetric flask. Following this, the volumetric flow rate at a fixed RPM for the 1.52mm and 1.14mm bore size tubing were measured in the same way, giving a flow rate ratio between the 2.79mm and 1.52 and 1.14mm tubing. Whilst reassembling the columns, 5ml of beads were added to each column making up to a total volume of 80ml in the system by supplementing the reservoir as described in Methods Section 2.3.

The large scale BAL system uses a volumetric flow rate ($mlmin^{-1}$) that propagates a 2-fold bead bed height. The flow velocity (linear flow rate) was determined for the large scale BAL using the calculations in Methods Section 2.3.4. The volumetric flow rate (mlmin-1) for the columns fed by the 2.79mm pump tubing was set to produce a 2-fold bed height, then the corresponding flow velocity (ms^{-1}) was calculated, illustrated in Table 4-4. The ratio calculated for the different volumetric flow rates between the 2.79mm and the 1.52mm and 1.14mm bore size tubing, was used to calculate the flow velocity (ms^{-1}) for the smaller pump tubing (Table 4-12).

4.2.1.3 Scale BAL Experiment for Cell debris

Materials

- Acute Liver Failure Plasma
- Phase Contrast Microscope
- PBS (Methods Section 2.1.1.1)
- 16mM EDTA

HepG2 cells encapsulated using the Jetcutter® system then grown in a fluidised bed for 12 days, was tested in the small scale BAL system (Methods Sections 2.3). Plasma from an acute liver failure patient was used to perfuse beads over 8 hours, taking samples from the bottom of the reservoir for analysis using FDA and PI staining (Methods Section 2.1.3.4) to determine cell viability of any intact cells which may have escaped from the biomass.

Sample Preparation to Visualise Intact Cells

Each plasma sample was placed in a 2ml microfuge tube for centrifuged at 1200g at 4°C for 6 minutes. Discarding the plasma, 1.5 ml of PBS was added to the microfuge tube, then pulse vortexed for 15 second to re-suspend the pellet. Following this, the solution was centrifuged as before, discarding the supernatant and replacing with 1.5ml of 16mM EDTA, again pulse vortexed to re-suspend the pellet and incubated at room temperature for 10 minutes, finally centrifuging as before and re-suspending in 1ml PBS. A volume of 250µl cell suspension was then ready for analysis using FDA and PI staining as detailed in Methods Section 2.1.2.4.

4.2.2. Encapsulated HepG2 Cell Number

The total cell number in the reservoir of the BAL scale model after 8 hours of perfusion with plasma from an ALF patient was determined using a haemocytometer as described in Methods Section 2.1.1.1.

4.2.3. QCPR Validation

The QPCR protocol described in the Methods Section 2.2.4 was used to determine total DNA in media and plasma samples as well as evaluating DNA integrity. Aspects of method validation were performed to ensure that the protocol could be utilised for pre-clinical and clinical testing.

4.2.3.1 Recovery Analysis

Recovery analysis involved spiking representative plasma or media samples with DNA, then determining concentration by Alu repeat QPCR after purification (as detailed in Methods Section 2.3.3) to ensure DNA recovery was not significantly affected. Untreated samples were concurrently analysed by QPCR to quantify the extent of inhibition or enhancement from components within the sample.

4.2.3.2. QPCR for Recovery Analysis with Spiked Media and Plasma Samples

Materials

- 100 µg/ml DNAse
- Alpha MEM media (PAA)
- Certified Human Genomic DNA (Bioline®)

Protocol

FFP Plasma or Media supplemented with 10% FFP (made as detailed in Methods Section 2.1.1.1), were made into 2ml aliquots for storage at -80°C. To remove background DNA, media and plasma aliquots were treated with a final concentration of 100µg/ml of DNAse I at 37°C for 4 hours, then to deactivate DNAse, heated at 70°C for 10 minutes. Following this, top DNA standards of 20pg/µl in media or plasma made by adding 20µl of 2ng/µl (1/100 dilution of the certified DNA stock certified in PCR water, appendix III), then serially diluting the top media or plasma standard with the same batch of media or plasma, to create identical final DNA concentrations to the DNA standards in water. A 20µl sample from each media or plasma standard concentration was treated using the purification protocol (outlined in Methods Section 2.2.4), also taking a corresponding set of samples to store on ice as the untreated samples. After treatment, DNA standards (in water), treated and untreated samples were analysed by QPCR as outlined in Methods Section 2.2.4.3.

Each sample was analysed in triplicate, with a total of five standard curves in media or plasma and water in separate QPCR runs, with both primers specific for 247bp and 115bp replicons. The data for the standard curves in water and media were pooled to provide a measure of variance, for comparison of recovery.

4.2.3.3. DNA Extraction from Apoptotic and Necrotic Cell Death

Materials

- Supplemented Alpha MEM media, Methods Section 2.1.1.1.
- 6 well culture plates (Falcon™).
- T80 Cell Culture flask (Thermo® Nunc®)
- 1µM staurosporine (Sigma-Aldrich®)
- HepG2 Cells

Cell culture

HepG2 cells were cultured in an 80cm^2 flask as described in Methods Section 2.1.1.1 over 7 days, then harvested by trypsinisation and re-suspended in media at a seeding density of 5.0 x 10^{5}cells/ml with supplemented media. Two Falcon™ 6-well plates were used adding 2ml of the cell suspension to each 9.6cm^2 well, totalling 1x10^6 cells in each well. The plates were cultured for 2 days; on the second day the media on one plate was replaced with 1ml fresh media containing 1µm staurosporine, cultured for a further 18 hours, after which cells were harvested and passed through a 27 gauge syringe to break up the cell clumps. The second plate was replenished with 1 ml fresh media, immediately transferred to a -80°C freezer overnight, removed and allowed to thaw at room temperature for 2 hours; these steps were repeated three time to encourage apoptotic cell death. The media was then removed and treated as part of the PCR purification protocol (Methods Section 2.2.4) for direct addition as a template to QPCR.

4.2.4 Caspase-GLO® Assay

Materials:

- Caspase 3/7 GLO kit (Promega G8091)
- Serum- and phenol red-free media
- White-walled plates
- Luminometer

Apoptosis is a tightly controlled process, occurring in response to environmental stresses via the intrinsic pathway, or activation of external cell receptors through the extrinsic pathway. Both the intrinsic and extrinsic pathways activate Caspase 3/7, which then go on to cleave other proteins with the DEVD amino acid sequence (Aspartic acid (D), Glutamic acid (E), Valine (V)). The activation of apoptosis can be quantified using the DEVD sequence engineered to instigate a luminescent signal when cleaved by Caspase 3/7, as shown in Figure 4-2.

Figure 4-2: Caspase-3/7 cleavage of the luminogenic substrate containing the DEVD sequence. Following Caspase cleavage, a substrate for luciferase (aminoluciferin) is released, resulting in the luciferase reaction and the production of light monitored on a luminometer[206].

Protocol

Sufficient reagent was made for the assay by adding equal volumes of the Caspase-GLO® Buffer to the Caspase-GLO® Substrate to make the Caspase-GLO® reagent, allowing it to equilibrate to room temperature. A volume of 100µl of Staurosporine-treated cell suspension was added to a 96- well plate and again allowed to equilibrate to room temperature, to providing 2.0 x 10^5 cells per well. To this 100µl of Caspase-GLO® reagent was added and mixed on a shaker at 300-500rpm for 30seconds, followed by incubating at 37°C for 1 hour. A 100µl sample from each well was transferred to a white walled 96-well plate and analysed using the luminometer.

4.2.5 Glucose and Lactate Quantification by Analox®

Material

- Analox® GM7 Direct Glucose and lactate analyser
- MilliQ treated RO H_2O
- Glucose oxidase reagent (Annalox®)
- Lactate oxidase reagent (Annalox®)
- 8mM Glucose Standard (Annalox®)
- 8mM Lactate standard (Annalox®)

The Analox® GM7 analyser works by exposing the sample to glucose or lactate oxidase, which consumes oxygen at a rate that is proportional to the concentration of analyte. Initially, all reagents were allowed to warm to room temperature. The glucose-oxidase reagent was added to the reagent reservoir, priming the system with reagent by running 6-8 analytical cycles. Using a positive displacement pipette 10µl of 8mM glucose standard was analysed, and repeated until the reading was ± 0.2mM of the 8mM standard. Prior to each sample addition, the positive displacement pipette and the Analox® system were flushed with MilliQ treated H_2O.

The same protocol was used for lactate analysis, using lactate-oxidase reagent and an 8mM lactate standard.

4.2.6. Preparation of Fresh ALF Plasma.

Materials

- Citrated blood collection vials

The tubes containing whole blood from normal and ALF patients were centrifuged at 1200g for 10 minutes at 4°C. The plasma supernatant was removed and carefully aliquoted into 2ml microfuge tubes for immediate freezing at -80°C. The blood cells were also frozen for DNA extraction as in Methods Section 2.2.1.

4.3. Results

4.3.1. Determination of Liver failure and Healthy Plasma

Both Plasma from acute liver failure (ALF) and healthy patients, used in subsequent experiments, were tested by the Royal Free Hospital Clinical Biochemistry Diagnostic laboratory to confirm characteristic parameters associated with ALF and healthy patients.

Alkaline phosphatase (ALP) and aspartate transaminase (AST) at the levels shown in Figure 4-5A and C were indicative of liver damage, being associated with Hepatic cells. Low levels of ALP suggested a breakdown of liver function causing a reduction in synthesis, whereas high levels of AST were suggestive of Hepatotoxicity, causing release from the intracellular environment of the hepatocyte into the blood. Both these proteins are indicative of ALF but not definitive, as AST is also found in skeletal muscle, and ALP is present more ubiquitously[32].

High alanine transaminase (ALT), shown in Figure 4-5B, provided definitive evidence of supporting ALF, due to exclusively being an intracellular hepatic transaminase, uniquely synthesised by hepatic cells, therefore release into the blood stream only occurs during liver damage. Along with ALP and AST concentrations, ALF was confirmed.

Further confirmation of ALF was provided by low albumin in Figure 4-3D suggesting inhibition of synthesis due to liver damage. Systemic inflammation due to liver failure as illustrated by elevated C-reactive protein shown in Figure 3-5E. Plasma from healthy patients were all within normal levels.

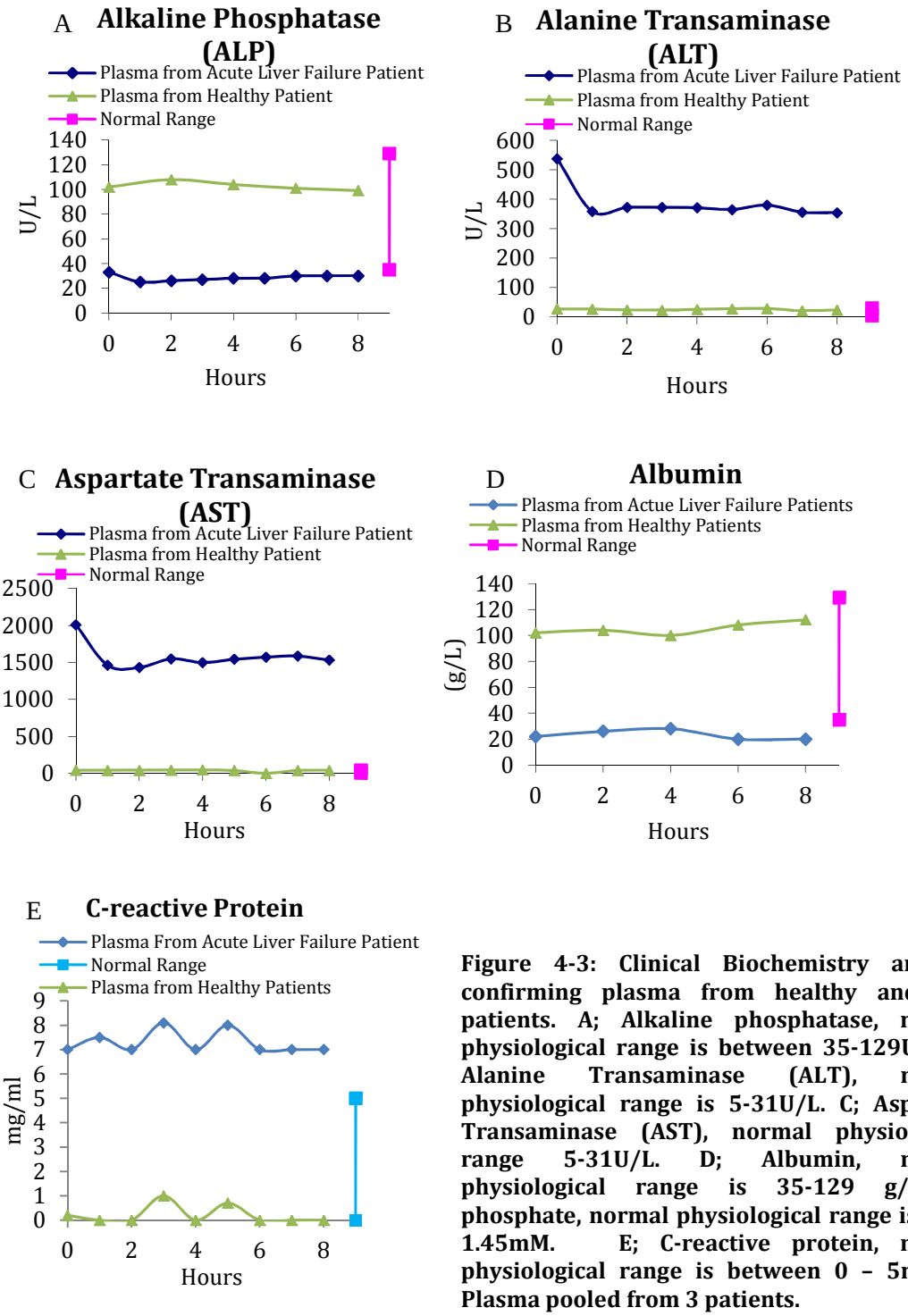

Figure 4-3: Clinical Biochemistry analysis confirming plasma from healthy and ALF patients. A; Alkaline phosphatase, normal physiological range is between 35-129U/L. B; Alanine Transaminase (ALT), normal physiological range is 5-31U/L. C; Aspartate Transaminase (AST), normal physiological range 5-31U/L. D; Albumin, normal physiological range is 35-129 g/L. D; phosphate, normal physiological range is 0.87-1.45mM. E; C-reactive protein, normal physiological range is between 0 – 5mg/ml. Plasma pooled from 3 patients.

4.3.2 Cell Debris in the BAL System

Cellular contamination from the biomass, as a direct result of fluidisation in plasma, was quantified by fluidising beads with healthy human plasma as part of a scale BAL model. The beads contained 56 x 10^6 ±11x^6 cell/ml, giving a total cell number of 280 x 10^6 cell/ml. Plasma samples taken from the bottom of the scale BAL system reservoir, after 8 hours of perfusion, were analysed using FDA PI staining, (described in Section 0,) showing intact viable and non-viable cells ( ).

Size of cell fragment	10µm± 4µm
Viable Cell Concentration	4 x 10^3± 3x10^2cells/ml
Non-viable cell concentration	6.2 x 10^3± 1.2 x 10^3/ml

Table 4-1: Cells escaping the beads in the small scale BAL model. Both viable and non-viable cells escaped from the fluidised bed and were detected in samples taken from the reservoir of the column experiment after 8 hours

The cell numbers above, form part of the contamination risk to the patient, it does not account for cells having already undergone apoptosis or necrosis and released DNA into solution, as plasma samples are taken from a sample port attached to the inlet of the reservoir.

4.3.3. Detection of DNA in Plasma

4.3.3.1 Theoretical calculations for expected DNA Concentration

A theoretical calculation was made to assess the potential DNA release from the BAL treatment phase, using the assumption that cell death is proportional to DNA release. This provided information for the DNA quantity the quality system may encounter and the potential LoQ necessary for the associated detection system; calculating according to mass of DNA in a single cell[207] and predicted cell number given in Table 4-1.

- 6.64 x 10^{-12}g ± 0.43 DNA in a Diploid cell[207]
- Proposed BAL cell number between:
- 7 x 10^{10} and 1 x 10^{11} HepG2 cells,

BAL Condition	BAL with $7x10^{10}$ cells	BAL with 1×10^{11} cells
Total DNA contained in Biomass (µg)	4.6×10^5	6.6×10^5
DNA concentration in 3.5L Human Plasma (µg/ml)	133	190
DNA concentration in 7L Human Plasma (µg/ml)	66	95
DNA concentration in 10L Human Plasma (µg/ml)	47	66
DNA concentration with 10% cell death in 7L Human Plasma (µg/ml)	7	10
DNA concentration with 1% cell death in 7L (µg/ml)	0.7	0.9

Table4-2: Theoretical calculations of DNA concentration within the BAL treatment phase with different cell numbers and total BAL volume, using the assumption that 1 cell contains $6.64 \times 10^{-12} \pm 0.43$g DNA[207] and that cell death is proportional to DNA release.

According to the calculations of cell death and DNA release, (assuming cell death is proportionate to DNA release) illustrated in Table 4-2, a 1% reduction in cell viability would release 0.7µg/ml DNA. Furthermore, to detect DNA from greater cell death, samples may need to be diluted to be within the standard curve range.

4.3.4. Fluorescence DNA Quantification by Hoechst Dye

Assessment of fluorescent DNA staining by Hoechst dye, utilised a nine point standard curve in water (Figure 4-4A), then comparing increased plasma dilutions to minimise any interfrence from plasma componnents, such as proteins. At 1% plasma concentration and below, a standard curve comparable to water was produced in terms of linear regression, although at lower DNA concentrations signal enhancement was observed (Figure 4-4B).

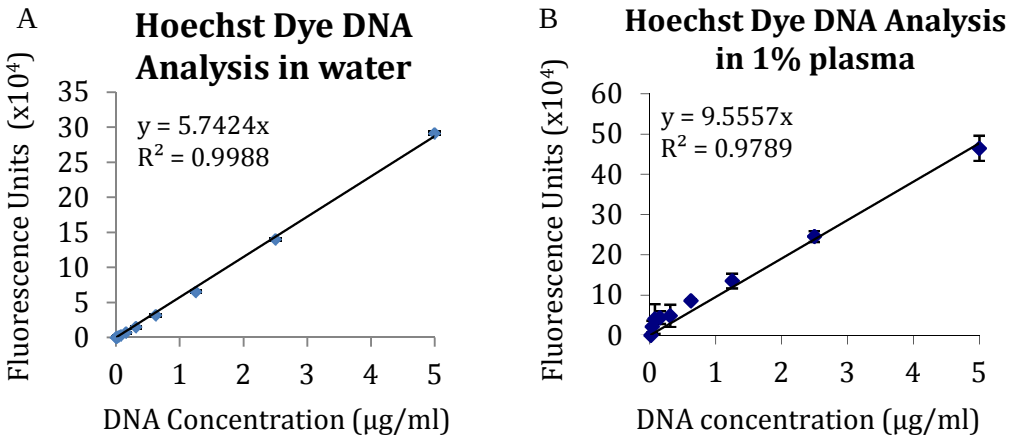

Figure 4-4: Plasma proteins caused inhibition of Hoechst dye DNA analysis, despite substantial dilution to improve linearity using a nine point DNA standard curve between 0 – 5µg/ml, analysed by Hoechst dye. A; Standard curve in water. B; standard curve in 1% Plasma. (N=5 for each point, error=standard deviation).

Calculating Hoechst Dye performance for a Large Scale BAL

By diluting plasma to 1%, the LoQ was 0.078µg/ml DNA. This is equivalent to 7.8µg/ml LoQ in 100% plasma. A BAL system with 7 x 10^{10} cells would contain a total DNA content of 4.6 x 10^5µg, with a DNA concentration of 46µg/ml in 10L plasma, requiring a reduction of 17% viability before reaching the LoQ of 0.078µg/ml. Table 4-3 illustrates the theoretical change in viability neccessary to provide sufficient DNA to meet the LoQ in different BAL sizes.

Cell Number in BAL	Total Cellular DNA (µg)	DNA in 3.5L Plasma (µg/ml)	% Cell Death Detectable	DNA in 10L plasma (µg/ml)	% Cell Death Detectable
7 x 10^{10}	4.6 x 10^5	133	6	46	17
1 x 10^{11}	6.6 x 10^5	190	4	66	12

Table 4-3: Assuming that cell death causes complete DNA release, the viability of DNA would have to drop between 4 - 17% to reach the LoQ of Hoechst dye assay, dependent on the plasma volume and cell number. These figures were based on 6.64 x 10^{-12} ± 0.43g DNA[207] .

4.3.5. DNA Quantification by QPCR

4.3.5.1 PCR Analysis by Gel Electrophoresis for Primer Optimisation

Initial PCR optimisation involved confirming the expected 115 nucleic acid base pairs (bp) and 247bp amplicon size at decreasing DNA template concentrations, by gel electrophoresis (Methods Section 2.2.4).

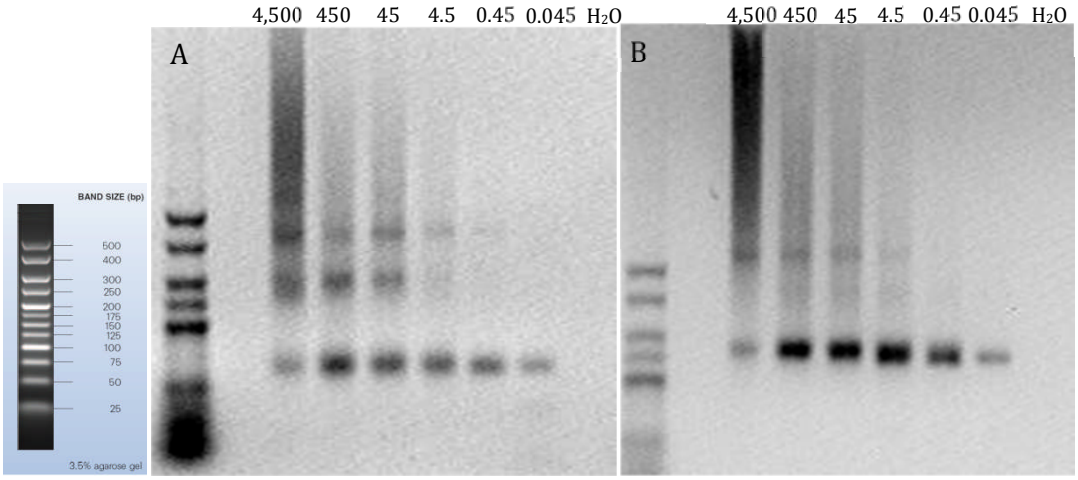

Figure 4-5: Reducing template concentration caused a reduction in non-specific PCR amplification, using primers specific to 115bp and 247bp Alu repeats consensus sequence Methods 2.2.3. A; 115bp Alu repeat amplicon, with decreasing DNA concentration. B; 247bp Alu repeat amplicon, with decreasing DNA concentration.

4.3.5.2 QPCR Method Development

Standard Curve

For both the 115bp and 247bp replicon primer sets, a 5 point Real Time Quantitative PCR standard curve was optimised for the conditions stated in the Methods Section 2.2. This included optimisation of primer and $MgCl_2$ concentration as well as establishing the limit of quantification (LoQ), producing the standard curves illustrated in Figure 4-6A and B.

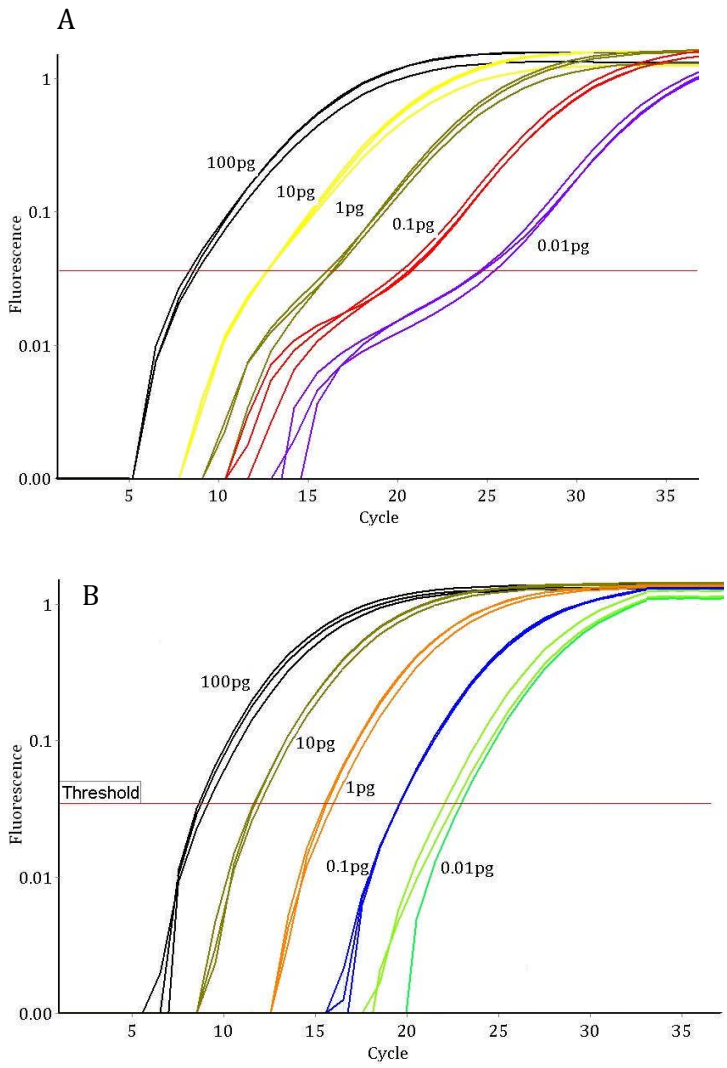

Figure 4-6: Optimised QPCR standard curves using Alu repeat primers. Amplifying from human genomic DNA samples from 0.01pg to 100pg total DNA per reaction; DNA was quantified using the threshold line providing a calculated measure of the most linear region of amplification. Each sample was performed in triplicate A; primer set specific for the 115bp Alu replicon. B; primer set specific for the 247bp Alu replicon.

4.3.5.3. Confirmation of Melt curve

Initial confirmation that the QPCR melt curve corresponded to the correct product size, analysis of the QPCR product was analysed on a 1% electrophoresis gel as illustrated in Figure 4-7. The QPCR melt curve reflects the unique temperature that the QPCR amplicons dissociate into single stranded DNA. This was used to confirm the correct replicon amplification, removing the necessity to analyse each QPCR by electrophoresis. A melt curve peaking at 90.5°C melting temperature matched with the 115bp amplicon size (Figure 4-7A and B) and the 87°C melt curve matched with the 247bp amplicon (Figure 4-7C and D). In addition, some non-specific DNA amplification was seen, especially in Figure 4-7 A, reflecting the numerous subfamilies of Alu repeats in the human genome.

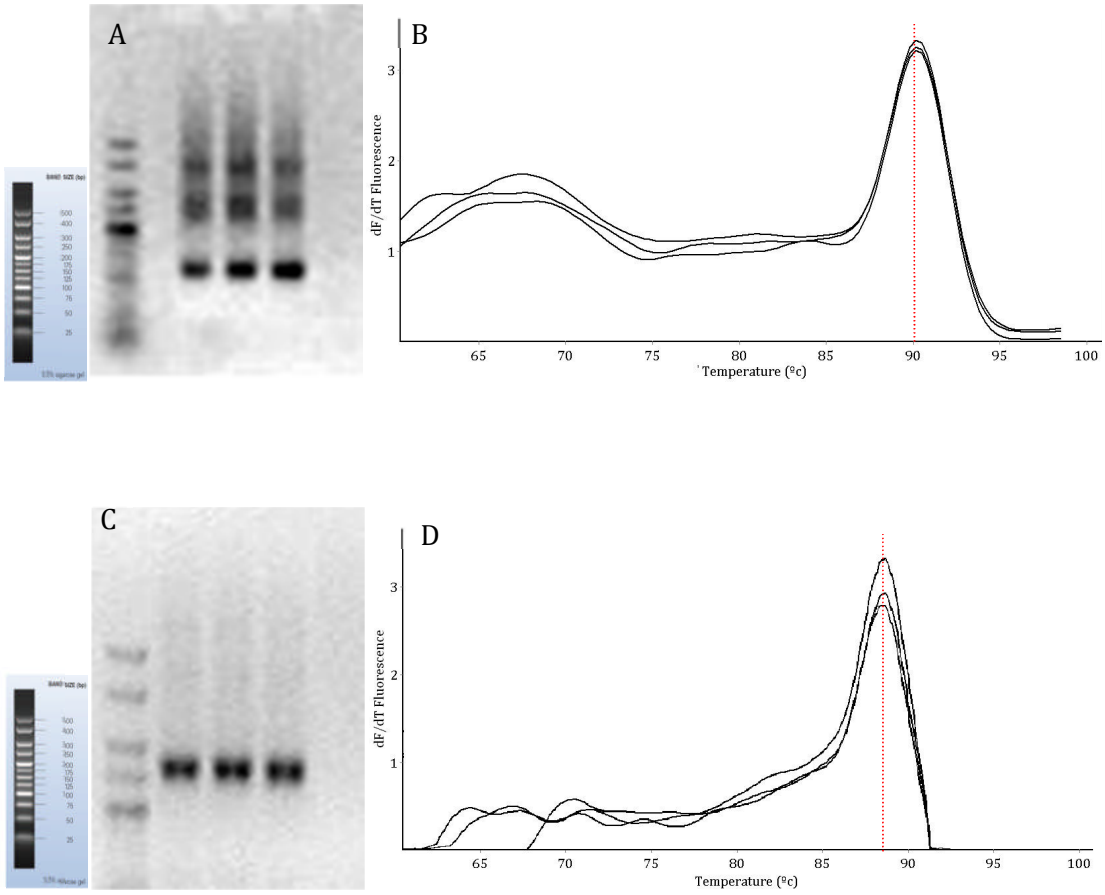

Figure 4-7: The QPCR DNA standards shown in Figure 4-6 also produced melt curves as outlined in Methods Section 2.2.4, analysing the QPCR product on a 1% agarose gel by electrophoresis, confirmed the amplicon size and the corresponding melting temperature for each primer set. A; Agarose gel electrophoresis analysis of the 100pg DNA standard, amplified by the 115bp Alu primer, showing some non-specific amplification as expected. B; melt curve peaking at 90.5°C, of the 100pg DNA standard amplified by the 115bp Alu primer C; Agarose gel electrophoresis analysis of the 100pg DNA standard amplified by the 247bp Alu primer. D; melt curve peaking at 87°C, of the 100pg DNA standard amplified by the 247bp Alu primer.

4.3.5.4. Efficiency of the PCR reaction

The efficiency and linearity of each DNA standard curve provided crucial information confirming successful amplification. Equation 4.2 shows the method of calculating the efficiency, from the gradient of the regression line presented Figure 4-8, comparing the result with the ideal -3.32 to provide a percentage measure of efficiency.

Equation 4.2: Efficiency = $10^{(-1/\text{slope})}$ -1.

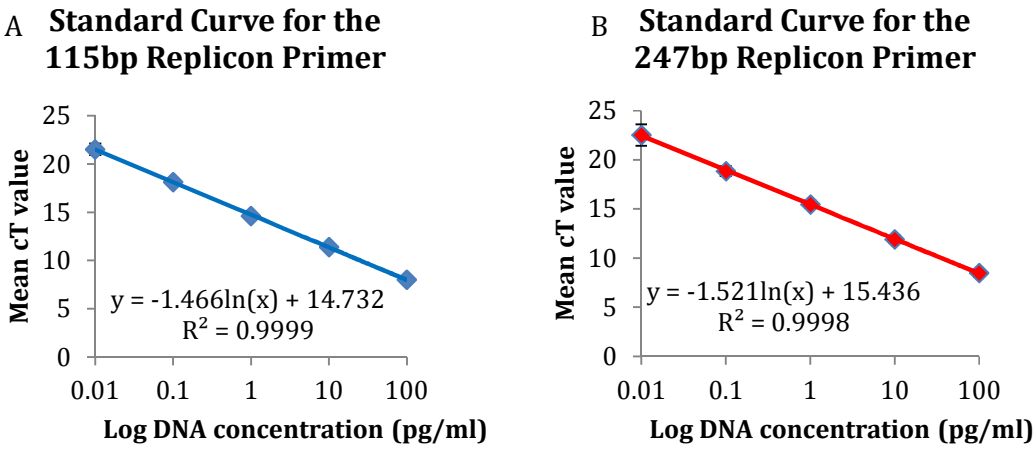

Figure 4-8: The mean linearity and efficiency of the QPCR reaction was determined by plotting the log of DNA template concentration vs. cT values, for each primer set. The efficiency was determined from the gradient of the line using equation 4.2. Linearity was evaluated using regression with n=20 for each sample. A; Regression line for the 115bp replicon primer, with a linearity of 0.9999 and efficiency of 106±1.2%. B; Regression line for the247bp replicon primer, with a linearity of 0.9998 and efficiency of 101±0.9%

4.3.6. QPCR Validation

4.3.6.1. Repeatability

Repeatability provides a measure of constitutive variation to be expected within the protocol by amplifying a single set of PCR standard concentrations, using identical: PCR machine, reagents, consumables and location, all performed on the same day. The standard DNA template was also kept constant using Human genomic DNA, certified both in purity and concentration (see appendix IV). Table 4-4 shows the variation between standard curves using the mean value and the standard deviation on 20 samples for each concentration performed over five runs.

	DNA Template (pg)				
Final DNA amount in PCR reaction (pg)	100	10	1	0.1	0.01
cT for 115bp amplicon	8.0±0.2	11.4±0.3	14.62±0.2	18.12±0.4	21.52±0.6
CV value (%)	2.5	2.6	1.4	2.2	2.8
cT for 247bp amplicon	8.47±0.4	11.9±0.4	15.46±0.4	18.83±0.5	22.52±1.1
CV value (%)	4.7	3.4	2.6	2.7	4.9

Table 4-4: The repeatability of the DNA standard curves, performed using identical DNA standards samples (diluted from certified DNA stock, shown in appendix IV), on the same PCR machine, with identical reagents and consumables, analysed on the same day. Four standard curves, with triplicate samples, were performed simultaneously in one run, with five runs in total (n=60 for each standard reaction). For each DNA concentration the % CV value illustrated the indicated the level of constitutive error.

4.3.6.2. Reproducibility

Reproducibility provides a measure of the extremes in precision when transferring the technique between PCR thermocyclers, analysts, PCR facilities, and over time. Consequently, the identical protocol and PCR samples were used with three PCR thermocyclers (including the in house Liver Group RotorGene® 3000 thermocycler used for all subsequent experiments) with different analysts, performing the analysis over the course of a year. Each standard sample was performed in triplicate as part of a 5 point standard curve, performed four times on three separate PCR machines then a year later the protocol was repeated with the same samples, kept at -80°C.

The standard curves produced on a single thermocycler (Rotorgene® 3000) in Table 4-4 were compared with the mean of standard curves produced by multiple analysts, on different thermocyclers, as illustrated in Table 4-5. A paired student's t-test was used to compare standard curves for each primer set. The primer set for the 115bp replicon performed on different thermocyclers showed a significant difference (p= 0.04, n=60). Whereas, when comparing standard curves using the primer set for the 247bp replicon performed on different thermocyclers, there was no significance between the means (p=0.99, n=60).

Both Repeatability and reproducibility analysis used the same standard curve DNA samples, incorporating the results from that experiment with those obtained from the two other PCR

machines, analysts, and laboratories. In total 180 samples were performed for each standard concentration. With Thanks to Dr Amy Thomas and Dr Miguel Centelles for providing the "other" analysts.

	DNA Template (pg)				
Final DNA amount in PCR reaction (pg)	100	10	1	0.1	0.01
cT for 115bp amplicon	8.1±0.4	11.62±1.0	14.8±0.9	18.7±1.2	22.2±2.2
CV Value (%)	4.9	8.6	6.1	6.4	9.9
cT for 247bp amplicon	8.1±1.2	11.5±1.5	15.48±1.3	19.3±1.1	22.7±1.1
CV Value (%)	14.8	13.0	8.4	5.7	4.8

Table 4-5: The same standard template samples were tested on different PCR machines, by different operators in different laboratories, calculating the mean and standard deviation between all standard curves. Each standard sample was in triplicate, with each 5 point standard curve performed four times on three separate PCR machines over a year. Four standard curves were performed simultaneously on one machine at a time, with each machine being used twice (n=180 for each standard concentration). The CV value reflects the level of error from changing the PCR machine.

4.3.6.3. Effect of Changing the PCR Thermocycler

The data from Table 4-5 was further reanalysed to focus on the change in PCR thermocycler using the same analyst. Therefore, for both 115bp and 247bp standard curves, the three PCR thermocyclers were compared and analysed using a paired, two tailed student's t-test as detailed in Table 4-6.

Each standard sample was performed in triplicate as part of a 5 point standard curve, with four standard curves performed on a single PCR run. The same standard concentration template was used for five separate PCR runs totalling n=60 for each sample. In all cases there was a significant difference between standards performed on different PCR thermocyclers, as shown in Table 4-6.

A

DNA	**RG3000**	**RG6000**	**RG3000**	**RG6000**
(pg)	115bp		247bp	
100	8.0±0.2	8.6±0.4	8.5±0.4	9.1±0.4
10	11.4±0.3	12.3±0.3	11.9±0.4	12.8±0.5
1	14.6±0.2	15.7±0.7	15.5±0.4	16.7±0.7
0.1	18.1±0.4	20.1±0.8	18.8±0.5	20.6±0.4
0.01	21.5±0.6	24.6±0.9	22.5±1.1	24.0±1.0
	P Value	**0.0288**	**P Value**	**0.0035**

B

DNA	**RG3000**	**Biorad®**	**RG3000**	**Biorad®**
(pg)	115bp		247bp	
100	8.0±0.2	7.7±0.3	8.5±0.4	6.8±0.3
10	11.4±0.3	10.4±0.4	11.9±0.4	9.9±0.4
1	14.6±0.2	14.0±0.6	15.5±0.4	14.2±0.7
0.1	18.1±0.4	17.8±0.8	18.8±0.5	18.5±0.6
0.01	21.5±0.6	20.5±0.9	22.5±1.1	21.7±1.1
	P Value	**0.0165**	**P Value**	**0.0151**

C

DNA	**RG6000**	**Biorad**	**RG6000**	**Biorad**
(pg)	**115bp**		**247bp**	
100	8.6±0.4	7.7±0.3	9.1±0.4	6.8±0.3
10	12.3±0.3	10.4±0.4	12.8±0.5	9.9±0.4
1	15.7±0.7	14.0±0.6	16.7±0.7	14.2±0.7
0.1	20.1±0.8	17.8±0.8	20.6±0.4	18.5±0.6
0.01	24.6±0.9	20.5±0.9	24.0±1.0	21.7±1.1
	P Value	**0.0158**	**P Value**	**0.001**

Table4-6: QPCR amplification for primers specific to the 115bp and 247bp replicon show significant difference at 95%, between the Liver Group Rotorgene 3000 and the other PCR machines tested. All standard curves were performed by the same analyst, with 4 standard curve on each PCR run, repeating the run 5 times with the same original DNA standard template (n= 60).

The % CV value was calculated for each primer set on separate PCR machines, as illustrated in Table 4-7. For each specific PCR machine the %CV was relatively low for both primer sets, whereas when transferring the protocol between PCR machines there was a significant difference in cT value as illustrated in Table 4-6.

	RG3000®		RG6000®		Biorad®	
DNA standard (pg)	CV 115bp (%)	CV 247bp (%)	CV 115bp (%)	CV 247bp (%)	CV 115bp (%)	CV 247bp (%)
100	2.5	4.7	4.6	4.4	3.4	4.4
1	1.4	2.6	4.6	4.2	4.3	4.9
0.01	2.8	4.9	3.6	4.2	5.1	5.1

Table 4-7: CV values for both 115bp and 247bp replicon primers performed on different PCR machines.

4.3.7 Recovery of DNA from Spiked Media and Human Plasma Samples

4.3.7.1. DNA Recovery from Media

DNA recovery was measured to evaluate the level of inhibition or enhancement incurred by addition of raw media to the PCR reaction, and to determine the difference between standards in water and treated samples, prepared as outlined in Section 4.2.3. For primers specific to the 115bp amplicon, the mean DNA recovery of treated samples was 98.8±2.4%, whereas untreated samples showed an average DNA recovery of 62.8±36.2%, shown in Table 4-8. DNA recovery for the primer specific to the 247bp replicon showed a mean 101±3.55% recovery after treatment, with a 58±41.85% recovery before treatment.

Standards (pg)	Treated Media (pg)	% recovery	Un-treatment Media (pg)	% Recovery
100	101±4	101	89±10	89
10	9.88±1	99	6.7±2	67
1	0.96±0.3	96	0.85±0.2	85
0.1	0.102±0.06	102	0.073±0.003	73
0.01	0.0101±0.003	101	0	0

Table 4-8: Using the Primers specific for the 115bp replicon, treatment of media removed inhibition and enhancement of the fluorescent signal as well as significantly reducing the standard deviation of samples. Each sample was performed in triplicate over five PCR runs alongside a standard curve (n=5).

Standards (pg)	Treated Media (pg)	% recovery	Un-treatment Media (pg)	% Recovery
100	99±3	99	78±11	78
10	10.2±1	102	15±4	15
1	1.06±0.7	106	0.3±0.1	30
0.1	0.97±0.1	0.97	0.047±0.01	47
0.01	0.0103 ± 0.002	103	0.12±0.1	120

Table 4-9: Using the Primers specific for the 247bp replicon, treatment of media removed inhibition and enhancement of the fluorescent signal as well as significantly reducing the standard deviation of samples. Each sample was performed in triplicate over five PCR runs alongside a standard curve (n=5).

As illustrated in Figure 4-9, media added raw to the PCR reaction caused a mean inhibition of 21.5±10.2% across the standard curve. After medium samples were treated using the purification protocol outline in the Methods Section 2.4 of the media, inhibition was reduced to a mean 0.2±1.2%.

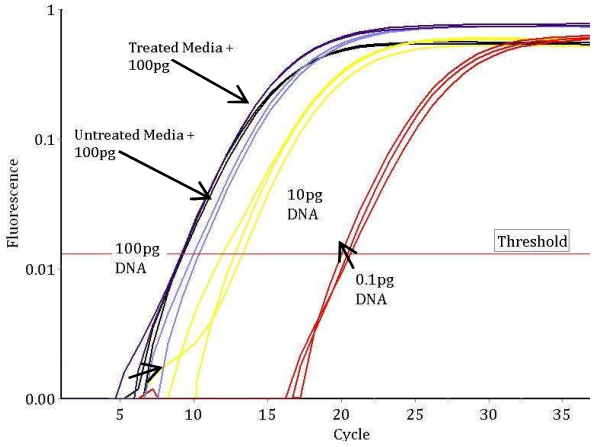

Figure 4-9: Un-treated media containing 10% FFP added to the PCR caused 21±10.2% inhibition. Treatment of the media prior to addition reduced inhibition to 0.2%±1.2%. Media samples were spiked to give the media and standards identical final DNA final concentration (each sample n=3). Only the media samples spiked with 100pg DNA is shown above for clarity.

4.3.7.2. DNA Recovery from Human Plasma

The same recovery protocol used with media was applied to human plasma for both primers specific to 115bp and 247bp replicon. The application of untreated human plasma directly to the PCR reaction showed greater inhibition than addition of untreated media, as illustrated in Table 4-10 and Table 10-11. Despite this, by treating plasma the mean recovery was restored to 98.8±3.27% for the 115bp replicon primer, and 101.5± 3.5% for the 247bp replicon primer (Table 4-10 and 4-11).

Standards (pg)	Treated Plasma (pg)	% Recovery	Un-treatment Plasma (pg)	% Recovery
100	101±3	101	74±15	74
10	9.4±2	94	6.9±4	69
1	1±0.7	100	0	0
0.1	0.097±0.05	97	0	0
0.01	0.0102 ±0.009	102	0	0

Table 4-10: Using the Primers specific for the 115bp replicon, treatment of plasma removed inhibition and enhancement of the fluorescent signal as well as significantly reducing the standard deviation of samples. Untreated samples with 1, 0.1 and 0.01pg DNA spike were inhibited to below the LoQ of the assay. Each sample was performed in triplicate over five PCR runs alongside a standard curve (n=5).

Standards (pg)	Treated Media (pg)	% recovery	Un-treatment Media (pg)	% Recovery
100	99±3	99	78±11	89.00
10	10.2±1	102	15±4	67.00
1	1.06±0.7	106	0.3±0.1	85.00
0.1	0.97±0.1	97	0	73.00
0.01	0.0.103 ± 0.02	103	0	0.00

Table 4-11: Using the Primers specific for the 247bp replicon, treatment of plasma removed inhibition and enhancement of the fluorescent signal as well as significantly reducing the standard deviation of samples. Untreated samples spiked with 0.1 and 0.01pg DNA spike were inhibited to below the LoQ of the assay. Each sample was performed in triplicate over five PCR runs alongside a standard curve (n=5).

Untreated plasma samples spiked with 1pg of DNA showed a lower cT value than treated plasma with a 1pg DNA, producing the same cT value as 1pg DNA in water, illustrated in Figure 4-10. In addition, untreated plasma with no DNA spike showed enhancement of DNA signal showing DNA concentration of 1.2±0.98pg/µl compared with no DNA levels below the LoD for treated plasma with no DNA spike.

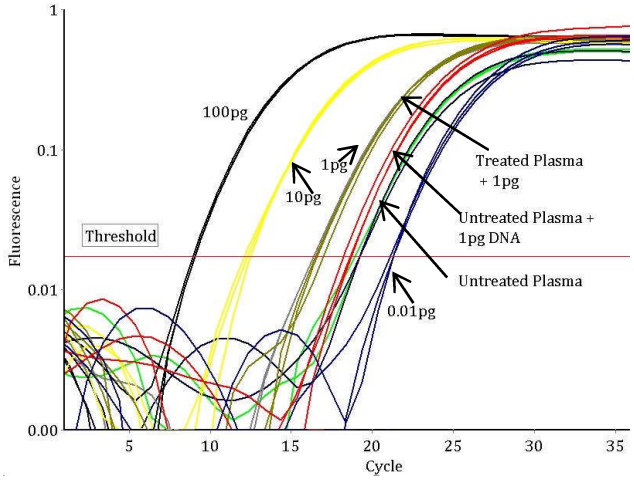

Figure 4-10: Untreated plasma added to the PCR caused inhibition. Treatment of the plasma prior to addition significantly reduced inhibition (as illustrated in Table 4-10 and Table 4-11). Plasma samples were spiked with DNA to give identical final concentrations (each sample n=3). Error! Reference source not found.**Only the plasma samples spiked with 1pg DNA are shown above, for clarity.**

4.3.8 DNA Integrity

DNA integrity provided a means of measuring the ratio of DNA from apoptotic and necrotic cell death. Cells cultured in 6-well plates were treated with 1µM Staurosporine over 18 hours to induce apoptosis or subjected to 4 freeze/thaw cycles between -80°C and 37°C to induce necrosis. Then DNA was tested using the QPCR with the 115bp and 247bp Alu replicon primers to assess the validity of the DNA integrity ratio.

4.3.8.1. Inducing Apoptosis and Necrosis

To ensure the cells had undergone apoptosis, pictures were taken under a phase microscope, as illustrated in Figure 4-11, confirming using the Caspase GLO® assay on a sample of cells treated with Staurosporine, shown in Figure 4-12.

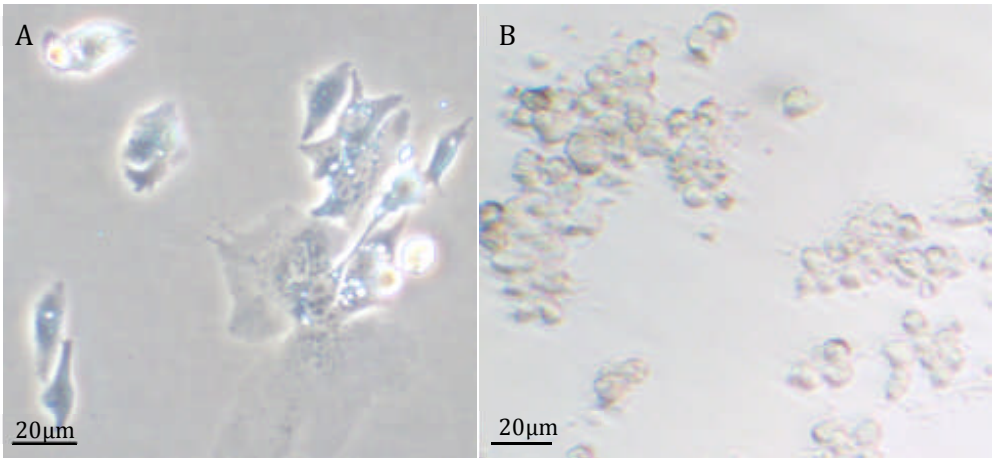

Figure 4-11: Inducing HepG2 apoptosis HepG2 cells cultured in monolayer were treated with 1µM Staurosporine for 18 hours, showing apoptotic cell morphology. A; HepG2 cells prior to addition of Staurosporine. B; HepG2 cells after 18 hours of treatment with Staurosporine.

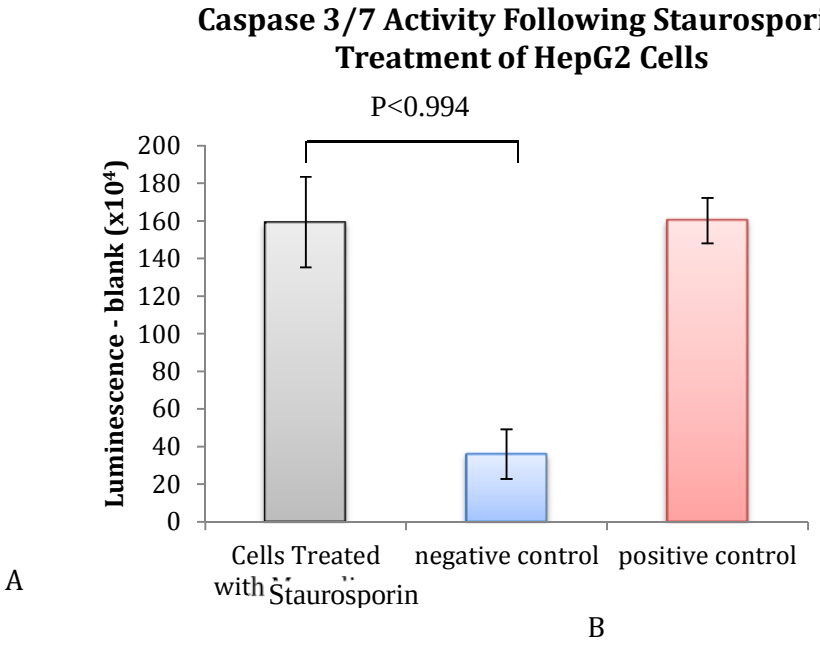

Figure 4-12: Caspase GLO® assay for apoptosis. Cells treated with Staurosporine showed a significant increase in Caspase 3/7 activation, the negative control represents background apoptosis of untreated HepG2 cells (n=5, unpaired t-test p<0.994).

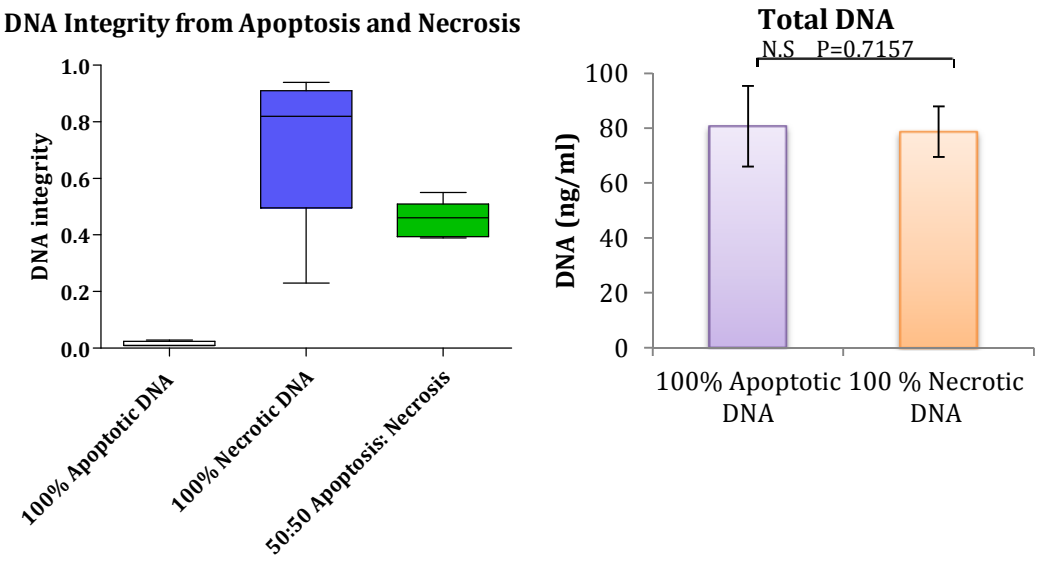

Figure 4-13: Validation of DNA integrity. DNA integrity was calculated on DNA extracted from apoptotic cell death with a mean DNA integrity of 1.7 x 10^{-3}± 8.0 x 10^{-4}. DNA integrity of necrotic cell death showed a mean DNA integrity of 0.90±0.036. A 1:1 mixture of DNA from apoptotic cell Death: DNA from necrotic cell death showed a mean DNA integrity of 0.45±0.07. All conditions at n=5.

DNA integrity was determined in media (after purification) using the 115bp and 247bp replicon primers to evaluate necrotic and total DNA concentration, as illustrated in Figure 4-7A. From this DNA integrity was calculated as described in Equation 4-1. The DNA integrity when mixing 1:1 DNA from necrotic and apoptotic cell death, increased from 1.7 x 10^{-3}± 8.0 x 10^{-4} to 0.45±0.07, as shown in Figure 4-7A. There was no significant difference in total DNA concentration for DNA from both necrotic and apoptotic cell death (Figure 4-7B).

4.3.9. "Worst Case Scenario" Model to Confirm Upper Limit of DNA Standard Curve

A model for "worst case scenario" was developed to condition plasma by simulating complete cell death, using the same beads to plasma ratio as the large scale BAL system, as outlined Methods Section 2.3.5. DNA concentration in the conditioned plasma was used to determine the upper standard curve for the Alu repeat QPCR.

Encapsulated HepG2 cell viability, was 95.6±2% immediately after harvesting (Figure 4-8A and B). A volume of 2ml beads in 40ml of plasma from healthy patients was incubated for 48 hours at 37°C under constant vigorous agitation, to achieve mechanical cell damage, causing a reduction in viability to 26±6% (Figure 4-8C and D). The initial DNA integrity measured immediately after bead harvesting was 0.34±0.05 increasing to 0.48±0.07 after 48 hours conditioning. This confirmed that DNA release from cells that underwent mechanical stress was from necrotic cell death. In addition, total DNA concentration increased by 62.2ng/ml confirming that a loss in viability causes DNA release.

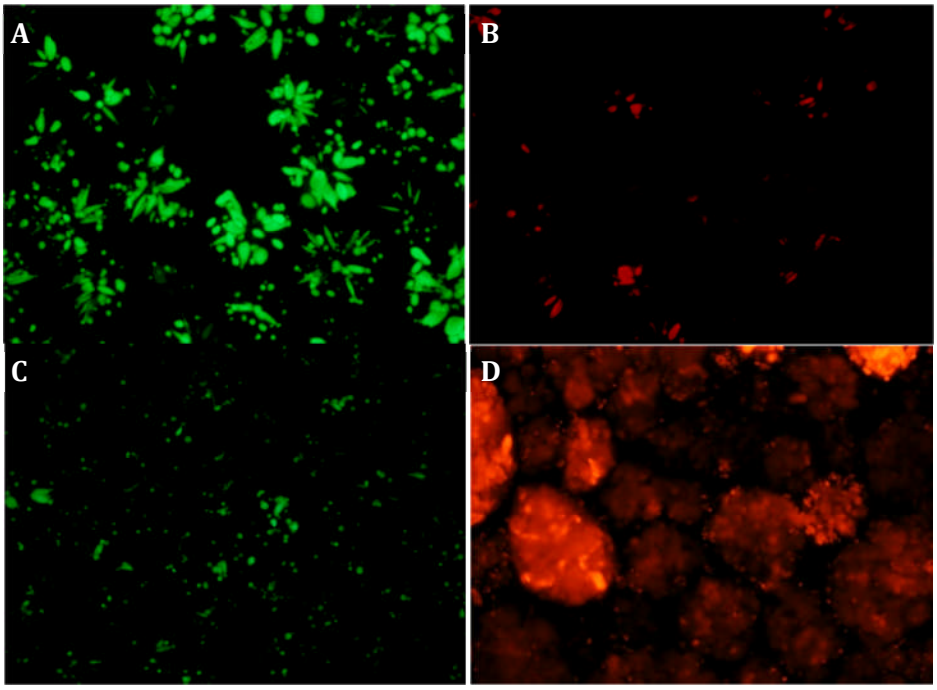

Figure 4-14: Mechanical damage of cell to induce necrosis. Encapsulated HepG2 Cells incubated at 37°C for 48 hours in HEPES buffered plasma from healthy patients, under constant agitation, showed decreased viability from 95.6±2% immediately after harvesting to 26±6%. A; FDA stained beads immediately after harvest from the BAL growth phase. B; pI Stained cells immediately after harvest from the BAL growth phase. C; FDA staining of beads after incubation. D; pI staining of beads after incubation.

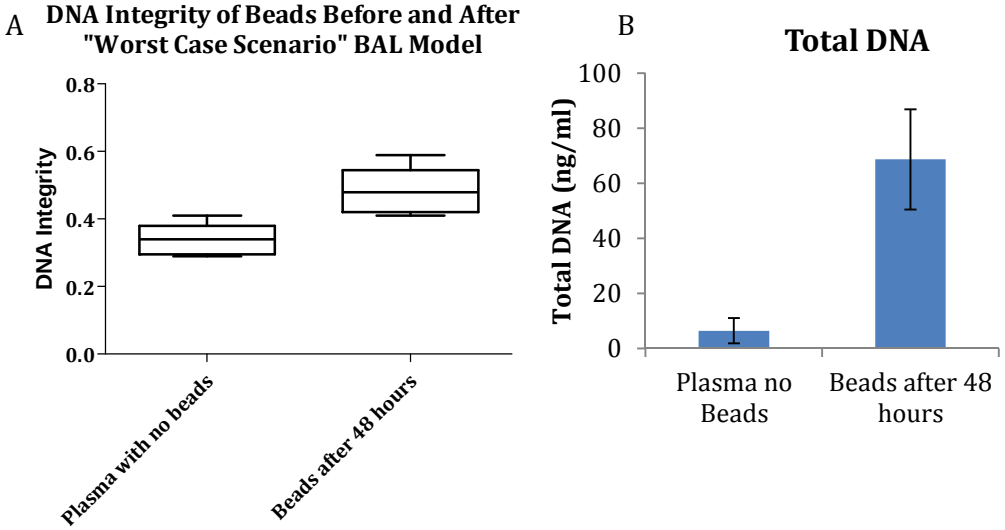

Figure 4-16: DNA integrity and total DNA for beads under mechanical stress (i.e. increased DNA from necrotic cell death) concentration increased by incubating 2ml of encapsulated HepG2 cells in human 40ml of plasma from healthy patients, over 48 hours, as outlined in. A; mean DNA integrity of 0.34±0.05 with beads incubated in human plasma and 0.48±0.07 with beads freshly harvested from the BAL growth phase (n=5). B; Total DNA concentration in plasma sampled at the end of 48 hours incubation compared with DNA in the plasma immediately after adding the beads (n=5).

4.3.10. Determination of DNA Release using the Small Scale BAL Model

The small scale BAL system was used to measure the potential DNA release in the large scale BAL treatment phase, indicating the amount of DNA a filter must remove. Plasma from both

ALF and healthy patients were used in the scale BAL system to show changes in viability and DNA release. From this, DNA integrity was determined to assess the nature of DNA release over treatment time. In addition, other parameters, such as glucose consumption and protein synthesis, were determined to indicate the cause of cell death.

Five separate sets of encapsulated HepG2 cells and scale BAL models were used to gain statistical power, making beads using the Jetcutter® encapsulator system and culturing beads in the large scale growth phase. The mean cell density between experiments was 51.9 x 10^6 ± 1.12 x 10^6 cells/ml of beads (FBB 22, 26, 27, 30 and 32), where a volume of 5ml from each encapsulation was used in each scale BAL model experiment, testing each plasma condition in duplicate.

4.3.10.1. Perfusion of Beads in Plasma from Healthy and ALF Patients

Viable cell numbers were significantly reduced when perfused with plasma from the ALF patients, from 51.9 x 10^6 ± 1.12 x 10^6 cells/ml of beads to 37.9 x 10^6 ± 2.2 x 10^6cells/ml of beads (Figure 4-17). A two-tailed t-test showed a significant difference with p<0.0001 with n=10 (error bars representing standard deviation). However, perfusion with plasma from healthy patients showed no significant difference in viable cell number, (using a two tailed t-test p=0.3674, n= 10, error bars representing standard deviation).

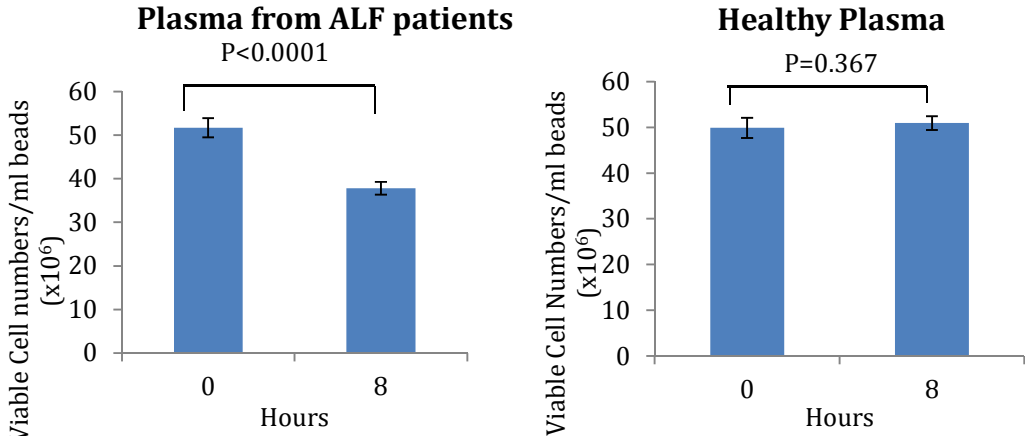

Figure 4-17: viable cell number for encapsulated HepG2 cells, perfused with plasma from ALF patients, reduced from 51.7x10⁶ ± 2.2x10⁶cells/ml beads to 37.9x106± 1.5x10⁶cells/ml beads. Perfusion with healthy plasma had no significant effect. A; ALF plasma caused a significant reduction in viable cell number, paired t-test, n=10, P<0.0001, error bars represent standard deviation. B; Plasma from healthy patients had no significant effect of viable cell numbers, paired t-test, n=10, p=0.367, error bars represent standard deviation.

4.3.10.2. Glucose and Lactate Consumption as a Measure of Metabolic Activity

Glucose consumption by encapsulated HepG2 cells perfused with either plasma from healthy or ALF patients showed no significant difference as illustrated in Figure 11A and B (Paired two tailed t- test, p=0.1079, n=10). However, lactate levels in the same experiment were different between plasma from healthy and ALF patients (paired two tailed t-test p=0.0058, n=10). This result may be due to higher lactate levels in liver failure patients, causing the difference to be attributable to higher background levels. The rate of lactate increase during the experiment was not significantly different (regression analysis p=0.5914) Figure 4-11B.

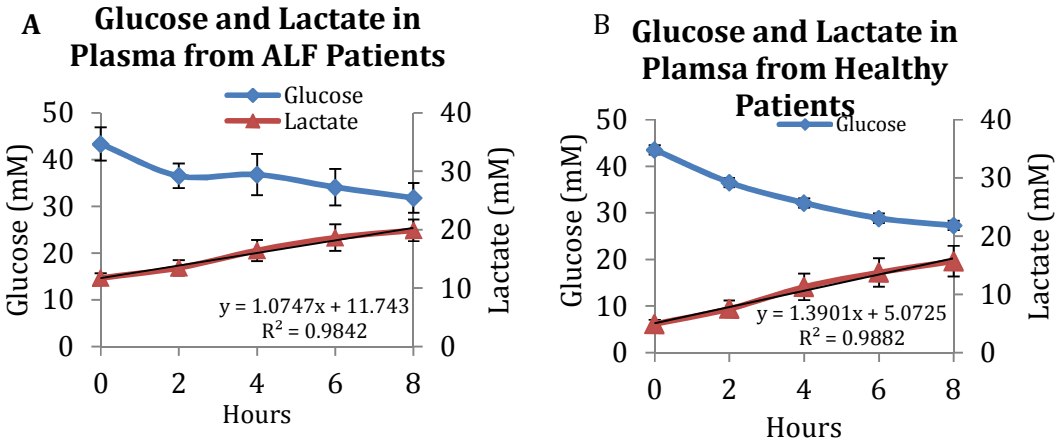

Figure 4-11: Glucose consumption and lactate accumulation. No significant difference in glucose metabolism was observed in beads perfused for 8 hours with either plasma from ALF or healthy patients, (Paired, two way t-test, n=10, p=0.1079, error bars representing standard deviation). Lactate levels were significantly higher in plasma from liver failure patient compared plasma from healthy patient, (paired two way t-test, with n=10 giving, p=0.0558, error bars representing standard deviation). The rate of lactate increase was not significantly different (regression analysis, p=0.05914). A; change in glucose and lactate concentration in plasma from ALF patients. B; change in glucose and lactate concentration in plasma from healthy patients.

4.3.10.3. AFP Production

Encapsulated HepG2 AFP production showed no significant difference between beads perfused with either plasma from healthy or liver failure plasma, shown in Figure 4-12 (regression analysis p=0.7633 n=10).

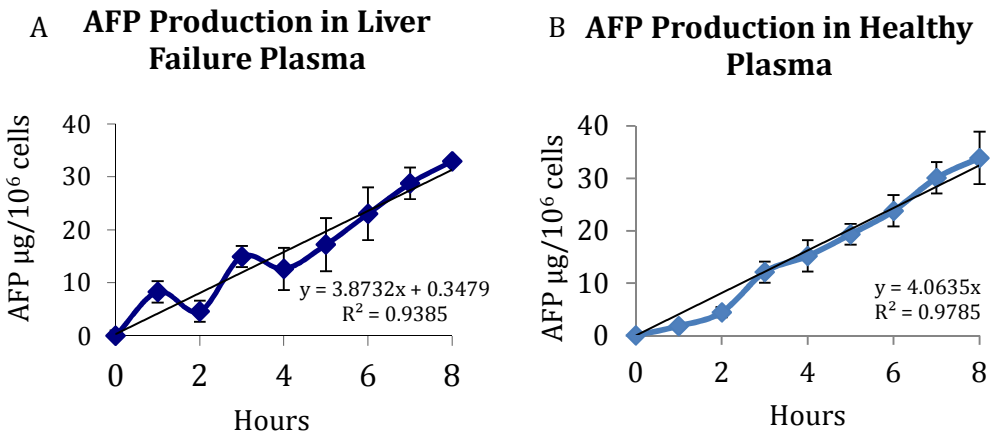

Figure 0-1: encapsulated HepG2 cells were perfused for 8 hours with either plasma from healthy or liver failure patients. AFP production was not significantly different in these conditions (regression analysis p=0.7633). A; AFP production in plasma from liver failure patient. B; AFP production in plasma from healthy patients.

4.3.10.4. DNA Integrity of Beads Perfused with Liver Failure Plasma

DNA integrity showed no significant difference before and after 8 hours of perfusion with plasma from the ALF patient (Figure 4-2, p=0.7221). However, DNA concentration increased 4-fold every hour during the perfusion with liver failure plasma, with a background DNA level of 11±2ng/ml measured at time 0. This was coupled with a 13.8 x 10^6cell/ml beads reduction in cell viability as illustrated in Figure 4-2, totalling 69.0 x 10^6cells death from 5 ml of beads over the 8 hours.

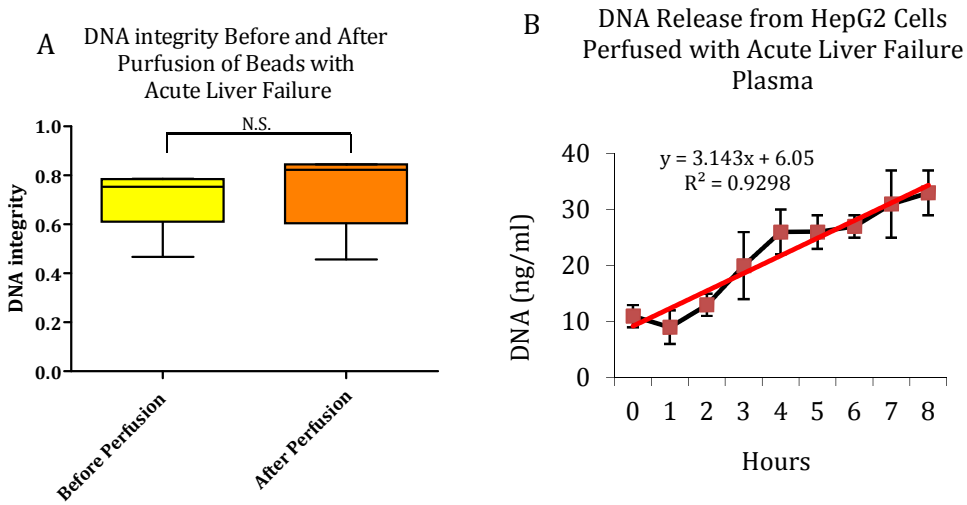

Figure 4-2: Encapsulated HepG2 cells perfused with plasma from an ALF patient over 8 hours. A; no significant difference in DNA integrity before and after perfusion (n=10 p=0.7221 two tailed t-test). B; an increase in DNA concentration over 8 hours, with a 3-fold increase in DNA concentration every hour, (n=10, error bar show standard deviation).

4.3.10.5. DNA Integrity between Plasma from Healthy and Acute Liver Failure Patients

A fresh sample of plasma, obtained from a patient suffering from ALF, was obtained for method validation, and analysed for DNA integrity and total DNA concentration. DNA integrity in plasma from the patient with ALF was significantly higher (0.72±1.7) than plasma from healthy patients (0.336±15) (p=0.006, two tailed t test), demonstrating an increased level of DNA from necrotic cell death, Figure 4-21A. In addition, total DNA concentration in plasma increased from a mean of 0.23±0.0012ng/ml in healthy patients to 86±4ng/ml in patients with ALF, further confirming the increased DNA release from patients with acute liver failure due to hepatic cell death by necrosis, Figure 22B.

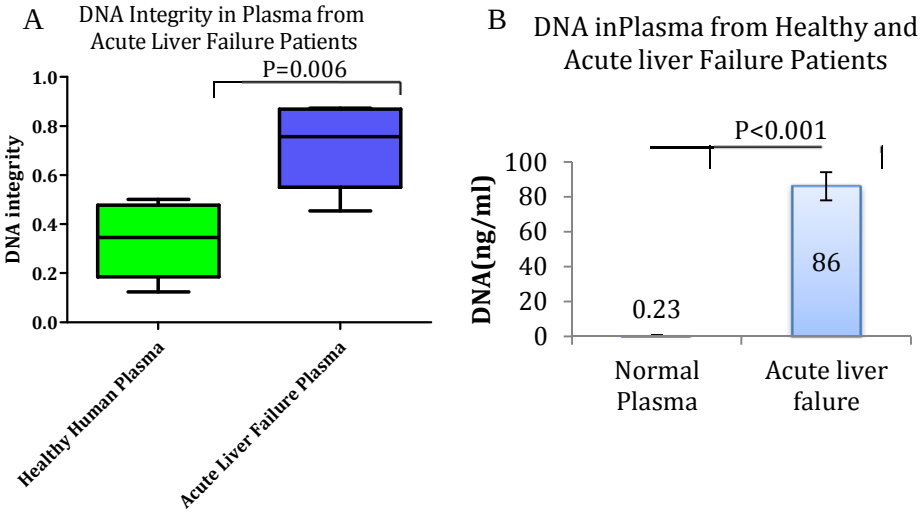

Figure 0-3: DNA in healthy and ALF plasma. A; DNA integrity significantly increases in plasma from a patient with ALF (0.72±1.7) compared with plasma from healthy patients (0.33±0.15), indicating an increased level of necrotic DNA. B; Total DNA concentration significantly increased between from 0.23±0.012ng/ml to 86±7ng/ml.

4.3.10.6. Changes in DNA as a function of Flow Velocity in the BAL model System

Despite a reduction in viable cell numbers, no significant changes in metabolic activity were found with plasma from ALF patients. Another parameter that may cause changes in viability is flow rate in the BAL system; there are two ways in which this could occur: an alteration in bead bed height causing reduction in mass transfer, or shear stress from the laminar flow. Therefore, healthy plasma was perfused at different flow rates measuring DNA integrity and cell viability.

As outlined in Section 4.1, flow velocities (ms^{-1}) in the scale BAL system were selected to fall either side of the large scale BAL flow velocity (Methods Section 2.3.4). The flow velocities of the scale BAL were $510mlmin^{-1}$, $191mlmin^{-1}$, and 101 $mlmin^{-1}$ for the 2.79mm, 1.52mm and 1.14mm bore size tubing respectively, compared with 3.8 x $10^{-}4$ in the large scale BAL, as listed Table 4-12Table 4-1.

BAL Type	Chamber height (m)	Chamber internal diameter (m)	Total volume (m^3)	Volumetric flow rate ($mlmin^{-1}$)	Linear flow rate (ms^{-1})
Large scale BAL Chamber	0.24	0.15	4.2×10^{-3}	400	3.8×10^{-4}
Small scale with 2.79mm pump tubing	0.18	0.01	1.4×10^{-5}	2.25	4.8×10^{-4}
Small scale with 1.52mm pump tubing	0.18	0.01	1.4×10^{-5}	0.837	1.8×10^{-4}
Small scale with 1.14mm pump tubing	0.18	0.01	1.4×10^{-5}	0.45	9.5×10^{-5}

Table 4-1: Chamber and flow characteristics in the large scale BAL chamber to achieve a 2-fold bead bed height, compared with the small scale BAL. At $400mlmin^{-1}$ the large scale BAL system shows a 2-fold bed height with a linear flow rate of $3.8 \times 10^{-4}ms^{-1}$. The small scale BAL with 2.79mm bore size tubing, at $2.25mlmin^{-1}$, showed a two-fold bed height; where 1.52mm and 1.14mm bore tubing showed lower bed heights of 1.5-and 1.2-fold, respectively. The linear flow rate was used to provide flow conditions comparable to that of the large scale BAL.

4.3.10.7. DNA Release from Beads in Plasma

Although no significant change in viability was detected after perfusion with healthy plasma over 8 hours, using FDA and PI staining (Figure 4-15C), some DNA release was detected (Figure 4-15A). As a result, some cell death, undetectable by fluorescent staining, produced an increase in DNA integrity from 0.081 ± 0.082, to 0.56 ± 0.15 (Figure 4-15C). This suggests that DNA in the plasma was from predominantly apoptotic origin, and over the 8 hours, any cell death that did occur was necrotic, possibly due to the laminar flow of the plasma causing low levels of cellular disruption.

An increase in necrotic DNA during the first two hours of perfusion followed by stabilisation, illustrated in Figure 4-15B, suggests that some cell death occurred during this time. It also became clear that, increased flow rates did not contribute to cell death as there was no significant difference in DNA release over the 8 hours, as illustrated in Figure 4-15C (paired t-tests with n=10, 2.79mm vs. 1.52 with P=0.2984, 1.52mm vs. 1.14mm with P= 0.0560 and 2.79mm vs. 1.14 with P=0.1605).

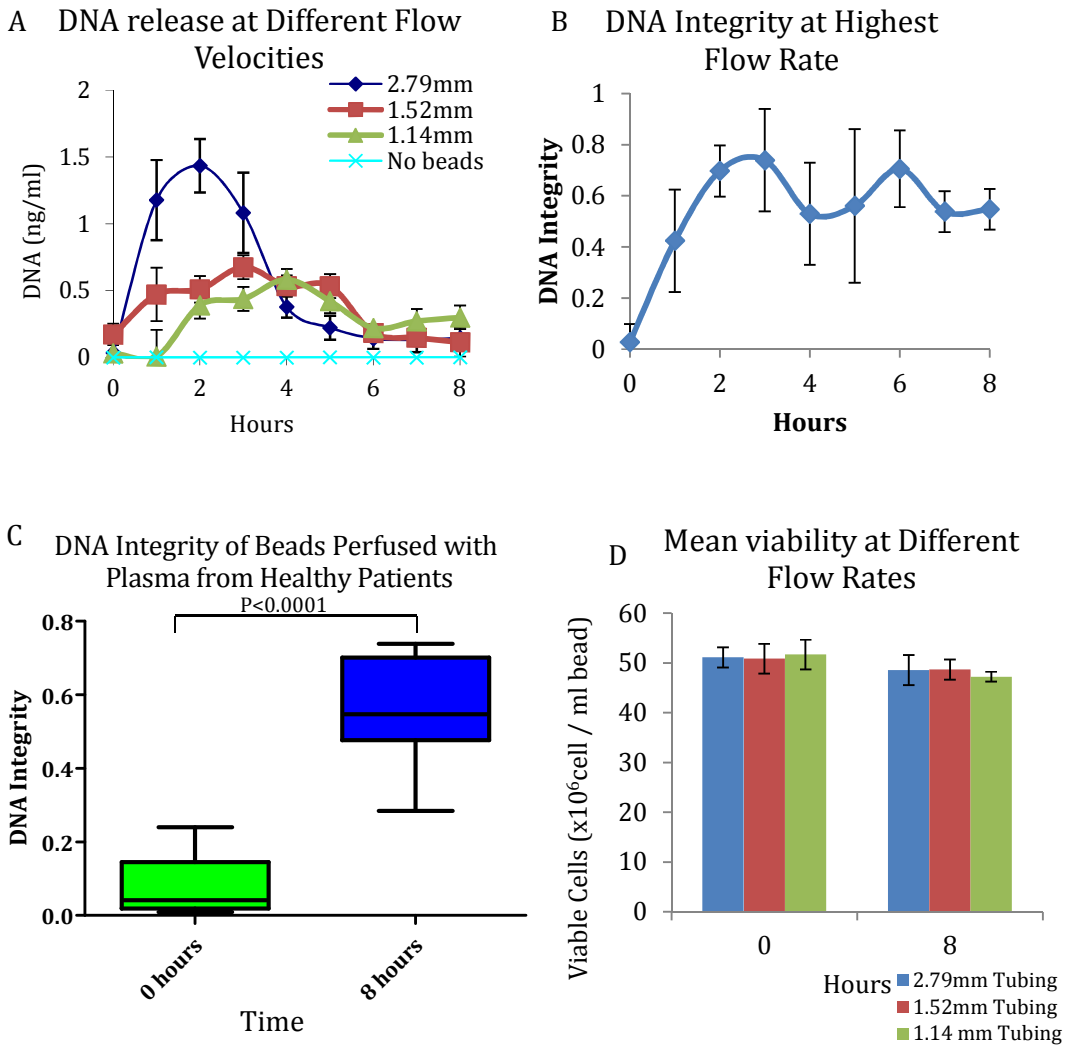

Figure 4-15: DNA release from a scale BAL system. Total DNA concentration was measured in samples taken every hour, over 8 hours perfusion with plasma from healthy patients, using the 115bp replicon primer. Amplification with the 247bp replicon primer provided DNA integrity (methods Section 2.2.3). A; total DNA concentration showed no significant difference with increased flow velocity, (t-test with n=10, 2.79mm vs. 1.52 with P=0.2984, 1.52mm vs. 1.14mm with P= 0.0560 and 2.79mm vs. 1.14 with P=0.1605, all error bars represent standard deviation). One way ANOVA analysis on all samples vs. no beads showed a significant difference in DNA level (P=0.0083, n=10). B; DNA integrity of beads perfused using the 2.79mm bore size tubing, showing an initial increase in DNA integrity up to 2 hours where there was no significant difference thereafter, (ANOVA, n=10, P=0.00062, error bars represent standard deviation). C; change in DNA integrity with perfusion using 2.79mm bore size tubing from initial DNA integrity to that after 8 hours, illustrating the change from mainly apoptotic DNA (0.081 ± 0.082, to 0.56 ± 0.15) to necrotic. D; Viable cell number before and after perfusion with healthy plasma for 8 hours showed no significant decrease viability for all tubing size (one tailed paired t-test p<0.0001).

4.3.11. Calculating Total DNA Release during a BAL Experiment

In the small scale BAL with 5ml beads and a starting HepG2 cell density of 51.7 x 10^6cells/ml, showed a 22ng/ml DNA release into 80ml from 69.0 x 10^6 dead cells over 8 hours, giving 1.76µg total DNA.

A large scale system of 7L of plasma with a bead cell density of 51.7x10^6cells/ml beads requires 1353ml of beads to provide the 7.0 x 10^{10}cells/ml predicted to be sufficient for treatment. Therefore, if 5ml of beads at this density released 1.76µg, 1353ml beads at the same cell density would release a total of 476.6µg of DNA in 7L, assuming a 23% drop in viability shown in the scale BAL. A final DNA concentration of 68ng/ml DNA would be expected after 8 hours of perfusion, in the large scale BAL. According to the theoretical calculation in Table 4-2, a 27% drop in viability with 7x10^{10} cells would release 19µg/ml DNA, over 200-fold greater than the amount measured in the scale BAL. DNA concentrations with a final BAL design of different volumes and total cell numbers are outlined in Table 4-13 as calculated from the scale BAL.

BAL Condition	Volume of beads with 7x10^{10} cells (ml)	Volume of Beads with 1x10^{11} cells (ml)	DNA concentration with BAL with 7x10^{10} cells (µg/ml)	DNA concentration with 1 x 10^{11} cells (µg/ml)
3.5L Plasma	1353	1934	136	195
7L Plasma	1353	1934	68	97
10L Plasma	1353	1934	48	68

Table 0-2: potential DNA concentration in large scale BALs with increasing total plasma from liver failure patient volume, with a bead density of 51.7 x 10^6cells/ml beads and a mean 19 ±3.7% reduction in cell viability.

4.3.12. Endotoxin

As previously mentioned, endotoxin contamination may originate from the BAL system, but may be eclipsed by the amount originating from a patient suffering from ALF. In order to reduce or remove endotoxin levels for both therapeutic and regulatory reasons, an endotoxin assay was optimised for use in human plasma.

4.3.12.1. Endotoxin Standard Curve

The LoQ of endotoxin in water was established by initially using a zero calibrator, and serial endotoxin dilutions. The zero calibrator involved repeating negative endotoxin free sample with n=20 which gave a mean value of 64±2.4 Fluorescence units (FU). According to accepted models[154,208], the limit of detection (LoD) should be set at two standard deviations above the

zero calibrator, giving 68.4FU. The limit of detection should be set at ten-fold the standard deviation above the zero calibrator, at 88 FU. As a result, any endotoxin reading below 88FU was disregarded, and so the LoQ for this assay was set at 0.01pg, showing a mean 112±7 fluorescence units (n=20), shown in Figure 0-4.

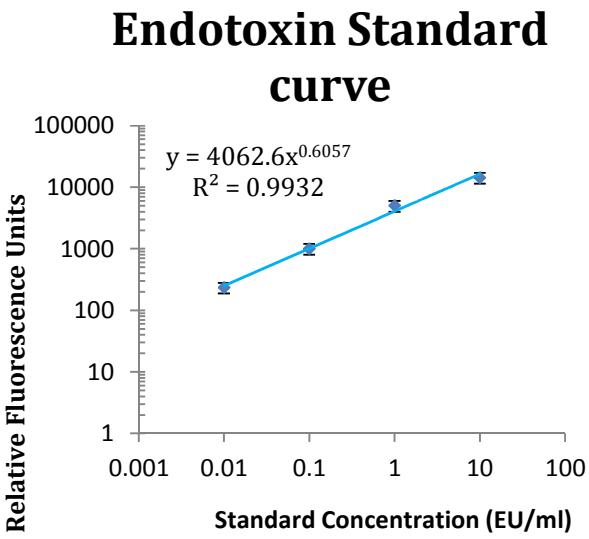

Figure 0-4: Endotoxin standard curve with LoQ of 0.01EU/ml, in water. Each sample n=5 using certified Endotoxin standard extracted from *Escherichia coli* O55:B5.

Removal of inhibition from plasma was achieved using two approaches: reduction in protein inhibition through dilution; heat treatment causing inactivation of proteins and endotoxin release from other proteins (Methods Section 2.7). Dilution of plasma down to 0.5% and heat treatment removed inhibition from plasma to an insignificant level, shown in Figure 4-17 (paired two way t-test with P=0.68, n=5).

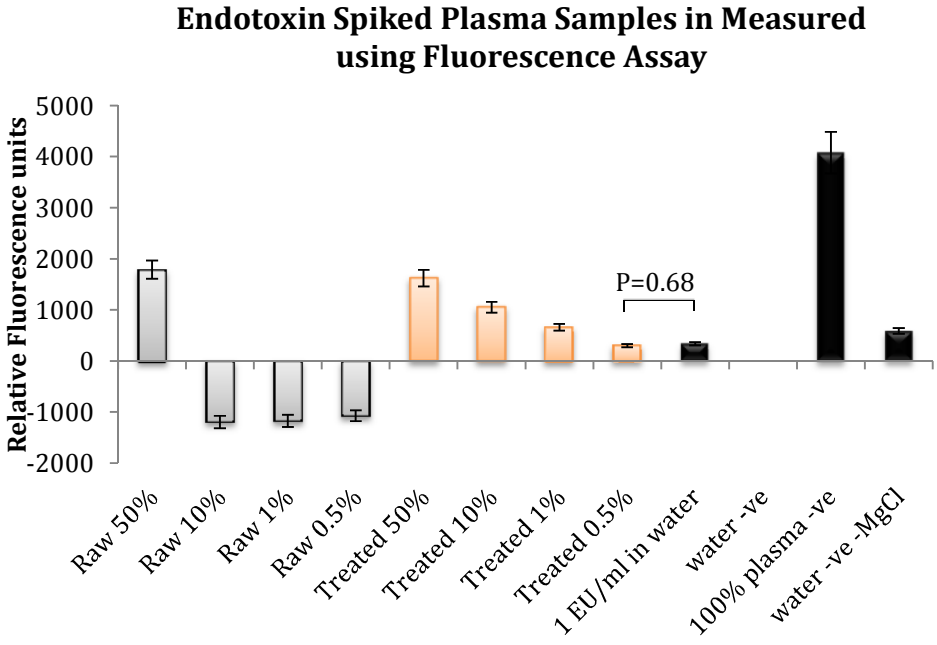

Figure 4-17: Endotoxin levels in plasma. Plasma samples were spiked with 1EU/ml of endotoxin for fluorescence analysis, requiring a 0.5% dilution and heat treatment to remove inhibition (n=5, p=0.68, two tailed). Raw samples denote untreated plasma spiked with 1EU/ml endotoxin, followed by the dilution. Treated samples denote samples heated as outline in Methods Section 2.6.5 followed by dilution. The same undiluted, untreated plasma used for other samples was added to the endotoxin assay.

4.4. Discussion

This chapter involved establishing detection methods for contaminants, including, cell debris and endotoxin, but mainly focusing on DNA detection. Development of a DNA detection system was initially based on predicted release, (particularly QPCR) to be optimised in a plasma environment. Thereafter, the scale BAL model enabled the refinement of the detection methods by demonstrating realistic levels to be expected in the large scale BAL. Those DNA levels also provided information regarding the necessary capacity of a filtration system, which was tested in later chapters.

In addition to DNA release, the Scale BAL model also provided an indicator of cellular response to plasma from one ALF patient. As previously mentioned, during the priming process healthy plasma would be used to prime the system. Therefore, at the beginning of the experiment, healthy plasma is constantly diluted by ALF plasma from the patient. Consequently, the scale BAL model provides an environment, reflecting extreme conditions, in the absence of this dilution effect.

4.4.1. Method Validation

To fulfil the criteria for regulatory market approval for manufacture of a medical device, each contaminant measurement within the BAL system will require validation[77,117,118,209-211]. The process of validating an analytical assay for use with a medical device requires a process of testing a wide variety of parameters, which include the analyst, the instruments and the preparation environment[77,209]. For a research laboratory, many of the processes necessary are hugely impractical without substantial investment that is inappropriate for a research laboratory. These considerations will be discussed in more detail in later chapters.

As a result, an approach was used to validate methods to a stage that were deemed adequate for pre-clinical trials, with the view that extending the methodology for incorporation into a manufacturing quality control mechanism would require minimal added development. The QPCR methodology was validated to provide a robust, precise and reliable analytical method in the Liver Group laboratory, using the Rotorgene 3000 thermocycler. Extending this into a GLP quality control laboratory would require further developments including validation of new thermocyclers and an expansion of the quality manual and related SOPs to incorporate regulatory compliant and standardised training documents, detailed in later Chapters.

4.4.2. Alu Repeat QPCR Development

A key aspect towards eventual Alu repeat QPCR validation was to determine the reliability of the reaction, for both standards and the samples treatment process. Attaining efficiency values between 80% and 110% have been shown to be sufficient for accurate DNA quantification, if the sensitivity of the PCR is adequate for the application[212,213]. An efficiency less than 100% suggests PCR reaction inhibition, whereas greater than 100% is indicative of non-specific

amplification, enhancement of fluorescent signal or DNA contamination[214-216]. Ultimately, the efficiency values obtained provide a measure of proportionality[217]. Despite clear non-specific amplification (illustrated in Figure 4-5A and C) by smearing above the band of interest, both replicon primers proved to amplify template concentration proportionately, confirmed by high R^2 values for standard amplification (in Figure 4-9A and B), with amplification efficiencies close to the desired 100%, at 106±1.2% and 101±0.9%, for the 115bp and 247bp replicon primers, respectively.

To substantiate the efficiency, the melt curve analysis illustrated that a single product was being amplified although some background was clearly evident (Figure 4-8). For most QPCR applications, a set of primers for a specific gene is used, producing a much more distinct peak for the melt curve, essential in ensuring that the primers do not cross amplify other genes and the PCR product is not contaminated[107,145,218]. The non-specific amplification alluded to here was attributable to the Alu primers being specifically designed to amplify as many of the Alu repeat subfamilies as possible to increase sensitivity, reflected in melt curve and electrophoresis analysis showing non-specific amplification. Others using Alu repeat primers and other tandem repeat sequences have observed the same phenomenon, coming to the conclusion that a melt curve with background is inevitable as long as linearity and efficiency are proven[219,220].

4.4.3. QPCR Validation

Different aspects of QPCR validation provide information to support the reliability of the results by establishing the limits and ensuring the method was fit for purpose. Furthermore, as discussed in later chapters, legal requirements for work to be carried out in certified laboratories, such as GLP compliance, rely not only on the quality of method development, initiated in this chapter, but also on the quality of the supporting documentation and management systems[199].

Important validation parameters outlined in Section 4.1.2 were: precision (as measured by repeatability and reproducibility), recovery, linearity, and sensitivity. As part of defining precision, repeatability analysis determined the constitutive error within the protocol by calculating the % CV values, to provide values reflecting the tightest form of precision measurement. In all cases, the % CV value was between 2.5% and 4.9%, showing the low level of constitutive error achieved. Two QPCR methods passed by the FDA for detecting the H1N1 RNA in human plasma between them showed %CV values spanning 0.6% - 4.6%[221,222]. Therefore, the values obtained for Alu repeat QPCR for total blood would be within these limits, if performed on a single thermocycler.

Using identical samples reproducibility analysis provided a less robust measure of precision by incorporating changes to analyst and QPCR thermocycler over time. As a result, the data was grouped for different analysts, PCR thermocyclers and tests performed over a year, showing a

significant increase in %CV values ranging from 8.1% to 14.8%. This clearly demonstrated that the QPCR method loses precision when incorporating changes in analyst, PCR machine, and increased time between analyses.

Another important indicator for the reduction in precision was the significant difference between the cT values obtained from different PCR thermocyclers, as illustrated in Table 4-6. The %CV figures for each primer set on individual PCR machine were within acceptable limits, albeit the %CV increased slightly for the RG6000® and BioRad® thermocyclers, due to initial PCR optimisation being performed on the RG3000®. It was clear, therefore, that changing the QPCR thermocycler had a significant effect on cT values, but results performed on specific thermocyclers maintained reliability, consequently requiring re-validation only if changing between thermocyclers.

Conventionally, an analytical method as part of a GLP laboratory involved with quality control of a manufacturing process would be validated on a single PCR thermocycler. Other variables, such as changing an analyst, would be addressed in a GLP Laboratory through formal training on a specified instrument, with extra analysis during changeover of analysts, to ensure the reliability of the results[223].

4.4.3.1. Recovery Analysis

Spiking plasma and media samples with a known concentration of DNA, then purifying and analysing samples, as described in Section 4.1.2, provided a measure of DNA recovery. The purification protocol (Methods Section 2.2.3.2) improved recovery in both plasma and media from between 58.0±41.85% - 62.8±36.2% to 98.8±2.4% - 101.5± 3.5%, quantifiable down to the LoQ of 0.01ng/ml. These figures are within acceptable limits for recovery analysis, for validated QPCR methodology[217,224,225] enabling the accurate analysis of DNA in media and human plasma for reliable total DNA quantification and DNA integrity analysis.

4.4.3.2. DNA Integrity

The concept of DNA integrity was used to establish DNA from apoptotic and necrotic cell death in differing BAL treatment states. Apoptosis was induced by Staurosporine treatment, which was confirmed by the Caspase 3/7 GLO® assay (Figure 4-6 and Figure 4-7A) typically yields a low DNA integrity ($1.7 \times 10^{-3} \pm 8.0 \times 10^{-4}$). Conversely, necrotic DNA from multiple freeze thaw cycles, at -80°C, showed a significantly higher DNA integrity at 0.90±0.036. Finally, mixing the apoptotic and necrotic DNA to a 1:1 ratio was reflected in the DNA integrity of 0.45±0.07 (Figure 4-7A). Importantly, the DNA concentration of both remained unchanged; confirming that the DNA integrity reflected the induction of apoptosis or necrosis in HepG2 cells in culture. The utilisation of this technique has been demonstrated as providing a potential cancer diagnostic tool, with an increase in DNA integrity representing necrotic cell death[115,147,148,225].

Expanding the use of DNA integrity to the "worst case scenario" BAL model of cell death provided an indication of DNA concentration if cells died in large numbers. Over 48 hours of incubation in healthy plasma, 69% reduction in viability produced a 62.2ng/ml increase in DNA concentration, as well as an increase in DNA integrity from 0.34±0.05 to 0.48±0.07. The increase in DNA integrity illustrated that DNA release from HepG2 cells under mechanical and environmental stress underwent necrotic cell death (Figure 4-9). In addition to this, a background level of cfcDNA was detected in plasma with no beads, although predominantly apoptotic, some DNA from necrosis was detected. A similar observation was made with cancer diagnostics using Alu QPCR, where a background of cfcDNA from necrotic origin was represented in the DNA integrity which showed a predominantly apoptotic DNA origin[99,148], unlike tested DNA integrity from induced cell necrosis by freeze thawing in Figure4-6.

4.4.3.3. DNA integrity in ALF plasma

The background DNA level in plasma from the ALF patients used in the small scale BAL was 11±2ng/ml. Analysis of DNA integrity showed DNA predominantly from necrotic cell death. As a result, when perfusing alginate encapsulated HepG2 cells with plasma from the ALF patient, in the small scale BAL experiment, the DNA integrity was not significantly different (Figure 4-13), due to the background necrotic DNA being too great for the QPCR protocol to detect any changes.

Although no significant change in DNA integrity was observed, a trend towards a higher DNA integrity could be seen, with a possible addition of DNA from HepG2 necrosis (Figure 4-10). In addition to this, perfused with plasma from ALF patients, HepG2 cells showed a 27% reduction in viability, releasing 22ng/ml or 1.76µg total DNA, which is over 200-fold less than the 19µg/ml calculated using the theoretical calculation shown in Table 4-2. Therefore, cell death does not correspond to DNA release with the same efficiency that was assumed for the theoretical calculation. Despite this, a lower DNA concentration will place a lesser burden on a filtration system.

4.4.4. DNA Integrity as a Diagnostic Tool

In the same way that DNA integrity may be used for cancer diagnostics, the technique could be applied to changes in cfcDNA in ALF patients. Some interest has been has been reported on this topic, where a recent conference proceeding at The American Association for the Study of Liver Disease (AASLD) reported using primers specific for the β-actin gene, showing a significant difference in cfcDNA concentration in sera of chronic liver failure patients compared with healthy patients[226]. This method goes further in being able to distinguish between background apoptotic DNA and necrotic DNA, as well as potentially improving sensitivity by virtue of amplifying Alu repeats, which are ubiquitously found across the genome. Furthermore, the DNA concentration in a fresh plasma sample collected from a patient and frozen at -80°C within 6 hours showed a DNA concentration of 86±7ng/ml as opposed to 11±2ng/ml, which could

have been due to variation between patients, as a result of storing the plasma used to perfuse cells at -20°C, or a difference in the method of collection, namely direct phlebotomy vs. plasma exchange where the plasma is lymphocyte and platelet depleted.

To fulfil the potential as a diagnostic tool, a trial should include patients suffering from ALF and healthy patients with sufficient replicates for statistical power. In addition to this, variations in state of liver disease including chronic liver diseases, could be investigated to confirm whether cell death by necrosis can be correlated with either the extent of liver damage, the rate of liver damage and the cause of damage[31,227,228].

A background level of cfcDNA was detected in plasma without beads; although predominantly apoptotic, some DNA from necrotic origin was detected. A similar observation was made with cancer diagnostics using Alu QPCR, where a background of DNA from necrotic origin was represented in the DNA integrity otherwise reflecting a predominantly apoptotic origin[99,148].

4.4.4.1. Cell Debris

The largest contaminant within the plasma will be from cell and alginate debris. Conventionally in process manufacturing, these would be removed through filtration or centrifugation. To analyse the effectiveness of the method, electron microscopy or nucleic magnetic resonance imagery would show the presence of cell debris on the filter membrane, or in the centrifuged pellet, as well as particulate analysis by laser light obscuration to confirm absence in the clarified liquid[188,229,230].

Particulate analysis of filtered plasma to remove cell debris will be discussed in later chapters. In this chapter, viable and non-viable whole cells were detected in the reservoir of the scale BAL system. Currently a 200µm physical barrier prevents large particulates entering the patient, if the alginate/cell fragments are smaller than 200µm they would pass into the patient. The most efficient way of preventing cells from entering the patient would be to introduce a filter with a nominal porosity sufficient to retain hepatocytes, typically between 10-40µm in diameter[231]. The porosity of charged depth filters discussed in later chapters were all below 10µm nominal porosity, being ideal for cell retention.

4.4.4.2. Endotoxin Analysis

As previously mentioned, the main source of endotoxins within the BAL system will originate from the patient, the control of which is necessary mainly for clinical benefit. Initial validation of the endotoxin standard curve showed a LoQ of 0.01pg using a zero calibrator. However, to remove plasma inhibition, samples were diluted to 0.5% followed by heat treatment (Methods Section 2.7). As a result, the LoQ of the endotoxin assay was 2EU/ml or 200pg/ml of endotoxin. For parenterals 25EU/ml is the limit required[201]; but for further method development and validation a more accurate method of analysis may be required, to determine reduction in

endotoxin concentration in ALF patients, previously shown to be 58.2±12.3pg/ml[232] or 0.582±0.123EU/ml, below the current LoQ. The use of kinetic end point chromogenic LAL assay has been reported to have sufficient sensitivity to measure endotoxin in healthy donor's blood[223].

The validation process for endotoxin removal was not as extensive as the QPCR methodology for two reasons; the LoQ would be insufficient for a valid analytical method[223], and for research purposes the assay was sufficient in showing the endotoxin removal capabilities of a quality system. A kinetic fluorogenic approach may be more appropriate which has a lower LoQ of 0.005EU/ml in water, performed in a facility that is dedicated to endotoxin analysis.

The next chapter will seek to remove the DNA and endotoxin, which were shown to be present in the scale BAL models, by filtration. Initially a scale filtration model was developed to test the efficacy of the filtration system for removal of DNA from the BAL system.

4.5. Conclusions

For the Purposes of measuring reduction in DNA or endotoxin in the full scale BAL system, QPCR was validated in human plasma to show reduction or even absence by a removal system. Endotoxin analysis although not validated to the same extent as QPCR, was sufficiently sensitive to show endotoxin removal down to 2EU/ml. DNA and endotoxin removal was then tested in the small scale BAL detailed in the next chapter.

Scaled Down Model for Filtration

This Chapter details filtration of plasma using 3M Cuno Filters to remove DNA, endotoxin, and particulates, with a scaled down model of the BAL system.

5. Scaled Down Model for Filtration

5.1. Introduction

Selection of an appropriate filter membrane is central to the BAL quality management scheme and relies on measuring two main parameters: volumetric capacity (volume throughput before filter blocks) and breakthrough capacity (volume throughput before selected impurity is found in filtrate). It is essential to have this information before embarking on pre-clinical trials, because problems of inadequate filtration would be difficult to correct once a BAL run has started.

5.1.1.1. Filtration Principles

Filtration of blood and plasma has been used in many medical contexts as described in Introduction Section 1.6.2. To establish the required efficacy of a filtration system, three equally important and interrelated principles need to be considered: the sieve capacity, total volumetric capacity and molecular binding capacity.

Sieve capacity relates to the physical retention of macromolecules and particulates on/in the membrane, such as proteins and platelets, respectively. Depending on the porosity of the filter, macromolecules and particulates retention by size exclusion may lead to filter fouling, resulting in a reduction in total volumetric capacity and abnormal pressure build up in the circuit. In addition to this, molecular interactions in the form of hydrophobic, ionic or charge based adsorption can add to retention of substrates needed to be retained in the circulating fluids of the BAL[234,235]. In many cases, retention of certain macromolecules or particulates may be desirable, for example in the BAL retention of particulates over 1μm, constituting mainly cell debris and potentially particulates from the alginate[236].

Retention of macromolecules and particulates, however desirable or unwanted, strongly influence the volumetric capacity of the filter. Some of the ways particulates may settle onto a filter are illustrated in Figure 5-1, showing effect of filter porosity and the size distribution of particulates. Mathematical models, detailed in Sections 5.1.2, describe the way particulates block filters, to allow us to predict the volumetric capacity of the full-size BAL using a scaled down circuit, small filter and where volume throughput can be measured.

The filter binding capacity reflects the number of molecular binding sites available for interaction between molecular compounds dissolved in the plasma, such as DNA and endotoxins, and the filter membrane[236]. Retention of larger particulates and macromolecules may reduce the number of binding sites; simply by impeding access, but molecular binding capacity does not ordinarily impact on total volumetric capacity[236,237]. All three filter principles, sieve capacity, volumetric capacity and binding capacity, were quantified using

the small scale filter model, which I designed for the BAL treatment phase. The methodology followed the following process:

- The scaled down filtration model was used to pass plasma through selected filter media, as described in Methods Section 2.5.
- During the filtration, pressure and volumetric throughput were measured in real time.
- The filtration experiment was stopped if the differential transmembrane pressure reached 1.6bar, or supply of plasma was exhausted (based on information supplied by 3M Cuno® engineers).
- Membrane resistance over time was plotted to provide the data to model kinetics of filter blockage.
- Using mathematical models for filter blockage, the volume throughput for the filter media were calculated (Lm-2).
- The volumetric flow through the filter media was applied to specific filter sizes as defined in the Introduction Section 1.6.2.3.

5.1.1.1. Estimation of DNA capacity

The DNA capacity of the 3M® Cuno® EXP® filters, including the capacities of the ZA, LP and S series filters, have not previously been determined in plasma, due to the predominant use for purification and clarification of bioprocessing fluids[188,230]. Previous studies determined DNA removal using a 3M® Cuno® 90SP single layered charged depth filters (nominal porosity of 0.1µm) with 10µg/ml calf thymus DNA in culture broth at pH 7.4, measuring circulating DNA in the presence of Hoechst dye. The filter continually removed 10µg/ml of DNA, with DNA breakthrough eventually occurring at 53.8L/m^2 of filter media. Using a filter with a 25cm^2 (0.0025m^2) filter media area (utilised in the scale filtration model), the following DNA capacity was calculated:

- 53.8Lm-2 x 0.0025m2 = 0.1345L capacity before breakthrough with 10µgml-1 dose.
- 134ml x 10µgml-1 = 1345µg = 1.35mg of DNA capacity in a 25cm2 filter.
- In Chapter 4, the DNA concentration in a 7L BAL, with 1353ml of beads, at 5.7 x 10cellsml-1 beads was expected to release 68ngml-1, totalling 0.476mg DNA over 8 hours.

With an entire large scale BAL treatment phase predicted to release 0.476mg total DNA over 8 hours, theoretically a 25cm^2 3M® Cuno® 90LP filter, with a filter capacity of 1.35mg DNA, has sufficient capacity. Even if the extra cfcDNA (cell free circulating DNA) from the patient is included, at 78µg total DNA over 8 hours, totalling 0.553mg, the 25cm^2 filter would still be sufficient. However, the calculations are based on two assumptions: the filter will remove DNA from culture broth with same efficiency as human plasma, and the 25cm^2

filter capacity would provide sufficient volumetric capacity for the entire BAL treatment phase.

5.1.1.2. Principle of Particulate Adsorption

To model the ability for a 25cm^2 filter to provide sufficient capacity for 8 hours of plasma perfusion, the plasma constituents contributing to filter blockage were investigated. Plasma constituents that may cause physical filtration blockage could range from protein aggregates, lipids, cell debris, platelets, and whole cells. These constituents will be collectively referred to as particles for simplicity. Two factors govern the adsorption of particles onto a filter membrane are: hydrodynamic forces, which are the opposing forces to an object in the liquid flow and body forces that affect the entire body of the fluid such as gravity and electrostatic forces. Body forces do not significantly affect filtration capacity of depth charged filters and will not be included in calculations[238].

5.1.1.3. Hydrodynamic Forces

Different hydrodynamic forces affect the movement of particles in a liquid with competing influence, dependant on the size of the particulate and viscosity of the solution. Competing hydrodynamic forces are expressed as particulate velocities, with the highest velocity having the overriding influence on particulate behaviour. Characteristic velocities associated with the specific hydrodynamic forces are outlined in Table 5-1. The dominant force for macromolecules of around 100Å (proteins, Figure 5-3) is Brownian diffusion, so that adsorption onto the filter membrane is dictated by intermolecular equilibrium. As the particles radius increases, the effect of Brownian diffusive velocity decreases in influence at a ratio of $1/r_s^2$ (where r_s is equal to particle radius). At an r_s of 1µm, random particle motion, particle-particle interactions, and inter-particle collisions become the dominant forces, collectively named shear induced diffusion[239,240]. For larger particles, the inertial lift velocity becomes the overriding force, caused by the viscous flow of liquid against the particles to cause movement[238].

		Characteristic Velocity (m/sec)		
Force	Velocity equation	r_s = 100Å	r_s = 1µm	r_s = 10µm
Viscous Drag	$U_{visc} = J_v$	10^{-5}	10^{-5}	10^{-5}
Brownian Diffusion	$U_{Brown} = D_B/r_s$	10^{-3}	10^{-7}	10^{-9}
Shear Induced Diffusion	$U_{shear} = 0.1\ \gamma_w r_s$	10^{-6}	10^{-4}	10^{-3}
Inertial Lift	$U_{lift} = \gamma_w^2 r_s^3/v$	10^{-12}	10^{-6}	10^{-3}

Table 5-1: Characteristic velocities associated with different particle and macromolecular forces. Results are in water with the following conditions; Jv = 10-5msec-1 (equation 4), µ = 0.01kgm-3 (density), γw = 103sec-1 (weight), T = 300K (temperature), ρ= 1.0020 (dynamic viscosity) cP v = 10-6m2sec-1 (kinematic viscosity is ratio of density and dynamic viscosity, v = µ/ρ). DB was determined by Stokes-Einstein equation[241], r indicates radius of the particle, with 100Å representing a protein macromolecule, whereas a radius of 1µm and 10µm represents particles.

The adsorption of particulates onto the filter membrane dictates the volumetric filter capacity, measured using filter blockage models, which can be expressed as a function of changes in pressure.

5.1.2. Filter Blockage Models to Determine Volumetric Filter Capacity

Ideally, to determine the volumetric capacity of a filter, plasma should be passed through a scale filter until the volumetric capacity is reached, as defined by a pre-determined maximal back pressure, or break through of the selected impurities. However, due to a practical limitation of plasma supply, volumes of up to 3L were passed through a scaled down sized filter, measuring pressure and volume throughput as described in the Methods Section 2.5. Blockage models were used to predict the filter capacity as expressed by filter media flux (Lm^2). This flux was then applied to larger scale filters to predict the total capacity for use with the BAL treatment phase as shown in Table 5-6. To provide a robust filtration system, high filtration fluxes are desirable to minimise filter fouling and maximise throughput, allowing greater use of the entire depth of filter media, rather than just the filter surface for the capture of particles[236,238,242,243].

5.1.2.1. Theoretical Model of Liquid Passing through a Filter

Three main filter blockage models are used to describe the most common ways particle deposit onto a filter media: pore blockage, pore constriction, and cake blockage, illustrated in Figure 5-1. They are best understood by modifying Darcy's Law, which describes the linear flow rate of liquid through a porous filter media, taking into account the viscosity and pressure drop over the filter media distance, shown in Equation 5-1[244].

Equation 5-1:
$$Q = \frac{-kA\,(P_b - P_a)}{\mu L}$$

Where the total linear flow rate Q (m^3s^{-1}) is equal to the product of the filter media permeability k (m^2) and filter media area A (m^2), and the pressure before P_b (Pa) and after P_a (Pa) the filter media, divided by the product of the length of the filter membrane L (m) and the viscosity of the solution μ (Pas).

The permeability (k) of the filter media can be converted into a form applicable to a filter model by using the assumption that the filter media is formed of a series of single cylindrical pores. As a result, permeability takes on the dimensions of L^2 and can be expressed as part of Hage-Poiseuille's law, as an expression of fluid velocity[245]:

Equation 5.2:
$$V = \frac{r^2 \Delta P}{8 \mu \delta_m}$$

Where the velocity (m^3) equals the product of the pore radius r (m) squared and transmembrane differential pressure difference ΔP (Bar) all divided by 8 times the product of the viscosity μ (Pas) membrane thickness δ (m^2).

From this, the membrane resistance before filtration can be modelled by rearranging the Hagen-Poiselle's law to make resistance the subject assuming the membrane resistance is equal to the transmembrane differential pressure[238,246]:

Equation 5.3: $$R_m = \frac{8\delta_m}{N\pi r_p^{\,4}}$$

Where the membrane resistance equals 8 times the filter media thickness δ_m (m^2) divided by the product of the pore density N (m^{-2}) the radius of the pores r_p (m) to the power 4.

The Hagen-Poiseulles law is expanded to predict one of the blockage models below:

- Complete pore blockage shown in Figure 5-1A where particles are larger or similar size to the pores causing complete blockage, both internally and at the surface of the filter media.
- Gradual pore blockage shown in Figure 5-1B, where particles are smaller than the pore and gradually form layers to block the filter.
- Cake blockage shown in Figure 5-1C, where particles are larger than the pores and form a layer on the surface of the filter.

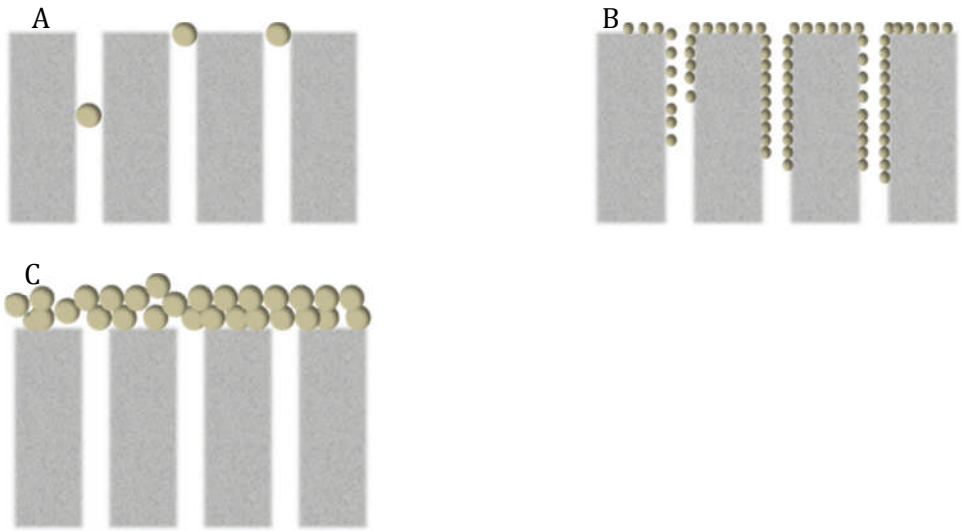

Figure 5-1: Representation of filter media blockage models. A; complete pore blockage, where particles completely constrict the cylindrical pore. B; gradual pore blockage, where smaller particles adsorb and gradually block the cylindrical pores. C; cake filtration, where particles form a layer over the filer media and do not penetrate the pore.

5.1.3.Measurement of Increasing Filter Resistance to Determine Filter Fouling Model

To establish the mode of blockage the relative resistance can be plotted over filtration time, producing distributions indicative of the blockage model as illustrated in Figure 5-2. Both

pore blockage and gradual pore blockage models show a concave shaped curve with increased filtration time, with pore blockage expressing a polynomial curve to the order of 3 and gradual pore blockage to the order of 2. Cake filtration shows a linear increase in resistance as particulates deposit on the surface of the filter membrane[246,247].

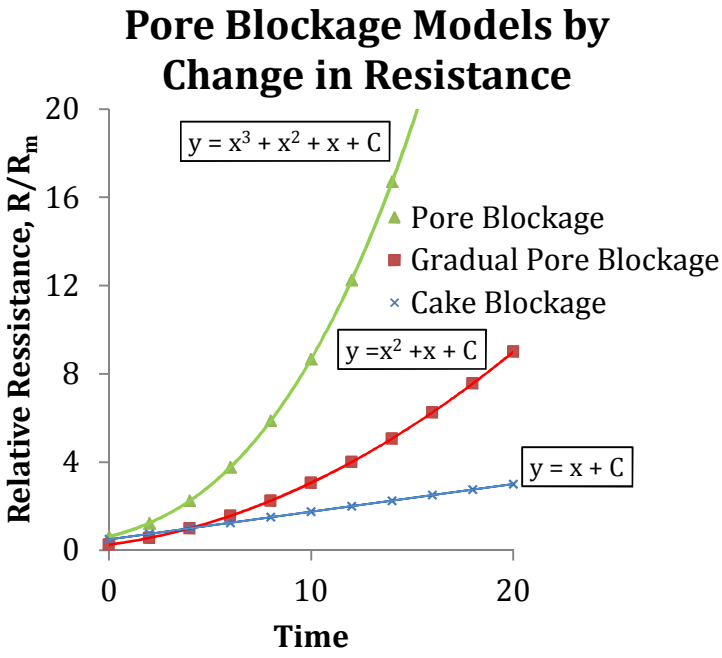

Figure 5-2: Representation of change in resistance over time indicating different filtration blockage models. By applying a trend line to the data, the best R^2 value signifies the equation for the line and corresponding blockage model[238,247].

Relative resistance is measured by normalising the resistance from the membrane before filtration and the resistance during filtration as shown in Equation 5-4:

Equation 5-4: $$R_r = R_t / R_m$$

Where normalised R_r (dimensionless) is equal to total resistance R_t (m^{-1}) divided by the resistance of the membrane before filtration R_m (m^{-1}).

Where R_t is:

Equation 5-5: $$R_t = \frac{\Delta P}{\mu J_f}$$

Where total resistance R_t is equal to transmembrane pressure ΔP (Bar) divided by the product of the viscosity μ (Pas) and the filter flux J_f (Lm^2).

5.1.3.1. Measuring Filter Flux for Blockage Models

Once the blockage model has been determined, the volume prediction for capacity can be made using the time law for each blockage model based on a modified form of the Hagen-Poiseulle equation (Equation 5-5), incorporating both Equation 5-2 and 5-3[238].

Equation 5-6: $$J_f = \frac{\Delta P}{\mu(R_m + R_s)}$$

Where the flux J_f ($Lm^{-2}min^{-1}$) is equal to differential pressure ΔP (Pa) divided by the product of the viscosity μ (Pas) and the sum of the internal R_m (m^{-1}) and surface filter media resistance R_s (m^{-1}).

5.1.3.2. Pore Blockage Model

The pore blockage model (Figure 5-1A) is described with a time law for the volume flow based on equation 5.5, where the filter flux at a given time is calculated from the initial flux[242]:

Equation 5-7: $$Jf\ (t) = Jf\ (0)\ e\text{-}At$$

Where the volume of throughput velocity, J_f (m^3s^{-1}), during the filtration time, t (s), equals the product of the initial throughput velocity J_f (0) (m^3s), and e (Euler's number 2.71828...) to the power of the -1, multiplied by the product of the filtration time t (s) and complete and intermediate blockage constant A.

Where A is:

Equation 5.8: $$A = K_A v_0$$

Where the blockage constant, A (s^{-1}), is equal to the product of the surface area blocked per unit of volume passed through the filter media, K_A (m^{-1}), and the mean initial flow velocity, v_0 (ms^{-1}).

Where v_0 is:

Equation 5-9: $$v_0 = \frac{J_f(0)}{A_0}$$

Where the mean initial flow velocity, v_0 (ms^{-1}), equals the initial throughput velocity, $J_f(0)$ (m^3s^{-1}), divided by the porous surface area of the filter media, A_0 (m^2).

The predicted total volume throughput relative to time was expressed by:

Equation 5-10: $$V_{(t)} = \frac{J_f(0)}{A} \times (1 - e^{-At})$$

Where the volume throughput, $V_{(t)}$ (L) is equal to the initial velocity (m^3s^{-1}) divided by the complete and intermediate blockage constant, A (s^{-1}), (Equation 5-4) multiplied 1- e to the power of the product of A and time, t (s).

5.1.3.3. Gradual Pore Blockage Model

Particles may arrive at the membrane and deposit onto the internal pore walls causing gradual pore blockage, as illustrated in Figure 5-1B. The time law for volume throughput is described by[242]:

Equation 5-11: $$J_f(t) = \frac{J_f(0)}{(1 + Bt)^2}$$

Where the volume flow, J_f (m^3s^{-1}), is equal to the initial volume flow $J_f(0)$ (m^3s^{-1}) divided by the product of the standard blocking constant B (s^{-1}) and time (s) plus 1, squared.

Where B is:

Equation 5-12: $$B = K_B v_0$$

Where the standard blocking constant, B (s^{-1}), is equal to the product of the decrease in cross sectional area of the pores K_B (m^{-1}) and the initial velocity of volume throughput, v_0 (ms^{-1}).

From this, the predicted volumetric flow through is:

Equation 5-13: $$V_{(t)} = \frac{J_f(0)t}{1+Bt}$$

Where the predicted volumetric throughput, $V_{(t)}$ (L) is equal to the product of volume flow, $J_f(0)$ (m^3s^{-1}), and time, t (s), divided by the product of the standard blockage constant, B (s^{-1}), and time, t (s), plus 1.

5.1.3.4. Cake Filtration

Cake filtration describes the process when particles arrive at the surface of the filter media and block or partially block the filter without penetrating into the media, then other particles aggregate with the existing particles to form a cake layer, illustrated in Figure 5-2C. The time law is described by:

Equation 5-14: $$J_f(t) = \frac{J_f(0)}{\sqrt{(1 + Ct)}}$$

Where the total volume flow velocity, $J_f(t)$ (m^3s^{-1}), equals the initial volume flow, $J_f(0)$, divided by the square root of the product of the constant, C (s^{-1}), and time, t (s), plus 1.

Where C equals*:*

Equation 5-15: $$C = (2R_r)K_c v_0$$

Where the constant cake filtration constant C (s^{-1}) equals the products of twice the ratio of the cake resistance (dimensionless), the area of the cake deposited cake (m^{-1}) and initial mean velocity of the fluid through the membrane v_0 (ms^{-1}).

Where R_r is:

Equation 5-16: $$R_r = \frac{R_c}{R_m}$$

Where R_r (dimensionless)is equal to resistance of the cake R_c (m^{-1}) divided by the resistance of the clean membrane R_m (m^{-1}).

The volume flow prediction is given by:

Equation 5-17: $$V_{(t)} = 2J_f(0) \quad x \quad \frac{(\sqrt{1 + Ct}) - 1}{C}$$

Where the predicted volume throughput, $V_{(t)}$, is equal to twice the initial flow velocity, $J_f(0)(m^3s^{-1})$, divided by the cake filtration constant, C (s^{-1}), all multiplied by the square root of the product of C (s^{-1}) and time, t (t), plus 1, all subtracted by 1.

5.1.4. Sieve Capacity

The size exclusion of a filter for particular substances is dictated by the nominal porosity and structure of the filter membrane. The nominal porosity of the filtration system for the BAL treatment phase needs to be sufficient to allow passage of circulating and newly synthesised proteins whilst binding DNA and endotoxin. Common blood components that may be present in plasma are illustrated in Figure 5-3.

Figure 0-1: Size comparison of common, non-cellular components of blood, showing size of ions in Å and protein size kDa. Modified from Membranes for Life Sciences[237].

The means of measuring the nominal porosity varies as outlined in the Introduction Section 1.6.2.1, although the sieve coefficient can be calculated for specific proteins using Equation 5.17.

Equation 5-18:

$$SC = \frac{2C_f}{C_{Bi} + C_{Bo}}$$

Where the Sieve Coefficient (SC) is equal to twice the concentration of the protein in the filtrate, C_F (ng/ml), divided by the sum of the filter input concentration, C_{Bi} (ng/ml), and the filter output concentration in the blood of the patient, C_{Bo} (ng/ml).

For the purposes of the scale BAL system, the protein concentration in the patient's blood (C_{Bo}) will be assumed as being identical to filtrate concentration (C_f).

5.2. Methods

5.2.1.Model for Plasma Filtration

For plasma types outlined in Sections 5.3.3 and 5.3.4, the predicted total volumetric filter media flux, V_t (Lm^{-2}), was calculated for each filter media using the blockage models detailed in Section 5.1.1. A predicted volumetric capacity for each filter was determined with Equation 5.18:

Equation 5.18: $V_t = V \times A$

Where the total volumetric filter media flux V_t (L) is equal to the product of predicted volumetric throughput $V(Lm^{-2})$ and filter media area (m^2).

Plasma was passed through the filters at 90ml/min, as this is the expected plasma flow rate of the Cobe Spectra as part of the large scale BAL treatment phase[248].

5.2.1.1. Fresh Frozen Plasma (FFP) Filtration

Fresh Frozen Plasma (FFP) (Methods Sections 2.3), was passed through the 3M® Cuno® 30SP and 60ZA05A filters (detailed in the Introduction Section 1.6.2.3) in order to assess volumetric filter media flux, V_t (Lm^{-2}). The filtration model was assembled as outlined in Methods Section 2.5, calculating the mode of blockage using the principles outlined in Section 5.1.1.

5.2.1.2. Plasma from Cobe® Spectra® Therapeutic Plasma Exchange Filtration

Plasma from Cobe® Spectra® therapeutic plasma exchange (CSTPE) was passed through the 3M® Cuno® 10SP, 30SP, 60ZA05A, 60LP and 90LP filters (detailed in Introduction 1.6.2.3) to determine volumetric filter media flux, V_t (Lm^{-2}). Followed by, using the blockage principles outlined in Section 5.1.1 to assess filter capacity. In addition to DNA removal, DNA filter capacity was assessed using the PCR protocol outlined in Methods Section 2.2.4.

5.2.2.ELISA Protocols for Measurement of Circulating Protein

5.2.2.1. AFP, Fibrinogen, Albumin and α-1-antitrypsin Concentration in Filtered Plasma

During the scale filtration model (Methods Sections 2.5), plasma samples were taken hourly and analysed for AFP, fibrinogen, albumin and α-1-antitrypsin as described in Methods Section 2.4. Table 5.2 shows the dilution factors used to reduce plasma protein concentration to within the range of the 0-200ng/ml standard curve.

Protein	Sample	Dilution Factor	Comment
AFP	All samples	10	AFP in Cobe Spectra Aphaeresis (CSA) plasma filtrate
Fibrinogen	All samples	1,000	Fibrinogen in CSA plasma filtrate
Albumin	All samples	10,000	Albumin in CSA plasma filtrate
α-1-antitrypsin	All samples	10,000	α-1-antitrypsin in CSA plasma filtrate

Table 0-1: Dilution factors for the specific protein ELISAs in both types of plasma using the protocol described in Methods Section 2.5, as part of experiments outlined in Section 5.2.1.

5.2.3.BCA total protein

Materials

- **Reagent A,** (pH 11.25):
  - 26mM sodium bicinchoninate (Sigma, D8284)
  - 189mM sodium carbonate (BDH, 102404H)
  - 87mM sodium tartrate (Sigma, S4797)
  - 100mM sodium hydroxide (BDH, 102524X)
  - 113mM sodium bicarbonate (BDH, 102474V)
- **Reagent B** (4% cupric sulphate):
  - 4% Cupric (II) sulphate 5-hydrate (BDH, 26270)
- Standard BSA solution, 1mg/ml (Sigma, P0834-10X-1ML)
- 96-well micro-plate
- 1.5ml Eppendorf® microfuge tubes
- Anthos® Multi-well spectrophotometric plate reader

Bicinchoninic acid (BCA) Protocol

A series of standards were prepared from 31.25µg/ml-1000µg/ml using serial dilution from the 1mg/ml BSA standard solution in MilliQ™ treated RO water.

Reagents A and **B** were mixed to a ratio of 50:1, respectively. Samples were diluted 1/1000 in MilliQ™ treated RO water, running both standards and samples in triplicate, adding 20µl volume for both standards and samples to the 96 well plate. To each well, 200µl of pre-mixed reagent A and B solution was added, sealing the plate, and gently mixing on a plate shaker for 30 seconds, followed by incubating at 37°C for 30 minutes. Allowing the plate to cool to room temperature, the absorbance of the plate was read at 550-570ηm, using the Anthos Multi-well Spectrophotometric Plate reader.

5.2.4. PMAS SBSS Liquid Particulate Counting with Plasma

Particulates in plasma were measured using the PMASS SBSS Liquid Particulate counter, using the protocol outlined in Methods Section 2.8. Samples were diluted to 1% in MilliQ™ treated RO water, to reduce the incidences of the particulate counter measuring superimposed particulates. This was confirmed by measuring reduction in particulate numbers at 2%, 1%, 0.5% and 0.25% dilutions, ensuring a linear reduction of particulates.

5.2.5.Filters used in the Scaled-down Filtration Model

Table 5-3 shows the filters that were actually used in the scaled down filtration model, where plasma was passed through the filters to calculate capacity for use with the BAL, using the filtration blockage models.

Zeta Plus® Formulation	Filter Media	Filter Aids	Pharmaceutical Grades	Primary Application
S Grade	**Cellulose**	**DE, perlite**	**05SP, 10SP, 30SP, 50SP, 60SP, 90SP**	**Final sterile membrane protection** **Buffer/solvent pre-filtration** **Chromatography column protection** **Reduction of contaminating DNA** **Endotoxin reduction**
LP series	**Cellulose (optimised for no β-glucan release)**	**DE, perlite**	**30LP, 60LP, 90LP**	**Blood fractionation** **Membrane protection** **Endotoxin reduction**
ZA series	**Cellulose**	**DE, Pre-extracted acid washed**	**30ZA05A, 60ZA05A, 90ZA05A**	**Endotoxin reduction in water** **DNA removal**

Table 0-2: Filters used in the scaled down filtration model. Plasma was passed through to assess capacity. DE refers to diatomaceous earth.

5.3. Results

5.3.1. Theoretical Filter Capacity for a BAL Treatment Phase

In order to select the appropriate filter for the BAL system the total volumetric throughput over 8 hours was calculated at different flow rates as illustrated in Table 5.4.

Volumetric Flow rate (ml/min)	Estimated Total Volumetric throughput (L)
10	4.8
40	19.2
60	28.8
90	43.2
120	57.6

Table 5-4: Theoretical volumetric throughput of the BAL system during 8 hours at different flow rates.

5.3.2. Filtration of Plasma using 3M® Cuno® Filters.

Volumetric filter media flux, V(t) (Lm^{-2}), for each filter media (Methods Section 2.5) was evaluated as described in Section 5.1.1. The mode of filter blockage was determined by plotting membrane resistance over time, from which V(t) was calculated using the mathematical models for the relevant blockage model as shown in Table 5-5. Then filters were tested for DNA removal capability and large particulate removal (over 1µm). In order to calculate the V(t) the blockage models were determined as follows.

5.3.2.1. Determination of Blockage Model in Fresh Frozen Plasma (FFP)

As mentioned in Chapter 4, FFP was obtained from whole blood donations, with a predefined set of cellular constituents. Filtration experiments were first performed with FFP to establish the filtration capacity with a readily available source of plasma that could potentially be incorporated into the BAL system for priming.

Both the single layered 30SP and the double layered 60ZA05A filters showed a distinctive cake blockage curve as illustrated in Figures 5-4 and 5-5 when plotting relative resistance over time.

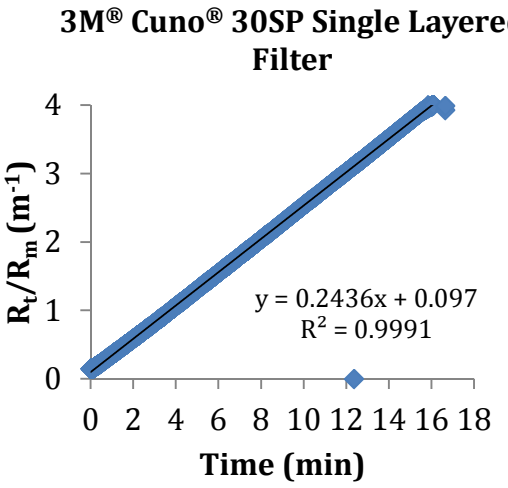

Figure 5-4: Relative resistance over filtration time with freshly frozen plasma passed through a 3M® Cuno® 30SP filter at 90ml/min, showing a curve indicative of cake blockage[238]. The curve shows individual data points over a single experiment, providing a measure of variance in relative resistance during filtration. 30SP filters have a nominal porosity of 0.6-3µm. Due to the high frequency of data point collection, the curve shows individual data points over a single experiment, providing a measure of variance in relative resistance during filtration. The anomalous measurements not on the line were attributed to electronic interference and did not affect the results.

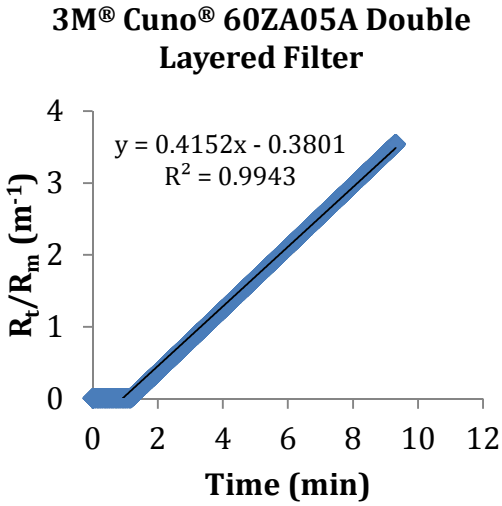

Figure 5-5: Relative resistance over filtration time with freshly frozen plasma passed through a 3M® Cuno® 60ZA05A double layered filter at 90ml/min, showing a curve indicative of cake blockage[238]. 30SP filter have a nominal porosity of 0.6-3µm. The 60ZA05A filters are constructed of a "30" filter media with nominal porosity of 0.6-3µm protecting a less porous "60" filter media with nominal porosity of 0.3-0.75µm. Due to the high frequency of data point collection, the curve shows individual data points over a single experiment, providing a measure of variance in relative resistance during filtration.

5.3.2.2. Filter Capacity with FFP

The 30SP and 60ZA05A filters, shown in Figures 5-4 and 5-5, quickly reached 1.6bar requiring the filter experiment to be terminated. As a result, the filter volumetric throughput

in Table 5-5 for the 25cm^2 filter was the measured value, using the figure from this to calculate the flux to apply to the larger filter sizes.

The 30SP filter was identical to the upstream protectant layer of the 60ZA05A filter (the 05A component), in terms of nominal porosity (0.6µm – 3µm). Although the 30SP filter did show a higher volumetric filter media flux of 10.8Lm^{-2} compared with 5.7Lm^{-2}, when calculated for the larger filter sizes, the capacities were insufficient for large scale application, illustrated in Table 5-4.

Filter Type	Mean Initial Flow Velocity (J_v) (m^3s^{-1})	Mean Flow Velocity (ms^{-1})	Volumetric Filter Media Flux (Lm^{-2})	Measured 25cm² Filter Capacity (L)	Predicted 650cm² Filter Capacity (L)	Predicted 1300cm² Filter Capacity (L)
30SP	4.22 x 10^5	1.35 x 10^4	10.8	0.027	0.702	1.4
60ZA05A	1.29 x 10^5	4.2 x 10^4	5.7	0.014	0.371	0.74

Table 5-5: Prediction of total volume throughput using the filter models with FFP passed through each filter. Mean initial volumetric flow rate was determined. Due to the filter quickly reaching 1.6bar, the volume throughput for the 25cm² filter reflects the measured volume, calculating the volumetric flow through for the larger filter sizes. Mean flow velocity was measured from over total filtration time from the volumetric flow rate, as measured by reaching 1.6bar differential pressure. (n=1)

5.3.2.3. Blockage Model in Plasma from Cobe® Spectra® Aphaeresis.

The plasma derived from Cobe® Spectra® Therapeutic Plasma Exchange (CSTPE) is more refined than FFP[248], illustrated later in Figure 5-16. Accordingly, it would be expected that the filter capacity should be improved compared to FFP.

Plotting the relative resistance against time, the 10SP filter (nominal porosity of 0.8-5µm), showed a distribution indicative of gradual pore blockage when filtering CSTPE plasma, as illustrated in Figure 5-6.

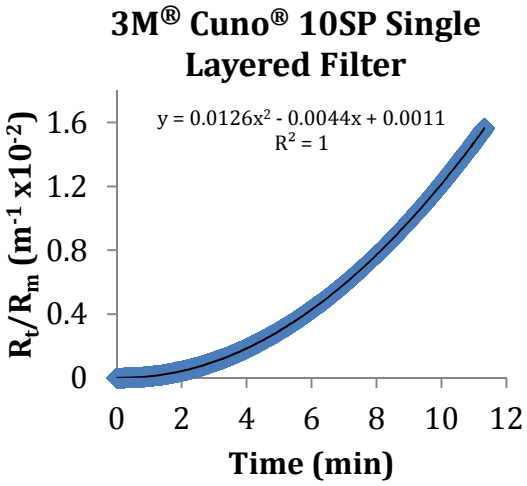

Figure 5-6: Relative resistance over filtration time with CSTPE plasma passed through a 3M® Cuno® 10SP filter at 90ml/min, showing a curve indicative of gradual pore blockage as detailed in Section 5.1.2. The curve shows individual data points over a single experiment, providing a measure for variance of relative resistance during filtration. The 10SP filter has a nominal porosity of 0.8 - 5µm.

As with the 10SP filter, the less porous 30SP filter (nominal porosity of 0.6µm – 3µm), shows a relative resistance distribution of a gradual pore blockage as illustrated in Figure 5-7.

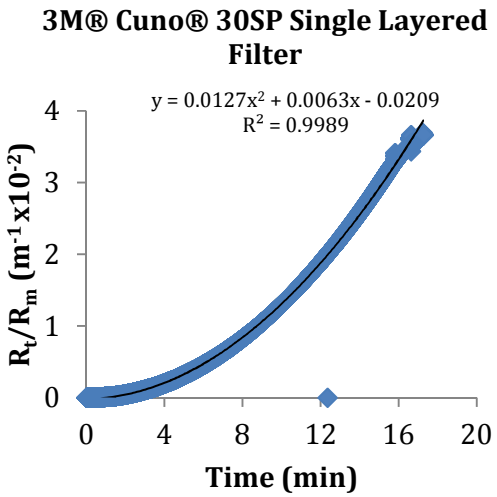

Figure 5-7: Relative resistance over filtration time with CSTPE plasma passed through a 3M® Cuno® 30SP filter at 90ml/min, showing a curve indicative of gradual pore blockage. The curve shows individual data points over a single experiment, providing a measure of variance for relative resistance during filtration. The 30SP filter has a nominal porosity of 0.6-3µm.

The 60ZA05A filter with CSTPE plasma, showed a relative resistance distribution of pore blockage, as illustrated in Figure 5-8.

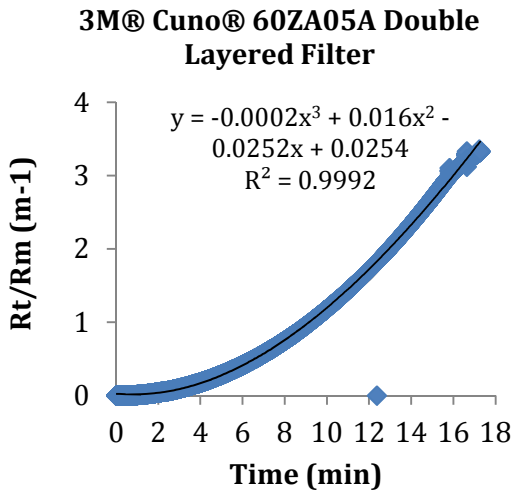

Figure 5-8: Relative resistance over filtration time with CSTPE plasma passed through a 3M® Cuno® 60ZA05A filter at 90ml/min, showing a curve indicative of pore blockage. The curve shows individual data points over a single experiment, providing a measure of variance for relative resistance during filtration. The 60ZA05A filters are constructed of a "30" filter media with nominal porosity of 0.6-3µm protecting a less porous "60" filter media with nominal porosity of 0.3-0.8µm 60ZA05A filter have an overall nominal porosity of 0.3-0.8µm.

Due to the single layered 60ZA filters no longer being available, the LP series were used in their place due to the same media construction and charge, differing only in lower potential release of β-glucans from the filter media itself[187]. Therefore, providing a measure for the 60ZA capacity, without the 05A protective layer. The 60LP single layered filter has the same nominal porosity as the lower layer of the **60ZA**05A double layered filter of 0.3µm-0.8µm. Passing CSTPE plasma through the 60LP filter showed a relative resistance distribution of pore blockage, as illustrated in Figure 5-9.

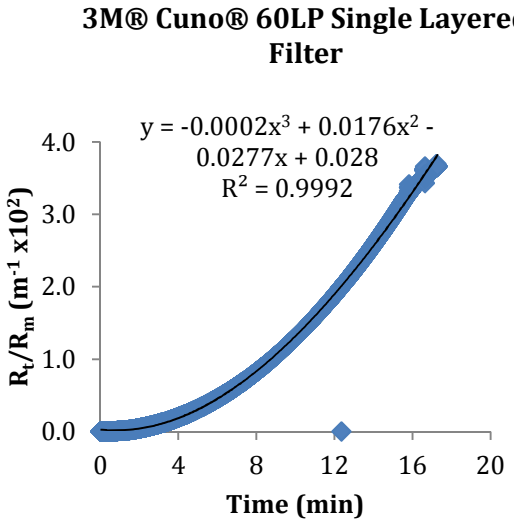

Figure 5-9: Relative resistance over filtration time passing CSTPE plasma through the 3M® Cuno® 60LP filter at 90ml/min, showing a curve indicative of pore blockage. The curve shows individual data points over a single experiment, providing a measure of variance for relative resistance during filtration. 60LP filter have a nominal porosity of 0.3-0.8µm.

The 90LP filter had the lowest nominal porosity of 0.05µm to 0.5µm, and showed pore blockage model as illustrated in Figure 5-10. This was tested to assess the potential capacity of a lower porosity filter in case it was necessary to reduce nominal porosity to increase contamination removal capacity.

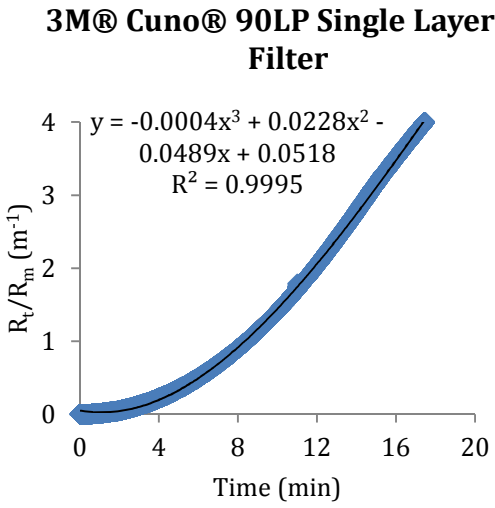

Figure 5-10: Relative resistance over filtration time with CSTPE plasma passed through a 3M® Cuno® 90LP filter at 90ml/min, showing a curve indicative of pore blockage. The curve shows individual data points over a single experiment, providing a measure of variance for relative resistance during filtration. 90LP filter have a nominal porosity of 0.05-0.5µm.

5.3.3.Predicted Total Volumetric Filter Flow Through

Having established the mode of filter blockage, the predicted volumetric filter media flux was calculated as shown in Table 5-6, using the blockage models in Section 5.1.2. As expected, the 10SP filter with the largest nominal porosity showed the greatest predicted volumetric filter media flux at $800Lm^{-2}$.

The 30SP filter showed a reduced volumetric filter media flux of $612Lm^{-2}$ due to the lower nominal porosity, but was significantly higher than the 60ZA05A filter at $491Lm^{-2}$. The 30SP filter has the same nominal porosity as the upstream protective layer of the 60ZA05A filter (i.e. the 05 layer). Comparing the 60LP (identical nominal porosity as the downstream 60ZA part of the 60ZA05A filter) with the 60ZA05A filter, the volumetric filter flux was further reduced to $22Lm^{-2}$ from $491Lm^{-2}$, as shown in Table 5-6. Therefore, the upstream 05 layer of the 60ZA05A filter does bestow some protection to the downstream 60ZA layer. The 90LP filter followed the trend of reduced volumetric filter media flux with lower nominal porosity at $7Lm^{-2}$, due to tightness of the media.

The volumetric filter media flux provides a predicted capacity as a unit of filter area, when applied to actual filter sizes the usable capacity was provided. Comparing these values with the theoretical volumetric throughput of the large scale BAL, described in Table 5-4, only the 10SP, 30SP and 60ZA05A filter would provide sufficient capacity using the $1300cm^2$ filter capsule.

Filter Type	Mean Initial Volumetric Flow Rate J_v (m^3s^{-1})	Mean Flow Velocity (ms^{-1})	Predicted Volumetric Filter Media Flux V (Lm^{-2})	Predicted V_t for $25cm^2$ Filter Area (L)	Predicted V_t for $650cm^2$ Filter Area (L)	Predicted V_t for $1300cm^2$ Filter Area (L)
10SP	6.99×10^{-4}	2.1×10^{3}	**800**	**2**	**52**	**104**
30SP	5.38×10^{-4}	1.0×10^{3}	**612**	**1.5**	**40**	**80**
60ZA05A	1.82×10^{-4}	9.6×10^{4}	**491**	**1.2**	**32**	**64**
60LP	4.31×10^{-4}	4.8×10^{4}	**22**	**0.06**	**1.4**	**2.9**
90LP	0.98×10^{-4}	1.0×10^{4}	**7**	**0.02**	**0.5**	**0.9**

Table 5-6: Prediction of total volume throughput using the filter models with CSTPE plasma passed through each filter. Mean initial volumetric flow rate was determined over the first 20 seconds of filtration measured from the time plasma filtrate started to exit the filter. Mean flow velocity was measured from total filtration time from the volumetric flow rate.

5.3.4. DNA removal with different filter Types

Both the ZA (60ZA05A) and LP series (90LP and 60LP) filters showed complete DNA removal from CSTPE plasma, mostly showing no DNA amplification or amplification occurring at below the LoQ when analysed by QPCR. However, the S filter series only showed a reduction in DNA level of 11% and 14% for the 10SP and 30SP filters, respectively, as illustrated in Table 5-7.

Filter	Mean DNA Concentration After Filtration (ng/ml)	Volume passed through filter (L)	Total DNA removal (µg)	% DNA Removal
60ZA05A	0.0 ± 0.00	0.771	39	100
90LP	0.0 ± 0.00	0.426	22	100
60LP	0.0 ± 0.00	0.523	27	100
30SP	32.98 ± 7.8	0.853	15	14
10SP	46.06 ± 9.7	1.423	65	11
Non Filtered	50.63 ± 5.0	n/a	n/a	n/a

Table 5-7: total DNA removal capability for each filter, using CSTPE plasma source was from different patients for each filter experiment, (each experiment representing n=5 for a single filter type, and error representing standard deviation). Where 100% reduction indicates DNA level below the LoQ. The total DNA was calculated from cumulative DNA over the total filter volume throughput, where capacity was limited by filter fouling.

5.3.5. DNA Removal Capacity

As previously mentioned, a 7L large scale BAL with $7x10^{10}$ cells was calculated to release 0.553mg total DNA over 8 hours. The 1.325mg DNA capacity of a $25cm^2$ 90SP filter was therefore sufficient for the large scale BAL system[139]. In Table 5-8 the DNA capacity of the ZA and LP series filters was calculated for plasma, using the amount of DNA clearance with the measured volume throughput from the scale filtration model, then calculating a multiplication factor (MF) for the predicted volumetric flow though for each filter. The product of the MF and quantity of DNA actually removed during filter model provided the theoretical DNA capacity of the filter shown in more detail in Equations 5-19 and 5-20:

Equation 5-19: $$MF = \frac{V_m}{V(t)}$$

Where the filter multiplication factor MF is equal to the measured volume throughput, V_m (L), divided by the predicted capacity, V(t) (L), from the blockage models.

Equation 5-20: $$V_{DNA} = MF \times \text{Total DNA removal}$$

Where the DNA capacity (mg) is equal to the product of the multiplication factor and the total DNA removal (mg).

	Volume Passed Through (L)	25cm² MF	Predicted DNA Capacity (mg)	850cm² MF	Predicted DNA Capacity (mg)	1300cm² MF	DNA Capacity (mg)
60ZA05A	0.771	1.3	0.051	54.5	**2.1**	107.7	**4.2**
90LP	0.426	0.047	0.001	1.4	**0.031**	2.1	**0.046**
60LP	0.523	0.115	0.003	3.6	**0.098**	5.5	**0.150**

Table 5-8: Predicted DNA capacity based on the measured volume passed through the filter, and the total predicted DNA capacity calculated from equation 15 and 16. The 25cm² filter was used for the scale filter model; the DNA capacity for larger filters then calculated from the predicted volume throughput from the blockage models

The DNA capacity of the 90SP filter used for cell broth[139] was calculated for 850cm^2 and 1300cm^2 filter sizes, shown in Table 5-9. After comparing the predicted DNA capacity of the LP and ZA filter series with CSTPE plasma and the 90SP filter, the LP and ZA filter series were substantially higher than the calculated amounts shown in Table 5-9.

90SP Capacity (Lm^{-2})	Filter Media Size (cm^2)	DNA Capacity (mg)
53	25	1.325
53	850	45.1
53	1300	68.9

Table 5-9: DNA capacity of the 90SP filters whilst passing cell broth with increasing filter size. DNA concentration of 10ng/ml was passed through a 90SP filter until breakthrough was detected at 53Lm^{-2}. This data was adapted from *Dorsey et.al* paper for different filter sizes[139].

5.3.6. Transit of Proteins through the Filters

5.3.6.1. Total Protein

Initially, total protein concentration was measured by BCA assay detailed in Methods section 5.2.3, to ensure no major reduction in protein by filtration. Figure 5-11 illustrates that there was no significant change in total protein content in CSTPE plasma through any of the filters tested ($p=0.34$, $n=6$).

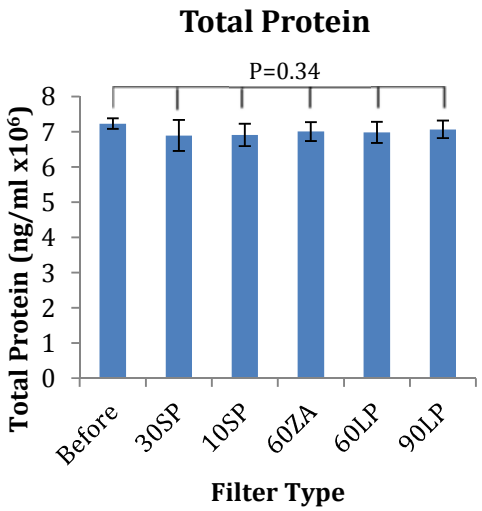

Figure 0-2: Total protein before and after filtration was not significantly different, (using ANOVA, n=6 for each filter, with error bars representing standard deviation).

5.3.6.2. Specific Protein Measurement by ELISA

Total protein measured by BCA indicated level of protein transit, but this assay was not sufficient to determine the transit of specific proteins essential for the therapeutic efficacy of the BAL. Therefore, protein transit was measured by ELISA for specific proteins as detailed in Methods Section 2.5 and Section 5.2.

Alpha-Feto-Protein (AFP)

AFP, which can be used to monitor HepG2 specific metabolic activity within the BAL, as it is not normally found in human plasma, was not significantly affected by filtration with any of the filters used as illustrated in Figure 5-12 (one way ANOVA P=0.99, n=6).

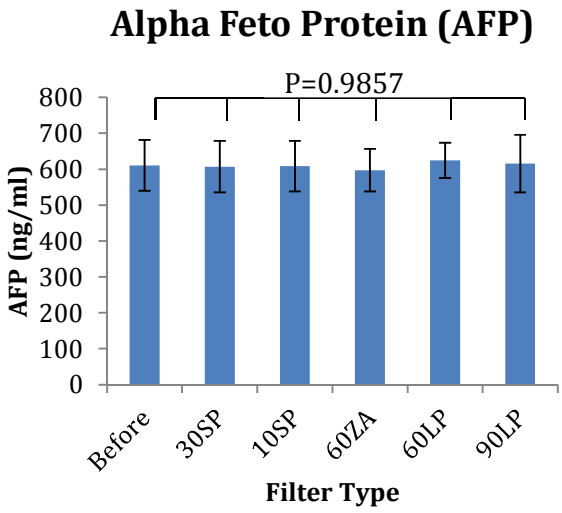

Figure 5-12: Alpha-fetoprotein concentration before and after filtration was not significantly changed, (using ANOVA analysis, n=6 for each filter, with error bars representing standard deviation).

Fibrinogen

Fibrinogen, which is an essential clotting factor often depleted in ALF patients[32], showed no significantly difference after filtration with any of the filters tested (one way ANOVA, p=0.83, n=6).

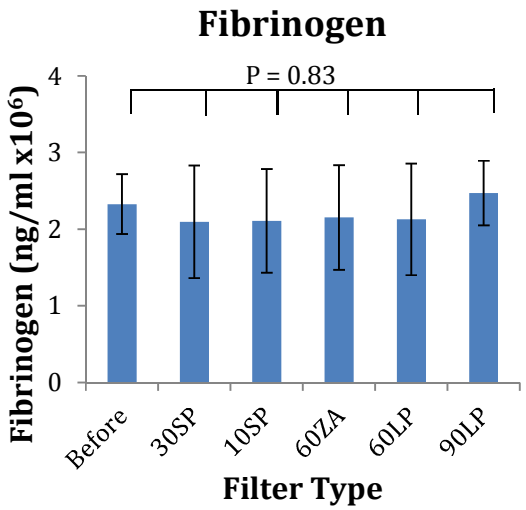

Figure 5-13: Fibrinogen concentration before and after filtration was not significantly changed, (using ANOVA, n=6 for each filter, with error bars representing standard deviation).

Albumin

Albumin is essential for detoxification as a carrier protein for many poorly soluble xenobiotics and maintenance of colloidal osmotic pressure, and is often low in patients with ALF[32]. No significant difference was observed between unfiltered CSTPE plasma and plasma filtrate as illustrated in Figure 5-14.

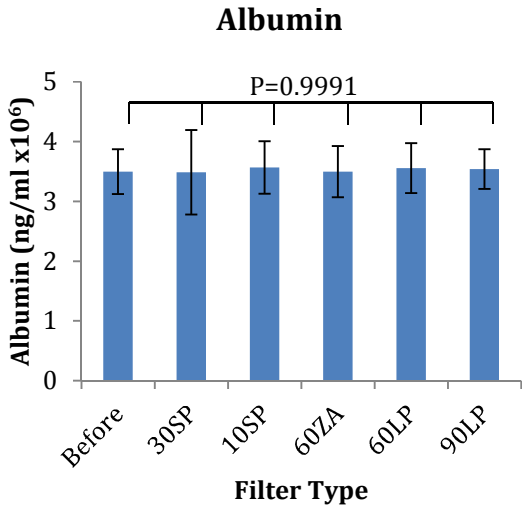

Figure 5-14: Albumin concentration before and after filtration was not significantly changed, (using ANOVA analysis, n=6 for each filter, with error bars representing standard deviation).

α-1-Antitrypsin

α-1-Antitrypsin is a protease inhibitor, synthesised in the Liver, which neutralises trypsin that which may be present following inflammation. No significant difference in α-1-Antitrypsin concentration was shown after filtration, as illustrated in Figure 5-15 (one way ANOVA p=0.07, n=6)

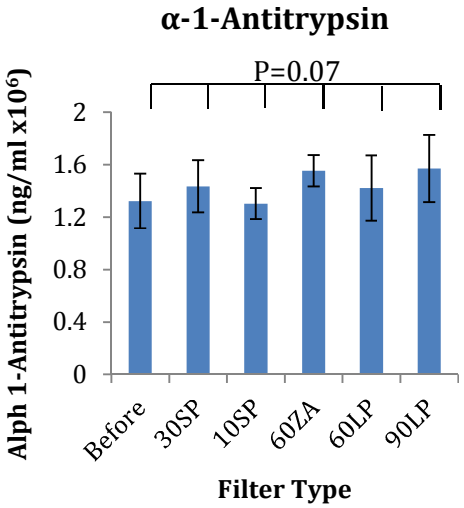

Figure 5-15: Alpha 1-antitrypsin concentration before and after filtration was not significantly changed, (using ANOVA, n=6 for each filter, with error bars representing standard deviation).

5.3.6.3. Sieve Capacity

To show the ELISA data in a form that can be compared with other filtration regimes, sieve capacity was analysed[236]. This showed no significant difference in protein concentration before and after filtration (Table 5-10).

Filter	AFP Sieve Co-efficient	Fibrinogen Sieve Co-efficient	Albumin Sieve Co-efficient	α-1-Antitrypsin Sieve Co-efficient
30SP	1.00	1.00	1.00	0.96
10SP	1.00	1.00	0.99	1.00
60ZA	1.00	0.99	1.00	0.91
60LP	0.98	1.00	0.99	1.00
90LP	1.00	0.93	1.00	0.95

Table 5-10: Sieve capacity of proteins through each depth charged filter using CSTPE plasma, showing no reduction in protein content in any of the filtration.

5.3.7. Particulate Removal from Plasma

Measurement of particulate levels in CSTPE and FFP supported the assumption that CSTPE would have lower levels (Figure 5-16). This could be attributable to fewer platelets, usually 1-3µm in diameter[249], and very few nucleated cells. The 10SP filter with the largest porosity reduced particulates with less efficiency than 60ZA05A filter, reflecting the much lower porosity and double layered nature of the 60ZA05A filter.

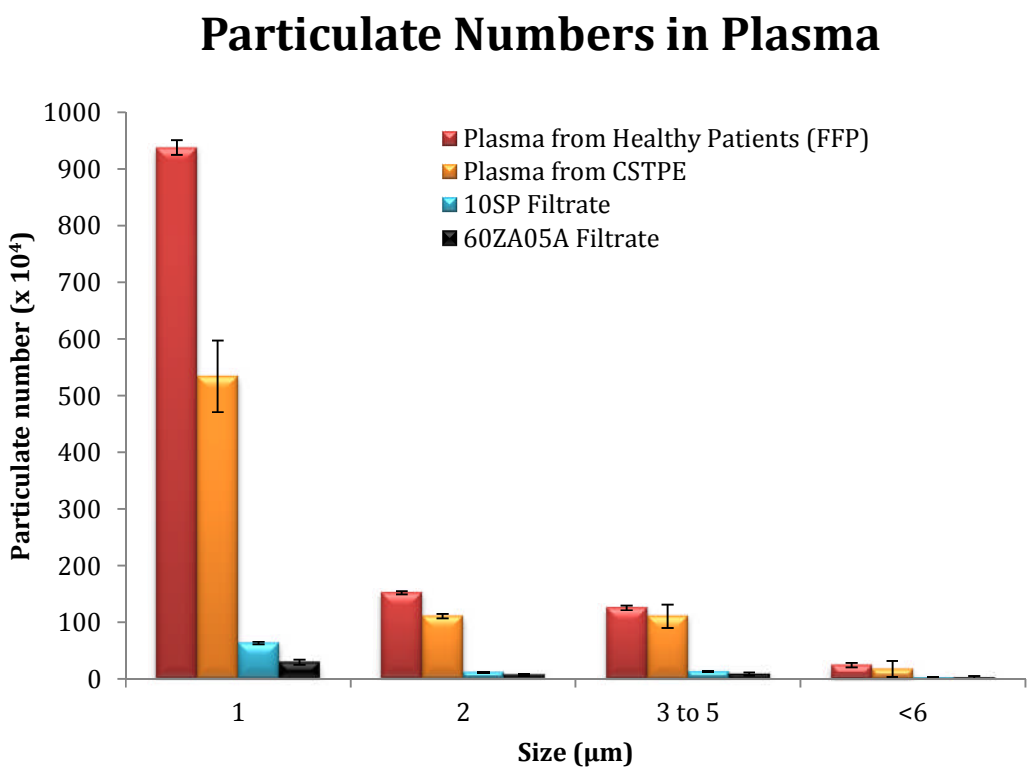

Figure 5.16: Particulate levels in plasma filtered by depth charge filters. Particulate levels in plasma filtered by 60ZA05A were not significantly different to 10SP (two tailed paired t-test, n=5, P=0.2425). Plasma passed through both 10SP and 60ZA05A filters had significantly fewer particulates than unfiltered FFP (two-tailed t-test, n=5 P<0.0001, error bars represent standard deviation). Particulate levels were significantly lower in CSTPE compared with FFP.

5.4. Discussion

The requirement of a BAL filter system is to both remove DNA and cell debris, whilst allowing transit to proteins, already in the circulation or synthesised by the BAL biomass. This includes both volumetric capacity and adsorption capacity for DNA.

5.4.1. DNA removal Capacity

The theoretical DNA capacity calculated in Section 5.1.1.1 showed that a 25cm^2 90SP filter would be sufficient in removing the expected DNA concentration from the large scale BAL system. The filtration model confirmed DNA removal (but not capacity) with both the ZA (e.g. 60ZA05A) and LP (e.g. 60LP) series filters of all nominal porosities tested, whereas the S series (e.g. 30SP) filters did not show the same DNA removal efficiency. This was because the S series filters are designed for bioprocessing clarification and DNA/endotoxin reduction; therefore carry a lesser positive charge compared with the ZA and LP series filters, which are designed for end stage purification and DNA/endotoxin removal[138,187,188,250].

Previous literature for the 60ZA05A, 90LP, and 60LP filters showed greater DNA binding capacity than the 90SP filters previously tested in cell broth[138,139,]. When calculating the DNA binding capacity of 60ZA05A, 90LP, and 60LP filters, the assumption was made that DNA binding capacity would not be reached before the volumetric capacity, predicted using the filter blockage models. Therefore, the calculation for DNA removal capacity in Section 5.3.5 using Equation 5-19 and 5-20 (plasma passed through the filter divided by the predicted volume, multiplied by the DNA concentration removed in the experiment) essentially expressed the DNA binding capacity according to measured volumetric flow-through relative to predicted flow-through. As a result, although the capacity expressed in Figure 5-8 show lower DNA binding capacity than those measured by *Dorsey et al.* in Figure 5-9[138,139], the true DNA capacity is likely to be greater due to the 90SP filter having fewer charged molecules on the filter media compared with the ZA and LP filter series. I.e. volumetric capacity is reached before binding capacity.

Furthermore, other S series filters did show DNA removal of 11 and 14% for the 10SP and 30SP filters, respectively. The lower nominal porosity increases the DNA removal efficiency, shown during tests with the 90SP filter removal efficiencies of between 60-80% in de-ionised H_2O containing 100ng/ml of bovine serum albumin[139]. The answer to the true DNA binding capacity of these filters will be tackled in the next chapter where a large scale filter system was used with DNA spikes to assess the DNA capacity of the filter over 8 hours of filtration with CSTPE plasma.

5.4.2.Filter Capacity with FFP

The volumetric filter capacity of the 60ZA05A and 30SP filters in FFP was significantly lower than the CSTPE plasma. The consequence of this was the pressure quickly increased to 1.6bar during filtration, prompting the termination of the experiment. Using the filter capacity up to the point of termination with 25cm^2, the filter flux was calculated and applied to the 850cm^2 and 1300cm^2 filters sizes (Table 5-5), showing a capacity clearly insufficient for a large scale BAL. The implications of these results are that FFP cannot be used directly to prime the BAL system. In its place either pre-separated CSTPE plasma must be used, or whole blood passed through the Cobe® Spectra®, attached to the BAL system, to produce CPTPE plasma for inline priming. The later technique has in fact been chosen as the current means of priming the system in the large scale BAL treatment phase. In the large scale pig model for acute liver failure, blood is obtained from an abattoir for separation by the Cobe® Spectra® to prime the BAL system.

5.4.2.1. Filter Capacity with CSTPE

Despite the tightly controlled parameters associated with FFP[205], filter capacity using CSTPE plasma was increased in comparison to FFP. This was due to CSTPE plasma containing lower particulates, as shown in Figure 5-16. These particulates could be attributed to platelets, which are between 1-3µm in diameter[249], which were reduced in number as a consequence of centrifugation, as part of the CSTPE process.

With the knowledge that the S series filters having less DNA removal efficiency compared to the ZA and LP filters, the 10SP and 30SP filters were tested in the context of upstream protectors. Both the filters showed a relative resistance distribution indicative of gradual pore blockage (Figure 5-4), suggesting sufficient nominal porosity to favour a slow build-up of particles as shown in Figure 5-1B.

The 10SP filter was placed upstream of the 60ZA05A filter in an attempt to increase the capacity of the downstream 60ZA05A filter. Unfortunately, the addition of this filter had no effect on the filter capacity of the 60ZA05A filter, (data not shown). This suggests that the particles that are causing blockage of the LP and ZA series filters are able to pass through the 10SP filter with nominal porosity of 0.8 - 5µm, which provides an insight into the properties of these filters in terms of nominal porosity. The filter media within each capsule is made up of a complex network of permeable channels, therefore giving a large range in nominal porosity of 0.8 - 5µm. Consequently, it is difficult to draw any conclusions as to the size of particulates causing downstream blockage based on this information. Transition electron microscopy could be used to measure particulates on the filter to visualise what is actually being retained.

The 30SP filter provided the same nominal porosity (but not charge) as the 05A layer of the dual layered 60ZA**05**A filter, thereby testing the effectiveness of the 05A filter media as a physical protectant to the 60ZA layer within the dual layered capsule. The 60LP has the same nominal porosity and charge as the 60ZA section of the **60ZA**05A filter. Both the 60ZA05A and 60LP filters, with a nominal porosity of 0.3-0.8µm, showed a relative resistance distribution of complete pore blockage models shown in Figure 5-2A, where single particles completely block the smaller pores. Importantly, the same distribution of relative resistance between the 60LP and 60ZA filter shows that the protection from the 05A layer does not prevent the penetration of all the particulates involved with 60ZA layer blockage. Therefore, blockage occurs due to a build-up of particles on both layers. Despite this, the substantial increase in volumetric throughput is a testament to the effectiveness of the upper protectant layer in reducing extent of particle build-up of the downstream 60ZA layer.

5.4.2.2. Removal of Contaminants and Protein Transit

An important aspect of a filtration system is the removal of contaminants whilst permitting transit of proteins synthesised by the BAL biomass. In all cases, the protein concentration was not significantly affected by filtration. This was reflected by the sieve coefficient, which provides a comparable measure of protein removal between filters. In all cases, the sieve coefficient was one or nearly one, illustrating the transit of protein. This is particularly important for validation of the system, where even large proteins such as fibrinogen can be systemic and secreted through the alginate and are not removed by the filtration system, such that that they are available for the patient.

5.4.3.Limitations of the Filter Model

5.4.3.1. For DNA removal

With all the ZA and LP series, filter complete DNA removal was observed. However, two features of the filtration model limit the application of the data to the final BAL system. Firstly, the DNA capacity cannot be guaranteed as the assumption was made that the DNA capacity would be maintained throughout the predicted total volumetric capacity, based on the results from DNA removal in cell broth[139]. Secondly, the filtration model is not a recirculating system taking fresh whole blood to produce plasma for treatment then re-combining components to whole blood in the way that the large scale BAL does. Consequently, some of the plasma characteristics may not be representative. For example, due to freeze thawing of the plasma; platelet aggregation was observed as shown in Appendix V, despite platelet levels being extremely low. This would not occur during plasma separating from a patient.

5.4.3.2. General Limitations

Other issues include dead volume within the large scale filters as part of the design. The 25cm^2 filters used for the filtration trials have a dead volume of 39ml. However, the larger scale filters are designed with a different housing, which contains relatively high dead space. Despite the 850cm^2 and 1300cm^2 being 34 and 52-fold greater in media area, the void volume is 2.2L and 2.8L, respectively. This may have a detrimental effect on the BAL system as it would require incorporation of a second large reservoir of plasma in addition to the main circuit volume. The chamber holding the encapsulated HepG2 biomass is currently 4L in volume, the Cobe® Spectra TPE dual needle set carries a tubing volume of 285ml, and the BAL tubing holds 890ml the total void volume equals 5.285L; an additional 2.2L of volume space would increase total volume by 41%. As a consequence, the higher the total BAL volume is, the less effective the biomass may become, due to dilution of the synthesised proteins and other solutes vital to BAL therapeutic functionality.

In addition, there is a concern with the use of cellulosic filters in a medical setting, due to potential extractables from the filter itself. When initially flushing the filters before sterilisation, a significant level of extractables leave the filters causing discolouration of the water, after which the levels reduce to below the levels documented by the FDA as suitable levels of particulates for plasma use.

5.4.3.3. Potential for Endotoxin Removal

Endotoxin removal by the ZA and LP series filters was not tested in this chapter due to the filter model used not providing an endotoxin controlled environment. In Chapter 6, the filter model was modified to reduce the potential for background endotoxin contamination.

5.5. Conclusions

Of the filters tested, the 60ZA05A filter was the most helpful for BAL application if used at 1300cm^2 filter media area and above. However, there remains a concern of the size of the void volume in the filters of this size, which could be tackled by using the same filter media in different housing but would require development with our 3M Cuno partners. Furthermore, the use of cellulosic compounds may be a potential problem in terms of release of particulates for medical use. If the use of the filter is shown to remove DNA and endotoxin in a large BAL whilst keeping particulates to below levels found in medical grade parenterals this may mitigate concerns for use of cellulosic material regulatory approval as part of a medical device. This will be further explored in the discussion chapter.

Chapter 6
Large Scale BAL

This chapter details the use of a filtration system in a full scale BAL to remove endotoxin, DNA and particulates as part of the large scale BAL system.

6. Large Scale BAL

6.1. Introduction

6.1.1. The Current Liver Group BAL System

The current Liver Group BAL comprises two independent circuits in terms of flow rate. The primary circuit contains the Cobe® Spectra® Apheresis System, which removes blood from the patient and provides plasma to the BAL system at a flow rate of between 20-150ml/min, (90ml/min most often used). Both the outlet and inlet of the Cobe® Spectra® system are controlled by the same pump with a double head to ensure that the input and output of plasma into the BAL are identical. The secondary circuit flows at between 100-600ml/min to provide a 2-fold bead bed height for the encapsulated HepG2 cells housed in the chamber and to provide a number of treatment cycles for the plasma passing through the biomass, before returning to the patient.

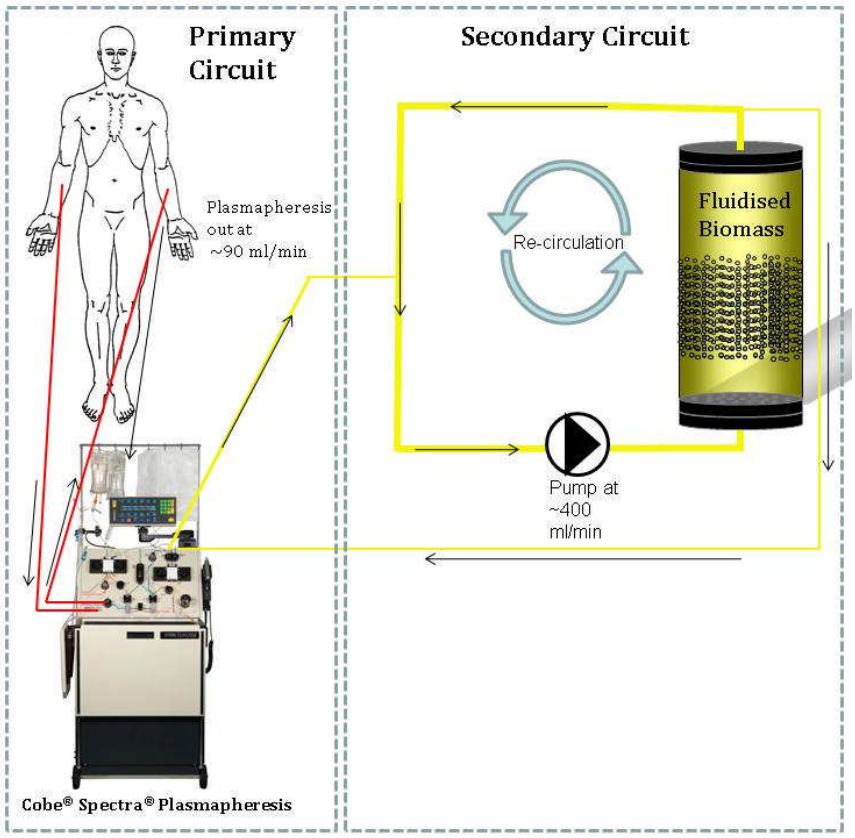

Figure 6-1: The large scale BAL system. Comprised of two sections, the primary and secondary circuit. The primary circuit, containing the Cobe® Spectra® therapeutic plasma exchange unit, operating at between 20ml/min -150ml/min[240]. The secondary circuit circulates in isolation at ~400ml/min to create a 2-fold bed height in the chamber holding the encapsulated HepG2 cells Plasma leaving the secondary circuit re-enters the primary circuit to rejoin the blood cells for return to the patient.

6.1.2. Important Parameters to Establish a Filtration System for the BAL

The direction and flow rates around the BAL system dictate the extent of treatment of a patient's plasma will receive and is reliant on two factors: firstly, the contact time between the biomass and a given volume of plasma will dictate the amount nourishment and detoxification which can be delivered; secondly, the maintenance of a maximum stable bead bed height within the BAL is crucial in facilitating maximal mass transfer and cell functionality[74,75]. In order to model the movement of fluid around the system, pressure measurements were made with changes to flow rate in the primary and secondary circuit. This data will provide a means of determining the effect of adding in a filtration system as well as potentially determining the flow rate to maximise the efficacy during treatment.

6.1.2.1. BAL Circuit with Added 3M® Cuno® Filter

By adding a filtration system to the BAL, the dynamics of the system flow may change. The measurement of pressure in the system before and after addition of a filter system provided an invaluable means of predicting potential challenges. One essential modification for the system was the addition of a reservoir after the filter, as illustrated in Figure 6.4, to mitigate the reduction in flow due to filter resistance over time. Another important feature of the BAL with the inline filter was the addition of a bypass circuit to allow the filter to be removed from the circuit in the event of excess pressure build-up due to filter blockage.

6.1.2.2. Addition of Contaminants

Spiking with Endotoxin

The normal levels of plasma endotoxin in healthy patients are usually between 0.1 - 0.4EU/ml, rising to 0.6-1Eu/ml with acute liver failure[184,232]. Endotoxin levels and associated endotoxemia are related to the levels of gram negative bacteria in the patient's blood or organ systems. ALF patients often suffer secondary complications such as septicaemia due to reduced immunological protection from compromised liver function[251,252]. The levels of endotoxin in a patient will therefore rise in line with bacterial presence. To model this endotoxin increase, the BAL treatment phase would require constant infusion of endotoxin over the treatment time. This could be problematic due to the large volume of plasma and the potential for endotoxin to adsorb on to the tubing or other circuit components. Therefore, several large endotoxin spikes were introduced into the blood at 50EU/ml, 100-fold the native level found in the ALF patients, thus increasing the likelihood of detecting endotoxin in a large plasma volume, to show subsequent clearance.

Spiking with DNA

As previously reported in Chapter 2, 86±4ng/ml DNA was released in plasma by dead HepG2 cells as part of the scale BAL model. At the same time as spiking endotoxin, DNA spikes were also added, at a concentration of 100ng/ml.

6.2. Summary of Chapter

With the information provided by previous chapters, a large scale BAL experiment will be performed with a 3M® Cuno® EXP® Filter in place, comparing the results with the BAL system without a filter.

6.3. Methods

6.3.1. Measuring Pressure in a Modified BAL system.

Materials

- 2L Biomass Chamber
- 200ml Empty alginate beads encapsulated using the Jetcutter™ encapsulator system (Methods Section 2.1.2.6.)
- 3L Rhesus negative, group B Fresh Frozen Plasma (FFP)
- 20U/ml Heparin
- Three Watson-Marlow® 520DU peristaltic pumps
- BAL treatment phase tubing set up as illustrated in Figure 4.
- Autoclaved 5L beaker,
- 100Uml/Penicillin/0.1mg/ml Streptomycin (Lonza®)
- 1.25µg/ml Fungizone (Invitrogen™)
- 5L sterile water
- Medex™ Pressure transducers read using the ADintruments PowerLab® and LabChart4® system modified as described in Methods Section 2.6.

A large scale model BAL treatment system was set up, as illustrated in Figure 6.2 (replacing the Cobe® Spectra® with Watson-Marlow® pumps), in order to measure pressures changes at key points as flow rates were altered.

To a 5L autoclaved beaker held in a category 3 tissue cabinet, Penicillin/Streptomycin, Fungizone and Heparin were added before pooling 3L of FFP. Pre-autoclaved BAL system tubing was setup, priming the system with sterile water for calibration the three Watson-Marlow® Pumps. Water was then removed, purging with air and replacing with plasma.

Moving the chamber to the tissue cabinet, 200ml empty alginate beads suspended in media were first washed with plasma, by dilution, and then added to the chamber, introducing some media to the system. Pressure measurements were made using modified Medex™ pressure transducers as described in Methods Section 2.5, as the flow rate of the pumps representing the Cobe® Spectra® were changed simultaneously from 20–80ml/min, whilst keeping the secondary circuit pump at 400ml/min. Then the secondary circuit pump was changed from 100–600ml/min, whilst keeping the pumps representing the Cobe® Spectra® at 40ml/min. During this, the bead bed height was measured with increased secondary circuit flow rate.

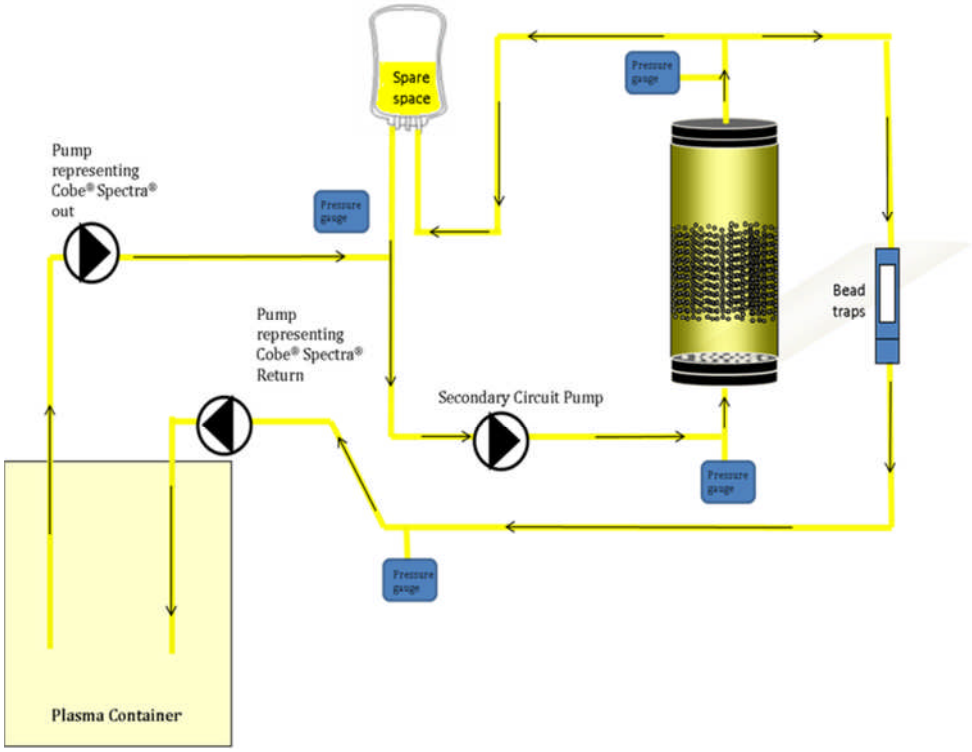

Figure 6-1: Model BAL treatment Phase to assess changes in pressure with increased flow rates. The Cobe® Spectra® was replaced by two Watson-Marlow® pumps set at identical flow rates. The first pump took plasma from a 5L container in a tissue cabinet, at between 20-80ml/min, to the secondary circuit. A second pump re-circulated the plasma through a 2L chamber containing empty alginate beads, at between 100-600ml/min. A third pump in the primary circuit removed plasma from the secondary circuit as the identical flow rate as the first pump, returning the plasma to the 5L container.

6.3.2. Adding a Filter to the Large Scale BAL System to Remove DNA and Endotoxin

Materials

- Same materials as Section 0. with the exception of:
- 3M® Cuno® EXT® 60ZA05A filter.
- 3M® Cuno® EXT® filter top manifold.
- 3M® Cuno® EXT® filter bottom manifold.
- 3M® Cuno® EXT® small filter holder.
- PTFE Bonded EPDM autoclave resistant Gaskets (Value Plastics®).
- Glass Reinforced White Nylon 1" to 1.5" sanitary fitting clamp (Value Plastics®).
- 1.5" sanitary fitting, mini-flange to 600 series 6.4mm barb adaptor, Kynar PVDF.
- Cobe® Spectra® Aphaeresis system
- Therapeutic Plasma Exchange (TPE) set for the Cobe® Spectra® Aphaeresis system
- 30L sterile MilliQ treated RO water
- 2L Rhesus negative, blood group B FFP, from donations to the NBS
- Red blood cells blood group B, from donations to the NBS
- 0.2µm hydrophobic air filter.
- 6L total volume (2L plasma, 2L filter, 2L in chamber)

The functionality of the 3M® Cuno® EXT® 60ZA05A filter as part of the large scale BAL was tested for removal of DNA and endotoxin, whilst allowing the transit of specific proteins. Prior to assembling the circuit, the filter was flushed with 10L of sterile water, then autoclaved alongside the filter manifolds, followed by assembling both the Cobe® Spectra® TPE tubing as detailed in Appendix VI, and the BAL circuit in isolation, sealing tubes to maintain sterility.

Human blood was reconstituted from FFP and blood cell bags and stored in a sterile 5L container situated in a sterile tissue cabinet. The Cobe® Spectra® TPE circuit was aseptically attached the autoclaved BAL circuit, clamping at the inlet and outlet of the BAL system.

Priming of the TPE set was initiated by passing the blood through the Cobe® Spectra® system to separate into plasma and blood cells, followed by priming the BAL system by first filling the "Priming Plasma" bag in Figure 6-4. Once the bag was filled with 6L of plasma, the BAL system was connected for priming from the BAL, setting the Cobe® Spectra® pumps as fast as possible to reduce priming time. At this stage the filter was bypassed to allow the BAL system to be fully primed then the waste bag was clamped allowing flow from the Cobe® Spectra® directly into and out of the BAL, as illustrated in Figure 6-4. During this time, the BAL system pump was maintained at 400ml/min, and then briefly varied from 100ml/min to 600ml/min to assess the effect on pressure. Once the system was fully running, the filter was added, opening the air vent (with a 0.2μm hydrophobic air filter) to allow the filter to be primed. For the large BAL experiment, no beads were added as in previous experiments, the pressure was unaffected as a result of beads.

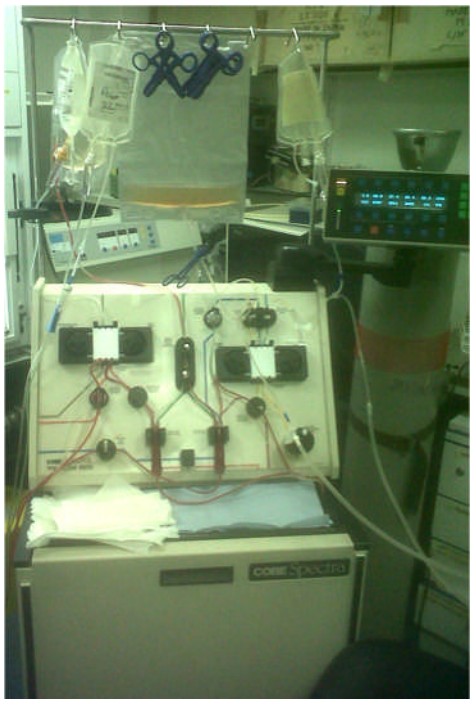

Figure 6-2: Cobe® Spectra® Aphaeresis system with the TPE set assembled.

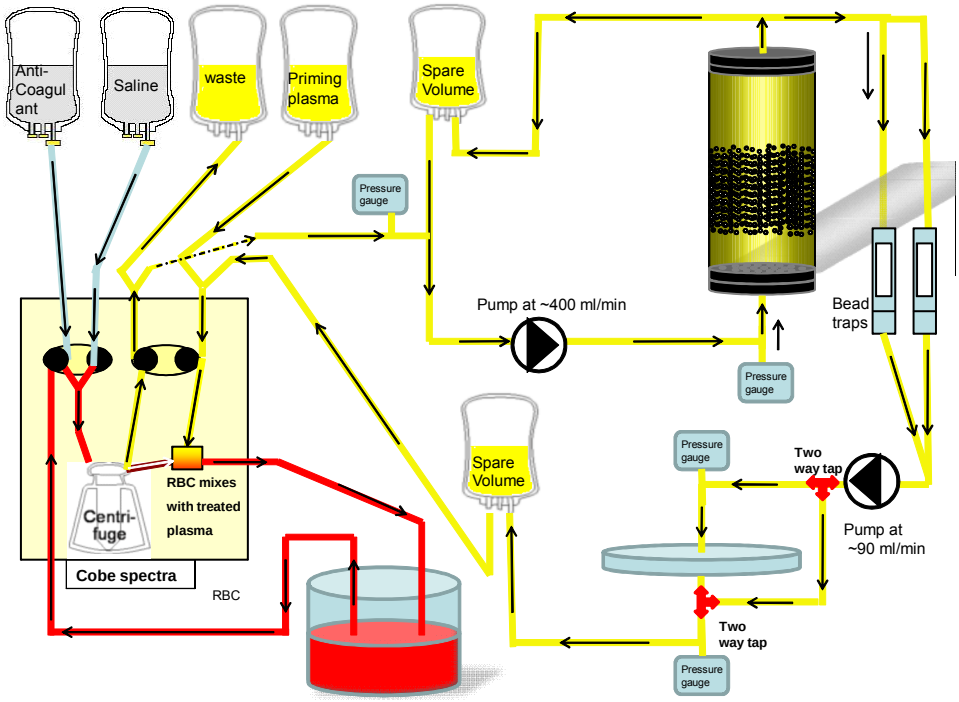

Figure 6-3: Detailed diagram of the BAL treatment phase. Blood was separated from the Cobe® Spectra® therapeutic plasma exchange unit, passing plasma to the BAL system where it was passed through the secondary circuit containing the chamber (not containing beads) at 400ml/min, then passing the plasma back to the Cobe® Spectra® to re-join the patient.

6.3.3. Endotoxin Measurement in Plasma using the Lonza® Fluorometeric *Limulus* Amoebocyte Lysate Assay.

Measurement of endotoxin in plasma before and after filtration through the 3M® Cuno® 60ZA05A EXT® Filter, as part of the BAL treatment phase.

Materials

- Same materials as Methods Section 2.6.
- 1129±465 EU/ml stock endotoxin, isolated from E.Coli as described in Methods Section 2.6.1.
- 2ml Cryovials (Nunc™).
- Liquid nitrogen stored in a small Dewar.

The methodology for endotoxin quantification by fluorogenic LAL assay was used, as detailed in Methods Section 2.6. The blood reconstituted for the BAL experiment (detailed in Section 0) was spiked with 62µl of the 1129 EU/ml to provide 50EU/ml endotoxin in the blood. This was used to prime both the Cobe® Spectra® and the BAL system prior to addition of the filter system. Immediately after the filter was primed and filtrate began exiting into the system, three 1.5 ml samples were taken and immediately snap frozen in liquid nitrogen, then stored at -80°C until assayed. At 4 and 6 hours, a further 262µl of 1,129,465 EU/ml stock endotoxin was added.

6.3.4. Extraction of HepG2 DNA for Spiking in the BAL Treatment Phase.

Materials

- T80 Tissue Culture Flasks (Nunc™)
- ND1000 Nanodrop® Spectrophotometer
- 27G sterile, DNA, DNAse and RNAse free syringe needle
- 2ml sterile, DNA, DNAse and RNAse free syringe

HepG2 cells were initially cultured as detailed in Methods Section 2.1.1.1, using three T80 culture flasks. After seven days, cells were harvested and DNA extracted using the protocol detailed in Methods Section 2.2.1.2 and Methods Section 2.2.2, respectively. The extracted DNA was sheared by passing the solution through with a 27G needle ten times. Finally, DNA concentration was then quantified using the Nanodrop® Spectrophotometer at 260ηm and 280ηm, pooling the DNA from the three flasks giving a total DNA concentration of 876 ± 39ng/µl.

6.3.5. DNA Spiking for Alu Repeat Analysis by QPCR

To determine DNA levels from spiking blood used in the BAL treatment phase with the addition of the filtration system.

Materials

- Same Materials as Methods Section 2.2.4.
- 876ng/µl HepG2 DNA extracted as described in Section 0.

Protocol

The same protocol as detailed in Methods Section 2.2.4 was used to analyse DNA in plasma samples taken from before and after filtration in the BAL treatment phase. At the same time as spiking endotoxin, 684µl of 876 ± 39ng/µl of DNA was added to the blood as part of the BAL treatment phase (Section 0).

6.3.6. ELISA for Fibrinogen, Albumin and α-1-antitrypsin

Materials

Same as Methods Section 2.4

ELISA Protocol

Plasma samples were taken hourly and analysed for AFP, fibrinogen albumin and α-1-antitrypsin as described in Methods Section 2.4. Table 6-1 shows the dilution factors used to reduce plasma protein concentration to within the range of the 0-200ng/ml standard curve.

Protein	Sample	Dilution Factor	Comment
Fibrinogen	All samples	1,000	Fibrinogen samples taken after 6 hours before and after the EXT® filter
Albumin	All samples	10,000	Albumin taken after 6 hours before and after the EXT® filter
α-1-antitrypsin	All samples	10,000	α-1-antitrypsin taken after 6 hours before and after the EXT® filter

Table 6-1: ELISA dilution factors for different proteins. Plasma samples taken at 6 hours of the BAL treatment phase were tested from Fibrinogen, Albumin and α-1-antitrypsin concentration using ELISA protocol detailed in Methods Section 2.4. Dilution factors were applied to allow the protein concentration to be quantifiable within the 0-200ng/ml standard curve

6.3.7. BCA assay

Materials

- Reagent A, (pH 11.25):
  - 26mM sodium bicinchoninate (Sigma-Aldrich®, D8284).
  - 189mM sodium carbonate (BDH, 102404H).
  - 87mM sodium tartrate (Sigma-Aldrich®, S4797).
  - 100mM sodium hydroxide (BDH, 102524X).
  - 113mM sodium bicarbonate (BDH, 102474V).
- Reagent B (4% cupric sulphate):
  - 4% Cupric (II) sulphate 5-hydrate (BDH, 26270).
- Standard BSA solution, 1mg/ml (Sigma, P0834-10X-1ML).
- 96-well micro plate.
- 1.5ml microfuge tubes.
- Anthos Multi-well spectrophotometric plate reader.

BCA Protocol

A series of standards were prepared from 31.25ug/ml-1000ug/ml using serial dilution from the 1mg/ml BSA standard solution in MilliQ™ treated RO water. Reagents A and B were mixed to a ratio of 50:1, respectively. Samples were diluted 1/1000 in MilliQ™ treated RO water, running both standards and samples in triplicate, adding 20µl volume for both standards and samples to the 96 well plate. To each well, 200µl of pre-mixed reagent A and B solution was added, sealing the plate, and gently mixing on a plate shaker for 30 seconds, followed by incubating at 37°C for 30 minutes. The plate was cooled to room temperature, the absorbance of the plate was read at 550-570ηm, using the Anthos Multi-well Spectrophotometric Plate reader.

6.4. Results

6.4.1. Physical Characterisation of BAL Pressure Profile

Pressure measurements were made at crucial points in the BAL system containing plasma, to provide baseline measurements to compare when the filter is added to the BAL treatment phase. Initially the Cobe® Spectra® was replaced by two pumps set at identical flow rates, as illustrated in Figure 6-5, but will be referred to as the Cobe® Spectra® for clarity. With a filter in place plasma was spiked with endotoxin and DNA to assess removal, whilst measuring filter capacity using pressure measurements.

6.4.2. Measuring Pressures in the BAL System with CSTPE

Pressure measurements were taken at the positions 1-4 independently, shown on Figure 6-4.

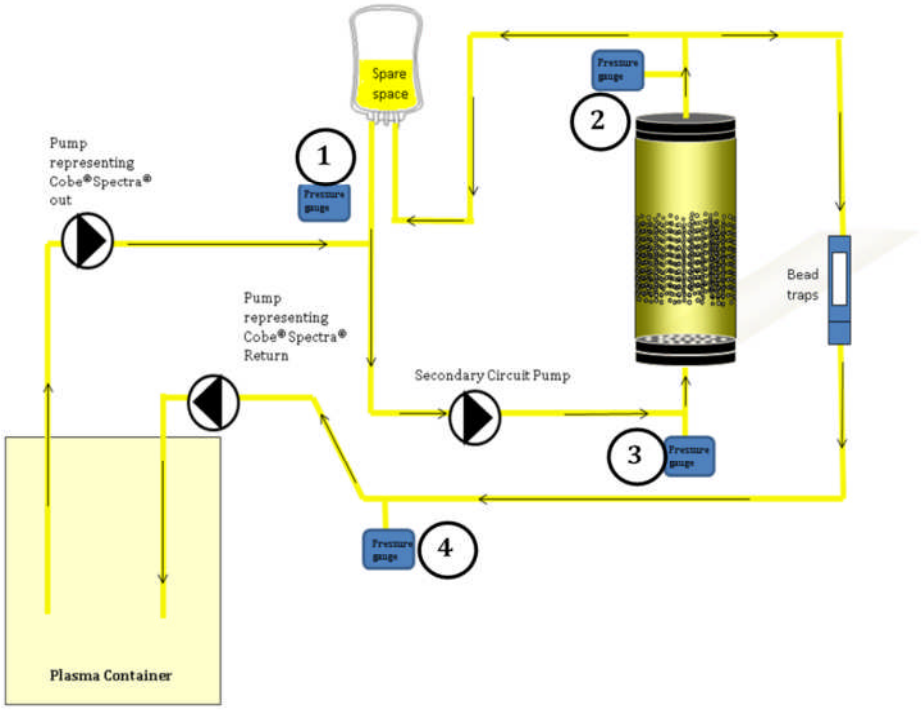

Figure 6-4: Locations of pressure measurements across the BAL. Positions of pressure readings corresponding to

6.4.2.1. Pressure Measurements at Exit and Entrance of Cobe® Spectra®

Position 1 was the pressure measurement taken at the exit of the pump representing the Cobe® Spectra® and position 4 was the pressure measurement at the return to the Cobe® Spectra®. As the flow rate of the pumps representing the Cobe® Spectra® increased from 20 – 40ml/min, the pressures at position 1 decreased by 0.21Bar to -0.0346Bar at 80ml/min, and increased at positions 4 by 0.115Bar to -0.08Bar at 80ml/min. The secondary circuit flow rate had a greater effect on pressure changes at positions 1 and 4, increasing from 0.388Bar to 0.389Bar at 600ml/min at position 4 and decreasing by 0.133Bar to -0.134Bar at 600ml/min (Figure 6.6).

Summary:

- As Cobe® Spectra® flow rate↑, pressure in secondary circuit ↓.
- As secondary circuit flow rate ↑, pressure at Cobe® Spectra® return ↑↑, and the pressure at Cobe® Spectra® outlet ↓↓

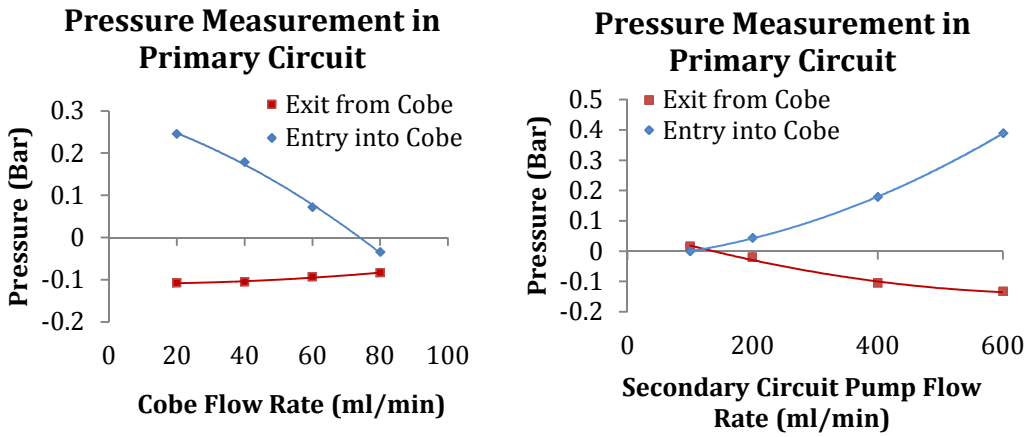

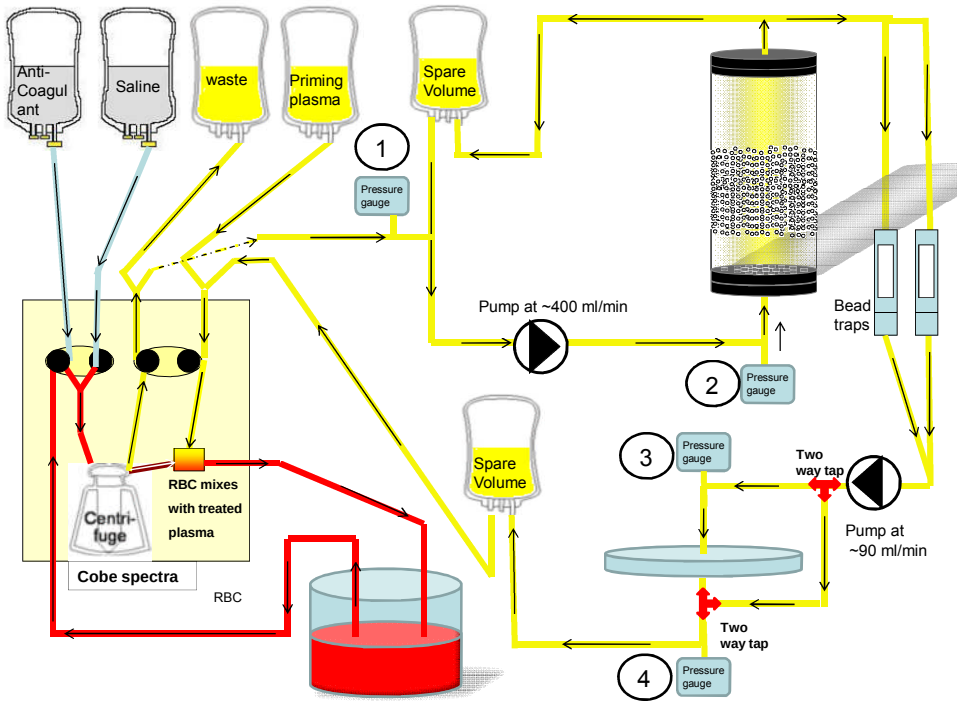

Figure 6-5: Pressure measurements taken at the Cobe Spectra exit and entrance to the BAL (position 1 and 4 as shown in Figure 6-4), representing the entrance and exit of the Cobe® Spectra® to the BAL system using CSTPE plasma. A; Pressure measurement as the flow rate of the Cobe® Spectra® pump was increased and the secondary circuit pump staying at 400ml/min. B; Pressure measurement as the flow rate of the Cobe® Spectra® is kept constant and the secondary circuit pump is increased.

6.4.2.2. Pressure Measurements at Exit and Entrance of Cobe® Spectra®

Position 2 was the pressure measurement taken before the chamber, and position 3 was the pressure measurement after the chamber. The differential pressure before and after the

chamber was determined, to assess the extent that the 200µm mesh at the bottom of the chamber influences the differential pressure. Altering the flow rate of the Cobe® Spectra® caused minimal changes in pressure at position 2 and 3, decreasing by 0.0685Bar and 0.0605Bar, respectively. As expected, increasing secondary circuit flow rate from 100ml/min to 600ml/min changed pressures at positions 2 and 3 by 1.197Bar and 0.609Bar at positions 2 and 3, respectively (Figure 6-7).

The rate of pressure change was identical before and after the chamber, as the Cobe® Spectra® flow rate increased from 20ml/min to 80ml/min, with the pressure after the chamber being consistently 0.32bar lower than before the chamber, as illustrated in Figure 6-6A. The distance between pressure gauges was relatively small for such a large change in pressure. Three parameters could cause this discrepancy: the loss of pressure due to friction from the chamber and tubing; the elevation of liquid between the bottom and top of the chamber; or resistance from the 200µm mesh.

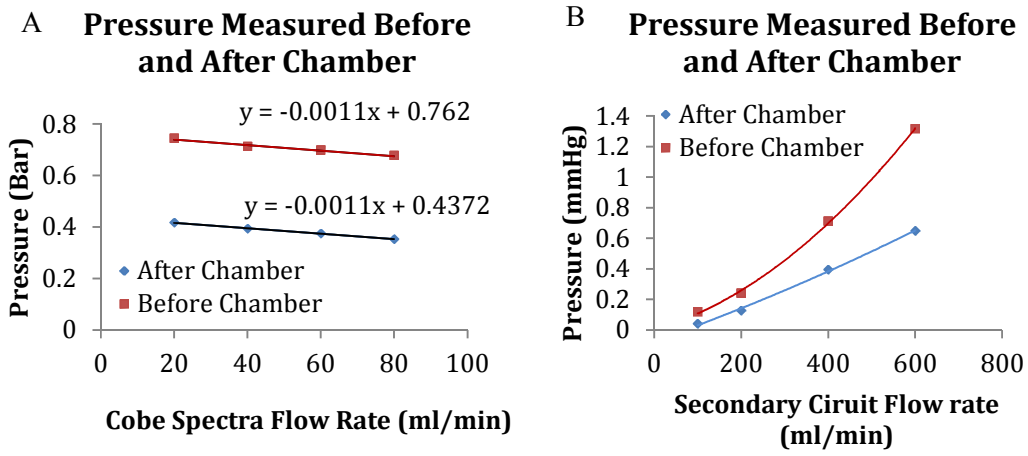

Figure 6-6: Pressure measurement before and after the BAL chamber using CSTPE plasma. A; Pressure changes whilst keeping the secondary circuit flow rate at 400ml/min and increasing the Cobe® Spectra® flow rate. B; Pressure changes whilst keeping the Cobe® Spectra® flow rate at 40ml/min and increasing the secondary circuit flow rate.

The change in pressure due to liquid elevation, i.e. gravitational effects, was calculated using Equation 6-1[253]:

Equation 6-1: $\Delta P_s = Z \times \rho \times SG$

Where the pressure difference at static fluid flow, ΔP_s ($kgcm^{-2}$), is equal to the product of the distance of elevation, Z (m), the density of the liquid, ρ (kgm^{-3}), and the specific gravity for the liquid, SG (dimensionless).

The specific gravity of Human plasma is 1.0310[254], the density of plasma 1025 kgm^{-3} [3, 255], and the static pressure difference was measured as 0.1002Bar.

⇨ 0.251m x 1025kgm^{-3} x 1.031= 265 kg/m^2 = 0.0265Bar

Therefore, the height of the chamber provides approximately a quarter of the contribution to the pressure differential of the plasma before and after the chamber.

Pressure loss due to friction was calculated using the Darcy-Weisbach law in Equation 6.2:

Equation 6-2: $\Delta P = \lambda \times \frac{1}{d_n} \times \frac{(\rho \times v^2)}{2}$

Where the loss in pressure, ΔP (Pa), is equal to the product of D'Arcy-Weisbach friction coefficient, λ (dimensionless), and the inverse of the hydraulic diameter, d_n (m), multiplied by the product of the liquid density, ρ (kgm^{-3}), and the volumetric flow rate, v (m^3s^{-1}), divided by 2.

Where the friction coefficient λ is dependent on the roughness of the tubing and whether the flow is laminar, transient or turbulent. This is dictated by Reynolds number as part of the parameter below[256]:

- laminar when *Re < 2300*
- transient when *2300 < Re < 4000*
- turbulent when *Re > 4000*

Reynolds number is calculated using Equation 6.3[256]:

Equation 6-3: $Re = \frac{\rho \times u^2}{\mu \times (u / L)}$

Where Reynolds number, Re (dimensionless), is equal to the dynamic pressure expressed by the product of the solution density, ρ (kgm^{-3}), and the liquid velocity squared, u (ms^{-1}), divided by the shear stress as defined by the dynamic product of the dynamic viscosity, μ (Pas), and the liquid velocity divided by the length of the tubing.

⇨ $\frac{1.25kgm^{-3} \times 7.02x10^{-4}ms^{-1}}{3x10^{-3}Pas \times (7.02x10^{-4}ms^{-1}/0.231)} = 554$

The plasma in this scenario has a low Reynolds allowing the calculation of the friction factor using Equation 6-4:

Equation 6-4: $\lambda = 64/\mathrm{Re}$

Where $\lambda = 0.1155$, and Re is Reynolds number expressing the ratio of inertial force to viscous force for a given solution.

$$\Rightarrow \frac{0.1155 \times 1 \times}{0.11\mathrm{m}} \quad \frac{(1025\mathrm{kgm^{-3}} \times (7.02\times10^{-4})^2)}{2} \quad = 3.0 \times 10^{-9}\ \mathrm{Bar}$$

As a result, the level of pressure loss due to friction was negligible, leaving the main source of loss in pressure to be caused by the presence of the 200µm mesh as illustrated in Figure 6-6.

6.4.3. Bead Bed Height in the BAL System with CSTPE

As flow rate increased, the bead height increased with a polynomial distribution, using empty beads in CSTPE plasma. A flow rate giving a 2-fold increase in bead bed height from the initial height with no flow had been established with alginate beads containing HepG2 cells with 2% glass bead concentration encapsulated. Using the Jetcutter system described in Methods Section 2.1.3, this was achieved at 349ml/min using empty beads in CSTPE plasma (Figure 6-8). This figure is variable depending on the overall density of beads, altered by changing the percentage glass beads in the alginate mix.

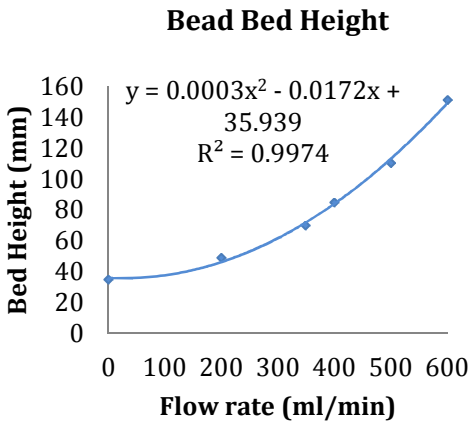

Figure 6-7: The alginate beads bed height, with CSTPE plasma passed through 35ml beads at between 0ml/min and 600ml/min, contained in a 2L chamber.

6.4.4. Large Scale BAL with In-line Filter

Testing the large scale BAL with the 3 M® Cuno® EXT® 60ZA05A filters evaluated any changes to the BAL system as a consequence of the alterations within the system, illustrated in Figure 6-8. These changes would predominantly originate from the back pressure that may build up behind the filter and the addition of a spare volume bag after the filter, as part of the primary circuit.

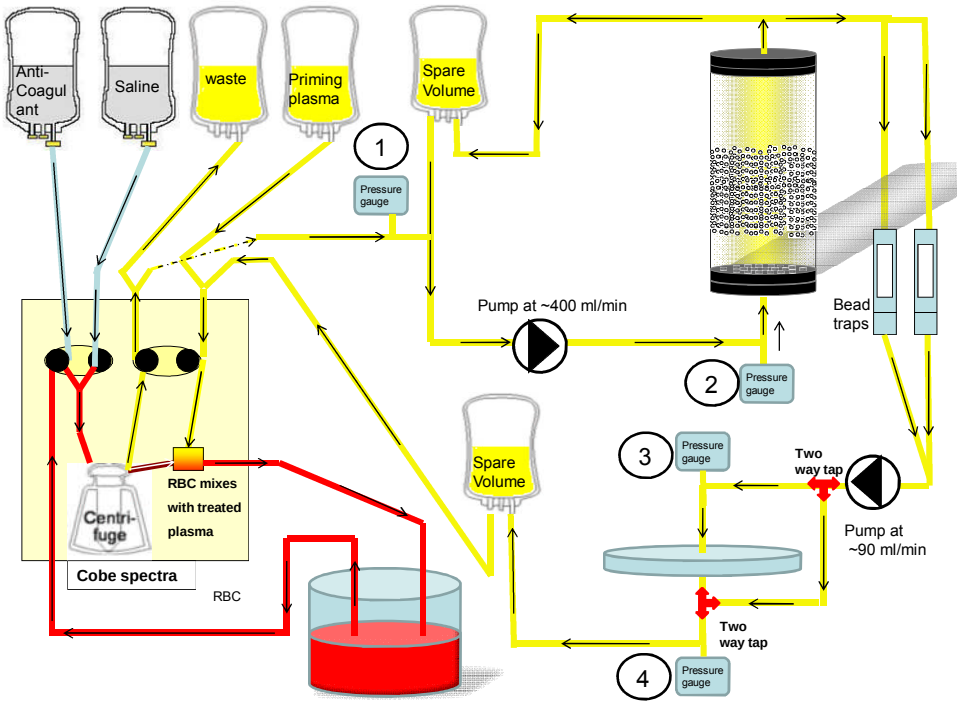

Figure 6-8: BAL treatment phase with an inline 3M® Cuno® EXT® 60ZA05A filter. In the primary circuit, blood was separated into plasma and cells by the Cobe® Spectra® aphaeresis system, to be passed into the secondary circuit at between 20-90ml/min, with the secondary circuit pump being maintained at between 100-600ml/min. Pressure readings were made at the exit and entrance of the Cobe® Spectra®, position 1 and 4, as well as before the chamber, at position 2, and before the filter, at position 3.

6.4.5. Pressure Changes in the BAL Over 8 Hours of Perfusion

As a result of modifying the BAL system with the addition of the filter, a pump and another spare volume bag, the distribution of pressures around the system were profoundly altered. Consequently, the flow rates used in the large scale BAL to test changes in flow rate, detailed in Section 0, could not be replicated in the large scale BAL with the added filter. Despite this, the changes in pressure were monitored throughout the experiment to evaluate the potential mechanism for changes in pressure.

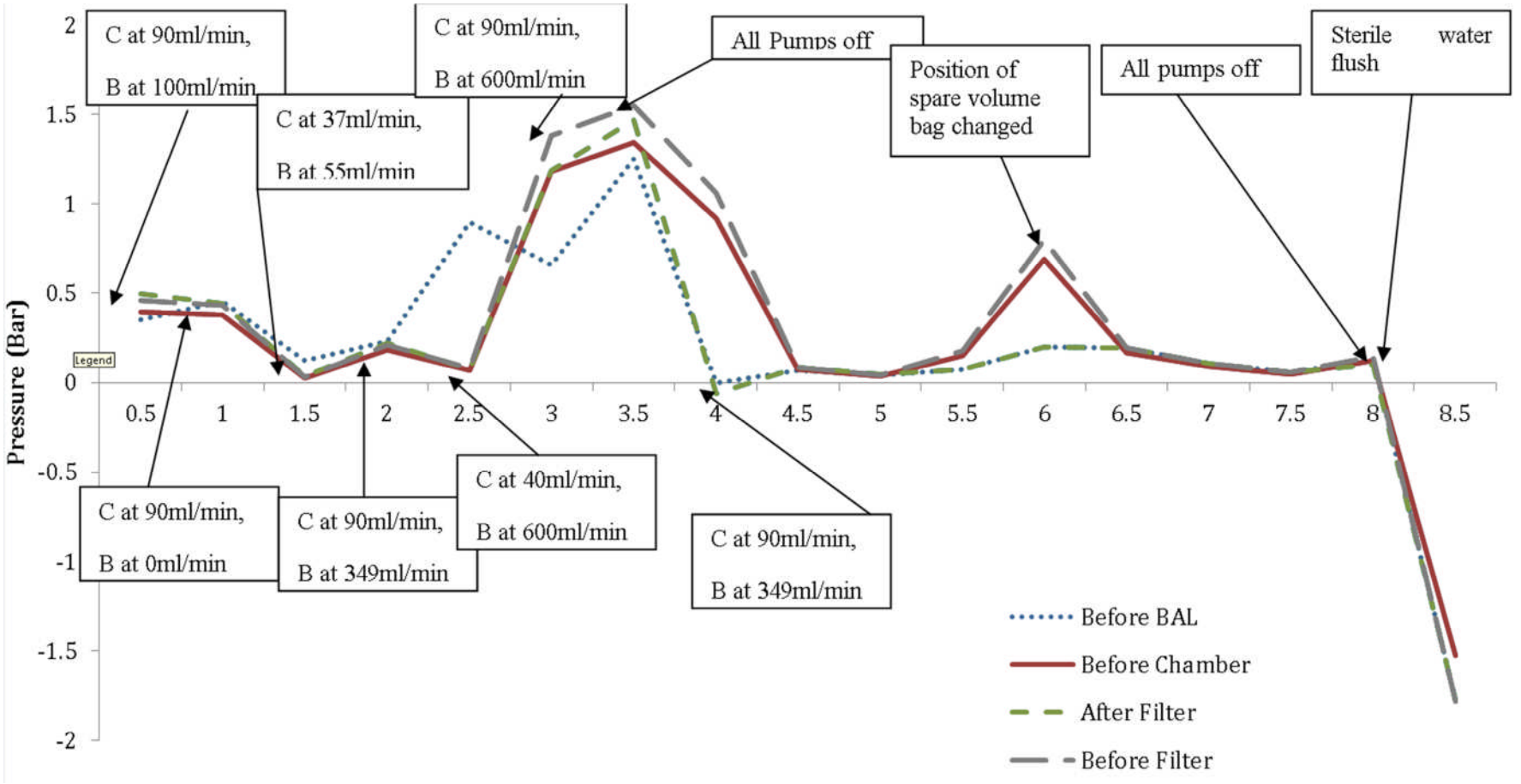

Figure 6-9: Pressure changes over 8 hours in the large scale BAL with an inline filter. Labels indicate changes to flow rate of either the Cobe ® Spectra® denoted by C, and the BAL pump denoted by B. The experiment was run for 8 hours after which a 25L sterile water flush was performed of the whole BAL system and the filter. The TPE tubing as part of the Cobe® Spectra® was disposed of as described in the essential Cobe® Spectra® user guide[257]. Samples were taken after 30 minutes, with DNA and endotoxin spikes added to the blood before filtration, at 4 hours and 6 hours.

During the experiment, the distribution of liquid in the two reservoir bags seemed to be dictated by two parameters: the distribution of pressure producing a lag between the change in flow rate and pressure; air space within the filter may have caused changes to pressure build up in each reservoir, causing the bag to either fill or empty depending on its gravitational position of the bag and flow rate of the Cobe® Spectra®. For example, at 2 hours the Cobe® Spectra® flow rate was increased from 37ml/min to 90ml/min and the BAL flow rate was increased from 55ml/min to 349ml/min. During the experiment without the filter, this would have caused a large increase in BAL pressure, a more negative pressure at the Cobe® Spectra® exit, and a less negative pressure at the Cobe® Spectra® entrance. The pressure readings in Figure 6-6 showed an increase in pressure coming out of the Cobe® Spectra® (before BAL), whilst the pressure either side of the filter decreased. The pressure was being transmitted into the reservoir bag in the secondary circuit, which rapidly filled with plasma. When the secondary circuit flow rate was increased to 600ml/min and the Cobe® Spectra® was decreased to 40ml/min, the pressure after the Cobe® Spectra® decreased and the pressure before and after the filter increased rapidly, whilst the spare volume bag in the primary circuit began to fill. The implication of this is the distribution of plasma in the circuit and extent of contact with the biomass has with a given volume of plasma, potentially altering detoxification and nourishment efficiency.

In terms of backpressure due to filter blockage, with the large filter flux, little pressure build-up was observed. At 3.5 hour when all the pumps were turned off, the pressure before the filter registered a lag in declining pressure compared with the pressure after the filter, possibly due to the resistance of the filter media. Despite this, when the system was allowed to stabilise for pressure setting the flow rate at 90ml/min for the Cobe® Spectra® and 349ml/min for the BAL pump, there was no detectable pressure differential before or after the filter, being identical to the pressure coming out of the Cobe® Spectra®. One point of pressure build up did occur, when the spare volume bag in the primary circuit was held below the height of the filter to assess the effect of gravity on the pressure within the system. As a result, the backpressure before the filter was increased as the reservoir volume reached its maximum.

Despite the changes to the BAL system, the filter showed little build up in pressure or resistance over the 8 hours of perfusion, owing to the large filter area utilised.

6.4.5.1. Filter Capacity

Unlike the experiments in chapter 5, the filter capacity does not require prediction for total capacity, as significant differential pressure was not produced during the 8 hours of perfusion with plasma. The capacity was sufficient to be able to reduce the filter size significantly from the $0.23m^2$ to a $0.1m^2$ filter or possibly less. At the end of the filtration experiment, the total volume throughput was 49.23L according to the Cobe® Spectra® readout.

6.4.6. Endotoxin and DNA Removal in the BAL Treatment Phase

6.4.6.1. Endotoxin and DNA Removal in the BAL Treatment Phase

Spiked endotoxin levels, as detailed in Section 0, were reduced to unquantifiable levels by the 3M® Cuno® EXT® 60ZA05A filter over the 8 hours of the BAL treatment phase (Figure 6-11). As a result, the endotoxin capacity of the filter was calculated to be 1.152 x 10^6EU total endotoxin binding. According to previous studies, a depth charged filter similar to the 60ZA05A filter would have a capacity of 29.9µg of endotoxin[258]. However, during this experiment a total of 76.13µg of endotoxin was added to the blood, all of which was removed, showing no breakthrough, even towards the end of the 8 hours.

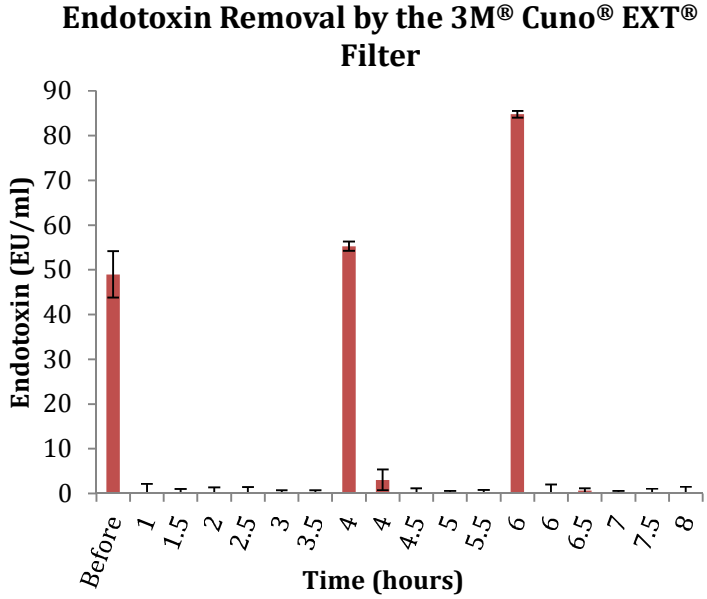

Figure 6-10: Endotoxin concentration in CSTPE plasma over 8 hours of the BAL treatment phase, adding endotoxin spikes before the experiment, after 4 hours and 6 hours. Double time points represent samples were taken before and after the filter in the BAL circuit after 15 minutes of endotoxin addition. (n=5)

6.4.6.2. DNA Removal

Spiked DNA levels were reduced to below the LoD by filtration with the 3M® Cuno® EXT® 60ZA05A filter (Figure 6-11), spiking with DNA before, at 4 and 6 hours of the BAL treatment phase, as described in Section 0. The DNA capacity calculated in Chapter 5, predicted a total DNA removal capacity of 39µg of DNA for a 25cm^2 3M® Cuno® 60ZA05A filter. A 0.23m^2 filter with the same filter media would provide a 3.59mg of DNA capacity. During the experiment, a total of 1.56mg of DNA was added to the system, which would have been representative of the level expected with plasma from an ALF patient and with a HepG2 cell viability of 73% (resulting in a potential DNA release from ~30% of the BAL cell content). Therefore, even if double the level of DNA was released into the system, the filter would still have sufficient capacity, based on the calculations in Chapter 5.

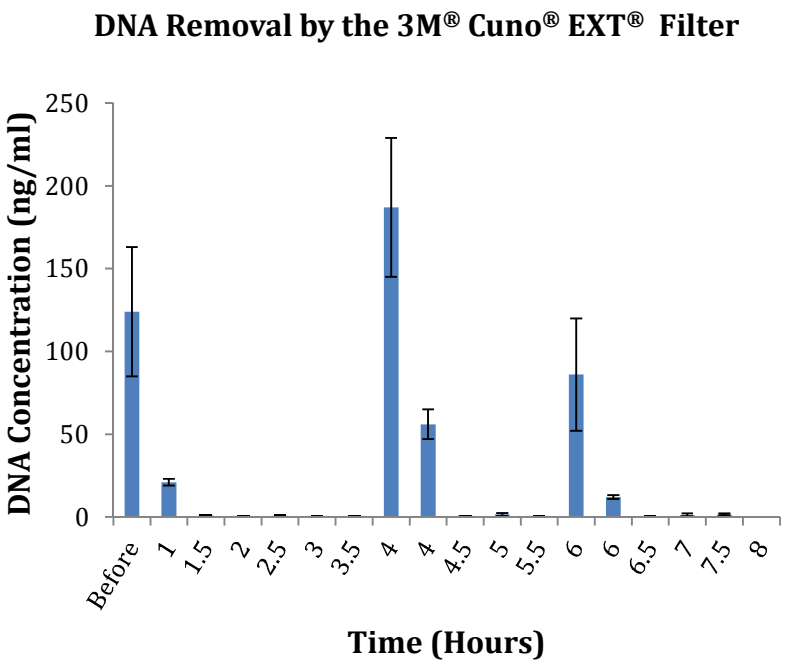

Figure 6-11: DNA concentration in CSTPE plasma in the BAL treatment phase over 8 hours, adding DNA spikes before filtration, at 4 and 6 hours, as detailed in Section 0. Double time points represent samples were taken before and after the filter in the BAL circuit after 15 minutes of DNA addition. (n=5)

6.4.7. Protein Transit through the 3M® Cuno® EXT® 60ZA05A Filter

Protein transit was measured by analysing plasma samples taken after 6 hours of filtration through the EXT® filter. In all cases, there was no significant difference in specific proteins before or after purification measured using ELISA, detailed in Section 0, and total protein using BCA assay, as shown in Figure 6.13.

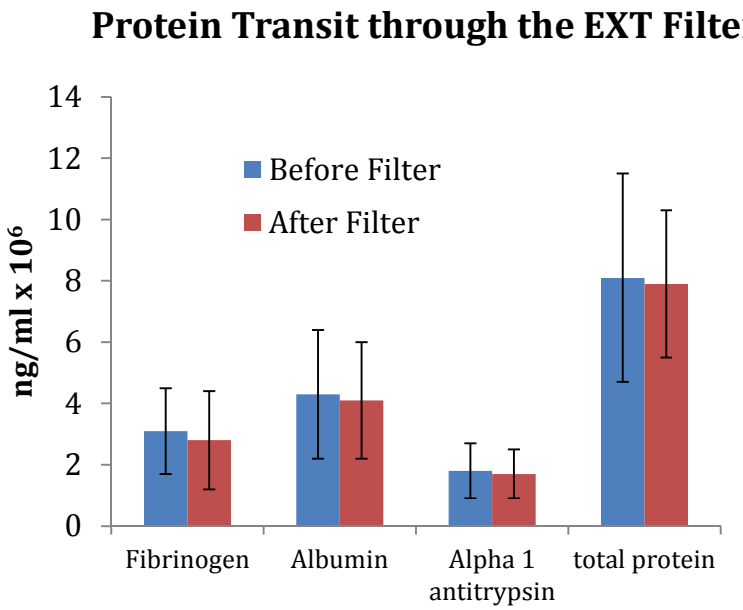

Figure 6-12: Plasma samples taken at 6 hours from the BAL treatment phase, detailed in Section 0, were analysed by ELISA showing no significant difference before and after filtration with p<0.99 for fibrinogen, p<0.88 for Albumin, p<0.98 for α-1-antitrypsin, and 0.99 for total protein with all proteins analysed in isolation (paired two-way t-test with n=5, error bars indicate standard deviation). Samples were taken before and after the filter.

6.5. Discussion

The BAL system without the inline- filter showed the dynamics of the complete circuit with changing flow rates. By adding the filter and introducing the subsequent modifications to the BAL system, the dynamics of the system were significantly altered, which would be expected, but required confirmation and quantification in order to be able to move towards pre-clinical trials.

In the BAL system without the filter, the greatest effect on the pressure was the flow rate of the BAL pump, whereas changing the flow rate of the Cobe® Spectra® had a relatively minor effect on the pressures within the system. Another important characteristic of this system was the resistance imparted by the 200µm mesh at the bottom of the chamber. When changing the BAL chamber flow rate, the pressure either side of the chamber did not change proportionally, with a 1.197Bar increase before that the chamber and a 0.6087Bar increase after. Consequently, the importance of ensuring the 200µm mesh within the chamber does not block is of vital importance to the robust function of the system. The maintenance of effective heparin concentration to avoid thrombin formation is the only means of preventing any clot formation, as other frequently used anticoagulants also chelate divalent cations, which would cause the alginate beads to dissolve.

An added dimension that could be combined with the analysis of the changes in flow rate around the BAL system is mathematically modelling the amount of biomass exposure a given plasma quantity received, providing a single unit of measurement to optimise the system and to quantify the implications of altering the system. In order to do this, computational fluid dynamics should be used, incorporating many of the principles covered in this thesis.

One way that a computational fluid dynamics program would provide vital information as to changes in the BAL system is by evaluating the changes to flow as a result of adding the filter, pump and the spare reservoir bags to the BAL system. Clearly, the addition of these components dramatically altered the pressure conditions in the system, illustrated by the slow and unexpected responses to changes to flow rate. An inference can be made that the spare volume bags were dictating the way the flow was distributed across the system, as observed during the large scale experiment. Previously a single spare volume bag in the secondary circuit mitigated any flow discrepancy between the inlet and outlet of the Cobe® Spectra® pump pushing plasma into and out of the circuit. However, with the addition of a new pump into the system, which was not controlled by the Cobe® Spectra®, and a second reservoir bag, the pressure in the system resulted in one bag to filling whilst the pressure increased in the secondary circuit, as illustrated Figure in 6-1. When the flow rates were changed and the pressure balance was shifted to the primary circuit the spare volume bag in the primary circuit

began to fill and the other bag began to empty. During the experiment, efforts were made to reach equilibrium for flow in and out of the two bags, achieved after 4.5 hours. However, to ensure that the plasma was maintaining the same level of BAL exposure as a system without the filter, computation of fluid dynamics could evaluate the theoretical treatment contact a given proportion of plasma would receive with different BAL designs, determining the extent to which the inclusion of the reservoir bags affect the system.

The increase in backpressure due to the reservoir bag filling showed the sensitivity of the system in terms of the effect of using two reservoirs. Furthermore, the addition of an extra pump not controlled by the Cobe® Spectra® system potentially introduced a discrepancy between the two systems, despite accurately calibrating both during system assembly. Accordingly, alternative system designs could be attempted to mitigate the issues raised.

One potential way of bypassing the necessity of having an extra pump and a spare bag may be to use the filter in a slightly different way. The 3M® Cuno® EXT® filters have four ports: a fluid entrance, a fluid exit and two air vents either side of the filter membrane. If the secondary circuit fluid is passed into the filter entrance and on the same side as the filter membrane, using the air vent, a fluid exit is provided as illustrated in Figure 6-13. As a result, the flow will still pass throughout the secondary circuit at between 100-600ml/min, as the easiest exit through the filter would be over the top and out of the air vent. At the same time, the Cobe® Spectra® would provide negative pressure downstream of the filter in the primary circuit, encouraging some of the liquid to pass through the filter. In previous experiment, 60ZA05A filters were tested for the ability to pull liquid through in this manner, rather than pushing, i.e. placing the pump downstream of the filter. This caused the liquid to degas. However, if the filter experiences an upstream positive pressure from the secondary circuit, with a negative pressure from the Cobe® Spectra®, the negative pressure may not be sufficient to cause degassing. However, this would need to be explored empirically.

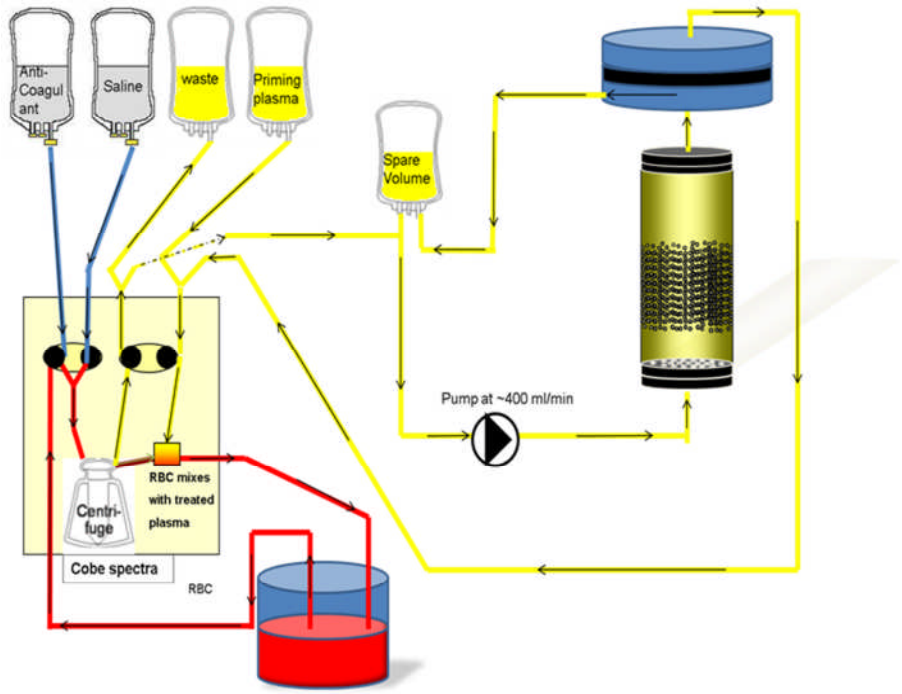

Figure 6-13: Large scale BAL design with the filter placed in the secondary circuit. Both the entrance and exit of the filter are positioned on the same side of the filter media, therefore causing the plasma to preferentially bypass the filter due to negative pressure downstream of the filter due to the Cobe® Spectra® some plasma will be encouraged to pass through the filter.

6.6. Conclusions

Despite the changes to the BAL system, the capability of removing endotoxin and DNA were extremely encouraging. In both cases, all the biological challenges were removed, reducing concentration to background levels. The DNA capacity was twice that predicted in Chapter 5, using the blockage models. In addition, the endotoxin capacity of the EXT filter in this chapter exceeded the calculated capacity for depth charge filters in previous studies[258], although the filters in these studies were preliminary versions of the S series filters, which have been shown to have a lower binding capability (Chapter 5). In the final filter design, there would need to be two filters, to mitigate any malfunction in one filter and to meet regulatory requirements if there was complete cell death, and then a second filter will be needed to ensure that no contaminant reached the patient. Although in the event of such a malfunction, the treatment would be prematurely terminated.

Since the start of writing this thesis, the large scale BAL system, without the filter, has been used as part of pre-clinical trials in a pig model for acute liver failure. The use of this system has shown successful integration of the Cobe® Spectra® and BAL systems, perfusing the biomass with plasma from the pig for up to 12 hours.

`

Chapter 7
Overall Discussion

This chapter will discuss the main outcomes of the previous results chapters and indicate areas for further development.

7. Overall Discussion

7.1 Initial Aims

The initial aims of the project were to establish a system to maintain plasma quality returning to the patient, focusing on contaminants from the BAL biomass as part of the treatment phase and particulates in alginate as a starting material. For the BAL treatment phase, the central requirement was to remove DNA and endotoxin from the BAL system whilst allowing transit of essential components synthesised by the biomass. Using 3M® Cuno® Zeta® plus charged depth filters, DNA and endotoxin were removed whilst allowing transit of specific proteins measured by ELISA and maintenance of total protein as measured by a BCA assay.

Alginate particulate content was reduced using both sand and charged depth filtration, but both caused detrimental changes to alginate properties causing the cell function and proliferation to be altered. Preliminary results from gas cyclonic filtration, reduced particulates to a comparable level to depth charged filtration and sand filtration whilst maintaining the alginate properties important for maintaining bead integrity, cell proliferation, and cell function.

7.2 Filtration system for BAL treatment Phase

The application of the 3M® Cuno® Zeta® plus charged depth filters to the BAL system showed sufficient capacity for the BAL treatment phase in both model and large scale experiments. In addition to this, DNA and endotoxin binding capacity was shown to be adequate for BAL treatment phase application. However, further developments are required to advance the system. Firstly, the measurement of specific proteins ensured that core synthetic proteins from the BAL system were not depleted; to complete this analysis other compounds important to therapeutic action of the BAL need to be assessed, to evaluate any changes in plasma composition beyond protein content.

7.3 Future Adaptation of Current Methods

Some of the methods used in modelling the system could be further expanded to other aspects of the project.

7.3.1. Scale BAL Growth Phase

The Scale BAL model was used to replicate the treatment phase, over 8 hours of perfusion. It could potentially be altered to model the growth phase, which provides an environment for encapsulated HepG2 cell growth, over 8-12 days using microgravity to promote mass transfer. However, a number of developments would be necessary. Firstly, two layers of silicon tubing line the inside of the large scale BAL chamber, passing oxygen into the BAL biomass. The glass columns used for the scale BAL model are too small to incorporate a

similar oxygenation system, instead incorporating it into the reservoir, holding the culture media. However, this would have 4 tubes entering and exiting a relatively confined space of the reservoir (even if larger reservoir bottles are used). Furthermore, with the potential of having nine replicates, the tubing could easily become tangles and twisted during the 10 days, potentially reducing fluid movement and increases in pressure leading to leakage.

To circumvent this challenge, a "circuit board" of tubing could be developed in the same manner as the Cobe® Spectra® system, where tubing is held in place so that connections are made correctly, any blockages are easily located and that tubing cannot kink. In addition to this, pH buffering may need to be transferred from exclusively using 5% CO_2 concentration in the incubator, to a combination of 5% CO_2 and a chemical solution. In the large scale bioreactor system CO_2 and N_2 are bubbled through the culture media, causing a decrease or increase in pH, respectively. After ~ 8 days when the cell density becomes greater, a feed of 7.5% bicarbonate is used to increase the pH. These three pH control methods are automatically controlled by the bioreactor system, using a pH probe in the bioreactor reservoir. The current scale BAL system design would rely on changes in the culture media to control pH, which may not be adequate for long term experiments over days. As a result, the design of the scale BAL model system could be changed to incorporate small pH probes connected to the ADintruments® PowerLab® system (used in the filter model), which could be used to control a pump for feeding bicarbonate into the reservoirs. Miniature pH electrodes are available that could be incorporated into the reservoir, measured at 14.6mm by 1mm, allowing real-time precise feedback pH control analogous to the large scale BAL.

7.3.2. Pressure Measurements across the Large Scale BAL Treatment Phase

Pressure measurements performed as part of the scale filtration model could be adapted to the large scale BAL treatment phase, to model the movement of fluid and relate it to mass transfer between the plasma and the cells. Mass transfer is crucial to successful treatment, and is reliant on the functionality of cells, the properties of the alginate, the speed of the plasma passing through the biomass, and the height of the biomass. By measuring the pressure, the plasma flow through the system can be monitored, allowing the contact time between cells and plasma to be calculated. Incorporating the contact time between a given portion of plasma and the cells into a mathematical model of the system with the other parameters mentioned could allow the development of the optimum mass transfer conditions and BAL design.

7.4 Alginate Purification as a Starting Material

7.4.1 Regulatory Requirements for Alginate as a Starting Material

The use of alginate in biomedical and pharmaceutical applications is well established, in artificial organs such as artificial pancreas[259,260] and artificial kidney[261], drug delivery for treatment of Parkinson's disease[262], and cell matrix for nerve regeneration[233]. Furthermore, alginate is featured on the Generally Recognised as Safe[264] (GRAS) list compiled under the FDA Code for Federal Regulation[265] (21 CFR 184.1724). This states that sodium alginate, but not magnesium, is suitable for human consumption, but does not guarantee use as a pharmaceutical product. The ASTM, originally known as the American Society of Testing and Materials, have been accepted as the international standardisation body, who outline the use of alginate as a pharmaceutical product, with a dedicated division for tissue engineering medical devices[266]. The standard set by the ASTM form the basis for medical application of alginate as part of cGMP, cGLP and cGTP, and FDA approval[267].

Two documents from the ASTM specifically relate to alginate as a starting material[23] and alginate in the context of cell encapsulation[159]. Neither stipulates specific requirements to achieve medical grade alginate, instead stating the necessary measurements of alginate parameters for regulatory submission, mainly referring to requirements relating to alginate used as a parenterals for drug delivery and for tissue implantation, and crucially requiring illustration of biocompatibility with the specific parameters measured.

An important alginate parameter stipulated under "alginate as a starting material" is impurity levels, defined as the presence of extraneous substances and materials in the alginate, including endotoxin, particulates, microbial burden, heavy metals, and protein. Of these impurities, endotoxin levels permitted in alginate are identical to parenterals, as described in Chapter 5 (5EU/kg of body mass) and are directly related to microbial burden in the alginate, relating to potential patient reaction to endotoxin[251]. Protein contamination in parenterals have been linked to hypersensitivity in patients[268], and the marine source of alginate presents a risk of heavy metal contamination, including lead and mercury[269].

In response to these regulations and the potentially detrimental clinical consequences, purification of alginate as a starting material is essential in moving towards a product certified as medical grade for use with human patients. Many other groups who aim to produce medical grade alginate go through multi-stage purification protocols which often alter the properties of the alginate[156,162,183]. However, many of the studies focused on alginate for cell transplantation into human to prevent immune access to the cells, and thereby prevent immune rejection. It is therefore likely that such an extensive alginate purification protocol will not be necessary to gain approval for use of alginate as a starting material for the BAL system.

7.4.2. Alginate Purification by Filtration

Alginate testing in this thesis initiated the process of creating medical grade alginate for the purposes of the BAL system. Filtration of alginate in solution caused changes to alginate properties for encapsulation. Whereas preliminary results of air classification (gas solid cyclonic filtration) in dry state showed no difference in alginate properties as defined by viscosity, cell function and proliferation.

Prior to going into an extensive study of gas solid cyclonic filtration, the particulates need to be characterised to know the composition and nature, in addition to measuring the other parameters outlined. The process of air classification uses two processes to separate dry components of a heterogeneous mixture: sieving, which utilises a variety of meshes to remove large particulates; air stream classification, which uses air flow to separate components based on particle size and density, into grades based on predefined cut off points[270]. It has been shown that protein levels can be manipulated using this method, although these reports concern protein recovery in food manufacturing[271]. Despite this, protein content, which is an important parameter of alginate purity, may be controlled using this method. As a result, the protocol could be an important improvement on filtration of alginate for other industrial applications.

Characterisation of particles should be performed in accordance with ASTM F-1877 (2010)[272], entitled "Standard Practice for Characterization of Particles". It details the methods for particulate composition, morphological characterisation, number, size, and size distribution of particles; including sieve analysis, optical, SEM (scanning electron microscopy), NMR (nuclear magnetic resonance) and HPLC.

7.5. The Development of the BAL System as a Medical Device

One of the main reasons for pursuing a system that manages plasma quality returning to the patient is to remove contaminants, which may have adverse clinical effects, and to initiate the process of regulatory compliance. Therefore, by reviewing some of the regulatory requirements the project can be better directed for eventual market approval. This development will require the implementation of a wide variety of management practices and detailed analysis of the BAL parameters. An overview of regulatory issues will be discussed, focusing mainly on analytical method development, medical device manufacture, and guidelines pertinent to the Liver Group BAL.

7.5.1. Overview of Regulatory Documents

Four main types of standards are internationally recognised for specific levels of medical device accreditation, ISO9001:2000, ISO17025:2005, ISO15189:2003 and cGLP (including cGMP and cGTP). The ISO standard (International Standards Organisation) guideline ISO9001:2000 mainly focuses on quality management systems for manufacturing concerning overall processes involved with administering the manufacture, quality

management, and delivery of the device[273]. As part of this, inspections take place from relevant organisations, depending on the location of market approval and with whom the certification is held, for example the BSI (British Standards Institute) in the UK.

With the relatively generalised nature of ISO9001:2000, ISO17025:2005 dictate many of the management criteria that need to be met in ISO9001:2000 but provides specific technical guidelines principally concerning topics such as calibration and testing laboratories. Again, inspection regimes ensure compliance, for example UKAS (*United Kingdom Accreditation Service)* in the UK. The third document which links both ISO9001:2000 and ISO17025:2005 is ISO15189:2003, which specifically concerns medical laboratories, being particularly pertinent for the BAL manufacture and further development. It matches the quality management requirements of ISO9001:2000 with the technical requirements of ISO17025:2005, covering details such as method development and validation, sampling regimes and, patient medical outcome, cost effectiveness, ethics and many other aspects of pre-and-post investigative issues. Finally, the most stringent standard is cGLP (current Good Laboratory Practice), which is maintained by cGLPMA (GLP monitoring authority) in the UK, incorporating all the ISO regulations mentioned and is crucial for manufacture and distribution of medicinal goods. In actual fact, depending on the application of GLP, different permutations of these guidelines are applicable, for example, cGMP, (manufacturing) and cGCP (clinical) each certification requiring extensive validation, in depth documentation of management processes and analytical methods, and strictly controlled facilities[118,186,274,275].

The implementations of these regulatory requirements depend upon the stage of development. The Liver Group BAL development is perfectly adequate for preclinical trials. To progress to clinical trials involving humans, the European Parliament and Council Directive 2001/20/EC[276] have stipulated requirements concerning implementation of cGCP (current Good Clinical Practice), which have become standardised across the European Union with introduction of this legislation in 2004. As a consequence, clinical trials must be conducted with the focus on safety of the participants with the manufacturing process complying with local GMP standards. Therefore, core analytical methods used for the clinical trials must focus on process validation with the specific requirements for validation being dependant on the stage of the device development. Throughout this development a comprehensive scope must be presented for each method at each stage of medical device development, within this scope relevant documentation substantiating the case for validation and regulatory compliance can be presented[277].

7.5.2. Application of Regulations to the BAL System

The transition of a device from research to a medical device can be a long and expensive process, often requiring years of pre-clinical testing to obtain the required data for regulatory approval by organisations such as the FDA[118]. As a result integrating processes to facilitate regulatory submission is important to prevent the need to repeat data and to speed the development of the project.

The validation of the QPCR protocol is adequate for research and pre-clinical trial purposes, to confidently show reduction or elimination of DNA in plasma. In addition to this, due to the incorporation of traceability of both method development and the source of components used in method validation the protocol could easily be extended for incorporation into clinical trials. The ELISA protocols and Nucleocounter® cell number protocols too could be extended for use in clinical trials, as a result of prior validation performed by others. Furthermore, many of the Liver Group BAL components are currently being documented for the purposes of traceability and are in the process of development for eventual validation. Finally to prepare for clinical trials, data gathered from pre-clinical trials must comply with 21CFR312, which outlines the process of applying for a new drug application, including drugs intended to treat life-threatening and severely-debilitating illnesses, such as the Liver Group BAL.

An overview will be presented of some developments that will facilitate progression of a project for use with clinical trials and beyond.

7.5.2.1 Quality Manual (QM)

A quality manual (QM), forms the core for further development, including the next significant step of producing a small scale manufacture process for clinical trial. It provides the governance for other related documents stipulating management responsibilities, infrastructure of the organisation, health and safety, quality procedures, and SOPs. For example, the scope of the SOPs in the QM incorporates instructions describing the laboratory environment that match the regulatory requirements for all subsequent SOP's[199].

7.5.2.2. Protocols used with the BAL System

As part of the QM, a battery of analytical methods used to evaluate specific therapeutic and contaminant parameters, would need to be incorporated into an in-depth management system. This must include detailed and robust documentation and tightly controlled environments for analytical detection of all the BAL parameters including DNA and other contaminants. In addition to this, the laboratory will have to comply with certain regulatory compliances to attain accreditation to guarantee the quality of the results[199].

Traceability

The central concept of validating an analytical protocol is traceability, of which two levels exist. Experimental traceability of an entire methodology includes reagents, sample identifiers, and analytical instruments, using documentation to detail batch numbers, source of samples and servicing logs. Metrological traceability relates to the ability to trace the experimental development back through different comparisons and justifications, and validation using reference standards[199]. Both aspects of traceability are important in producing a valid analytical protocol, forming part of a much wider network of traceability and documentation that can encompass management structures, training records, instrument maintenance and ownership, and laboratory design. For example, a pharmaceutical manufacturing plant will have specific requirements from an analytical method and management structure around traceability, which would be excessive and far too costly for a University research group. The important aspects of these concepts must be chosen and applied to the needs of the organisation.

Management Structure

A management structure is core to the implementation of the specific aspects concerning both types of traceability. A distinct management structure carrying out defined aspects of documentation aids the process of developing a compliant product, including staff training, maintenance of standard operating procedures (SOPs). For example, SOPs should be monitored by a number of proficient individuals at different levels of management, including people who are not directly involved with the methodology, to ensure that the protocol is followed in a compliant manner on all levels, from the bench to the documentation.

Equipment must be fit for purpose, requiring evidence in the form of experience of members of staff using it, standard instruments used by others, adequacy of the instrument for the task, validation of software. Ownership of equipment is necessary to ensure that instruments are properly maintained in both in terms of day to day use and servicing. The owner needs to be properly trained, with supporting documentary evidence.

Calibration underpins metrological traceability, ensuring experimental values agree with values of CRM (certified reference material), where available. For both GLP and ISO17025:2005 evidence of system suitability is required, requiring validation in the same manner as the QPCR protocol in Chapter 5. A schedule of calibrating and recording calibration must be put in place. Testing the performance of equipment independently is also necessary.

All reagents including all water used must be documented and fit for purpose and sufficient grade for the task in hand, incorporating complete traceability of all components, including storage conditions and stability of the reagents.

Implementation of Quality Management Principles for QPCR

The depth at which each of the management processes are implemented depends on the requirements of the project. For the purposes of developing and validating a QPCR protocol for use within a pre-clinical research setting, a number of management systems were put in place. This was in preparation for further more detailed development for clinical trials. These included laboratory environment, instrumentation used, and method validation performed around the framework of traceability.

The environment was strictly controlled by using separate areas for PCR reaction setup, amplification process, and analysis; separated not only in location but also in the consumables and instruments. This ensured that no accumulation of template could occur to cause contamination of samples and false positives. In addition, records of batches and material numbers, as well as detailed account of each experiment fulfilled the same aspects of metrological and experimental traceability.

All areas of the BAL process will need to be managed in the same manner as the QPCR protocol, to collect appropriate data for regulatory submission to carry out clinical trials. Many of these processes are in place or are in development in-line with the needs of improving the system. For example, the growth phase of the BAL system is performed in a clean room to reduce likelihood of contamination, although to gain regulatory approval the clean room would require certification, as well as continuing to document all data and materials used for both meteorological and experimental traceability.

Specific Principles for Developing the BAL System Manufacturing Device

As mentioned the development of the BAL system to a clinical setting requires the implementation of a variety of processes and quality management systems. This thesis mainly focused on specific contaminants, namely DNA, endotoxin, and particulates, which form part of the banner of biocompatibility. An ASTM guideline (ASTM F748 2006) outlines selecting biological tests to establish biocompatibility.

The central theme of ASTM F748 2006, is the biocompatibility of the medical device. It states that each device is considered on individual merits regardless of what other applications of similar technologies have shown. The use of animal models (using as few as possible) is central to this, ensuring that the components of the device do not affect the outcome of the health. The tests performed do rely on the nature of the device or product and the exposure time, with the BAL treatment phase categorised as an inter-operative device, due to its relatively short treatment time. As an indication of minimal requirements necessary for a BAL, the following tests must be complete:

- Cell culture cytotoxicity
- Sensitization studies

- Systemic toxicity, acute or sub-acute
- Blood compatibility
- Haemolysis
- Pyrogen testing
- Immune response.

Initial screening tests of biomaterials are also essential, as if any adverse tissue response is detected later, it may be impossible to ascertain which component of the device caused the issue. For the BAL this includes the alginate and the impurities. The entire encapsulation, growth, and treatment phase and all of the components involved, such as media components, polymerisation buffers and other preparation fluids. Furthermore, parameters such as sterility must be determined.

Biocompatibility testing requires evaluating the levels of extractables from the constituents of the device, using methods with sufficient sensitivity to detect to trace levels, if possible, such as HPLC (High Performance Liquid Chromatography), GC (Gas Chromatography), or AA (Atomic Absorbance Spectroscopy). Following this, the biocompatibility of the extracts from components of the medical device and the device itself should be undertaken, to ensure that even undetectable levels of extractables are not causing adverse effects.

Two other guidelines provide further information for safety and toxicology testing[278,279]: ISO 10993, called "Biological evaluation of medical devices"; ASTM F748 – 06 (2010) entitled, "Standard Practice for Selecting Generic Biological Test Methods for Materials and Devices". These document detail studies, which relate to the whole BAL project in addition to the alginate as a starting material and as a matrix for cell encapsulation, Analysis such as reproducibility in the manufacture of compounds is extremely important and is explicitly outlined in the Code for Federal Regulation 21CFR211[274].

7.6. Conclusions

Adding a filter to the Liver Group BAL system could represents a significant change in the fluid dynamics of the system. Consequently, the work in this thesis represents preliminary work to be used to allow focused testing using customised filters and ensuring that the analytical methods work correctly when applied to more realistic situations. For example, using plasma from many different patients to provide statistical power and test cells in both small and large scale that have previously been cryo-preserved. The BAL circuitry needs to be adjusted to prevent a filter changing the amount of treatment patient plasma gets. These dynamics need to be modelled, as well as testing more filters on a small scale to provide statistical power. Finally, the Alu repeat PCR protocol has the potential to become an early diagnostic tool for liver damage. If this protocol is tested with different patient plasma samples and optimised for diagnostic purposes, it could provide a new tool in diagnosing

specific types of liver cell damage, thereby helping clinicians provide the correct treatment as soon as possible.

8. Reference List

1 A Hollander, et al., "The first stem cell-based tissue-engineered organ replacement: implications for regenerative medicine and society.," 4(2), 147 (2009).

2 Harald C. Ott, et al., "Regeneration and Orthotopic transplantation of a bioartificial lung," Nat Med 16(8), 927 (2010).

3 Harald C. Ott, et al., "Perfusion-de-cellularized matrix: using nature's platform to engineer a bioartificial heart," Nat Med 14(2), 213 (2008).

4 A Saito, K Sawada, and S Fujimura, "Present status and future perspectives on the development of bioartificial kidneys for the treatment of acute and chronic renal failure patients," 15(2), 183 (2011).

5 J Rozga and P Malkowski, "Artificial liver support: quo Vadis?," 15(4), 92 (2010).

6 R. N. M. MacSween, et al., macsween's pathology of the liver (Elsevier Churchill Livingstone, 2007).

7 G. Schneider, et al., MRI of the liver: imaging techniques, contrast enhancement, differential diagnosis (Springer, 2006).

8 AH McIndoe and VS Counseller, "The Bilaterality of the Liver," Arch. Surg. 15, 589 (1927).

9 R. V. Krstiç, human microscopic anatomy: an atlas for students of medicine and biology (Springer-Verlag, 1991).

10 P Kamath, "Vascular Disease of the Liver," in Mzy Clinic Gastroenterology and Hepatology Board Review, edited by S Hauser, D Pardi, and J Poterucha (Mayo Clinic Scientific Press, Rochester MN, 2005), pp.348-356.

11 D Hausinger, WH Lamers, and AF Moorman, "Hepatocyte Heterogeneity in the Metabolism of Amino Acids and Ammonia," 46, 72 (1992).

12 K Jugermann and T Kietzmann, "Zonation of parenchymal and non-parenchymal metabolism in liver," 16, 179 (1996).

13 DE Malarkey, et al., "New Insights into Functional Aspects of Liver Morphology," 33, 27 (2005).

14 AV Loud, "Quantitative Stereological Description of Ultrastructure of Normal Rat Liver Parenchymal Cells," 37, 27 (1968).

15 "American College of Surgeons," https://www.socialtext.net/acs-demo-wiki/index.cgi?couinard_s_segments. Accessed on 27/6/2011

16 "National Institute on Alcohol Abuse and Alcoholism," http://www.niaaa.nih.gov/Pages/default.aspx. Accessed on 27/6/2011

17 RP Oude-Elferink and AK Groen, "Mechanisms of Biliary Lipid Secretion and their Role in Lipid Homeostasis.," Semin Liver Dis. 20(3), 293 (2000).

18 J. Rodges, J. P. Benhamou, and M. Rizzetto, textbook of hepatology: from basic science to clinical practice (Blackwell, 2007).

19 Albert L. Jones, et al., "A quantitative analysis of hepatic ultrastructure in rats during enhanced bile secretion," Anat. Rec. 192(2), 277 (1978).

20 R Daoust, "Histochemical Comparison of Focal Losses of RNAse and ATPase Activities in Preneoplastic Rat Liver," 27(2), 653 (1978).

21 P. H. Sugarbaker, "Surgical decision making for large bowel cancer metastatic to the liver," 174(3), 621 (1990).

22 P. Soyer, et al., "Hepatic metastases from colorectal cancer: influence of hepatic volumetric analysis on surgical decision making," 184(3), 695 (1992).

23 M Wimmer and D Fette, "Microphotometric Studies on Intra-acinus Enzyme Distribution in Rat Liver," 64, 23 (1979).

24 T Kietzmann, et al., "Arterial Oxygen Partial Pressures Reduce the Insulin-Dependent Induction of the Perivenously Located Glucokinase in Rat Hepatocyte Cultures: Mimicry of Arterial Oxygen Pressures by H2O2." 321, 17 (1997).

25 K Jugermann and N Katz, "Functional Specialization of Different Hepatocyte Populations," (1989).

26 S. S. Gropper, J. L. Smith, and J. L. Groff, advanced nutrition and human metabolism (Wadsworth Engage Learning, 2008).

27 W. H. Elliott and D. C. Elliott, biochemistry and molecular biology (Oxford University Press, 2009).

28 Georg Hennemann, et al., "Plasma Membrane Transport of Thyroid Hormones and Its Role in Thyroid Hormone Metabolism and Bioavailability," Endocr. Rev 22(4), 451 (2001).

29 Makoto Naito, Go Hasegawa, and Kiyoshi Takahashi, "Development, differentiation, and maturation of Kupffer cells," Microsc. Res. Tech. 39(4), 350 (1997).

30 Ekihiro Seki, et al., "TLR4 enhances TGF-[beta] signalling and hepatic fibrosis," Nat Med 13(11), 1324 (2007).

31 P Gines, et al., "Effect of Liver Failure on Organ Systems," in Chronic Liver Failure: Mechanisms and Management, (Humana Press, London, New York, 2010), pp.171-189.

32 S. Sherlock, S. Sherlock, and J. Dooley, diseases of the liver and biliary system (Blackwell Science, 2002).

33 J. H. Chow and C. Chow, the encyclopaedia of hepatitis and other liver diseases (Facts on File, 2006).

34 H. C. Thomas, S. M. Lemon, and A. J. Zuckerman, viral hepatitis (Blackwell Pub., 2005).

35 W. J. Marshall and S. K. Bangert, "Acute and Chronic Liver Disease," in Clinical biochemistry: metabolic and clinical aspects, 2 ed. (Churchill Livingstone/Elsevier, 2008), pp.274-295.

36 LL Kjaergard, et al., "Artificial and Bioartificial Support Systems for Acute and Acute-on-Chronic Liver Failure," 289(2), 217 (2003).

37 J. Rodes, JP Benhamou, and M Rizzetto, "Toxic Liver Injury," in Textbook of Hepatology: from basic science to clinical practice, edited by J Rodes, et al. (Blackwell, 2007), pp.1268-1276.

38 C Dart, et al., "Acetaminophen poisoning: an evidence-based consensus guideline for out-of-hospital management," 44(1), 1 (2006).

39 S johns, HPA Report No. 1, http://www.hpa.org.uk/web/HPAwebFile/HPAweb_C/1235032869649. Accessed on 14/02/2011.

40 RD Recknagel and EA Glende, "Carbon tetrachloride hepatotoxicity: An example of lethal cleavage," 263 (1973).

41 Han Chu Lee, "Acute liver failure related to hepatitis B virus," 38, S9-S13 (2008).

42 M Kennedy and S Alexopoulos, "Hepatitis B virus infection and liver transplantation." 15(3), 310 (2010).

43 TE Starzl, CG Groth, and L Brettschneider, "Extended Survival in 3 Cases of Orthotopic Homo-transplantation of the Human Liver." 63, 549 (1968).

44 Bernan, Increasing the Supply of Donor Organs Within the European Union: 17th Report of Session 2007-08: Vol. 2 Evidence: House of Lords Paper 123-II Session 2007-08 2008.

45 JA Tector, et al., "Use of Extended Criteria Livers Decreases Wait Time for Liver Transplantation without Adversely Impacting Post transplant Survival," 244(3),

46 Stephen R. Ash, "Powdered Sorbent Liver Dialysis and Apheresis in Treatment of Hepatic Failure," 5(5), 404 (2001).

47 L, Highleyman, "MARS and Prometheus Artificial Liver Devices Offer Some Benefits for Patients with Liver Failure, but Did Not Improve Survival," in (EASL (European Association for the Study of the Liver), Vienna, 2010).

48 GK Michalopoulos, "Liver Regeneration," in Molecular Pathology of Liver Diseases, edited by SPS Monga (Springer, Pittsburgh, 2010), pp.261-278.

49 I Massie, et al., "Cryopreservation of Encapsulated Liver Spheroids for a Bioartificial Liver: Reducing Latent Cryoinjury Using an Ice Nucleating Agent," 14(7) (2011).

50 U. Meyer, et al., fundamentals of tissue engineering and regenerative medicine (Springer, 2009).

51 Daniel Mueller, et al., "In-depth physiological characterization of primary human hepatocytes in a 3D hollow-fibre bioreactor," J Tissue Eng. Regen. Med, n/a (2011).

52 Y. Nahmias, F. Berthiaume, and M. L. Yarmush, "Integration of technologies for hepatic tissue engineering," 103, 309 (2007).

53 NJ Muller, et al., "Microbial safety in xenotransplantation," 16(2), 201 (2011).

54 Qian Yang, et al., "Fluidized-bed bioartificial liver assist devices (BLADs) based on microencapsulated primary porcine hepatocytes have risk of porcine endogenous retroviruses transmission," 4(4), 757 (2010).

55 N Amimoto, et al., "Hepatic Differentiation of Mouse ES Cells and IPS cells during Organoid Formation in Hollow Fibres," (2011).

56 Leonard H. Damelin, et al., "Altered mitochondrial function and cholesterol synthesis influences protein synthesis in extended HepG2 spheroid cultures," Archives of Biochemistry and Biophysics 432(2), 167 (2004).

57 T. M. Rahman, et al., "Alginate-encapsulated human hepatoblastoma cells in an extracorporeal perfusion system improve some systemic parameters of liver failure in a xenogeneic model," Artif. Organs 28(5), 476 (2004).

58 Norifumi Harimoto, et al., "The Newly Established Human Hepatocyte Cell Line: Application for the Bioartificial Liver," 42 ed.2005), pp.557-564.

59 S Enosawa, et al., "In vivo estimation of bioartificial liver with recombinant HepG2 cells using pigs with ischemic liver failure." 10(4-5), 429 (2001).

60 Demetra Mavri-Damelin, et al., "Cells for bioartificial liver devices: The human hepatoma-derived cell line C3A produces urea but does not detoxify ammonia," 99(3), 644 (2008).

61 T Usui, Y Saitoh, and F Komada, "Induction of CYP3As in HepG2 Cells by Several Drugs.—Association between Induction of CYP3A4 and Expression of Glucocorticoid Receptor," 26(4), 510 (2001).

62 I Jasmund, R Simmoteit, and A Bader, "An Improved Oxygenation Hollow Fibre Bioreactor of Cultivation of Liver Cells," in Animal cell technology: from target to market : proceedings of the 17th ESACT Meeting, TyloÂsand, Sweden, June 10-14, 2001, edited by E Lindner-Olsson, N Chatzissavidou, and E Lullau (Kluwer Academic, 2001), pp.545-548.

63 ES Tzanakakis, et al., "Extracorporeal Tissue Engineering Liver-Assist Devices," 2, 607 (2000).

64 A. A. Demetriou, et al., "Prospective, randomized, multi-center, controlled trial of a bioartificial liver in treating acute liver failure," 239(5), 660 (2004).

65 A. J. Ellis, et al., "Pilot-controlled trial of the extracorporeal liver assist device in acute liver failure," 24(6), 1446 (1996).

66 I. M. Sauer and J. C. Gerlach, "Modular extracorporeal liver support," 26(8), 703 (2002).

67 UNOS, Annual Report of the U.S. Organ Procurement and Transplantation Network and the Scientific Registry of Transplant Recipients: Transplant Data 1994-2006.2007.

68 WM Hsu, et al., "Liver-Assist Device with a Microfluidics-Based Vascular Bed in an Animal Model," 252(2), 351 (2010).

69 Julia Schutte, et al., "Artificial micro organs, microfluidic device for dielectrophoretic assembly of liver sinusoids,", 1 (2011).

70 GuoLiang Lv, et al., "Bioartificial liver system based on choanoid fluidized bed bioreactor improve the survival time of fulminant hepatic failure pigs," , n/a (2011).

71 J. M. Millis, et al., "Initial experience with the modified extracorporeal liver-assist device for patients with fulminant hepatic failure: system modifications and clinical impact," 74(12), 1735 (2002).

72 Igor M. Sauer, et al., "Extracorporeal Liver Support Based on Primary Human Liver Cells and Albumin Dialysis and Treatment of a Patient with Primary Graft Non-Function," in 39 ed.2003), pp.649-653.

73 E Morsiani, et al., "Early experiences with a porcine hepatocyte-based bioartificial liver in acute hepatic failure patients." Int J Artif Organs. 25(3), 192 (2002).

74 S. M. Coward, et al., "Proliferation rates of HepG2 cells encapsulated in alginate are increased in a microgravity environment compared with static cultures," 29(2), 152 (2005).

75 S. M. Coward, et al., "Alginate-encapsulated HepG2 cells in a fluidized bed bioreactor maintain function in human liver failure plasma," 33(12), 1117 (2009).

76 SL Nyberg, et al., "Primary hepatocytes outperform Hep G2 cells as the source of biotransformation functions in a bioartificial liver." Ann Surg. 220(5), 59 (1994).

77 B Burlington, "Design Control Guidance for Medical Device Manufacturers, "in 1997).

78 B. H. A. Rehm, alginates: biology and applications (Springer, 2009).

79 C Wandrey, A Bartkowiak, and S Harding, "Materials for Encapsulation," in Encapsulation Technologies for Active Food Ingredients and Food Processing, 1 ed. edited by N. J Zuidam and V Nedovi-ç (Springer, 2009), pp.55-57.

80 O Smidsrod and A Haug, "A Light Scattering Study of Alginate," 22, 797 (1968).

81 O. Smidsrod and G. Skjak-Braek, "Alginate as immobilization matrix for cells," 8(3), 71 (1990).

82 D. Quong, et al., "External versus internal source of calcium during the gelation of alginate beads for DNA encapsulation," 57(4), 438 (1998).

83 CJ Burek, et al., "Calcium induces apoptosis and necrosis in hematopoietic malignant cells: Evidence for Caspase- 8 dependent and FADD-autonomous pathway," 7, 173 (2003).

84 C. Schwinger, et al., "High throughput encapsulation of murine fibroblasts in alginate using the JetCutter technology," 19(3), 273 (2002).

85 Julie Dusseault, et al., "Evaluation of alginate purification methods: Effect on polyphenol, endotoxin, and protein contamination," J. Biomed. Mater. Res. 76A(2), 243 (2006).

86 U. Zimmermann, et al., "Production of mitogen-contamination free alginates with variable ratios of mannuronic acid to guluronic acid by free flow electrophoresis," 13(5), 269 (1992).

87 SK. Tam, et al., "Impact of residual contamination on the biofunctional properties of purified alginates used for cell encapsulation," 27(8), 1296 (2006).

88 KH Lee, et al., "Diffusion-mediated in situ alginate encapsulation of cell spheroids using micro scale concave well and Nano porous membrane," (11), 1168 (2011).

89 CM Shi and Cheng TM, "Differentiation of dermis-derived multipotent cells into insulin-producing pancreatic cells in vitro," 10(17), 2550 (2004).

90 Erica Ollmann Saphire, et al., "Crystal Structure of a Neutralizing Human IgG Against HIV-1: A Template for Vaccine Design," 293(5532), 1155 (2001).

91 J. C. Petricciani and F. N. Horaud, "DNA, dragons and sanity," 23(3), 233 (1995).

92 P Mandel and P Metais, "Les acides nucléiques du plasma sanguin chez l'homme (Nucleic acids of the blood plasma in man)," Ann. N. Y. Acad. Sci. 142, 241 (1948).

93 A. N. Butt, et al., "Circulating nucleic acids and diabetic complications," Ann. N. Y. Acad. Sci. 1075, 258 (2006).

94 V Swarup, et al., "Quantification of Circulating Plasma DNA in Friedreich's Ataxia and Spinocerebellar Ataxia Types 2 and 12." Ahead of printing (2011).

95 C Tag, et al., "Improved Method for Isolating Cell-Free DNA," 51(8), 1561 (2005).

96 S. N. Tamkovich, et al., "Circulating nucleic acids in blood of healthy male and female donors," Clin. Chem. 51(7), 1317 (2005).

97 S. N. Tamkovich, et al., "Circulating DNA and DNase activity in human blood," 1075, 191 (2006).

98 N. Umetani, "Higher amount of free circulating DNA in serum than in plasma is not mainly caused by contaminated extraneous DNA during separation," Annals of the New York Academy of Sciences 1075, 299 (2006).

99 N. Umetani, et al., "Prediction of breast tumour progression by integrity of free circulating DNA in serum," J Clin Oncol. 24(26), 4270 (2006).

100 P. Anker and M. Stroun, "Immunological aspects of circulating DNA," Ann. N. Y. Acad. Sci. 1075, 34 (2006).

101 J. A. Walker, et al., "Human DNA quantitation using Alu element-based polymerase chain reaction," 315(1), 122 (2003).

102 S. N. Tamkovich, et al., "[Circulating nucleic acids in blood of patients with stomach and colon neoplasms]," 51(3), 321 (2005).

103 WHO Study Group on Cell Substrates for Production of Biologicals http://www.who.int/biologicals/publications/meetings/areas/vaccines/cells/Cells.FINAL.MtgRep.IK.26_Sep_07.pdf. Accessed on 05/01/2011

104 N Umetani, et al., "Increased Integrity of Free Circulating DNA in Sera of Patients with Colorectal or Periampullary Cancer: Direct Quantitative PCR for ALU Repeats," 52(6), 1062 (2006).

105 S. Nagata, et al., "Degradation of chromosomal DNA during apoptosis," 10(1), 108 (2003).

106 C. S. Potten and J. W. Wilson, apoptosis: the life and death of cells (Cambridge University Press, 2004).

107 "HotStar Hi-Fidelity PCR Handbook for Sensitive and Reliable High-Fidelity Hot-Start PCR Sample 2007-2008,"in 2008).

108 W. R. Hudlow, et al., "A quadruplex real-time qPCR assay for the simultaneous assessment of total human DNA, human male DNA, DNA degradation and the presence of PCR inhibitors in forensic samples: a diagnostic tool for STR typing," 2(2), 108 (2008).

109 B. G. Wang, et al., "Increased plasma DNA integrity in cancer patients," 63(14), 3966 (2003).

110 L Raptis and HA Menard, "Quantitation and Characterisation of Plasma DNA in Normal and Patients with Systemic Lupus Erythematosus," 66, 1391 (1980).

111 TH Rainer, et al., "Derivation of a Prediction Rule for Posttraumatic Organ Failure Using Plasma DNA and Other Variables," Annals of the New York Academy of Sciences 945(1), 211 (2001).

112 M. B. Giacona, et al., "Cell-free DNA in human blood plasma: length measurements in patients with pancreatic cancer and healthy controls," 17(1), 89 (1998).

113 A. K. Pathak, et al., "Circulating cell-free DNA in plasma/serum of lung cancer patients as a potential screening and prognostic tool," Clin. Chem. 52(10), 1833 (2006).

114 M Giancona, et al., "Cell-Free DNA in Human Blood Plasma: Length Measurements in Patients with Pancreatic Cancer and Healthy Controls," 17(1), 89 (1998).

115 Sabine Jahr, et al., "DNA Fragments in the Blood Plasma of Cancer Patients: Quantitation's and Evidence for Their Origin from Apoptotic and Necrotic Cells," 61(4), 1659 (2001).

116 A Abbas, N Fausto, and R Mitchell, basic pathology, 8 ed. (Saunders Elsevier, 2007).

117 FDA, "Guidance for Industry, "in Q6B Specifications: Test Procedures and Acceptance Criteria for Biotechnological/Biological Products,1999).

118 A Kaplan, et al., "Medical Device Development, "in 2008).

119 SP Pillay, et al., "Endotoxin Levels in Donor and Recipients during Orthotopic Liver Transplantation," Aust. N. Z. J. Surg. 67, 187 (1997).

120 Stephen H. Gregory and Edward J. Wing, "Neutrophil-Kupffer cell interaction: a critical component of host defences to systemic bacterial infections," 72(2), 239 (2002).

121 Zuo Jin Liu, et al., "Up-Regulation of IRAK-M is Essential for Endotoxin Tolerance Induced by a Low Dose of Lipopolysaccharide in Kupffer Cells," Journal of Surgical Research 150(1), 34 (2008).

122 Jan Henning Fruhauf, et al., "Porcine endogenous retrovirus released by a bioartificial liver infects primary human cells," 29(10), 1553 (2009).

123 Giuseppe Di Nicuolo, et al., "Long-term absence of porcine endogenous retrovirus infection in chronically immunosuppressed patients after treatment with the porcine cell based Academic Medical Centre bioartificial liver," 17(6), 431 (2010).

124 Kazuyoshi Hanasawa, "Extracorporeal Treatment for Septic Patients: New Adsorption Technologies and Their Clinical Application," 6(4), 290 (2002).

125 SM Vesentini, GB Fiore, and A Redaelli, "Mechanisms of Polymyxin B Endotoxin Removal from Extracorporeal Blood Flow: Molecular Interactions," 167, 45 (2010).

126 E. A. Burgstaler and A. A. Pineda, "Therapeutic plasma exchange: A paired comparison of Fresenius AS104 vs. COBE Spectra," J. Clin. Apheresis 16(2), 61 (2001).

127 T. Burnouf, et al., "Assessment of complement activation during membrane-based plasmapheresis procedures," 19(3), 142 (2004).

128 K. Sutherland, "Filter Media," in Filters and filtration handbook, (Elsevier/Butterworth-Heinemann, 2008), pp.92-106.

129 H. C. Vogel and C. L. Todaro, fermentation and biochemical engineering handbook: principles, process design, and equipment (Noyes Publications, 1997).

130 Elizabeth L. Brainerd, "Caught in the crossflow," Nature 412(6845), 387 (2001).

131 M. Y. Jaffrin and C. G. Caro, biological flows (Plenum Press, 1995).

132 K. Sutherland, filters and filtration handbook (Elsevier/Butterworth-Heinemann, 2008).

133 G. Stacey and J. Davis, medicines from animal cell culture (Wiley, 2007).

134 R. W. Baker, membrane technology and applications (J. Wiley, 2004).

135 U. Gottschalk, process scale purification of antibodies (John Wiley & Sons, 2009).

136 Cuno, "Cuno Zeta CP and SP Series of Filters," in 2007).

137 R Knight and E Ostreicher, "Charge-Modified Filter media," in Filtration in the Biopharmaceutical Industry, edited by T. H. Meltzer and M. W. Jornitz (Marcel Dekker, 1998), pp.95-125.

138 Cuno, "DNA Removal from Bioprocess Purification Processes," in 2002).

139 N Dorsey, J. Eschrich, and G Cyr, "The Role of Charge in the Retention of DNA by Charged Cellulose-Based Depth Filters," 10, 46 (1997).

140 B Tipton, et al., "Retrovirus and Parvovirus Clearance from an affinity column product using adsorptive depth filtration," 1, 43 (2002).

141 A. Haarstrick, U. Rau, and F. Wagner, "Cross-flow filtration as a method of separating fungal cells and purifying the polysaccharide produced," 6(4), 179 (1991).

142 M. C. Porter, handbook of industrial membrane technology (Noyes Publications, 1990).

143 P Laird, et al., "Simplified mammalian DNA isolation procedure," Nucleic Acid Research 19(15), 4293 (1991).

144 S. N. Tamkovich, et al., "Circulating nucleic acids in blood of healthy male and female donors," Clin. Chem. 51(7), 1317 (2005).

145 MD Timken, et al., Quantitation of DNA for Forensic DNA Typing by qPCR 2005.

146 van der, V and P. J. Pretorius, "The origin of circulating free DNA," Clin. Chem. 53(12), 2215 (2007).

147 B. G. Wang, et al., "Increased plasma DNA integrity in cancer patients," Cancer Res. 63(14), 3966 (2003).

148 N Umetani, et al., "Increased Integrity of Free Circulating DNA in Sera of Patients with Colorectal or Periampullary Cancer: Direct Quantitative PCR for ALU Repeats," Clinical Chemistry 52(6), 1062 (2006).

149 Joel R. Gillespie and Vladimir N. Uversky, "Structure and function of [alpha]-fetoprotein: a biophysical overview," Biochimica Et Biophysica Acta (BBA) - Protein Structure and Molecular Enzymology 1480(1-2), 41 (2000).

150 Luis Bachmann, et al., "Size and shape of fibrinogen, 1. Electron microscopy of the hydrated molecule," Die Makromolekulare Chemie 176(9), 2603 (1975).

151 J Levin and FB Bang, "The role of endotoxin in the extracellular coagulation of limulus blood," Bull John Hopkins University Hospital (115), 265 (1964).

152 J Levin and FB Bang, "Clottable protein in Limulus; its localization and kinetics of its coagulation by endotoxin." Thromb Diath Haemorrhage. 31(19), 186 (1968).

153 S Iwanaga and J Levin, "The limulus clotting reaction," Curr Opin Immunol. 5(1), 74 (1993).

154 "PyroGeneTM Recombinant Factor C Endotoxin Detection Assay,"in 2011).

155 P De Vos, et al., "Improved biocompatibility but limited graft survival after purification of alginate for microencapsulation of pancreatic islets," Diabetologia 40(3), 262 (2011).

156 S Heiligenstein, et al., "Evaluation of non-biomedical and biomedical grade alginates for the transplantation of genetically modified articular chondrocytes to cartilage defects in a large animal model in vivo," The Journal of Gene Medicine , n/a (2011).

157 Microfiltration and ultrafiltration by ACTEW Corporation Ltd http://www.actew.com.au/water2water/documents/MicrofiltrationandUltrafiltration.pdf Accessed on 24/3/2011.

158 ASTM international, Report No. ASTM F 2026, 2008.

159 ASTM international, Report No. ASTM F2315 - 11, 2003.

160 British pharmacopoeia 2011 (Stationery Office, The, 2010).

161 U. Leinfelder, et al., "A highly sensitive cell assay for validation of purification regimes of alginates," Biomaterials 24(23), 4161 (2003).

162 SK. Tam, et al., "Impact of residual contamination on the bio functional properties of purified alginates used for cell encapsulation," Biomaterials 27(8), 1296 (2006).

163 A Prokop and TG WANG, "Purification of Polymers Used for Fabrication of an Immuno-isolation Barriera," Annals of the New York Academy of Sciences 831(1), 223 (1997).

164 P Laird, et al., "Simplified mammalian DNA isolation procedure," 19(15), 4293 (1991).

165 Joel R. Gillespie and Vladimir N. Uversky, "Structure and function of [alpha]-fetoprotein: a biophysical overview," Biochimica Et Biophysica Acta (BBA) - Protein Structure and Molecular Enzymology 1480(1-2), 41 (2000).

166 D. A. Allcutt, D. Lort, and C. N. McCollum, "Final inline filtration for intravenous infusions: a prospective hospital study," 70(2), 111 (1983).

167 J. W. Puntis, et al., "Hazards of parenteral treatment: do particles count?" 67(12), 1475 (1992).

168 T. M. Rahman, et al., "Alginate-encapsulated human hepatoblastoma cells in an extracorporeal perfusion system improve some systemic parameters of liver failure in a xenogeneic model," 28(5), 476 (2004).

169 Marianne Khalil, et al., "Human Hepatocyte Cell Lines Proliferating As Cohesive Spheroid Colonies in Alginate Markedly Up regulate Both Synthetic and Detoxificatory Liver Function," in 34 ed.2001), pp.68-77.

170 M. R. Collins, M. J. D. Graham, and American Water Works Association, slow sand filtration: and international compilation or recent scientific and operational developments (American Water Works Association, 1994).

171 "Microfiltration and Ultrafiltration by ACTEW Corporation Ltd," in 2011).

172 Sang Ho Yoo, et al., "Microencapsulation of [alpha]-tocopherol using sodium alginate and its controlled release properties," International Journal of Biological Macromolecules 38(1), 25 (2006).

173 A. Martinsen, G. Skjak-Braek, G Smidsrod, "Alginate as immobilization material: III. Diffusional properties," 39(2), 186 (1992).

174 A. C. Hoffmann and L. E. Stein, gas cyclones and swirl tubes: principles, design, and operation (Springer, 2007).

175 U. Leinfelder, et al., "A highly sensitive cell assay for validation of purification regimes of alginates," 24(23), 4161 (2003).

176 P De Vos, et al., "Improved biocompatibility but limited graft survival after purification of alginate for microencapsulation of pancreatic islets," 40(3), 262 (2011).

177 K Sakugawa, et al., "Simplified method for estimation of composition of alginates by FTIR," J. Appl. Polym. Sci. 93(3), 1372 (2004).

178 S Heiligenstein, et al., "Evaluation of non-biomedical and biomedical grade alginates for the transplantation of genetically modified articular chondrocytes to cartilage defects in a large animal model in vivo," J. Gene Med. n/a (2011).

179 SX Ci, et al., "Molecular mass distribution of sodium alginate by high-performance size-exclusion chromatography," Journal of Chromatography A 864(2), 199 (1999).

180 A Prokop and TG WANG, "Purification of Polymers Used for Fabrication of an Immuno-isolation Barrier," Annals of the New York Academy of Sciences 831(1), 223 (1997).

181 DM. Updegraff, "Semi-micro determination of cellulose in biological materials," Analytical Biochemistry 32(3), 420 (1969).

182 D McHugh, Report No. 441, 2003. http://www.fao.org/docrep/006/y4765e/y4765e08.htm accessed 11/01/2011

183 Christopher G. Thanos, et al., "Intraperitoneal stability of alginate-polyornithine microcapsules in rats: An FTIR and SEM analysis," 27(19), 3570 (2006).

184 Z. Nadhazi, et al., "Plasma Endotoxin Level of Healthy Donors," 49(1), 151 (2002).

185 Benjamin Y. Klein, et al., "Immunogenicity of subcellular fractions and molecular species of MuLV-induced tumours. I. screening of immunogenic components by isopycnic ultracentrifugation and polyacrylamide electrophoresis of a tumour homogenate," 38(3-4), 325 (1980).

186 C Witten, "FDA Perspective/Review of Cell Scaffold Products," in 2007).

187 Cuno, "Zeta Plus Bio Cap Disposable Filter Capsules for Biotechnology and Pharmaceutical Industries," in 2007).

188 Cuno, "Zeta Plus Maximiser Dual Zone Depth Filter," 1999.

189 T. Takahashi, et al., "Novel wide-range quantitative nested real-time PCR assay for Mycobacterium tuberculosis DNA: development and methodology," 46(5), 1708 (2008).

190 V. Swarup, V, "Circulating (cell-free) nucleic acids--a promising, non-invasive tool for early detection of several human diseases," FEBS Letters 581(5), 795 (2007).

191 D. Grover, et al., "Alu repeat analysis in the complete human genome: trends and variations with respect to genomic composition," Bioinformatics. 20(6), 813 (2004).

192 Murat Abdurashitov, et al., "A physical map of human Alu repeats cleavage by restriction endonucleases," BMC Genomics 9(1), 305 (2008).

193 M. A. Batzer and P. L. Deininger, "Alu repeats and human genomic diversity," 3(5), 370 (2002).

194 G. B. Hutchinson, et al., "An Alu element retroposition in two families with Huntington disease defines a new active Alu subfamily," Nucleic Acids Res. 21(15), 3379 (1993).

195 D. Labuda and G. Striker, "Sequence conservation in Alu evolution," Nucleic Acids Res. 17(7), 2477 (1989).

196 A. J. Mighell, A. F. Markham, and P. A. Robinson, "Alu sequences," FEBS Lett. 417(1), 1 (1997).

197 M. R. Shen, M. A. Batzer, and P. L. Deininger, "Evolution of the master Alu gene(s)," J. Mol. Evol. 33(4), 311 (1991).

198 International Organisation for Standardisation, Report No. ISO 3534-2:2006, 2011.

199 J. T. Keer, essentials of nucleic acid analysis: a robust analysis (Royal Society of Chemistry, 2008).

200 J Hurley, "Endotoxemia: Methods of Detection and Clinical Correlates," 8(2), 268 (1995).

201 Centres for Drug Evaluation and Research, et al., Report No. HFN 320, 1997.

202 William A. Shaver, Harshika Bhatt, and Burton Combes, "Low serum alkaline phosphatase activity in Wilson's disease," 6(5), 859 (1986).

203 B. R. Bacon and J. G. O'Grady, "Specific Diseases of the Liver and Biliary Tree," in Comprehensive clinical Hepatology, edited by B. R. Bacon and J. G. O'Grady (Elsevier Mosby, 2006), pp.501-516.

204 "Diagnostic Tests," in Rheumatology: diagnosis and therapeutics, edited by J. J. Cush, A. Kavanaugh, and C. M. Stein (Lippincott Williams & Wilkins, 2005), pp.31-33.

205 Guidelines for the Blood Transfusion Services in the United Kingdom 7th Edition Report No. 179955 C15 9/05, 2005.

206 "Technical Bulletin: Caspase-GLO 3/7 Assay," in 2009

207 D Haag, C Tschahargane, and V Ehemann, "Isolation of single cell nuclei from human epidermis for cytophotometric DNA--measurements," 253(3), 301 (1975).

208 G. Walsh, "Drug Manufacturing Process," in Biopharmaceuticals: biochemistry and biotechnology, (J. Wiley, 2003).

209 Department of Health and Human Services, "Process Performance Qualification," in FDA > CDRH > Good Manufacturing Practice / Quality Systems > Medical Device Quality Systems Manual > Process Validation ed.2009).

210 FDA, "Food and Drugs Administration," in 2008).

211 U.S. Department of Health and Human Services Food and Drug Administration, "Guidance for Industry Bio-analytical Method Validation," in 2001).

212 S. A. Bustin, et al., "The MIQE guidelines: minimum information for publication of quantitative real-time PCR experiments," Clin. Chem. 55(4), 611 (2009).

213 Y. Karlen, et al., "Statistical significance of quantitative PCR," 8, 131 (2007).

214 WA Al-Soud, L Jönsson, and P Radstrom, "Identification and Characterization of Immunoglobulin G in Blood as a Major Inhibitor of Diagnostic PCR," 38(1), 345 (2000).

215 J Bessetti, "An Introduction to PCR Inhibitors," in 2007.

216 A. Borst, A. T. Box, and A. C. Fluit, "False-positive results and contamination in nucleic acid amplification assays: suggestions for a prevent and destroy strategy," 23(4), 289 (2004).

217 M. A. Valasek and J. J. Repa, "The power of real-time PCR," Adv. Physiol Educ. 29(3), 151 (2005).

218 L. A. Haff, "Improved quantitative PCR using nested primers," 3(6), 332 (1994).

219 Manuela Marullo, et al., "Expressed Alu repeats as a novel, reliable tool for normalization of real-time quantitative RT-PCR data," Genome Biology 11(1), R9 (2010).

220 J. Vandesompele, "Normalisation of Gene Expression: State of the Art and Preview on a New Strategy Using Expressed Alu Repeats," in 2005).

221 Intelligent MD, "Intelligent MDx IMDx 2009 Influenza A H1N1 Real-Time RT-PCR Assay Package Insert A," (2009).

222 Focus Diagnostics, "Influenza A H1N1 (2009) Real Time RT-PCR- A real-time polymerase chain reaction (PCR) assay intended for the in vitro qualitative detection of 2009 H1N1 influenza virus RNA.," (2009).

223 British Pharmacopoeia Commission, British pharmacopoeia 2009 (Stationery Office, 2008).

224 J. T. Keer, essentials of nucleic acid analysis: a robust analysis (Royal Society of Chemistry, 2008).

225 S. A. Bustin, et al., "Quantitative real-time RT-PCR--a perspective," 34(3), 597 (2005).

226 Y Hejun, et al., "Circulating Cell-Free Human Genomic DNA in the Serum of Patients With Drug-Induced Acute Liver Failure," in (American Association for the Study of Liver Disease (AASLD), 2010).

227 "Liver Disease," in Gastroenterology and Hepatology Medical Master Class, MRCP examination text, 2 ed. (Royal College of Physicians, 2008), pp.109-130.

228 N. Kaplowitz, "Liver and Biliary Diseases," in 2 ed. (Williams & Wilkins, Baltimore, 1996), pp.3-19.

229 "Zeta Plus Depth Filtration and Alternative Technologiesfor Cell Culture Clarification," in 2001).

230 M Prashad and K Tarrach, "Cell Clarification of Bioreactor Offloads," edited by Sartorius 2003).

231 E Kuntz and HD Kuntz, Hepatology: textbook and atlas: history, morphology, biochemistry, diagnostics, clinic, therapy (Springer, 2008).

232 L Li, et al., "Treatment of hepatic failure with artificial liver support system," 114(9), 941 (2001).

233 Z. Nadhazi, et al., "Plasma Endotoxin Level of Healthy Donors," Acta Microbiologica Et Immunologica Hungarica 49(1), 151 (2002).

234 M. E. Laska, et al., "Robust scale-up of dead end filtration: impact of filter fouling mechanisms and flow distribution," 92(3), 308 (2005).

235 A. Wang, R. Lewus, and A. S. Rathore, "Comparison of different options for harvest of a therapeutic protein product from high cell density yeast fermentation broth," 94(1), 91 (2006).

236 K. V. Peinemann and S. P. Nunes, membranes for life sciences (Wiley-VCH, 2007).

237 F Wiese, "Membranes for Blood Fractionation/Apheresis," in Membranes for life sciences, edited by K. V Peinemann and S. P Nunes (Wiley-VCH, Morlenbach, 2007), pp.69-90.

238 L. J. Zeman and A. L. Zydney, microfiltration and ultrafiltration: principles and applications (Marcel Dekker, 1996).

239 AL Zydney and CK Colton, "A Concentration Polarization model for the Filtrate Flux in Crossflow Microfiltration of Particulate Suspensions," 47(1) (1986).

240 A. Acrivos, et al., "Longitudinal shear-induced diffusion of spheres in a dilute suspension," 240, 651 (1992).

241 D Dobson, et al., "Experimental veri® cation of the Stokes± Einstein relation in liquid Fe± FeS at 5 GPa," 99(10), 773 (2001).

242 W. R. Bowen, J. I. Calvo, and A. Hernbndez, "Steps of membrane blocking in flux decline during protein microfiltration," 101(1-2), 153 (1995).

243 F Badmington, et al., "Vmax testing for practical microfiltration train scale-up in biopharmaceutical processing," 19, 64 (1995).

244 H Darcy, "Les Fontaines de la Ville de Dijon (the public fountains of the City of Dijon)," , 647 (1856).

245 L. W. Lake, enhanced oil recovery (Prentice Hall, 1989).

246 J Hermia, "Constant Pressure Blocking Filtration Laws: Application to Power-Law non-Newtonian Fluids," Trans. Inst. Chem. Eng. 60(183) (1982).

247 Eve M. Tracey and Robert H. Davis, "Protein Fouling of Track-Etched Polycarbonate Microfiltration Membranes," Journal of Colloid and Interface Science 167(1), 104 (1994).

249 B. J. Bain, "Blood Cells: a Practical Guide," in Blood cells: a practical guide, 3 ed. edited by B. J. Bain (Blackwell Science, Oxford, 2002), pp.112-114.

250 Cuno, "CUNO Filter Housings and Engineering Systems," in 2001).

251 C. Ronco, P. Piccinni, and M. H. Rosner, endotoxemia and endotoxin shock: disease, diagnosis and therapy (S. Karger AG, 2010).

252 Robert M. Ollodart, Ilse Hawthorne, and Safuh Attar, "Studies in experimental endotoxemia in man," The American Journal of Surgery 113(5), 599 (1967).

253 M Naqvi and MM Naqvi, "Laws of Resistance to Flow," in Design of linear drainage systems,(Thomas Telford, 2003), pp.89-92.

254 RJ Trudnowski and RC Rico, "Specific Gravity of Blood and Plasma at 4°C and 37°C," Clin. Chem 20(5), 615 (1974).

255 R. A. Freitas, nano-medicine (Landes Bioscience, 1999).

256 J. Happel and H. Brenner, low Reynolds number hydrodynamics: with special applications to particulate media (Kluwer Academic, 1991).

257 Gambro Ltd, "Cobe Spectra User Guide," in 2005).

258 KC Hou and R Zaniewski, "Depyrogenation by endotoxin removal with positively charged depth filter cartridge," 44(4), 204 (1990).

259 A. M. Sun, G. M. O'Shea, and M. F. Goosen, "Injectable microencapsulated islet cells as a bioartificial pancreas," Appl. Biochem. Biotechnol. 10, 87 (1984).

260 F. Lim and A. M. Sun, "Microencapsulated islets as bioartificial endocrine pancreas," 210(4472), 908 (1980).

261 Thomas M. S. Chang and N. Malave, "The Development and First Clinical Use of Semipermeable Microcapsules (Artificial Cells) as a Compact Artificial-kidney," 4(2), 108 (2000).

262 Dwaine F. Emerich, et al., "A novel approach to neural transplantation in Parkinson's disease: Use of polymer-encapsulated cell therapy," Neuroscience & Biobehavioral Reviews 16(4), 437 (1992).

263 Kyoko Suzuki, et al., "Regeneration of transected spinal cord in young adult rats using freeze-dried alginate gel," 10(14) (1999).

264 FDA, "Generally Recognised As Safe," in 2011).

265 FDA, "Food for Human Consumption Title 21, Part 184,"in 2011).

266 GL Picciolo, Report No. News 28, 2000. Regenerative medicine: tissue engineering standards come to ASTM. ASTM Standardization News 28: 7–8

267 C Witten, "FDA Oversight of Cell Therapy Clinical Trials," in 2005.

268 M. Martin, et al., "Analysis of cytokine secretion from lymphocytes of patients with hypersensitivity reactions to contaminated heparins," 164(1), 68 (2011).

269 PI Leonardi and JA Vasquez, "Effects of copper pollution on the ultrastructure of Lessonia spp.," 398/399, 375 (1999).

270 C Bernhardt, "Classification Methods in Streaming Fluids," in Particle size analysis: classification and sedimentation methods, edited by C Bernhardt (Chapman & Hall, 1994).

271 A. S. Grandison, and M. J. Lewis, separation processes in the food and biotechnology industries: principles and applications (Woodhead, 1996).

272 ASTM international, Report No. ASTM F1877 - 05(2010), 2010.

273 International Organisation for Standardisation, Report No. ISO/IEC 9001:2000, 2000.

274 FDA, "Code of Federal Regulations, Title 21, Part 211, Current Good Manufacturing Practice for Finished Pharmaceuticals," in 2011).

275 FDA, "Code of Federal Regulations, Title 21, Part 312, Investigational New Drug Application," in 2011).

276 European Union Council, "Directive 2001/20/EC of the European Parliament and the Council ," 1(5) (2001).

277 International Conference on Harmonisation (ICH), Report No. ICH Guideline Q2(R1), 1994.

278 ASTM international, Report No. ASTM F748 - 06(2010), 2011.

279 ISO, Report No. ISO 10993-13:2010, 2010.

Appendix I

Jetcutter™ encapsulation

Materials

- GeniaLab® Jetcutter™
- 2% alginate solution in PBS (section **Error! Reference source not found.**)
- Polymerisation buffer (section **Error! Reference source not found.**)
- 25 mM glucose complete alpha- MEM culture medium (section **Error! Reference source not found.**)
- D-MEM medium with:
  - 10% FCS
  - 100 U/ml Penicillin, 0.1 mg/ml Streptomycin
  - 1.25 µg/ml Fungizone
- Pyrex beakers baked (180 °C for 3 hours)
- Autoclaved Jetcutter™ components:
  - pressure vessel
  - inline filter
  - nozzle holder nozzle assembled and autoclaved
  - cutting tool, cutting disc, collection cover
- Autoclaved 5 L stainless steel basin
- Baked funnel for filling pressure vessel
- Plastic beaker for collecting waste from Jetcutter™
- 25 ml measuring cylinder for calibration of alginate flow rate
- Plastic bottomless beaker and elastic band
- 200 µm nylon mesh
- 200 µm glass beads
- Magnetic Stirrers
- Stainless steel spatula
- Sterile consumables including, 15 ml Nunc™ tubes, 50 ml Nunc tubes, 50 ml syringes, 25ml serological pipettes, Gilson tips and Nunc® triple culture flasks

Jetcutter™ principle

The JetCutter™ encapsulation enables the production of large volumes of beads, and is currently the method of choice for encapsulating cells for use with the full scale Bioartificial Liver system.

The Jetcutter™ system consists of a pressurised chamber which forces the alginate/cell/media mix through a nozzle at a controlled rate. The stream then passes through a cutting tool with asymmetrically arranged of wires, which are inclined relative to the vertical solid stream of liquid, resulting in a horizontal cut as the tool passes through the liquid stream. The cylindrical segment then forms a bead due to surface tension whilst descending to the polymerisation buffer. This machinery is operated by more experienced colleagues.

JetCutter™ Set Up

HepG2 cell culture for the Jetcutter® system was the as the Inotech®, in terms of preparation of HepG2 cells, the alginate and cell mix, and the media used to encapsulate, but to a larger scale. Cells were cultured in triple Nunc® flasks, described in section **Error! Reference source not found.**, and mixed with 2% alginate to a 1:1 ratio, giving 1% alginate, cell in high glucose medium mix (high glucose medium in section **Error! Reference source not found.**), to which 2% 200µm sterile glass beads were added, thoroughly mixed, and immediately poured into the pressure vessel. The lid of the pressure vessel contains a propeller unit, which is driven from the top by a motor set at 50 rpm, allowing constant agitation of cell, alginate and glass bead mix. Air pressure was provided using an air pump connected through a vent in the lid, then by opening an outlet located at the bottom of the vessel, the mix is forced out and the flow begins.

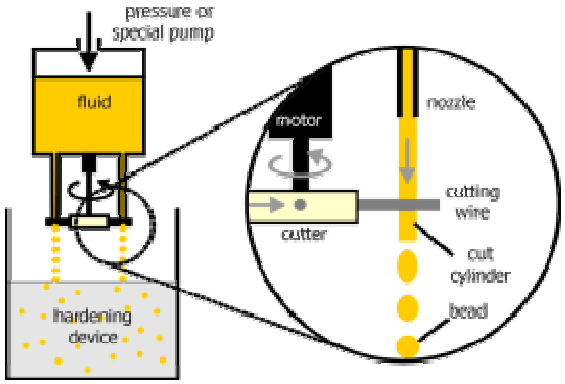

Figure i: Schematic diagram of the jet cutter system where the air pressure is produced to force the alginate, medium and cell mix through a 350 µm nozzle. The flow is cut by 100 µm wires on a circular cutting device to form beads by surface tension. The beads then descend into the polymerisation buffer containing Ca^{2+} causing cross linking between the alginate homopolymeric blocks, consisting of β-D-mannuronate and its C-5 epimer α-L-guluronate.

The flow passed through a 350 µm nozzle, which was calibrated to 0.33 ml/sec by adjusting the pressure, followed by temporarily discontinuing the flow to attach the cutting disk in the path of the flow.

A number of parameters relating to the cutter and the flow, directly impact bead characteristics as shown in Figure ii: the cutter, spreads the descending path of the beads reducing the probability of multiple beads forming; the angle of inclination of the flow to the cutting disk alters the size of the beads and the efficiency of encapsulation in terms of waste (Figure ii); lastly, the motor speed of the cutter set at 3600rpm, alters the size of the beads, by changing the volume of alginate mix that passes before cutting again.

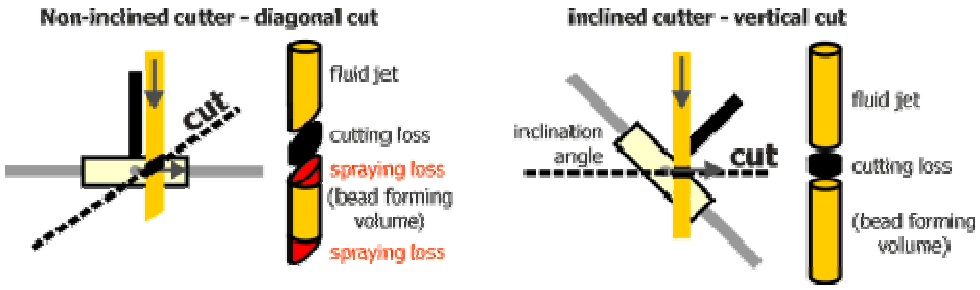

Figure ii: The inclination of the alginate flow to the wire cutter affects the amount of alginate cell mix wasted by the cutting process. Optimal inclination angle is determined by the GeniaLab® Beadsim™ program.

Optimal conditions were set using an algorithm provided by the BeadSim™ software which calculates the required flow rate, cutting speed and inclination angle for the required bead size of 500 µm.

"Feed and Bleed system"

We routinely produce between 500 and 1000 litres of beads for large scale experiments and treatment, which is measured after polymerisation, using the settled volume of beads. To polymerisation this volume, a 5 L container with 3 L of polymerisation buffer and a magnetic stirrer was placed beneath the flow of beads. We have previously observed that calcium ion concentration affects the rate of polymerisation and subsequently the quality of beads. When encapsulating high volumes of beads, however, the alginate sequesters the calcium in the buffer as well as causing a dilution effect. This was controlled by slowly bleeding 70% $CaCl_2$ into the 5 L container over the period of encapsulation, simultaneously an overflow pipe is located immediately above the 3L mark to remove excess polymerisation buffer, and reduce the dilution effect of the beads. The flow rate of the concentrated calcium infusion was identical to the flow rate of beads from the Jetcutter™, typically between 19.5 and 21ml/min.

Bead Collection

To begin the encapsulation, the outlet tap on the pressure vessel was opened to begin alginate mix flow and the Jet cutter motor was started. Prior to bead collection, the initial flow through was discarded whilst a clean alginate mix flow was established. After which the beads were collected into the polymerisation buffer over 1 hour, then poured from their collection basin through a beaker with a 200µM mesh bottom, retaining the beads on the mesh. To remove the polymerisation buffer, the beads in the mesh were placed at the bottom of a container, where D-MEM with 10 % FBS was poured over the beads whilst mixing gently, followed by transferring the beads into 50 ml centrifuge tubes to be used as required. Once beads had settled, the volume collected was estimated from the graduations marked on the side of the tubes.

Appendix II

Appendix III Certified PCR water

Product Insert
PCR Water

Product:
PCR Water

Catalogue Number:
BIO-37080 10 x 10ml

Features
- Ultra-pure 18.2MΩ
- DNase/RNase-free

Applications
- For use in all molecular biology applications.

Description
Bioline ultra-pure 18.2MΩ PCR Water is extremely pure molecular biology grade water, which is suitable for all PCR, RT-PCR and electrophoresis applications. Purification of ultra-pure water is carried out with a pharmaceutical-grade, absolute 0.22µm membrane filter that is recommended for most analytical applications. Further purification is achieved by filtration of water through a membrane filter with a molecular weight cut-off of 10 Kilo Dalton. Each lot is PCR-tested with universal primers and certified to be free of DNA contamination. For all applications involving RNA, we recommend using DEPC-treated Water, which is chemically treated to destroy any RNase contamination.

Product Specifications:

Batch details:
Batch No: **See bottle**

Storage Conditions:
PCR Water can be stored for 12 months at -20°C.

Shipping Conditions:
On Dry Ice or Blue Ice

Specifications:

Appearance	Clear Colourless Liquid
Molecular Formula	H_2O
Molecular Weight	18.02
Performance/Quality	DNase, RNase, Nickase and Protease activities not detected

Product Life: 1 year from date of purchase

Associated Products:

Product Name	Pack Size	Cat No
IMMOLASE DNA Polymerase	250 Units	BIO-21046
Thermo DNA Ligase	500 Units	BIO-27045
Quick-Stick Ligase	50 Reactions	BIO-27027
Agarose Tablets	300g	BIO-41027

Notes
1. This product insert is a declaration of analysis at the time of manufacture.
2. Research Use Only.

UK
Bioline
16 The Edge Business Centre
Humber Road
London, NW2 6EW
U.K

Tel: + 44 (0)20 8830 5300
Fax: +44 (0)20 8452 2822

Germany
Bioline GmbH
Im Biotechnologiepark TGZ 2
D-14943 Luckenwalde
Germany

Tel: +49 (0)33 7188 1239
Fax: +49 (0)33 7188 1244

email: info@bioline.com
website: www.bioline.com

USA
Bioline USA Inc.
305 Constitution Dr.
Taunton
MA 02780
USA

Toll Free: 888 257 5155
Tel: 508 880 8990
Fax: 508 880 8993

Australia
Bioline (Aust) Pty Ltd
PO Box 122
Alexandria NSW 1435
Australia

Tel: +61 (0)2 9209 4160
Fax: +61 (0)2 9209 4763

Appendix IV Human Genomic

Product Insert
Human Genomic DNA

Catalogue Number:
BIO-35025 1 x 500µl

Features
- Highly purified
- Fragments of up to 50Kb

Applications
- Southern blotting
- Genomic library construction
- Control template

Description
Human Genomic DNA is highly purified and isolated from human placenta. The average length of the DNA is greater than 50Kb and is suitable for Southern Blotting, genomic library construction and as a control template.

Product Specifications

Batch details:
Batch No: See vial
Pack Size: See vial

Storage Conditions:
Human Genomic DNA should be stored at -20°C for up to 12 months. Repeated freeze/thaw cycles should be avoided.

Shipping Conditions:
On Dry Ice or Blue Ice

Presentation:
Volume: 500µl
Concentration: 200ng/µl
Total amount: 100µg

Storage and Dilution Buffer:
1x TE (10mM Tris-HCl pH 8.0, 1mM EDTA)

Associated Products:

Product Name	Pack Size	Cat. No.
Agarose Tablets	150g	BIO-41025
18.2MΩ Water	10 x 10ml	BIO-37060
dNTP Mix	500µl	BIO-39025
MyTaq™ DNA Polymerase	250 Units	BIO-21046

References:
(1) Sambrook,J., Fritsch, E.F. and Maniatis, T. (1989) *Molecular Cloning: A laboratory Manual*, 2nd ed., Cold Spring Harbor Laboratory, Cold Spring Harbor, NY, 9.14

Notes
1. This product insert is a declaration of analysis at the time of manufacture.
2. Research Use Only.

UK
Bioline
16 The Edge Business Centre
Humber Road
London, NW2 6EW
U.K.

Tel: + 44 (0)20 8830 5300
Fax: +44 (0)20 8452 2822

USA
Bioline USA Inc.
305 Constitution Dr.
Taunton
MA 02780
USA

Toll Free: 888 357 5155
Tel: 508 880 8990
Fax: 508 880 8993

Germany
Bioline GmbH
Im Biotechnologiepark TGZ 2
D-14943 Luckenwalde
Germany

Tel: +49 (0)33 7188 1229
Fax: +49 (0)33 7188 1344

Australia
Bioline (Aust) Pty Ltd
PO Box 122
Alexandria NSW 1435
Australia

Tel: +61 (0)2 9209 4150
Fax: +61 (0)2 9209 4783

email: info@bioline.com
website: www.bioline.com

Appendix V Platelet Aggregation

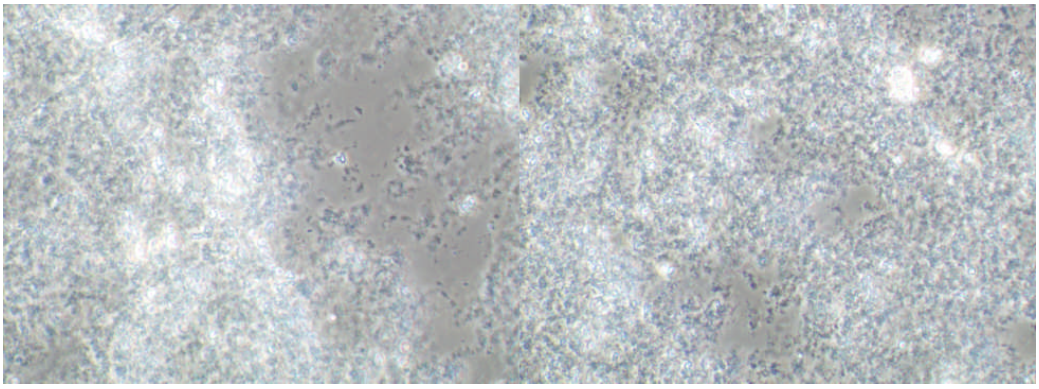

Figure I: Platelet aggregation in FFP under phase contrast microscopy.

Appendix VI Loading and removing the Cobe® Spectra® Therapeutic Plasma Exchange Tubing